



ulm university universität
uulm



Ulm University Hospital - Surgery Center
Department of General and Visceral Surgery

Medical Directors:

Prof. Dr. med. Doris Henne-Bruns (until 30.09.2020)

Prof. Dr. med. Christoph Michalski (from 01.10.2020)

Characterization of CK1 δ -mediated phosphorylation of tau and development of novel pharmacological approaches targeting CK1 δ in Alzheimer's disease

Dissertation submitted in partial fulfillment of the requirements for the degree of

“Doctor rerum naturalium” (Dr. rer. nat.)

of the International Graduate School in Molecular Medicine

submitted by

Aileen Roth

born in Weingarten

2023

Current dean of the Medical Faculty:	Prof. Dr. Thomas Wirth
Current chairman of the International Graduate School in Molecular Medicine:	Prof. Dr. Bernd Knöll
First supervisor:	PD Dr. Joachim Bischof
Second supervisor:	Prof. Dr. Holger Barth
Third supervisor:	Prof. Dr. Gopal Sapkota
External Reviewer:	Dr. Andrea Venerando
Day doctorate awarded:	13 th July, 2023

Results gained in this thesis have previously been published in the following publications:

Roth, A., Sander, A., Oswald, M. S., Gärtner, F., Knippschild, U., and Bischof, J. 2022. Comprehensive Characterization of CK1 δ -Mediated Tau Phosphorylation in Alzheimer's Disease. *Frontiers in molecular biosciences* 9, 872171.

Roth, A., Gihring, A., Bischof, J., Pan, L., Oswald, F., and Knippschild, U. 2022. CK1 Is a Druggable Regulator of Microtubule Dynamics and Microtubule-Associated Processes. *Cancers* 14, 5.

Drathen, T. von, Ure, E. M., Kirschner, S., **Roth, A.**, Meier, L., Woolhouse, A. D., Cameron, S. A., Knippschild, U., Peifer, C., and Luxenburger, A. 2022. C5-Iminosugar modification of casein kinase 1 δ lead 3-(4-fluorophenyl)-5-isopropyl-4-(pyridin-4-yl)isoxazole promotes enhanced inhibitor affinity and selectivity. *Archiv der Pharmazie* 355, 5, e2100497.

Traub, B., **Roth, A.**, Kornmann, M., Knippschild, U., and Bischof, J. 2021. Stress-activated kinases as therapeutic targets in pancreatic cancer. *World journal of gastroenterology* 27, 30, 4963–4984.

Roth, A., Gihring, A., Göser, F., Peifer, C., Knippschild, U., and Bischof, J. 2021. Assessing the Inhibitory Potential of Kinase Inhibitors In Vitro: Major Pitfalls and Suggestions for Improving Comparability of Data Using CK1 Inhibitors as an Example. *Molecules* (Basel, Switzerland) 26, 16.

Roth, A., Gärtner, F., Mayer, K., Beyrle, J., König, I., Knippschild, U., and Bischof, J. 2021. CK1 δ -Derived Peptides as Novel Tools Inhibiting the Interactions between CK1 δ and APP695 to Modulate the Pathogenic Metabolism of APP. *International journal of molecular sciences* 22, 12.

A complete list of all publications published during the preparation of this thesis can be found in the chapter “publications”.

Content

List of figures	VI
List of tables	VIII
List of abbreviations	IX
1 Introduction	1
1.1 Protein phosphorylation and protein kinases	1
1.2 The CK1 family	2
1.3 Roles of CK1 in biology	7
1.4 Contribution of CK1 to the development of human diseases	11
1.5 The role of CK1 in Alzheimer's disease	13
1.6 Protein kinases as targets in therapy	21
1.7 CK1-specific inhibitors and their therapeutic potential	23
1.8 Modulation of the CK1 activity with therapeutic peptides	26
1.9 Aim of the study	28
2 Materials and Methods	30
2.1 Materials	30
2.2 Molecular biological methods	45
2.3 Bacteria methods	48
2.4 Protein biochemical methods	55
2.5 Cell biological methods	62
2.6 Interaction analysis	68
2.7 Immunohistochemical methods	71
2.8 Computational methods	72
2.9 Statistical analysis	73
3 Results	74
3.1 Characterization of CK1 δ -mediated phosphorylation of tau	74
3.2 Identification of new CK1 δ -specific compounds for the treatment of AD	86
3.3 Identification of CK1 δ -derived peptides modulating AD pathology	104
4 Discussion	124
4.1 CK1 δ is a potential target for tau-mediated phosphorylation	124

4.2	Identification of new CK1δ-specific compounds for the treatment of AD	128
4.3	Identification of CK1δ-derived peptides modulating AD pathology	135
4.4	Conclusion	140
5	Summary	143
6	References	145
	Supplement	167
	Acknowledgement	170
	Statutory declaration	172
	Publications.....	173

List of figures

Figure 1: Phylogenetic tree of the human ePK superfamily.....	2
Figure 2: Domain structure of the CK1 isoforms.....	3
Figure 3: Molecular and domain structure of CK1 δ	4
Figure 4: Phosphorylation sites of CK1 δ targeted by cellular kinases.	7
Figure 5: The role of CK1 in the Wnt signaling.	8
Figure 6: Schematic overview of tau441 domains and its potential AD-associated phosphorylation sites.	15
Figure 7: The role of CK1 in tau hyperphosphorylation.	16
Figure 8: Schematic overview of APP695 domains and its potential phosphorylation sites.....	17
Figure 9: The potential role of CK1 in APP processing.....	18
Figure 10: The potential role of CK1 in the development of AD.....	20
Figure 11: Plasmids for the expression of 6xHis- and GST-tagged proteins.	50
Figure 12: Workflow for the establishment of standard conditions	58
Figure 13: Overview of the generation of the “Alzheimer’s-in-a-dish” cell culture model.	63
Figure 14: Principle of the NanoBiT [®] PPI system.	69
Figure 15: Establishment of the NanoBiT [®] PPI system.	70
Figure 16: Tau441 contains several putative target sites for CK1.	74
Figure 17: Mass spectrometric analysis of tau441.....	76
Figure 18: Generation and phosphorylation of tau441 fragments.....	77
Figure 19: Phosphopeptide analysis of tau441 fragments.....	78
Figure 20: Summary of the data obtained from <i>in silico</i> prediction, mass spectrometric analysis and biochemical approaches.....	79
Figure 21: Generation and phosphorylation of tau441 phosphomutants.	80
Figure 22: Phosphopeptide analysis of tau441 phosphomutants.	81
Figure 23: Identification of CK1 δ -specific tau phosphorylation sites in neuronal cells via Western blot analysis.	82
Figure 24: Immunofluorescence staining of CK1 δ and tau in neuronal cells.	84
Figure 25: Co-localization analysis of CK1 δ and tau.	85
Figure 26: Phosphorylation of tau441 by CK1 δ is linked to tau aggregation.	86
Figure 27: Calculation of the S/N ratio.	88
Figure 28: Determination of the V _{init} region of GST-tagged CK1.	89
Figure 29: Michaelis-Menten kinetics of GST-tagged CK1 α , CK1 δ and CK1 ϵ	90

Figure 30: Initial screening of benzimidazole derivatives.....	92
Figure 31: Initial screening of IWP-derived compounds.	93
Figure 32: IC ₅₀ determination of the most potent IWP-derived compounds.....	94
Figure 33: Initial screening of isoxazole derivatives.....	96
Figure 34: IC ₅₀ determination of the most potent isoxazole derivatives.....	97
Figure 35: Neuronal cell toxicity of CK1δ-specific inhibitors.	99
Figure 36: Effect of CK1δ-specific inhibitors on Aβ processing.	101
Figure 37: Effect of CK1δ-specific inhibitors on tau phosphorylation and aggregation.	103
Figure 38: Generation of APP695 fragments to facilitate the protein production.	105
Figure 39: Identification of CK1δ-derived peptides, which specifically bind to APP695 fragments.....	106
Figure 40: Effect of CK1δ-derived peptides on CK1δ-mediated phosphorylation of APP695 fragments.....	107
Figure 41: Establishment of the NanoBiT® APP695-CK1δ interaction system.	109
Figure 42: Domain structure of tau441 and tau383.	110
Figure 43: Identification of CK1δ-derived peptides, which specifically bind to tau.	111
Figure 44: Effect of CK1δ-derived peptides on CK1δ-mediated tau phosphorylation.	112
Figure 45: Identification of CK1δ-derived peptides blocking the interaction of tau441 and CK1δ by using NanoBiT®.....	113
Figure 46: Localization of APP695-/tau-interacting and -inhibiting CK1δ-derived peptides in CK1δ protein structure.....	114
Figure 47: Neuronal cell toxicity of CK1δ-derived peptides.	115
Figure 48: Cell entry of CK1δ-derived peptides into living neuronal cells.....	117
Figure 49: Effect of CK1δ-derived peptides on Aβ processing and amyloid plaque formation.	119
Figure 50: Effect of CK1δ-derived peptides on tau phosphorylation.....	121
Figure 51: Effect of CK1δ-derived peptides on tau aggregation.	123
Figure 52: Overview of potential CK1δ-specific tau phosphorylation sites.	128

List of tables

Table 1: Identified <i>in vitro</i> and <i>in vivo</i> substrates of CK1.	5
Table 2: Different types of PK inhibitors.	22
Table 3: Potent CK1-specific inhibitors.	25
Table 4: Overview of devices, which were used in this project.	30
Table 5: Chemicals and biochemicals.	31
Table 6: Overview of consumables and reagent systems.	33
Table 7: Bacteria and cell lines with their respective origin and genotype.	34
Table 8: Used bacteria and cell line with their respective culture media.	34
Table 9: Molecular weight markers.	34
Table 10: Proteins and enzymes.	35
Table 11: Procaryotic expression vectors.	35
Table 12: Eukaryotic expression vectors.	36
Table 13: Antibodies and streptavidin-conjugates.	37
Table 14: Sequences of primers used for cloning procedures.	38
Table 15: Sequences of primers used for sequencing.	40
Table 16: Software, databases and online tools.	40
Table 17: Commercially available or published inhibitors used in this study.	41
Table 18: Overview of the tested compounds.	42
Table 19: CK1 δ -derived peptide library	44
Table 20: PCR cycling conditions according to Q5 [®] Site-Directed Mutagenesis Kit.	45
Table 21: PCR cycling conditions with Phusion [®] High-Fidelity DNA polymerase.	46
Table 22: PCR cycling conditions with taq DNA polymerase.	47
Table 23: Results of LC-MS/MS analysis of phosphorylated tau441.	75
Table 24: AD-associated tau phosphorylation sites targeted by CK1 δ	83
Table 25: Determination of V _{init} region for GST-tagged CK1 α , CK1 δ and CK1 ϵ	90
Table 26: Summary of the established standard conditions	91
Table 27: IC ₅₀ determination of IWP-derived compounds.	94
Table 28: IC ₅₀ determination of isoxazole derivatives.	98

List of abbreviations

A	aa	amino acid
	A β	amyloid- β
	ABTS	2,2'-azino-bis(3-ethylbenzothiazoline-6-sulphonic acid)
	AGC	family of the protein kinase A/G/C
	AKAP	A-kinase anchoring protein
	Akt	Akt/protein kinase B
	ALS	amyotrophic lateral sclerosis
	APC	adenomatous polyposis coli
	aPK	atypical protein kinase
	APC	adenomatous polyposis coli
	APOE	apolipoprotein E
	APP	amyloid precursor protein
	APP-C	C-terminal fragment of APP695 (aa 613 – 695)
	APS	ammonium persulfate
	ATP	adenosine triphosphate
	ATP-BS	ATP binding site
	AU	absorption unit
	B	BACE
BBB		blood-brain-barrier
BCA		bicinchoninic acid
bFGF		basic fibroblast growth factor
BMP		bone morphogenetic protein
BSA		bovine serum albumin
C	CAMK	family of the Ca ²⁺ /calmodulin-dependent protein kinase
	CDK	cyclin-dependent kinase
	CK1	casein kinase 1
	CK2	casein kinase 2
	CMGC	family of the cyclin-dependent kinase
D	DAPI	4',6-diamidino-2-phenylindole
	DD	dimerization domain
	DISC	death-inducing signaling complex
	DMEM	Dulbecco's modified eagle's medium
	DMSO	dimethyl sulfoxide
	DNA	desoxyribonucleic acid
	dNTP	deoxyribonucleoside triphosphate
	DTT	dithiothreitol
	DVL	Disheveled
E	E2	APP695 fragment consisting of the E2 domain (aa 268 – 612)
	EC ₅₀	half maximal effective concentration
	ECL	enhanced chemiluminescence
	EDTA	ethylenediaminetetraacetic acid
	EGF	epidermal growth factor
	EGFR	epidermal growth factor receptor
	EGTA	ethylene glycol-bis-(beta-aminoethylether)-N,N,N',N'-tetraacetic acid
	ELISA	enzyme-linked immunosorbent assay
	endA1	endonuclease I
	ePK	eukaryotic protein kinase
F	FACS	fluorescence activated cell sorting

List of abbreviations

	FAD	familial Alzheimer's disease
	FADD	Fas-associated protein with death domain
	FAM83	Family of sequence similarity 83
	FCS	fetal calf serum
	FGFR	fibroblast growth factor receptor
	FITC	fluorescein isothiocyanate
	FPLC	fast protein liquid chromatography
G	GFP	green fluorescent protein
	GSK3	glycogen synthase kinase 3
	GST	glutathione-S transferase
H	HCl	hydrogen chloride
	HEPES	N-2-hydroxyethylpiperazine-N'-2-ethanesulfonic acid
	hNPC	human neural progenitor cell
	HRP	horseradish peroxidase
I	IC ₅₀	half maximal inhibitory concentration
	IF	immunofluorescence
	IMAC	immobilized metal affinity chromatography
	iPCR	inverse polymerase chain reaction
	IPTG	isopropyl- β -D-thiogalactopyranoside
	IWP	inhibitor of Wnt production
J	JAK	Janus kinase
K	KHD	kinesin homology domain
	K _i	inhibitory constant
	K _m	Michaelis constant
L	LB	lysogeny broth
	LC-MS/MS	liquid chromatography with tandem mass spectrometry
	LgBiT	large unit of the binary technology
	LRP	lipoprotein-related receptor protein
M	MAP	microtubule-associated protein
	MAPK	mitogen-activated protein kinase
	MDM2	mouse double minute 2 homolog
	MOC	Mander's overlap coefficient
	MT	microtubule
	MTT	3-(4,5-dimethylthiazol-2-yl)-2,5-diphenyltetrazolium bromide
N	N-APP	N-terminal fragment of APP695 (1 – 267)
	NFAT	nuclear factor of activated T-cells
	NFT	neurofibrillary tangle
	NLS	nuclear localization signal
	NP-40	Nonidet-P 40
O	OD ₆₀₀	optical density at 600 nm
P	PBS	phosphate buffered saline
	PCC	Pearson's correlation coefficient
	PCR	polymerase chain reaction
	PDB	protein data bank
	PDHK	pyruvate dehydrogenase kinase
	PHF	paired helical filaments
	PIKK	phosphatidylinositol 3' kinase related kinase
	PI3K	phosphoinositide-3-kinase
	PK	protein kinase
	PKA/C/G	protein kinase A/C/G
	PMSF	phenylmethylsulfonyl fluoride

List of abbreviations

	PNT	1,10-phenanthroline
	PPI	protein-protein interaction
	PRKACA	protein kinase cAMP-activated catalytic subunit alpha
	PRKAR2A	protein kinase cAMP-dependent type II regulatory subunit alpha
	PROTAC	proteolysis-targeting chimeras
	PSEN	presenilin
	PTM	post-translational modification
	PVDF	polyvinylidene fluoride
R	RBS	ribosome binding site
	recA1	recombinase I
	RGC	receptor guanylate cyclase
	ROI	region of interest
S	S/N	signal-to-noise
	SAD	sporadic Alzheimer's disease
	SCF	SKP1-Cul1-F-Box protein E3 ubiquitin ligase
	SDM	site-directed mutagenesis
	SDS	sodium dodecyl sulfate
	SISF	sarkosyl-insoluble fraction
	SmBiT	small unit of the binary technology
	SMI	small molecule inhibitor
	SSF	sarkosyl-soluble fraction
	STE	mitogen-activated protein kinase cascade family
T	tau	tubulin-associated unit
	TBS	Tris-buffered saline
	TCF	T-cell factor
	TDP-43	TAR DNA-binding protein of 43 kDa
	TEMED	N,N,N',N'-tetramethylethylenediamine
	TK	tyrosine kinase
	TNF	tumor necrosis factor
	TRAIL	TNF-related apoptosis-inducing ligand
	TRITC	tetramethylrhodamine
	TTBK	tau-tubulin kinase
	TV	transcription variant
V	V	velocity
	V _{init}	initial velocity
	V _{max}	maximal velocity
	VRK	vaccinia-related kinases
W	Wnt	wingless/int-1
	wt	wild type

1 Introduction

1.1 Protein phosphorylation and protein kinases

Protein phosphorylation is one of the most important signal transduction and cell signaling mechanism by which intercellular signals control crucial intracellular processes such as gene transcription and protein translation, cell cycle progression, cellular metabolism, cytoskeleton dynamics, cellular proliferation, differentiation, ion transport and hormone response [17, 55, 78]. Phosphorylation processes are mainly catalyzed by members of the huge superfamily of protein kinases (PK) that catalyze the transfer of the γ -phosphate derived from adenosine triphosphate (ATP) to a hydroxyl residue, which is attached to a protein substrate. A reverse reaction, also known as dephosphorylation, is mediated by protein phosphatases.

Recently, the human genome project has identified that approximately 20 % of the 32,000 human genes encode for proteins that are involved in signal transduction processes. Among the 32,000 human genes, approximately 1.7 % encode for 555 PKs, of which 497 PKs belong to the group of eukaryotic PKs (ePKs) with typical domain structures, while the other 58 PKs refer to atypical PKs (aPKs) [175]. According to the amino acid (aa) side chain kinases prefer to phosphorylate, three main types of PKs can be classified: Tyrosine kinases (TK) (phosphorylating the Tyr phenolic hydroxyl), serine-threonine kinases (phosphorylating the hydroxy group of these two aa) and histidine kinases (phosphorylating the nitrogen of His residues) [17]. Among the PKs, the majority of kinases belongs to the serine-threonine kinase family, whereas only 90 refer to TKs [226].

In 2002, Manning et al. revealed the PK complement of the human genome (the “kinome”) and classified ePKs in nine distinct ePK families involving TK (including several receptor kinases like epidermal growth factor receptor (EGFR) or fibroblast growth factor receptor (FGFR) and non-receptor TK-like Abl or Janus kinase (JAK)), TK-like, receptor guanylate cyclase (RGC), STE group (including mitogen-activated protein kinase (MAPK) cascade families), casein kinase 1 (CK1), AGC group (including protein kinase A, C and G (PKA/PKC/PKG)), CMGC group (including cyclin-dependent kinases (CDK)), CAMK group (including PK dependent on Ca^{2+} /calmodulin-dependent) and a group referred to “others” containing 83 family

members (Figure 1) [158, 226]. Members of the aPKs are classified into four groups including Alpha, phosphatidylinositol 3' kinase related kinase (PIKK), pyruvate dehydrogenase kinase (PDHK) and a group of RIO kinases (named after the "right open reading frame") [2, 105, 201, 231].

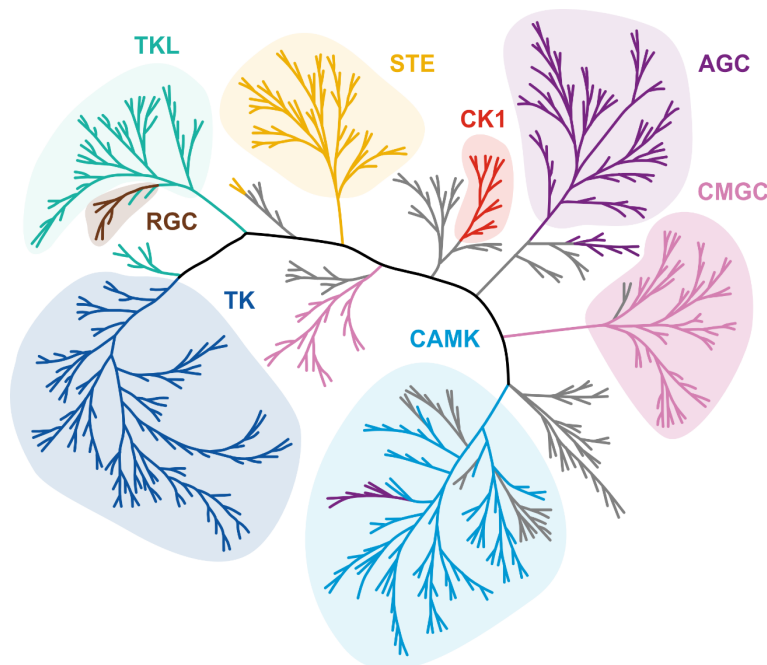


Figure 1: Phylogenetic tree of the human ePK superfamily. The phylogenetic tree represents the human kinome including nine PK families. The PK superfamily includes the family of tyrosine kinases (TK, blue), TK-like (TKL, green), receptor guanylate cyclase (RGC, brown), mitogen-activated protein kinase (MAPK) cascade family (STE, yellow), casein kinase 1 (CK1, red), protein kinase A/G/C (AGC, purple), cyclin-dependent kinase (CMGC, pink) and Ca^{2+} /calmodulin-dependent protein kinase (CAMK, light blue). Figure is based on [226].

1.2 The CK1 family

Members of the CK1 family, which build their own branch of the kinome tree, were among the first kinases described in literature. Currently, at least seven different CK1 isoforms (α , β , γ 1-3, δ and ϵ) and their transcription variants (TV) have been characterized in mammals (Figure 2A). All CK1 isoforms, except CK1 β , which is exclusively expressed in bovine animals, are present in the human organism [187, 299]. Within their kinase domain, all CK1 isoforms are highly conserved, whereas CK1 δ and CK1 ϵ share the highest homology with 98 %. However, CK1 isoforms differ significantly in length and sequence of the N-terminal domain (aa 4 to 40) and C-terminal domain (aa 39 to 122) resulting in different molecular weights (MW) ranging from 37 kDa (CK1 α) to 51 kDa (CK1 γ 3) (Figure 2A) [185, 299]. The closest

phylogenetic relationship to CK1 isoforms was identified for vaccinia-related kinases (VRK)1 to 3 and the tau-tubulin kinases (TTBK)1 and 2 (Figure 2B) [185].

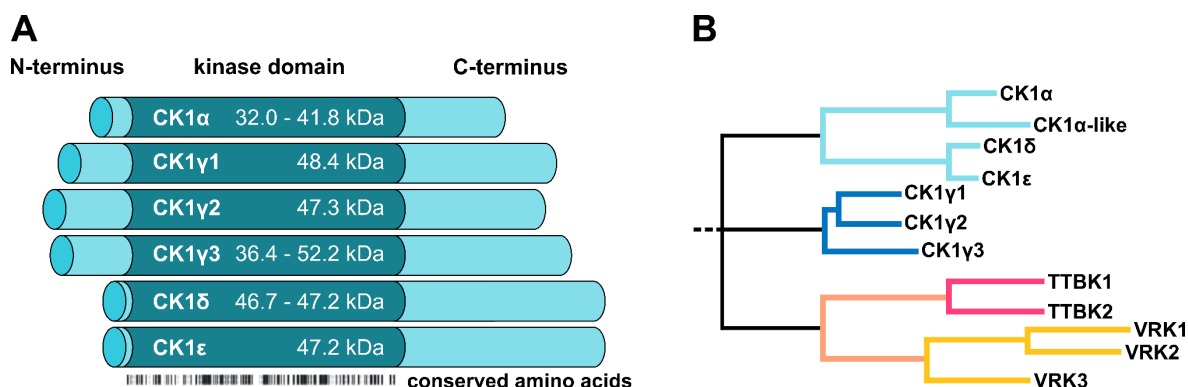


Figure 2: Domain structure of the CK1 isoforms. (A) Schematic illustration of human CK1 isoforms α , γ 1-3, δ and ϵ ranging from 32 kDa to 52.2 kDa. Despite differences in MW, all isoforms share high homology within the kinase domain. Figure is based on [187]. **(B)** Phylogenetic tree of the CK1 family members includes six human CK1 isoforms (α , γ 1-3, δ and ϵ), TTBK1/2 and VRK1/2/3. Figure was modified from [185], which is licensed under a Creative Commons Attribution 3.0 unported license (CC BY 3.0), <https://creativecommons.org/licenses/by/3.0/>. TTBK: Tau-tubulin kinase, VRK: Vaccinia-related kinase.

1.2.1 Structure and domains

Based on a bi-lobal structure, CK1 is composed of a small N-terminal and a large C-terminal lobe (Figure 3A). Both lobes form the catalytic cleft for ATP-substrate interaction and are connected by a single loop, which forms the hinge [221, 371]. The small N-terminal lobe is composed of five twisted anti-parallel β -sheets and one helix, which play an important role in the conformational regulation of kinase activity. Contrarily, the C-terminal lobe consists of five long anti-parallel α -helices as well as three short helices, four short β -sheets and three long loops, which are clustered around the surface of the catalytic cleft and are necessary for enzyme activity. Additionally, a kinesin homology domain (KHD), a putative dimerization domain (DD) and a putative nuclear localization signal (NLS) affecting substrate binding have been identified within the kinase domain of CK1 δ (Figure 3B). KHD was assumed to support the interactions of CK1 isoforms with components of the cytoskeleton as it is necessary for the interaction of kinesin with microtubules (MT) [29, 117, 284]. The ATP-binding site (ATP-BS) located in the N-terminal part of CK1 is mainly composed of three components including a deep hydrophobic region, which is bordered by a gatekeeper residue and a second large hydrophobic region.

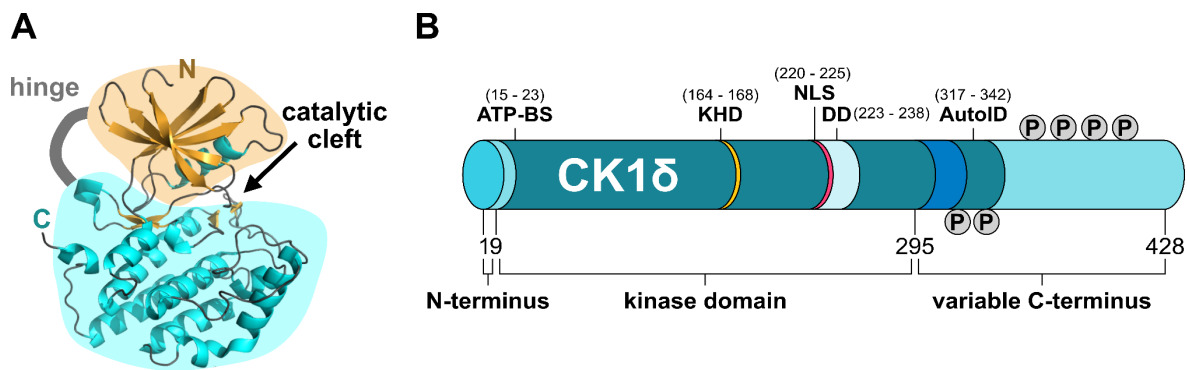


Figure 3: Molecular and domain structure of CK1 δ . (A) Three-dimensional cartoon diagram of the bi-lobal molecular structure of CK1 δ (PDB code 6GZM) including the N-terminal lobe (yellow) and the C-terminal lobe (turquoise) forming the catalytic cleft and which are connected by the hinge region (grey). (B) Schematic representation of the CK1 δ domain structure showing relevant domains including ATP-binding site (ATP-BS), kinesin homology domain (KHD), nuclear localization signal (NLS), dimerization domain (DD) and autoinhibitory domain (AutoID). Numbers indicate aa positions and P sites of phosphorylation. Figure was modified from [185], which is licensed under a Creative Commons Attribution 3.0 unported license (CC BY 3.0), <https://creativecommons.org/licenses/by/3.0/>. ATP-BS: ATP-binding site, AutoID: Autoinhibitory domain, DD: Dimerization domain, KHD: Kinesin homology domain, NLS: Nuclear localization signal.

1.2.2 Substrate specificity and consensus sequence of CK1

The milk protein component casein was described as one of the first substrates for CK1 [35]. Although it is not a physiological substrate for CK1 isoforms, it perfectly illustrates their preference for serine or threonine residues, which are N-terminally flanked by phospho-primed aa residues resulting in the canonical consensus sequence, which is represented by the motif pSer/pThr-X-X-(X)-Ser/Thr, where X is any aa and pSer/pThr denotes phospho-primed aa residues [116, 234, 235]. Since CK1 belongs to the group of acidotropic PKs, it does not exclusively phosphorylate phospho-primed motifs, but also serine or threonine residues, which are flanked by an agglomeration of negatively charged acidic aa including aspartic and glutamic acid [10]. Compared to primed phosphorylation, unprimed phosphorylation seems to be very slow indicating a regulatory function, which serves as rate-limiting steps for downstream phosphorylation [211, 227, 334]. In addition to the primed and unprimed canonical consensus sequence, non-canonical consensus sequences for CK1 isoforms were identified including Lys/Arg-X-Lys/Arg-X-X-Ser/Thr, which was described for sulfatide and cholesterol-3-sulfate binding proteins [178] and the Ser-Lys-Ser motif, which is present in β -catenin and the nuclear factor of activated T-cells (NFAT) [227]. Due to the great variety of CK1 substrate consensus sequences and a huge amount of cellular proteins harboring at least one of the CK1-specific consensus sequence, more than 140 *in vitro* and *in vivo* protein substrates for CK1

have been detected, so far. Although the physiological relevance of some *in vitro* identified substrates has not been verified *in vivo*, which can be attributed to challenging and complex intracellular regulatory mechanisms, the involvement in many different cellular processes dependent on the CK1-targeted substrates highlights its pleiotropic character [185, 270]. A small selection of *in vitro* and *in vivo* identified CK1 substrates is shown in Table 1.

Table 1: Identified *in vitro* and *in vivo* substrates of CK1. Small selection of CK1-targeted substrates within different functional groups. Table was modified from [185], which is licensed under a Creative Commons Attribution 3.0 unported license (CC BY 3.0), <https://creativecommons.org/licenses/by/3.0/>.

Substrate class	CK1-targeted substrates
DNA-/RNA-related proteins	Non-histone chromatin proteins [73], RNA polymerase I/II [89], topoisomerase II α [141], Star-poly(A) polymerase (Star-PAP) [133], Rec8 [165], DNA methyl-transferase (Dnmt1) [324], TAR DNA-binding protein of 43 kDa (TDP-43) [72], DEAD-box RNA helicase DDX3 [85], ubiquitin-like with PHD and RING finger domains 1 (UHRF1) [65]
Transcription, splice and translation factors	p53 [240], NFAT [386], β -catenin [211], armadillo [374], SMAD 1 to 3 and 5 [346], forkhead box G1 [277], SNAIL [372], tafazzin [213], yes-associated protein [383], initiation factors 4B/4E [145]
Receptors	β -subunit of the insulin receptor [273], tumor necrosis factor (TNF) α receptor [90], platelet derived growth factor (PDGF) [36], low density lipoprotein-related receptor protein 6 (LRP6) [91], type I interferon receptor (IFNAR1) [215], estrogen receptor α (ER α) [126], calmodulin [261], Ror2 [176]
Kinases	CDK5 [306], PKC [255], protein kinase D2 [39], cell division cycle 25 [155]
Microtubule-associated proteins	α - β -tubulin [29], microtubule-associated protein (MAP)1A [366], MAP4 [29], stathmin [29]; reviewed in [287]
Factors of neurodegenerative diseases	Tau [289, 312], amyloid precursor protein (APP) [352], presenilin-2 [351], β -secretase [350] and α -synuclein [256]

1.2.3 Regulation of CK1 activity

Although CK1 isoforms are ubiquitously expressed and described as constitutively active kinases, their expression levels are distinctly dependent on cell and tissue type [220, 336, 338]. Additionally, specific factors seem to influence the expression and activity of CK1 including stimulation with insulin [76] or gastrin [39], changed membrane concentrations of phosphatidylinositol-4,5-bisphosphate [140], the treatment with topoisomerase inhibitors and small molecule inhibitors (SMI) as calotropin [186] or γ -irradiation [297]. Regarding regulation of CK1 on the protein level, several mechanisms such as subcellular localization, structure-related regulation, interaction with certain partners and post-translational modifications (PTM) including autophosphorylation have been characterized [38, 85].

One prominent mode of CK1 regulation is based on the interaction with scaffold and anchoring proteins that control and coordinate the proper positioning of protein complexes. Acting as signalosomes, scaffold proteins bring kinases in close proximity to their protein substrate improving interaction and reaction efficiency through spatial control between partner proteins [134]. Additionally, scaffold proteins have been demonstrated to allosterically control their catalytic binding partners and thereby regulating their activity [27, 134]. Regarding the regulation of CK1, such scaffold proteins might control constitutively active CK1 isoforms in various ways, since scaffold proteins tether CK1 isoforms at specific subcellular localizations to direct CK1 toward or away from their protein substrates and, thus, leading to changes in the phosphorylation rate and CK1 activity [134, 179]. In fact, such scaffold proteins have been shown to exert substantial control over several kinase-mediated signaling pathways including CK1 family members. Examples for scaffold proteins interacting with CK1 include the A-kinase anchoring protein (AKAP)450, which was identified to interact with CK1 δ and CK1 ϵ and, thereby, recruit them to centrosomes [309], and the DEAD-box RNA helicase DDX3, which was shown to act as a scaffolding adaptor directly activating the kinase I κ B [142]. Additionally, DDX3 was shown to exert an allosteric function by interacting with CK1 ϵ in relation to the Wnt (wingless/int-1) signaling pathway promoting the phosphorylation of Disheveled (DVL) [85]. Conversely, CK1 might have a function in the regulation of DDX3, as CK1 isoforms have been demonstrated to phosphorylate DDX3 [85]. Recent studies have highlighted that the Family of sequence similarity 83 (FAM83) interacts and co-localizes with CK1 isoforms including CK1 α , CK1 δ and CK1 ϵ and thereby guiding CK1 isoforms into distinct subcellular compartments to facilitate CK1-dependent signaling [44, 118]. Moreover, in a study designed to screen protein binding partners recruiting CK1 to ubiquitinated lesions associated with neurodegeneration, a structural homolog of dysbindin binding to CK1 γ , δ , and ϵ was discovered. Regarding CK1 δ , dysbindin was shown to act as a dose-dependent inhibitor [377].

Furthermore, CK1 activity can be regulated by PTMs mainly including reversible phosphorylation occurring either through autophosphorylation or site-specific phosphorylation, which is mediated by cellular kinases including Chk1, PKA, PKC isoform α , CDK, Akt and CDC-like kinase 2 [38, 112, 127, 159, 238, 239]. In both

cases, phosphorylation of CK1 leads to inhibitory effects towards its intrinsic catalytic activity. Within the regulatory C-terminal domain of CK1 δ and CK1 ϵ autophosphorylation events can act as pseudo-substrates, which block the catalytic center of the kinase. Phosphorylation events mainly occur within aa sequences with the recognition motif pSer/pThr-X-X-Y (whereas Y denotes any aa except serine or threonine) [50, 54, 128, 137, 282].

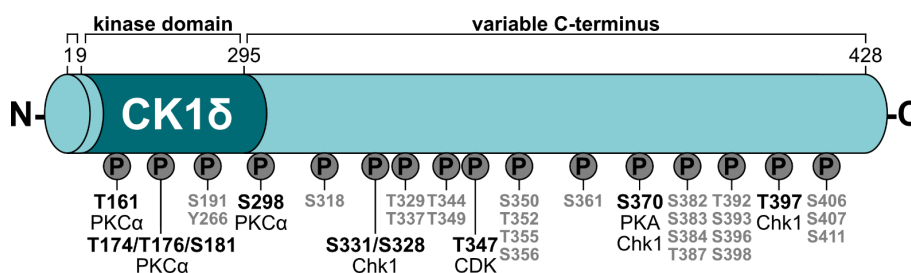


Figure 4: Phosphorylation sites of CK1 δ targeted by cellular kinases. Phosphorylation sites of CK1 δ for cellular kinases in the kinase and the variable C-terminal domain are indicated at their respective position. The figure was generated based on data for CK1 δ phosphorylation collected and provided by PhosphoSitePlus[®] [112, 127, 156, 159, 239]. *CDK*: Cyclin-dependent kinase, *Chk1*: Checkpoint kinase 1, *PKA*: Protein kinase A, *PKC α* : Protein kinase C isoform α .

1.3 Roles of CK1 in biology

Regarding the reported phosphorylation of hundreds of substrates by CK1 isoforms, it is not surprising that the CK1 family is implicated in many biological processes including membrane trafficking, vesicular transport, cytokinesis, ribosome genesis, DNA repair, the circadian rhythm, signaling pathways, apoptosis, MT dynamics and MT-associated processes [184, 187, 380]. The most prominent biological processes involving CK1 include the Wnt signaling pathway, apoptosis and MT-associated processes and will be introduced in the following chapters.

1.3.1 CK1 regulates components of the Wnt signaling pathway

Members of the CK1 family have been implicated in various signaling pathways including the canonical and non-canonical Wnt signaling pathway as well as Hedgehog and Hippo signaling pathway playing an important role in growth, homeostasis and tissue development [164, 219, 259, 384]. Mutated key regulator proteins and aberrant signaling are known to induce various cancer entities [22, 75, 183, 260, 292].

As one of the best known CK1-mediated processes, the Wnt signaling pathway plays an important regulatory role in cellular proliferation, differentiation and polarity

[52, 219, 232, 242, 283]. In short, activation of the Wnt-related receptors through Wnt ligands results in the nuclear translocation of β -catenin leading to the transcription of Wnt signaling-dependent target genes [225]. The absence of Wnt ligands leads to the sequestration of β -catenin by the β -catenin destruction complex involving the SKP1-Cul1-F-Box protein E3 ubiquitin ligase (SCF) substrate receptor β -TrCP, the scaffold proteins adenomatous polyposis coli (APC) and axin as well as the kinases glycogen synthase kinase 3 (GSK3) and CK1 (Figure 5) [319]. Looking inside the complex, CK1 phospho-primers β -catenin at Ser45, which is then sequentially phosphorylated on Thr41, Ser37 and Ser33 by GSK3 [11, 121, 211, 227, 378]. As a consequence the multiple phosphorylated β -catenin is ubiquitinated by the β -TrCP-SCF complex, which primes β -catenin for its degradation via the proteasome [84].

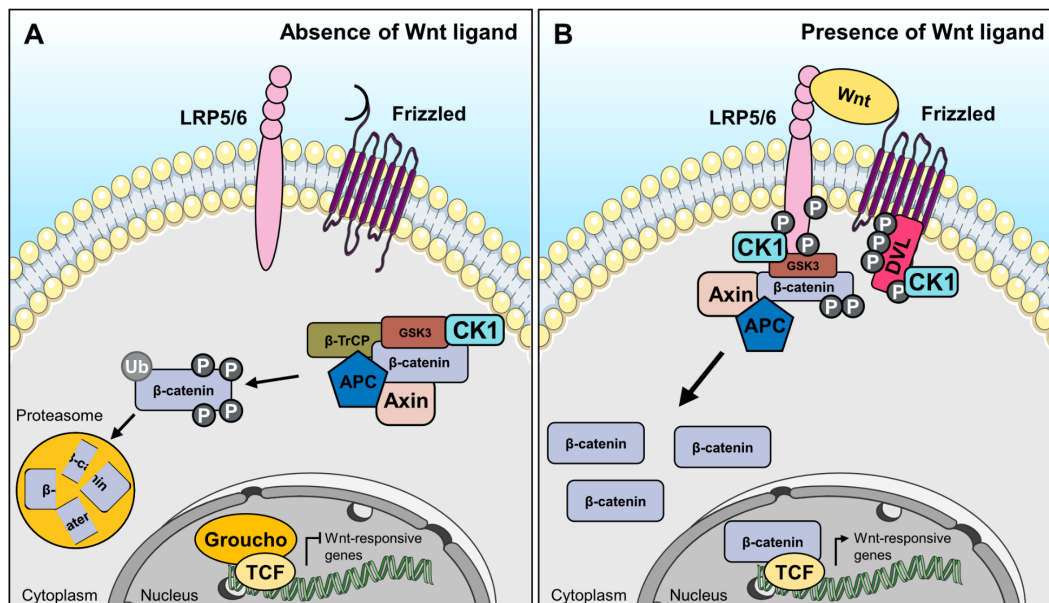


Figure 5: The role of CK1 in the Wnt signaling. (A) In the absence of the Wnt-ligand, β -catenin is hidden within the β -catenin destruction complex including β -TrCP-SCF, APC, axin, GSK3 and CK1 and is subsequently phosphorylated by CK1 and GSK3. Multiple phosphorylation events trigger the β -catenin ubiquitination mediated by β -TrCP-SCF and its proteasomal degradation. Within the nucleus, Groucho binds to TCF and blocks the transcription of Wnt-dependent target genes. (B) Following the presence of Wnt ligands binding to receptors Frizzled and LRP5/6, LRP5/6 becomes phosphorylated and induces the formation of Wnt signalosome mainly composed of DVL and axin. These phosphorylation events recruit the destruction complex to the membrane. Consequently, β -catenin is stabilized and migrates into the nucleus where it removes Groucho from TCF activating the transcription of Wnt-dependent target genes. CK1-mediated phosphorylation of DVL leads to increased affinity between the Wnt receptor complex and DVL promoting the Wnt signaling pathway. Parts of the figure were derived from Servier Medical Art templates, which are licensed under a Creative Commons Attribution 3.0 unported license (CC BY 3.0), <https://creativecommons.org/licenses/by/3.0/> [305]. Figure was modified from [185], which is licensed under a Creative Commons Attribution 3.0 unported license (CC BY 3.0), <https://creativecommons.org/licenses/by/3.0/>. APC: Adenomatous polyposis coli, DVL: Disheveled, GSK3: Glycogen synthase kinase 3, LRP: Lipoprotein-related receptor protein, TCF: T-cell factor.

When Wnt ligands are present, axin is excluded from the β -catenin destruction complex and phosphorylated β -catenin accumulates and saturates the destruction complex. Consequently, the newly translated β -catenin migrates to the nucleus, where it removes Groucho from T-cell factor (TCF) and initiates the transcription of Wnt-dependent target genes [84, 319, 332]. Although the Wnt signaling pathway is very well characterized, the exact distribution of roles within CK1 isoforms has not been solved in detail. However, several studies emphasized that all CK1 isoforms are involved and regulate the Wnt signaling pathway either positively or negatively [270]. In this context, CK1 ϵ was shown to phosphorylate the Wnt receptor-associated protein DVL, which is supposed to increase the affinity between the Wnt receptor complex and DVL and thereby promoting the Wnt signaling [49, 66, 96, 150]. In contrast to that positive regulatory function, CK1 has shown an inhibitory function within the destruction complex, which inactivates the Wnt signaling process.

1.3.2 CK1-associated functions in apoptotic processes

Programmed cell death, or also known as apoptosis, describes an important and controlled mechanism that clears abnormal or damaged cells within an organism. Proteins that are related to apoptosis and therefore called death receptors that includes Fas and tumor necrosis factor (TNF) receptor 1, are involved in the transduction of extrinsic apoptotic signals leading to the generation of the intracellular death-inducing signaling complex (DISC). Consequently, DISC recruits caspases in order to promote the apoptotic signal [111].

The involvement of CK1 family members in various apoptotic pathways has been shown by many studies. For example, CK1 isoforms were identified to phosphorylate the pro-apoptotic protein Bid at Ser64 and Ser66. Unphosphorylated Bid, which belongs to the family of Bcl-2, has been shown to be processed by caspase 8-mediated proteolysis and to be involved in cytochrome c-mediated apoptotic mechanisms. Accordingly, the inhibition of CK1-mediated phosphorylation of Bid was associated with accelerated Fas-induced apoptosis, whereas the overexpression of CK1 reduced the number of apoptotic cells as a result of increased phosphorylation of Bid, thereby preventing its caspase 8-mediated processing [99]. Moreover, members of the CK1 family were identified to

phosphorylate the TNF receptor p75, and thereby, regulate p75-mediated apoptosis negatively [31]. Additionally, silencing via RNAi of *CSNK1A1* encoding for CK1 α or pharmacological inhibition of CK1 was shown to sensitize tumor cells to TNF-related apoptosis-inducing ligand (TRAIL)-mediated apoptosis [166]. Furthermore, CK1 α has been reported to phosphorylate Fas-associated protein with death domain (FADD) at aa residue Ser194 *in vitro* and *in vivo*. As a consequence, CK1 α is assumed to be involved in the regulation of non-apoptotic functions mediated by FADD including nuclear localization of FADD, cell cycle interaction and increased sensitivity towards chemotherapeutics [6, 7].

1.3.3 CK1 controls MT-associated processes

CK1 isoforms are involved in important regulatory functions including genomic stability, cell cycle progression, MT dynamics, mitosis and meiosis [28, 29, 56, 138, 139, 172, 263, 264, 269, 294, 309, 322]. Unfortunately, the precise contribution of each CK1 isoform to specific roles in the regulation of the cell cycle is poorly understood. Nevertheless, CK1 δ was supposed to be associated with MTs, centrosomes and the kinetochore during mitosis pointing towards a regulatory checkpoint function within the cell cycle. The importance of CK1 isoforms is further highlighted by the fact that CK1 δ and CK1 ϵ are guided to the centrosome via the interaction of the scaffold protein AKAP450 enabling CK1 to phosphorylate the MT plus-end-binding protein 1, which is known as a relevant factor for centrosome positioning within T-cell activation [309, 388]. Besides CK1 δ and CK1 ϵ , also CK1 α is involved in mitosis and spindle positioning, which was confirmed by the observation that the injection of CK1 α -specific morpholinos induced mitotic arrest and caused defects of chromosomal misalignments observed in mouse oocytes [354]. Additionally, immunostaining approaches revealed CK1 α on mitotic spindles [46].

In addition to direct CK1-MT interaction, regulation of MT-associated processes including MT stability, polymerization and spindle dynamics are attributed to CK1-mediated phosphorylation of microtubule-associated proteins (MAP) [106]. So far, several MAPs including MAP1A, MAP2 and MAP4 as well as the MT-attached proteins stathmin and tubulin-associated protein (tau) were identified to be phosphorylated by CK1 [29, 197, 289, 312, 366]. Additionally, CK1 δ was shown to

directly modulate MT by the phosphorylation of its subunits α -, β - and γ -tubulin and thereby inducing stress-related functions at the centrosome and spindle apparatus [28, 29].

CK1 isoforms are not only involved in regulating cell cycle progression, but also have a function in the interaction between MTs and membranes as well as transport process along MTs. Regarding transport processes, CK1 ϵ regulates dynein-dependent transport process by phosphorylating the dynein intermediate chain component IC138 and thereby, activates the transport of membrane organelles [161, 375].

1.4 Contribution of CK1 to the development of human diseases

CK1 isoforms are involved in the phosphorylation and regulation of various key regulators within signaling pathways. Consequently, dysfunction or deregulation of CK1 isoforms regulating signaling pathways might lead to deregulated signal transduction, which is linked to the development of human diseases including various cancer entities and neurodegeneration.

Cancer-related functions of CK1 are closely associated with the role of CK1 in the beforementioned signaling pathways. Additionally, its oncogenic potential was demonstrated by the findings that CK1 modulate key regulatory proteins such as mouse double minute 2 homolog (MDM2), p53 and β -catenin, which are crucial regulators in tumor progression [184, 299]. So far, several mutations within *CSNK1D*, which encodes for CK1 δ , have been revealed and observed in different cancer entities (reviewed in [287]). Although the mutation rate of *CSNK1D* was observed very low, a TCGA database analysis obtained from different tumor cell lines and tissues indicated highest frequency of genomic amplification of *CSNK1D* in lung and bladder/urinary tract cancer [42, 209]. Additionally, changes in the expression levels of *CSNK1D* due to genomic alterations contribute to tumorigenesis and tumor progression of colorectal cancer [358], breast carcinoma [308], ductal pancreatic carcinomas [47] and blood cancer [168, 177]. The oncogenic potential of CK1 isoforms is exhibited by inhibiting apoptotic processes and promoting proliferation as well as genome instability caused by increased kinase activity due to mutations in *CSNK1D* and, in particular, CK1 δ overexpression in tumors [185].

Recently, it was described that most CK1 isoforms are expressed in the cortex and striatum of the brain, the latter being involved in motivation- and movement-related behaviors. Additionally, CK1 was shown to regulate glutamatergic synaptic transmission, which is mediated by N-methyl-D-aspartate receptors that have a central role in several pathological and physiological processes in the striatum and the central nervous system (CNS). Given the involvement in the regulation of synaptic transmission, CK1 might be seen as an important regulatory kinase in motivation- and movement-related behaviors [67]. However, altered activity and overexpression of CK1 in physiological processes have been linked to hyperphosphorylation of key proteins, which are involved in the development of neurodegenerative diseases, such as Alzheimer's disease (AD), Parkinson's disease (PD) and amyotrophic lateral sclerosis (ALS).

PD is a progressive bradykinetic disorder, which is characterized by the severe loss of pars compacta nigral cells and the accumulation of α -synuclein in specific brain stem and cortical regions and in the spinal cord. Most susceptible genes for the development of PD include glucocerebrosidase, leucine rich repeat kinase 2 and α -synuclein [265]. The protein α -synuclein was identified to be the major component of Lewy bodies, which represent one of the major hallmarks of PD [170]. Phosphorylation and dephosphorylation events were shown to regulate functions of the α -synuclein. It has been demonstrated that α -synuclein is constitutively phosphorylated at aa residue Ser129 by CK1 implicating a key role for CK1 in PD [256]. Furthermore, it is widely known that mutations in the parkin gene might have an important role in the pathogenesis of sporadic PD. Although its contribution to PD remains largely unknown, parkin might have neuroprotective functions, which can be affected by changes in its solubility. Recent studies have demonstrated that phosphorylation of parkin mediated by CDK5 and CK1 decrease parkin solubility resulting in its aggregation and inactivation [198].

The TAR DNA-binding protein of 43 kDa (TDP-43) was characterized as a major disease-associated constituent in frontotemporal lobar degeneration and in ALS [14]. Hyperphosphorylated cytoplasmic TDP-43 and its intranuclear inclusions were identified in brains derived from patients suffering from these neurodegenerative diseases. Among the TDP-43 phosphorylation sites, 29 residues were phosphorylated by CK1 *in vitro* [174].

During recent years, many studies highlighted the contribution of CK1 to the development of neurodegenerative diseases, especially in tauopathies like AD, which will be introduced in the following chapter.

1.5 The role of CK1 in Alzheimer's disease

AD is a multifactorial neurodegenerative disease first described in 1906 by the pathologist Alois Alzheimer. Classical symptoms include progressive memory loss as well as decline in other cognitive functions including disorientation, speech abnormalities, apraxia, hallucinations, etc. Patients who are affected by AD suffer personality changes (like emotional and behavioral disturbances), and the ability to perform personal and social activities decreases. As the disease progresses, patients become totally dependent, and typically other diseases can be fatal, such as pneumonia in particular, which is the leading cause of death in AD [194].

Although most of the AD cases are sporadic (SAD), rare, familial, early-onset and autosomal dominant forms of AD (FAD) have been characterized. Mutations or polymorphisms in genes, which are related to the development of FAD, encode for the amyloid precursor protein (APP), presenilin (PSEN)1 and PSEN2 [359]. To date, more than 25 mutations in the APP gene have been identified, some of them enhancing production of amyloid- β (A β) peptides and/or favor amyloid plaque formation such as the Swedish (K670N/M671L) [245] or London mutation (V717I) [130]. Remarkably, most of the mutations are localized in the region flanking the A β domain. Duplication of the APP gene may contribute to the early-onset of AD, which explains why individuals with trisomy of chromosome 21, where the APP gene is located, have an increased risk for the development of AD [152]. Missense mutations in APP are responsible for less than 0.1 % of all AD cases, while missense mutations in PSEN1 or PSEN2 genes are attributed to early-onset AD affecting people between 40 and 60 years of age and for aggressive forms of AD. Of note, mutations within these two genes might be responsible for the shift of substrate specificity of PSEN1 and PSEN1 from Notch to APP promoting A β production [195]. For SAD, the most prominent genetic risk factor is the presence of the apolipoprotein E (APOE)4, while its close relative APOE2 may provide protection against AD [80, 363]. Non-genetic risk factors, which have been

associated with higher risk of developing AD include aging, cerebrovascular diseases, hypertension, type 2 diabetes, obesity and dyslipidemia [310].

Amyloid plaques and intracellular neurofibrillary tangles (NFT) are widely accepted and have been extensively described as hallmarks of AD. These lesions were found in specific regions of the brain, which are associated with learning and memory processes including the hippocampus, neocortex and the entorhinal cortex. The presence and distribution of amyloid plaques, NFTs and synaptic degeneration correlate with the course and degree of cognitive decline [92, 144]. Remarkably, both histopathological hallmarks, amyloid plaques and NFTs, are related to phosphorylation events. More precisely, amyloid plaques are composed of A β peptides, whose production is modulated by the phosphorylation of APP mediated by kinases, whereas NFTs are a result of hyperphosphorylation events of tau [88, 120, 274, 275].

A potential role of CK1 in the development of AD was considered when it was shown that CK1 δ expression was increased by a factor of 30 in the hippocampal region of brains derived from AD patients compared with corresponding controls [125]. Subsequent experiments confirmed the upregulation of CK1 δ mRNA in brains of AD patients, which correlated with the degree of regional pathology, whereas no upregulation of CK1 δ was detected in peripheral organs [376]. These observations gave rise to further investigations regarding the role of CK1 in AD, in particular its role in the tau hyperphosphorylation and the phosphorylation of APP.

1.5.1 CK1 phosphorylates the tau protein

NFTs consists of aggregated abnormal paired helical filaments (PHF), which are composed of hyperphosphorylated tau proteins. The tau protein is a MT-associated protein, essential in MT dynamics, axonal transport and neurite outgrowth and regulated by phosphorylation. In the human adult CNS, six different tau isoforms are expressed, which are derived from alternative splicing of exon 2, 3 and 10 located on the *MAPT* gene, which vary in the number of N-terminal inserts (N) and C-terminal repeat domains (R) [131]. The longest tau isoform with two N and four R (2N4R) is the largest human tau with a total of 441 aa in length (tau441) (Figure 6). Since tau441 carries both the R2 and both N-terminal inserts and thus promotes the

binding of tau to tubulin, it proved to be the most effective tau for enhancing MT assembly [94, 95].

In its abnormally hyperphosphorylated state, tau detaches from the MT network leading to MT destabilization associated with neuronal cell toxicity [24]. In addition, hyperphosphorylated tau proteins have the ability to aggregate into small deposits (pre-tangles) that build β -sheet conformations in PHFs. As a result, these small aggregates assemble into large NFTs, whereby tau proteins undergo structural modifications including glycosylations, truncations and cross-linking [167, 228]. Therefore, alterations in signaling cascades leading to abnormal protein aggregation can potentiate formation of NFTs and neurodegeneration. Tau carries a huge number of potential phosphorylation sites including serine, threonine and tyrosine residues [19, 135]. For tau441, more than 80 potential phosphorylation sites have been described [18], which are likely targeted by several kinases such as GSK3 [147], MAPK [107], TTBK [331], CDK [147], MT-affinity regulating kinase [108], CAMK [254], PKA [147], PKC [43] and CK1 [147]. Phosphorylation events within the MT-binding domain decrease the binding affinity of tau to MTs [34]. Given that a variety of kinases is involved in tau hyperphosphorylation, tau might be primed by a specific kinase before subsequent phosphorylation mediated by another kinase [147]. So far, sequential phosphorylation events have been shown to be relevant in modulating protein functions [77].

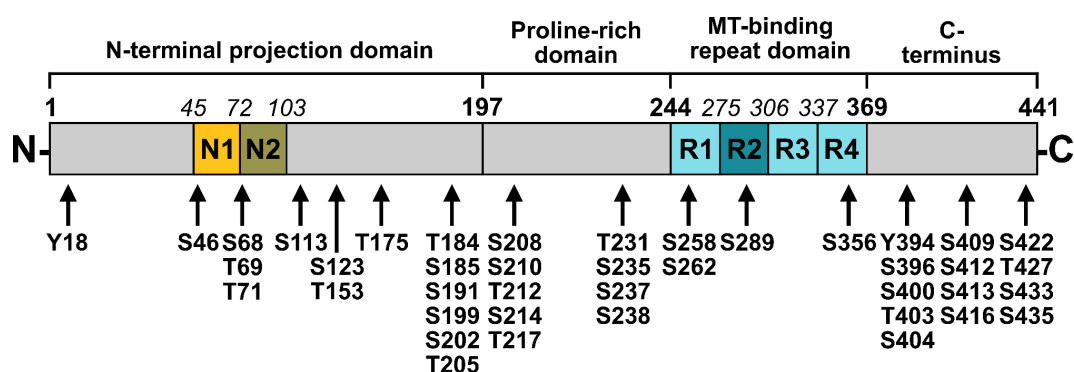


Figure 6: Schematic overview of tau441 domains and its potential AD-associated phosphorylation sites. Major tau441 domains include the N-terminal projection domain with N-terminal inserts (N1 and N2), proline-rich domain, MT-repeat binding domain with C-terminal repeat domains (R1 to R4) and the C-terminus. Figure was modified from [311], which is licensed under a Creative Commons Attribution 4.0 international license (CC BY 4.0), <https://creativecommons.org/licenses/by/4.0/>. MT: Microtubule, N: N-terminal insert, R: C-terminal repeat domain.

MT fractions are often used to determine, which of the MT- and tau-associated kinases most readily affects the phosphorylation of tau at AD-associated

phosphorylation sites demonstrating that CK1 belongs to this group of kinases [114]. Additionally, the overexpression of CK1 ϵ led to increased tau phosphorylation in mouse hippocampus resulting in an impaired spontaneous alternation behavior [63]. In addition to CK1 ϵ , the CK1 isoforms α and δ have been shown to be closely associated with neurofibrillary lesions in AD providing further evidence that CK1 is involved in PHF formation [197, 302]. Moreover, CK1 δ -specific phosphorylation was detected at tau residues Ser202/Thr205 as well as Ser396/Ser404 in lysates of human embryonic kidney 293 (HEK293) cells treated with IC261 by using immunodetection via phospho-specific antibodies [207]. Both CK1-specific sites, which were identified in this study, are involved in the tau-tubulin interaction emphasizing an important role of CK1 in tau aggregation [207]. In a more comprehensive study, mass spectrometry (MS) analysis revealed 33 sites of an *in vitro* phosphorylated recombinantly expressed tau protein specifically targeted by CK1 δ . However, the phosphorylation of tau residues mentioned before (Ser202/Thr205 and Ser396/Ser404) could not be verified in this study [149]. However, CK1 δ and GSK3 accounted for at least 15 phosphorylation sites phosphorylated in PHF-tau in AD. A combination of both kinase activities could lead to the phosphorylation of more than three-quarters of the serine/threonine phosphorylation sites, which were identified in PHF-tau, showing that CK1 δ might be involved, together with GSK3, in the pathogenesis of AD [265].

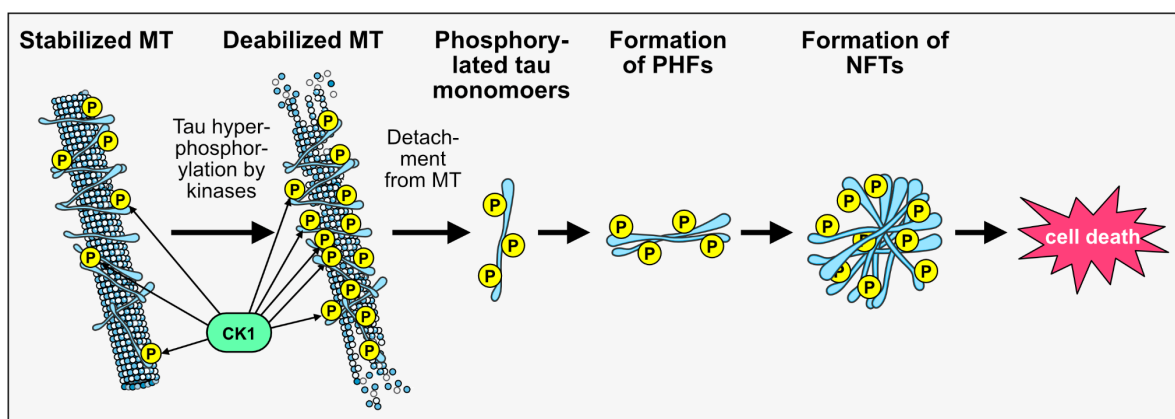


Figure 7: The role of CK1 in tau hyperphosphorylation. Tau, which was phosphorylated by various kinases including CK1 detaches from the MT leading to its destabilization. Phosphorylated tau monomers form paired helical filaments (PHFs), which aggregate ultimately into NFTs leading to neuronal cell death. Parts of the figure were derived from Servier Medical Art templates, which are licensed under a Creative Commons Attribution 3.0 unported license (CC BY 3.0), <https://creativecommons.org/licenses/by/3.0/> [114]. MT: Microtubule, NFT: Neurofibrillary tangles, PHF: Paired helical filaments.

1.5.2 CK1 is involved in the APP metabolism

APP is an ubiquitously expressed transmembrane protein, which exists in different isoforms resulting from alternative splicing of exons 7, 8 and 15 of the APP mRNA. The APP isoform with 695 aa (APP695) is the predominant form in neuronal cells and is composed of several domains including the E1 domain, acidic domain (AcD), E2 domain, juxtamembrane region (JMR), membrane located A β domain and the APP intracellular domain (AICD) (Figure 8)

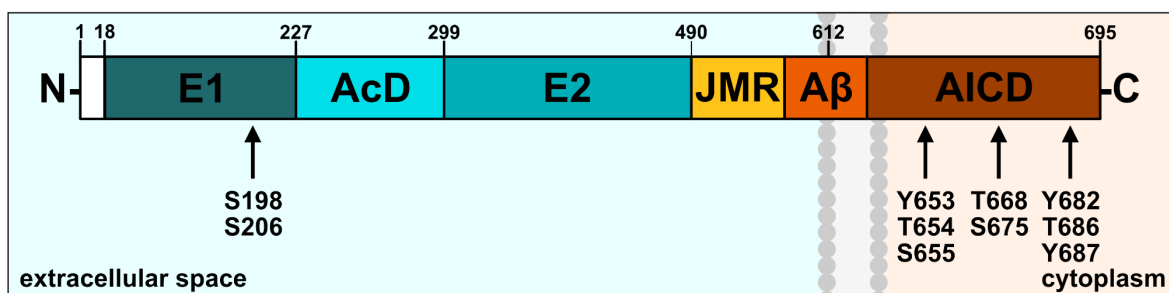


Figure 8: Schematic overview of APP695 domains and its potential phosphorylation sites. Major APP695 domains include the signal peptide (SP), E1 domain (E1), acidic domain (AcD), E2-domain, juxtamembrane region (JMR), A β and the APP intracellular domain (AICD). Parts of the figure were derived from Servier Medical Art templates, which are licensed under a Creative Commons Attribution 3.0 unported license (CC BY 3.0), <https://creativecommons.org/licenses/by/3.0/> [305]. Figure is based on [257]. *AcD*: Acidic domain, *AICD*: APP intracellular domain, *JMR*: Juxtamembrane domain.

APP can be processed by two different pathways, the non-amyloidogenic or amyloidogenic pathway. According to the non-amyloidogenic pathway, APP is cleaved by α -secretase within the membrane-located A β domain (Figure 9). The cleavage mediated by α -secretase results in the release of nearly the entire ectodomain (sAPP α) and production of a membrane bound α -C-terminal fragment (C83), which is subsequently cleaved by the γ -secretase complex into a non-toxic p3 peptide and the AICD. The non-amyloidogenic α -secretase-mediated pathway is the major and ubiquitous pathway of APP processing in most cells, which is regulated by various neurotransmitters, hormones, growth factors and PKC [210]. In the amyloidogenic pathway, which is enriched in neurons, APP is initially cleaved by β -secretase releasing sAPP β and β -C-terminal fragment (C99), which is directly cleaved by γ -secretase complex into A β peptide and AICD. Additionally, β -secretase is capable of cleaving APP β within the A β domain and thus generating a truncated A β species [382]. The β -secretases β -site APP cleaving enzyme (BACE)1 and BACE2 are able to cleave the APP β -sites and were associated with A β formation [341].

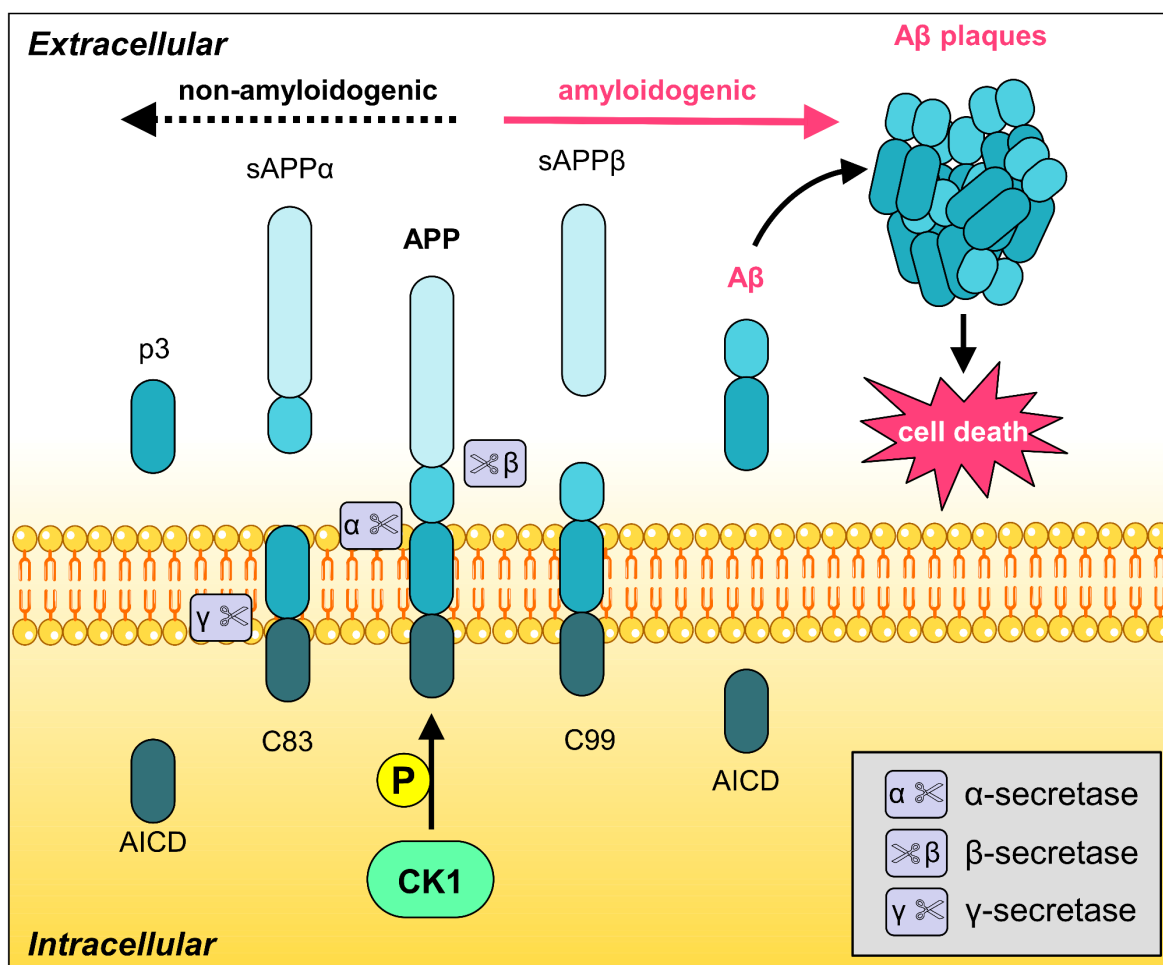


Figure 9: The potential role of CK1 in APP processing. Proteolytic processing of APP within the non-amyloidogenic and amyloidogenic pathway. In the non-amyloidogenic pathway APP is cleaved by α - and γ -secretase into soluble and non-toxic sAPP α , p3 and AICD. In the amyloidogenic pathway APP is cleaved by α - and β -secretase into sAPP β , AICD and the insoluble and toxic A β peptide. A β peptides form amyloid plaques, which lead to neuronal cell death. Phosphorylation by CK1 might lead to promotion of the amyloidogenic conversion. Parts of the figure were derived from Servier Medical Art templates, which is licensed under a Creative Commons attribution 3.0 unported license (CC BY 3.0), <https://creativecommons.org/licenses/by/3.0/> [305]. The figure is based on [132]. AICD: APP intracellular domain, APP: Amyloid precursor protein, C83: α -C-terminal fragment, C99: β -C-terminal fragment.

APP can be phosphorylated at several sites in both intra- and extracellular domains, especially at serine, threonine and tyrosine residues by various kinases including PKC [53, 129], CDK [160], CDC2 [327], GSK3 [13] and CK1 [352] (Figure 8). *In silico* analyses showed that APP contain multiple CK1 consensus sequences [115], which was confirmed by the findings that CK1 phosphorylates the soluble APP β *in vitro*. Additionally, a CK1-like ectoprotein kinase was identified to phosphorylate membrane-located and secreted forms of soluble APP β , which was discovered by using a set of selective kinase inhibitors [352]. These observations were supported by the findings that soluble APP β ectodomain is targeted by CK1 at residue Ser198

and Ser206 during secretory cleavage [349]. Unfortunately, the physiological relevance of APP phosphorylation is not clearly understood. However, several studies described a correlation between phosphorylation at specific sites and sAPP β fate [23, 275, 344].

1.5.3 CK1 and its role in the “cascade hypothesis”

As described, amyloid plaques are extracellular proteinaceous deposits found in brains derived from AD patients, which are mainly composed of A β peptide aggregates. Although A β peptides can be found in healthy individuals, amyloid plaques are observed in individuals with mild cognitive symptoms at higher levels than in healthy individuals of higher age [151], which shows that amyloid plaques are a strong predictive factor for AD. Additionally, the formation of amyloid plaques strongly correlates with clinical symptoms. Several studies defend the amyloid cascade hypothesis, which states that A β accumulation in the CNS is the first event initiating the pathogenic cascade resulting in neurodegeneration and neuronal death [119]. In the most widely accepted amyloid cascade hypothesis three main aspects are stated including the central role of A β depositions in disease process, A β depositions as an early event and mutations in APP β and other proteins that contribute to FAD and SAD. According to this hypothesis, several factors such as age, genetics and environmental factors lead to an imbalance in A β formation and clearance and key players such as γ -secretase enhance A β production, which are regulated by phosphorylation [180, 196, 257]. However, the amyloid cascade hypothesis has no reasons for all histopathological hallmarks, which are associated with AD, such as NFTs, although some results demonstrated that A β itself can influence NFT formation [253, 328]. In order to provide an explanation for the onset of this multifactorial disease and all AD-associated hallmarks, several hypotheses have been put forward for instance the dual pathway hypothesis, mitochondrial cascade hypothesis, metabolism cascade hypothesis, inflammatory cascade hypothesis and the cell cycle re-entry hypothesis (Figure 10). Regarding the dual pathway hypothesis, it was proposed that upstream factors could trigger A β and tau-mediated pathology. According to this hypothesis, downstream treatment targeting A β and tau pathology will be of therapeutic advantage. In this hypothesis, protein phosphorylation is a key event in amyloid plaque and NFT formation, although decrease in A β clearance could play a role [313].

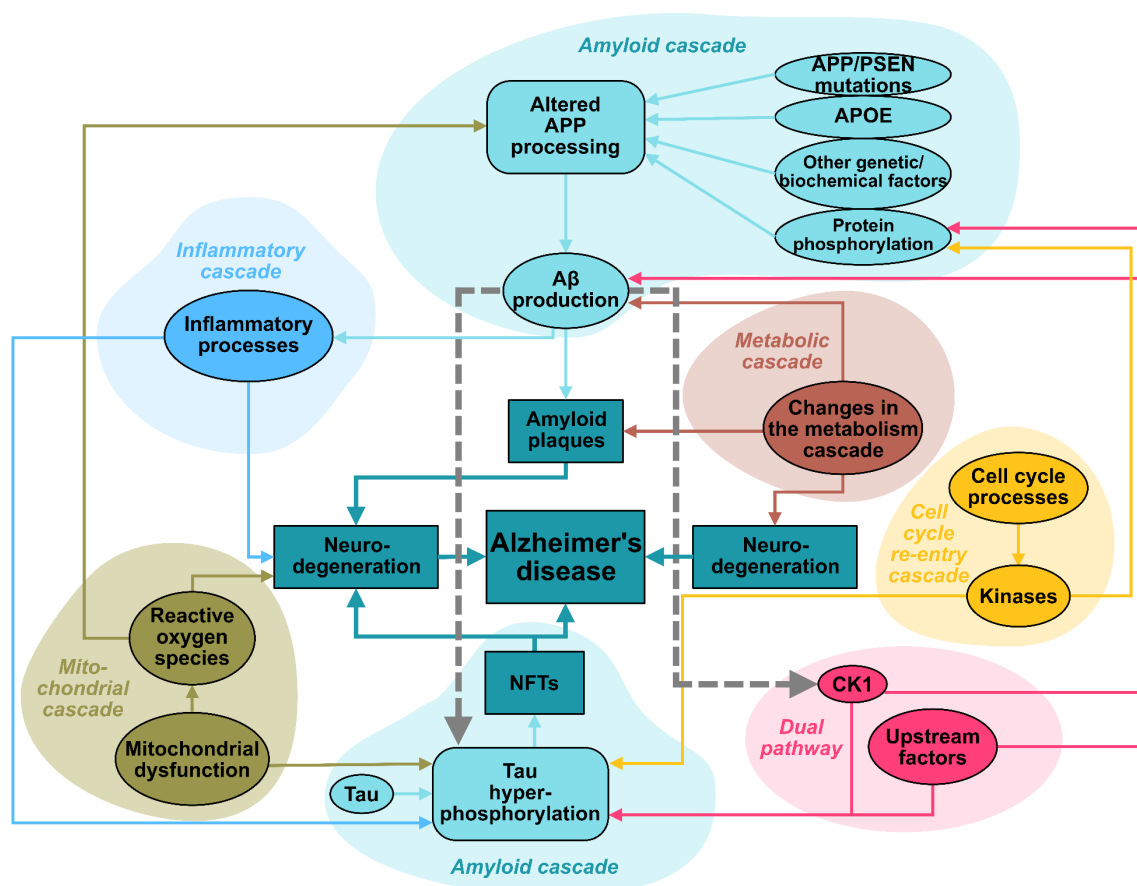


Figure 10: The potential role of CK1 in the development of AD. Overview of the most discussed cascade hypotheses for the development of AD pathology. The amyloid cascade starts with the proteolytic and amyloidogenic cleavage of APP into toxic A β peptides, which form oligomers and aggregates resulting in amyloid plaques and neuronal death. In addition, increased A β production leads to tau hyperphosphorylation and CK1 activation. Alternative pathological mechanisms, which are influenced by A β production or promote A β production, amyloid plaque formation, tau hyperphosphorylation or neuronal cell death include the inflammatory cascade (involving inflammatory processes), metabolic cascade, mitochondrial cascade (involving mitochondrial dysfunction and reactive oxygen species), cell cycle re-entry cascade (involving cell cycle processes and kinases) and the dual pathway (involving upstream factors, such as CK1, which trigger A β and tau pathology). The figure is based on [257]. APOE: Apolipoprotein E, APP: Amyloid precursor protein, NFT: Neurofibrillary tangle, PSEN: Presenilin.

During recent years, several studies have demonstrated the role of CK1 in the development of AD, especially in the amyloid cascade and dual pathway hypothesis. For example, overexpression of constitutively active CK1 ϵ was associated with an increase in A β peptide production. Additionally, endogenous A β production could be reduced by using three structurally dissimilar CK1-specific compounds, demonstrating that CK1-specific compounds act during γ -secretase cleavage, whereas Notch cleavage is not affected [115]. Moreover, A β peptides were identified to stimulate CK1 kinase activities, which contributes to abnormal protein phosphorylation associated with AD [58]. The administration of a BBB permeable CK1-specific inhibitor (PF-670462) in 3xTg-AD mice (displaying memory

impairments and circadian abnormalities similar to symptoms occurring in patients with AD) rescued hippocampal proteomic changes in several AD-associated pathways and resulted in normalized working memory and behavioral circadian rhythms [4].

1.6 Protein kinases as targets in therapy

PKs are key regulators in the majority of cellular signaling pathways, which are frequently connected to the development of diseases, and therefore used as therapeutic intervention points. The first kinase inhibitor, imatinib, targeting a TK for the treatment of chronic myelogenous leukemia, was approved by the U.S. Food and Drug Administration in 2001. Since then, many kinase inhibitors (most of them against TK) have been developed for therapies including SMIs, kinase-specific antibodies and antibody conjugates. Among them, most kinase inhibitors have been approved as anti-cancer therapeutics. Generally, kinase inhibitors are categorized into seven types according to their mode of target binding and mechanisms of action (Table 2).

Type I kinase inhibitors bind to the catalytic site of the kinase in its active conformation, with the DFG motif (Asp-Phe-Gly) of the activation loop pointing inside the ATP binding pocket and changing the structural conformation, thereby inhibiting the phosphotransfer [217]. Contrarily, a type II kinase inhibitor binds reversibly to the kinase in its inactive conformation, whereby the DFG conformation is changed and is directed away from the ATP binding pocket leading to the generation of single or multiple hydrogen bonds within the hinge [217].

Table 2: Different types of PK inhibitors. Figure was modified from [222], which is licensed under a Creative Commons Attribution 4.0 international license (CC BY 4.0), <https://creativecommons.org/licenses/by/4.0/>.

Type of PK inhibitor	Binding type	Binding site
I	Reversible	Active site (ATP binding pocket)
II	Reversible	Inactive site (ATP binding pocket, DFG pocket)
III	Reversible	Allosteric (within ATP binding pocket)
IV	Reversible	Allosteric (substrate binding domain)
V	Reversible	Allosteric (bivalent)
VI	Irreversible	Allosteric (covalent)
VII	Irreversible	Allosteric (extracellular)

ATP: Adenosine triphosphate, DFG: Asp-Phe-Gly motif.

Type III to VII inhibitors are classified as allosteric inhibitors. Type III inhibitors belong to the class of steady-state non-competitive/uncompetitive inhibitors with regard to the phosphate donor and bind within the small and large lobes of the ATP binding pocket. In contrast to type III inhibitors, type IV inhibitors bind remotely from the catalytic ATP binding pocket at the substrate binding site [124]. Type V inhibitors belong to the group of bivalent inhibitors binding irreversibly to active kinase sites and peptide motifs, which represent the protein substrate targeted by the kinase [199]. Due to its binding to the ATP binding pocket and the unique and specific structural feature of the kinase, bivalent kinase inhibitors are generally highly potent and selective [173]. Type VI inhibitors bind irreversibly to their kinase target via the covalent binding of the reactive electrophilic inhibitor groups with nucleophilic cysteine residues of the kinase [285]. Type VII inhibitors are non-classical allosteric inhibitors targeting the extracellular domain of receptor TKs [153].

During the last decades, several different strategies to treat human diseases, such as cancer, neurodegeneration or autoimmune diseases, were developed including kinase inhibitors, which were chemically synthesized or derived from natural compounds. To date, the U.S. Food and Drug Administration approved several SMIs, which target more than 20 types of PKs including members of the CK1 family [205].

1.7 CK1-specific inhibitors and their therapeutic potential

Pharmacological inhibition of CK1 has been explored as potential therapeutic strategy targeting several cancer types [299], neurodegenerative diseases [83], obesity [86], behavioral disorders [15] and opioid and alcohol addiction [267, 347]. So far, several highly selective and potent CK1-specific SMIs have been identified and some of them have already proven their therapeutic potential in animal models or clinical trials (Table 3). Most of the identified CK1-specific inhibitors belong to the class of ATP-competitive type I kinase inhibitors. Due to the use of different ATP concentrations, which are essential for the comparison of the half maximal inhibitory concentration (IC_{50}) between kinase inhibitors, the effectiveness of inhibitors is difficult to classify and compare.

CKI7, an isoquinoline-based derivative, was the first ATP binding inhibitor being identified to show potency and selectivity towards CK1 [370]. Later, IC261, an

indolinone-based derivative, has been proven as dual CK1 δ and CK1 ϵ -specific inhibitor through high-throughput screenings [229]. Two very potent compounds, PF-670462 and PF-4800567, which were developed by Pfizer Global Research and Development, were identified as highly potent and selective inhibitors for CK1 δ and CK1 ϵ , whereas PF-4800567 exhibits 22-fold stronger inhibition towards CK1 ϵ than CK1 δ [353]. Furthermore, the treatment of PF-670462 proved to be beneficial in the therapy of perturbed circadian behavior [237], bipolar disorders [15] and addictive behavior [267]. Compounds Peifer-1 and Peifer-2 are isoxazole-based derivatives, whereas Peifer-1 exerted dual inhibition towards p38 α and CK1 δ . However, Peifer-1 and the further developed Peifer-2 have low chemical stability, which negatively influences the usage *in vitro* and *in vivo* [262]. Additionally, the class of benzimidazole-based CK1-specific compounds have been characterized by several studies such as SR-3029, Bischof-5 and Bischof-6 [32, 37]. Especially SR-3029 was reported to exhibit high potency against CK1 δ and CK1 ϵ . In this context, the class of inhibitors of the Wnt production (IWP) were shown to have inhibitory effects on CK1 δ , which was explained by structural similarities to benzimidazole-based CK1-specific inhibitors [122]. The class of triazolo[1,5-c]quinazolines was initially identified to amplify signaling outputs in a bone morphogenetic protein (BMP) signaling-dependent manner without the alteration of closely related developmental pathways. Among this set, especially compound Wesseler-1a was characterized as an *in vitro* and *in vivo* active and osteogenic BMP signaling boosting dual-specific inhibitor inhibiting CK1 δ and ϵ as well as phosphoinositide-3-kinase (PI3K) α and γ [362]. Recently, within a series of very potent CK1-specific compounds based on a 1H-pyrrolo[2,3-b]pyridine-imidazole scaffold, the first very potent and highly CK1 α isoform selective compound, MU1742, was identified [247].

Furthermore, the list of CK1-specific inhibitors shown in Table 3 contains one compound (BTX-A51), which is currently undergoing the clinical trial phase I, and one inhibitor (umbralisib) that has already been approved. Regarding BTX-A51, a set of compounds was initially tested in preclinical studies showing high potency against CK1 α , induction of p53 and upregulation of β -catenin, which led to apoptosis of leukemia progenitor cells *in vitro* and further confirmed by animal experiments. BTX-A51 was also shown to inhibit CDK7 and CDK9 and other members of the CK1 family including CK1 δ , CK1 γ and CK1 ϵ [241]. Nevertheless, BTX-A51 has

successfully entered clinical trials phase I with focus on refractory acute myeloid leukemia and non-Hodgkin lymphoma [303]. Umbralisib was approved for the treatment of lymphoma and targets PI3K δ [97]. At higher concentrations, it was identified to act as CK1 ϵ inhibitor. Despite the relatively low potency towards CK1 ϵ , clinical results from umbralisib treatment showed that the inhibition of CK1 ϵ was well tolerated and had a beneficial therapeutic effect in lymphoma [60, 101].

Table 3: Potent CK1-specific inhibitors.

Inhibitor	Molecular/therapeutic effect	Target	Investigation phase	Ref.
CKI7	Inhibition of CK1	CK1	Preclinical	[68, 278]
IC261	Binding to tubulin leading to direct inhibition of MT polymerization	CK1, tubulin	Preclinical	[229, 278]
PF-670462	Selective inhibition of CK1 δ and CK1 ϵ	CK1 δ , CK1 ϵ	Preclinical	[353]
PF-4800567	Selective inhibition of CK1 ϵ	CK1 ϵ	Preclinical	[353]
Peifer-1/ Peifer-2	Dual inhibition of p38 α MAPK1 and CK1 δ , low chemical stability	p38 α , CK1 δ	Preclinical	[262]
SR-3029	Inhibition of overexpressed CK1 δ and CK1 ϵ	CK1 δ , CK1 ϵ	Preclinical	[32]
Bischof-5/ Bischof-6	Selective inhibition of CK1 δ /CK1 ϵ , inhibitory effects against proliferation of tumor cell lines	CK1 δ , CK1 ϵ	Preclinical	[37]
IWP-2/ IWP-4	Selective inhibition of CK1 δ , inhibited proliferation of cancer cell lines	CK1 δ	Preclinical	[122]
Wesseler-1a	Amplification of the BMP signaling by combined inhibition of PI3K and CK1 isoforms	CK1 δ / ϵ , PI3K α / γ	Preclinical	[362]
MU1742	Potent and highly selective inhibitor of CK1 α	CK1 α	Preclinical	[247]
BTX-A51	Inhibition of CK1 α , activation of p53-dependent cell death and inhibition of CDK7/CDK9	CK1, CDK7/9	Phase I	[241]
Umbralisib	Block the phosphorylation of translation initiation factor 4E binding protein resulting in the inhibition of c-myc translation and cellular death	PI3K δ , CK1 ϵ	Approved	[97, 101]

CDK: Cyclin-dependent kinase, IWP: Inhibitors of Wnt production, MAPK: Mitogen-activated protein kinase, PI3K: Phosphoinositide-3-kinase

1.7.1 CK1-specific inhibitors used in neurodegenerative diseases

As mentioned before, several compounds inhibiting CK1 are described in literature. Many of them do not selectively inhibit CK1 isoforms but might serve as a good starting point for drug development. Among the published inhibitors, the majority of results was published for inhibitors tested in cancer-related topics, but only a few

towards neurodegeneration. Cancer and neurodegeneration are both defined by the dysregulation or deregulation of the same signaling pathways, however, leading to opposite consequences. Aberrant signaling pathways might lead to increased cell survival and proliferation in tumorigenesis, whereas those alterations result in cell death and apoptosis in neurodegenerative diseases. One of the most altered signaling pathways in cancer is the Wnt signaling pathway, which is also implicated in neurodegenerative diseases such as AD and PD [340]. The development of CK1-specific inhibitors, which are able to cross the BBB is a promising approach for the treatment of proteinopathies such as ALS and AD. As an example, small brain-penetrating compounds were identified, which inhibit the neurotoxicity of TDP-43 through the inhibition of its phosphorylation mediated by CK1 *in vitro* [295].

Although several CK1-specific compounds were developed for the treatment of cancer, only very few kinase inhibitors for the treatment of neurodegenerative diseases, such as AD exist. Recently, an inhibitor, which was originally designed to inhibit A β binding alcohol dehydrogenase, which is involved in AD pathophysiology, showed high potency against CK1. The strategy to inhibit both enzymes, which are involved in two distinct AD-associated pathological processes, could be advantageous [30]. Dual-specific characteristics of an inhibitor was also used against CK1 and CDK, both involved in the production of A β peptides, resulting in decreased CK1-dependent production of A β peptides in a cell culture model [258]. However, the main hurdle in the design and development of compounds targeting the CNS is the successful penetration of the BBB, which is essential for the treatment of neurodegenerative diseases [21].

1.8 Modulation of the CK1 activity with therapeutic peptides

The regulation of biological cellular processes is mainly controlled through the interaction of two or more proteins, which can have a wide range of effects including initiating or modulating signal transduction, regulating gene transcription and protein translation, providing cytoskeletal stability and induce cellular replication or death [320]. The total amount of protein-protein interactions (PPI), which are necessary for cellular processes is called the “interactome” and has significant roles in physiological as well as pathological process [16, 248, 342]. Since the “interactome” is essential and huge, it theoretically contains many potential target sites at which a

drug could intervene. Unfortunately, the development of new synthetic SMIs targeting PPIs is challenging, because protein surfaces usually do not allow specific binding of low MW SMIs [365]. Although peptide-based candidates exhibit significant disadvantages, such as low cellular proteolytic stability and weak membrane permeability, their large molecular size allow specific interaction with the protein surfaces.

In many cases, the development of peptide inhibitors has resulted from an understanding of specific PPIs for a particular PK. Thus, peptide-based inhibitors can be derived from various sources such as biologically relevant interaction partners (including endogenous inhibitory proteins and kinase substrates), the PK sequence, anchoring or scaffold proteins (including AKAPs) and other binding partners [40]. Novel aa sequences for peptide-based inhibitors have usually been discovered in library screening approaches including screenings with full-length kinases, regulatory subunits or substrate fragments [40]. Peptide libraries can either contain synthetic generated and biochemically screened peptides or recombinantly expressed peptides, which were screened via phage display [40].

In a recent study, the modulation of CK1 δ - α -tubulin interaction was disturbed by using a CK1 δ -derived peptide, which was screened biochemically by using a synthetic generated CK1 δ -derived peptide library. A peptide, which encompasses aa 361 to 375 of CK1 δ was detected as a prominent interaction partner for α -tubulin [190]. The selected peptide has been shown to block the phosphorylation of α -tubulin mediated by CK1 δ and inhibits cell cycle progression of mitosis entering cells that finally leads to cell death [190]. In this context, a CK1 δ - and CK1 ϵ -derived library was screened, and selected peptides were shown to inhibit the interaction of CK1 δ and CK1 ϵ with the DEAD-box RNA helicase DDX3X. Mutations within DDX3X were identified to stimulate CK1 activity causing stimulation of CK1-mediated signaling pathways such as Wnt signaling pathway [85, 103]. Thus, the treatment with identified CK1 δ -/CK1 ϵ -derived peptides led to decreased activation of CK1 δ and CK1 ϵ by DDX3X in cell culture experiments, which was possibly caused by the prevention of CK1-DDX3X interaction mediated by the peptides [103]. Similar inhibiting effects were observed for interfering peptides that modulate the interaction of CK1 ϵ -axin1 and regulate CK1 ϵ -mediated phosphorylation of DVL and thus, the activation of the Wnt signaling pathway [150]. A similar approach was used to

prevent the interaction between MDM2 and CK1 α . In previous studies, CK1 α was identified to interact with MDM2 leading to the degradation of the tumor suppressor p53. A pharmacological inhibition of CK1 α already resulted in increasing protein levels of p53 and induced cell death. Reduced cell growth in a p53-dependent manner could also be achieved by using small CK1 α -derived peptides specifically inhibiting the CK1 α -MDM2 interaction [157].

1.9 Aim of the study

Altered activity and overexpression of CK1 in physiological processes have been associated with (hyper-)phosphorylation of key proteins like APP and tau, which are involved in the development of AD. Even though several studies proposed that CK1 is involved in the pathogenesis of AD, so far, not much is known about CK1-specific phosphorylation of tau and its influence on tau aggregation. Therefore, the first hypothesis of this study addressing this question was

- I.) CK1 δ is involved in the phosphorylation of AD-associated tau phosphorylation sites and has a functional influence on tau aggregation.

So far, only a few studies demonstrate the CK1 δ -mediated phosphorylation of tau at AD-associated sites. Unfortunately, most results are obtained by qualitative methods, and thus, a relation between CK1 δ -mediated tau phosphorylation, which was identified by immunodetection or LC-MS/MS analysis, and the effect of CK1 δ -mediated phosphorylation on tau aggregation remains to be investigated. To answer these questions, the CK1 δ -mediated phosphorylation of AD-associated tau phosphorylation sites was characterized *in vitro* by using LC-MS/MS analysis, *in vitro* kinase assay and two-dimensional phosphopeptide analysis. To confirm the results obtained from biochemical approaches, a cell-based assay and immunodetection using phospho-specific antibodies was performed. In addition, double immunofluorescence staining was performed to investigate co-localization of endogenous CK1 δ with tau. Finally, the effect of *in vitro* CK1 δ -mediated phosphorylation on tau aggregation was examined.

Since the tau hyperphosphorylation and aggregation into PHFs and NFTs as well as the production of A β peptides and the formation of amyloid plaques seem to be main drivers of the development of AD according to the amyloid cascade and dual

pathway hypothesis, inhibition of A β production, plaque formation, tau hyperphosphorylation and aggregation could have a major beneficial impact on the AD development. As CK1 seems to be involved in the tau hyperphosphorylation and APP metabolism, it represents an interesting point for therapeutic intervention, which was addressed in the next two hypotheses.

II.) CK1 δ -specific SMIs have beneficial therapeutic effects in the development of AD

The majority of previously developed CK1 inhibitors do not selectively inhibit CK1 isoforms but serve as good starting points for drug development. In cooperation with external partners newly developed compounds (including benzimidazole derivatives, IWP-derived compounds and isoxazole derivatives) were tested for their selectivity and potency towards CK1 δ . In addition, most of the already tested and published inhibitors were tested on cancer cell lines, but only a few in neurodegeneration-related approaches. In order to test well-described and promising newly developed inhibitors for their therapeutic biological effect in the development of AD, a cell culture-based assay (“Alzheimer’s-in-a-dish” model) mimicking AD pathology was first established and then used for inhibitor testing.

Since CK1 is involved in many essential cellular processes, general inhibition of CK1 δ -mediated phosphorylation by SMIs could be disadvantageous. Instead of using CK1 δ -specific SMIs small peptides could specifically inhibit pathophysiological phosphorylation with high selectivity by blocking CK1 δ -substrate interactions. Thus, the final main hypothesis of this study is

III.)CK1 δ -derived peptides are novel tools inhibiting the PPI and modulate pathogenic metabolism of APP and tauopathy in AD

To verify this hypothesis, a peptide library derived from the aa sequence of CK1 δ was used for the screening of peptides which specifically manipulate the interaction between CK1 δ and APP695 or tau and thus inhibit their CK1 δ -mediated phosphorylation. Furthermore, successful peptides were tested for their ability to penetrate neuronal cells without inducing toxic effects. Finally, the effect of CK1 δ -derived peptides on AD pathology including A β peptide production, amyloid plaque formation and tau hyperphosphorylation was investigated using the established “Alzheimer’s-in-a-dish” model.

2 Materials and Methods

2.1 Materials

2.1.1 Devices

Table 4: Overview of devices, which were used in this project.

Device	Manufacturer
Automated cell counter, LUNA™	Logos Biosystems, Anyang-si, South Korea
Bacteria incubator, Certomat BS-1	B. Braun Biotech International, Melsungen, Germany
Biacore™ X100	Cytiva, Marlborough, MA, USA
Biological safety cabinet, Herasafe™	Heraeus Instruments GmbH, Hanau, Germany
BioPhotometer	Eppendorf AG, Hamburg, Germany
Cell incubator, Heracell™ VIOS 250i	Heraeus Instruments GmbH, Hanau, Germany
Cell sorter FACSAria	BD, Franklin Lakes, NJ, USA
Centrifuge (5415R, 5417C, 5810R)	Eppendorf AG, Hamburg, Germany
Centrifuge (Biofuge stratos, Megafuge 1.0R)	Heraeus Instruments GmbH, Hanau, Germany
Cherenkov counter LC6000IC	Beckman Coulter, Brea, CA, USA
Confocal microscope, Leica SP8	Leica Mikrosysteme Vertrieb GmbH, Wetzlar Germany
Developer machine, Kodak X-OMAT	Eastman Kodak Company, Rochester, NY, USA
FPLC system Ettan™ LC storage compartment: Box-900 pH and conductivity detector: pH/C-900 UV detector: UV-900 pump: P-905 mixing valve: M-925 valve box: INV-917 fraction collector: Frac-950 communication module: CU950	Amersham Pharmacia Biotech, Amersham, UK
Imaging system Fuxion FX	Vilber, Collégien, France
Incubation shaker, CERTOMAT® BS-1	B. Braun Biotech International, Melsungen, Germany
Lyophilizer Savant Speed Vac® Refrigerated vapor trap, RVT400	Thermo Fisher Scientific Inc., Waltham, MA, USA
Mass spectrometer QExactive HF Orbitrap	Thermo Fisher Scientific Inc., Waltham, MA, USA
Microscope, Olympus IX81 camera: XM10	Olympus Europa, Hamburg, Germany
Mixer, Stuart™ Scientific roller mixer SRT1	Sigma Aldrich, St. Louis, MO, USA
Multimode plate reader, TriStar ² LB 942	Berthold Technologies, Bad Wildbad, Germany
Multimode plate reader, Tecan Spark 10M	Tecan, Männedorf, Switzerland
pH meter, MP220	Mettler Toledo GmbH, Greifensee, Switzerland

Table 4 continued: Overview of devices, which were used in this project.

Device	Manufacturer
Plate shaker, Wallac 1296-001	PerkinElmer, Waltham, MA, USA
Power supply, Model 1000/500	Bio-Rad Laboratories Inc., Hercules, CA, USA
Scale, MXX-2001	Denver Instrument, Bohemia, NY, USA
Scale, SBC-32	Scaltec Instruments GmbH, Göttingen, Germany
SDS-PAGE system, Mini-Protean® Tetra Cell	Bio-Rad Laboratories Inc., Hercules, CA, USA
Shaker, KS 205 basic	IKA Labortechnik, Staufen, Germany
Slab gel dryer, SGD 2000	Thermo Fisher Scientific Inc., Waltham, MA, USA
Syringe pump, Perfusor Secura FT	B. Braun Biotech International, Melsungen, Germany
Thermocycler, Labcycler	SensoQuest GmbH, Göttingen, Germany
Thermomixer, Thermomixer comfort	Eppendorf AG, Hamburg, Germany
UHPLC Easy-nLC 1200	Thermo Fisher Scientific Inc., Waltham, MA, USA
Ultracentrifuge, Optima XPN-80	Beckman Coulter, Brea, CA, USA
Ultrasonic device, Sonifier 250, Branson	Thermo Fisher Scientific Inc., Waltham, MA, USA
UV/Vis spectrophotometer, QIAxpert	QIAGEN, Hilden, Germany
Vacuum pump, MV10C vacuum pump	Vacuubrand, Wertheim, Germany

2.1.2 Chemicals and biochemicals

Table 5: Chemicals and biochemicals.

Chemical/biochemical	Manufacturer
[γ - ³² P] ATP	HARTMANN ANALYTIC, Braunschweig, Germany
2-propanol	Carl Roth GmbH & Co. Kg, Karlsruhe, Germany
β -mercaptoethanol	Sigma Aldrich, St. Louis, MO, USA
6x DNA loading dye	Thermo Fisher Scientific, Waltham, MA, USA
ABTS	Sigma Aldrich, St. Louis, MO, USA
Acetic acid glacial	VWR International GmbH, Radnor, PA, USA
Acrylamide (Rotiphorese® Gel 30)	Carl Roth GmbH & Co. Kg, Karlsruhe, Germany
Agarose	Biozym Scientific GmbH, Oldendorf, Germany
Ammonium persulfate	Carl Roth GmbH & Co. Kg, Karlsruhe, Germany
Ampicillin sodium salt	Carl Roth GmbH & Co. Kg, Karlsruhe, Germany
Aprotinin	Carl Roth GmbH & Co. Kg, Karlsruhe, Germany
ATP	Sigma Aldrich, St. Louis, MO, USA
Bacto™ agar	BD Biosciences, Franklin Lakes, NJ, USA
Benzamidine	Sigma Aldrich, St. Louis, MO, USA
Bromphenol blue	Sigma Aldrich, St. Louis, MO, USA
Calcium Chloride	Merck Millipore, Darmstadt, Germany
Coomassie Brilliant Blue G250	Waldeck GmbH & Co. KG, Münster, Germany
D-(+)-glucose	Sigma Aldrich, St. Louis, MO, USA
DAPI	Sigma Aldrich, St. Louis, MO, USA
Developer solution (G135, G354)	Agfa Healthcare AG, Mortsel, Belgium
dNTP mix	Thermo Fisher Scientific, Waltham, MA, USA

Table 5 continued: Chemicals and biochemicals.

Chemical/biochemical	Manufacturer
DMSO	Sigma Aldrich, St. Louis, MO, USA
DTT	Sigma Aldrich, St. Louis, MO, USA
Dulbecco's modified eagle medium (DMEM), DMEM/F12	Gibco/Life Technologies, Carlsbad, CA, USA
Dulbecco's phosphate buffered saline	Gibco/Life Technologies, Carlsbad, CA, USA
EDTA	Carl Roth GmbH & Co. Kg, Karlsruhe, Germany
EGTA	Sigma Aldrich, St. Louis, MO, USA
Ethanol	VWR International GmbH, Radnor, PA, USA
Fetal calf serum	Biochrom GmbH, Berlin, Germany
Formic acid	Sigma Aldrich, St. Louis, MO, USA
Glycerin	Sigma Aldrich, St. Louis, MO, USA
Hydrochloric acid (37 %)	Sigma Aldrich, St. Louis, MO, USA
Hydrogen peroxide (30 %)	Merck Millipore, Darmstadt, Germany
Imidazole	Sigma Aldrich, St. Louis, MO, USA
IPTG	Sigma Aldrich, St. Louis, MO, USA
Kanamycin	Sigma Aldrich, St. Louis, MO, USA
KnockOut serum	Gibco/Life Technologies, Carlsbad, CA, USA
Laemmli buffer 2x concentrate	Sigma Aldrich, St. Louis, MO, USA
Lipofectamine® 3000	Invitrogen™, Carlsbad, CA, USA
Luminol	Sigma Aldrich, St. Louis, MO, USA
Midori Green	NIPPON Genetics Europe GmbH, Düren, Germany
Magnesium sulfate	Merck Millipore, Darmstadt, Germany
MTT	Sigma Aldrich, St. Louis, MO, USA
Nonidet P-40	Sigma Aldrich, St. Louis, MO, USA
Penicillin/streptomycin solution	Gibco/Life Technologies, Carlsbad, CA, USA
Potassium chloride	Merck Millipore, Darmstadt, Germany
ProLong™ Glass Antifade Mountant	Invitrogen™, Carlsbad, CA, USA
Pyridine	Merck Millipore, Darmstadt, Germany
Reduced L-glutathione	Sigma Aldrich, St. Louis, MO, USA
SDS	Carl Roth GmbH & Co. Kg, Karlsruhe, Germany
Sodium chloride	Sigma Aldrich, St. Louis, MO, USA
Sodium phosphate (NaH ₂ PO ₄ , Na ₂ HPO ₄)	Merck Millipore, Darmstadt, Germany
TEMED	Sigma Aldrich, St. Louis, MO, USA
Thioflavin S	Sigma Aldrich, St. Louis, MO, USA
Tris	Sigma Aldrich, St. Louis, MO, USA
Tryptone	Carl Roth GmbH & Co. Kg, Karlsruhe, Germany
Yeast extract	Sigma Aldrich, St. Louis, MO, USA

2.1.3 Consumables and reagent systems (kits)

Table 6: Overview of consumables and reagent systems.

Consumable/reagent system	Manufacturer
96-well plates (MaxiSorp™, PolySorp™)	Thermo Fisher Scientific, Waltham, MA, USA
Amicon Ultra-0.5 mL centrifugal filters	Merck Millipore, Darmstadt, Germany
C18 StageTips	Thermo Fisher Scientific, Waltham, MA, USA
Cell counting slides (Luna™)	Logos Biosystems, Anyang-si, South Korea
Cell culture dish (10 mm)	Sarstedt AG & Co. KG, Nümbrecht, Germany
Cell culture plates (6-well, 24-well, 96-well)	Sarstedt AG & Co. KG, Nümbrecht, Germany
Centrifuge tubes (15 mL, 50 mL)	Sarstedt AG & Co. KG, Nümbrecht, Germany
cComplete™ His-Tag purification column	F. Hoffmann-La Roche AG, Basel Switzerland
CytoTox-ONE homogenous membrane integrity assay	Promega, Fitchburg, MA, USA
Flasks with baffles (500 mL, 1 L, 2 L)	VWR International GmbH, Radnor, PA, USA
Gibson Assembly® Master Mix	New England Biolabs, Ipswich, MA, USA
Glutathione Sepharose 4 Fast Flow	Cytiva, Marlborough, MA, USA
GSTrap™ FF column	Cytiva, Marlborough, MA, USA
Minisart® Syringe filter (0.45 µm)	Sartorius Stedim Biotech GmbH, Göttingen, Germany
Mix2Seq Kit	Eurofins Scientific SE, Luxembourg city, Luxembourg
NanoBIT® PPI MCS Starter Systems	Promega Corporation, Madison, WI, USA
Nano-Glo® Live Cell Assay System	Promega Corporation, Madison, WI, USA
Q5® site-directed mutagenesis kit	New England Biolabs, Ipswich, MA, USA
Quantikine® human Aβ (aa 1-42) immunoassay	R&D Systems, Minneapolis, MN, USA
Pasteur pipettes (150 mm, 230 mm)	VWR International GmbH, Radnor, PA, USA
PCR reaction tubes (0.45 mL)	VWR International GmbH, Radnor, PA, USA
PD-10 desalting column	Cytiva, Marlborough, MA, USA
Petri dishes	BD Biosciences, Franklin Lakes, NJ, USA
Pierce™ BCA protein assay kit	Thermo Fisher Scientific, Waltham, MA, USA
Pipette tips	Eppendorf AG, Hamburg, Germany
Plasmid Plus Midi kit	QIAGEN, Venlo, Netherlands
PVDF membrane	F. Hoffmann-La Roche AG, Basel Switzerland
Reaction tubes (0.5 mL, 1.5 mL, 2 mL)	Eppendorf AG, Hamburg, Germany
Stripette® serological pipette (5, 10, 25 mL)	Corning Inc., Corning, NY, USA
TALON® Metal Affinity Resin	Takara Bio, Kusatsu, Shiga, Japan
Thin-layer cellulose plates	Merck Millipore, Darmstadt, Germany
Whatman® qualitative filter paper	Sigma Aldrich, St. Louis, MO, USA
X-ray film, Amersham Hyperfilm MP	Cytiva, Marlborough, MA, USA

2.1.4 Bacteria and cell lines

Table 7: Bacteria and cell lines with their respective origin and genotype.

Bacteria/ cell lines	Description	Manufacturer/ provider
<i>E. coli</i> Subcloning Efficiency™ DH5α	cloning strain, mutation in <i>recA1</i> and <i>endA1</i> (gene for recombinase I and endonuclease I) prevents unwanted recombination and ensures increased insert stability, and improves yield and quality of plasmid [323]	Thermo Fisher Scientific, Waltham, MA, USA
<i>E. coli</i> SoluBL21™	expression strain, optimized for expressing insoluble proteins in soluble form [20]	Genlantis, San Diego, CA, USA
<i>E. coli</i> SHuffle® T7 Express	expression strain, constitutively expression of disulfide bond isomerase, deficient in protease <i>Lon</i> and <i>OmpT</i> , promotes right folding of recombinant proteins [20]	New England Biolabs, Ipswich, MA, USA
HEK293 (ACC305)/ HEK293T (ACC635)	highly transfectable human primary embryonal kidney cell line; HEK293T is a derivative of HEK293 carrying a plasmid containing the SV-40 large T-antigen	DSMZ, Hannover, Germany
ReNcell® VM	immortalized human neural progenitor cell (hNPC) line, able to differentiate into neurons and glial cells [70]	Merck Millipore, Darmstadt, Germany

2.1.5 Culture media

Table 8: Used bacteria and cell line with their respective culture media.

Bacteria/cell lines	Culture media
<i>E. coli</i> (each strain)	LB medium (10 g/L NaCl, 10 g/L peptone, 5 g/L yeast extract in dH ₂ O, sterilized by autoclaving) supplemented with 100 µg/mL ampicillin or 25 µg/mL kanamycin.
HEK293/ HEK293T	DMEM (Gibco/Life Technologies, Carlsbad, CA, USA) supplemented with 10 % (v/v) FCS and 100 U/mL penicillin-streptomycin solution
hNPCs differentiation medium	DMEM/F12 (Gibco/Life Technologies, Carlsbad, CA, USA) supplemented with 2 % B-27 neural supplement, 2 µg/µL heparin and 100 U/mL penicillin-streptomycin solution
hNPCs proliferation medium	hNPCs differentiation medium supplemented with 20 ng/mL human epidermal growth factor (EGF) and 20 ng/mL human basic fibroblast growth factor (bFGF)
Cell sorting medium	Phosphate buffered saline (PBS) supplemented with 2 % (v/v) B-27 supplement and 2 % (v/v) KnockOut serum

2.1.6 Molecular weight markers

Table 9: Molecular weight markers.

Molecular weight markers	Manufacturer
GeneRuler 1 kb DNA Ladder	Thermo Fisher Scientific, Waltham, MA, USA
Precision Plus Protein Standard (Dual Color)	BioRad, Hercules, CA, USA

2.1.7 Proteins and enzymes

Table 10: Proteins and enzymes.

Protein/enzyme	Manufacturer
α -casein (from bovine milk)	Sigma Aldrich, St. Louis, MO, USA
Accutase®	Sigma-Aldrich, St. Louis, MO, USA
Basic fibroblast growth factor	Reprocell Inc., Glasgow, UK
Bovine serum albumin fraction V	Sigma-Aldrich, St. Louis, MO, USA
<i>DpnI</i>	New England Biolabs, Ipswich, MA, USA
Epidermal growth factor	Sigma-Aldrich, St. Louis, MO, USA
Heparin	Stemcell Technologies Inc., Vancouver, BC, Canada
Lysozyme	Sigma-Aldrich, St. Louis, MO, USA
Phusion High-Fidelity DNA Polymerase	Thermo Fisher Scientific, Waltham, MA, USA
Illustra™ Taq DNA polymerase	Cytiva, Marlborough, MA, USA
TPCK-trypsin	Thermo Fisher Scientific, Waltham, MA, USA
Trypsin/EDTA (0.05 %/0.02 % in PBS)	Gibco/Life Technologies, Carlsbad, CA, USA

2.1.8 Vectors

Table 11: Prokaryotic expression vectors.

Vector	Description	Origin
pET28a(+)-6xHis-APP695	encoding for human 6xHis-tagged APP695	Biomatik, Toronto, ON, Canada
pET28a(+)-6xHis-tau441	encoding for human 6xHis-tagged tau441	Biomatik, Toronto, ON, Canada
pET28a(+)-6xHis-CK1 δ	encoding for human 6xHis-tagged CK1 δ (transcription variant 1)	Biomatik, Toronto, ON, Canada
pGEX-6P-3-GST-CK1 α	encoding for human GST-tagged CK1 α	-
pGEX-6P-3-GST-CK1 δ	encoding for human GST-tagged CK1 δ (TV 1)	-
pGEX-6P-3-GST-CK1 ϵ	encoding for hamster GST-tagged CK1 ϵ	-

APP: Amyloid precursor protein, GST: Glutathione-S transferase, tau: tubulin-associated unit

Table 12: Eukaryotic expression vectors.

Vector	Description	Origin
pBiT1.1-C	encoding for C-terminal large BiT (LgBiT)	
pBiT2.1-C	encoding for C-terminal small BiT (SmBiT)	
pBiT1.1-N	encoding for N-terminal LgBiT	
pBiT2.1-N	encoding for N-terminal SmBiT	
SmBiT-PRKACA positive control vector	encoding for the catalytic subunit α of protein kinase A (tagged with SmBiT)	NanoBiT [®] PPI starter systems, Promega, Fitchburg, MA, USA
LgBiT-PRKAR2A positive control vector	encoding for protein kinase cAMP-dependent type II regulatory subunit α (tagged with LgBiT)	
NanoBiT [®] negative control vector	encoding for HaloTag [®] -SmBiT, a structurally stable fusion partner	
pCDNA3.1-APP695	encoding for APP695; used as template for NanoBiT [®] constructs	-
AAVS1-CAG-rTA3-TauWT-2N4R-EGFP	encoding for tau441; used as template for NanoBiT [®] constructs	AAVS1-CAG-rTA3-TauWT-2N4R-EGFP was a gift from Gerold Schmitt-Ulms [3, 357]
pSPAX2	packaging vector for lentiviral particle production	kindly provided by Prof. Dr. Cagatay Günes (Ulm University Hospital, Ulm, Germany)
pMD2.G	envelope vector for lentiviral particle production	
pCSCW-GFP	lentiviral control vector (encoding for GFP) for establishing an “Alzheimer’s-in-a-dish” model according to [70] and [181]	
pCSCW-APPSL-IRES-GFP	lentiviral expression vector (encoding for full-length human APP695 with K670N/M671L/V717I (Swedish and London mutation) and GFP) for establishing an “Alzheimer’s-in-a-dish” model according to [70] and [181]	kindly provided by Prof. Dr. Doo Kim (Massachusetts General Hospital, Harvard Medical School, Massachusetts, USA)
pCSCW-mCherry	lentiviral control vector (encoding for mCherry) for establishing an “Alzheimer’s-in-a-dish” model according to [70] and [181]	
pCSCW-PSEN1(Δ E9)-IRES-mCherry	lentiviral expression vector (encoding for full-length human PSEN1 (Δ E9) and mCherry) for establishing an “Alzheimer’s-in-a-dish” model according to [70] and [181]	

APP: Amyloid precursor protein, BiT: Binary technology, GFP: Green fluorescent protein, LgBiT: Large unit of the binary technology, PRKACA: Protein kinase cAMP-activated catalytic subunit alpha, PRKAR2A: Protein kinase cAMP-dependent type II regulatory subunit alpha, PSEN1: Presenilin-1, SmBiT: Small unit of the binary technology, tau: Tubulin-associated unit.

2.1.9 Antibodies and streptavidin-conjugates

Table 13: Antibodies and streptavidin-conjugates.

	Antibody, clone	Usage/dilution	Manufacturer
Primary antibodies	anti-tau (HT7), MN1000	Western blot (1:1,000)/ IF staining (1:500)	Thermo Fisher Scientific Inc., Waltham, MA, USA
	anti-pSer202/pThr205-tau (AT8), MN1020	Western blot (1:500)	Thermo Fisher Scientific Inc., Waltham, MA, USA
	anti-pSer214-tau, DIQ2X	Western blot (1:1,000)	Cell Signaling Technology, Danvers, MA, USA
	anti-pSer416-tau, D7U2P	Western blot (1:1,000)	Cell Signaling Technology, Danvers, MA, USA
	anti- β -amyloid, 6E10	IF staining (1:500)	BioLegend, San Diego, CA, USA
	anti-CK1 δ , ab10877	IF staining (1:500)	abcam, Cambridge, UK
	anti- β -actin, AC-15	Western blot (1:5,000)	Sigma Aldrich, St. Louis, MO, USA
	anti- β -III-tubulin, MAB1637	IF staining (1:500)	Merck Millipore, Darmstadt, Germany
	anti-MAP2, Poly18406	IF staining (1:500)	BioLegend, San Diego, CA, USA
Secondary antibodies	HRP-conjugated anti-mouse, 7076	Western blot (1:10,000)	Cell Signaling Technology, Danvers, MA, USA
	HRP-conjugated anti-rabbit, 7074	Western blot (1:10,000)	Cell Signaling Technology, Danvers, MA, USA
	Alexa Fluor 647 anti-goat	IF staining (1:250)	Invitrogen™, Carlsbad, CA, USA
	Alexa Fluor 633 anti-rabbit	IF staining (1:250)	Invitrogen™, Carlsbad, CA, USA
	Alexa Fluor 488 anti-mouse	IF staining (1:250)	Invitrogen™, Carlsbad, CA, USA
	DyLight 488 anti-mouse	IF staining (1:200)	Thermo Fisher Scientific Inc., Waltham, MA, USA
	DyLight 350 anti-mouse	IF staining (1:500)	Thermo Fisher Scientific Inc., Waltham, MA, USA
Streptavidin-conjugates	HRP-streptavidin	streptavidin-linked interaction assay (1:8,000)	Thermo Fisher Scientific Inc., Waltham, MA, USA
	TRITC-streptavidin	IF staining (1:200)	Jackson ImmunoResearch Europe Ltd., Cambridgeshire, UK)

HRP: horseradish-peroxidase; IF: Immunofluorescence, MAP2: Microtubule-associated protein 2, tau: tubulin-associated unit, TRITC: Tetramethylrhodamine

2.1.10 Primer

Table 14: Sequences of primers used for cloning procedures.

	Designation	Primer sequence (5' → 3')
Generation of tau441 fragments & tau383 isoform	5'-tau441 ¹⁻¹⁵⁵	AACCCCGCGCTAAGCAGCCCCCG
	3'-tau441 ¹⁻¹⁵⁵	GCAATTTTGGTTTTTGCATCGGC
	5'-tau441 ¹⁵⁶⁻²⁴²	AGCAAATGGGTTCGCGGATCCGGTGCAGCCCCGCTGGT
	3'-tau441 ¹⁵⁶⁻²⁴²	TGGTGGTGGTGGTGCTCGAGTTAGCGGCTTTTGGCACTACTCGGAC
	5'-tau441 ²⁴³⁻⁴⁴¹	CTGCAGACCGCCCCGGTT
	3'-tau441 ²⁴³⁻⁴⁴¹	GGATCCGCGACCCATTTGC
	5'-tau383	AGGTCTGAAAGCAGAAGAAGCAGGTATTG
	3'-tau383	CTTCTTCTGCTTTCAGACCTGCATCGGTG
Generation of tau441 phosphomutants	5'-tau441 ^{S68A}	TGATGCAAAAAGCCACCCCGACCG
	3'-tau441 ^{S68A}	CTGGTTTCACTACCCGGT
	5'-tau441 ^{S68/69A+T71A}	GGCAGCAGAAGATGTGACCGCC
	3'-tau441 ^{S68/69A+T71A}	GGTGC GGCTTTTGCATCACTGGTTTC
	5'-tau441 ^{S202A}	CAGCCCGGGTGCACCGGGCACCC
	3'-tau441 ^{S202A}	CTATAACCACTGCGGTCAC
	5'-tau441 ^{S202A+T205A}	CAGCCCGGGTGCACCGGGCGCAC
	3'-tau441 ^{S202A+T205A}	CCCGGGCTGCTATAACCACTGCG
	5'-tau441 ^{S191A}	GTTATAGCAGCCCGGGTAGC
	3'-tau441 ^{S191A}	CACTGCGGTCACCTGCTTTC
	5'-tau441 ^{T212A}	GACCCCGCCTACACGTGAAC
	3'-tau441 ^{T212A}	GGCAGGCTCGGTGCACGAC
	5'-tau441 ^{T217A}	CTGCCGGCACCGCCTACAC
	3'-tau441 ^{T217A}	GCTCGGGGTACGACTACGG
	5'-tau441 ^{T212A+S214A}	TCGTGCACCGGCACTGCCGACCCCG
	3'-tau441 ^{T212A+S214A}	CTACGGCTACCCGGGGTG
	5'-tau441 ^{S214A+T217A}	TCGTACCCCGGCCCTGCCGGCAC
	3'-tau441 ^{S214A+T217A}	CTACGGCTACCCGGGGTG
	5'-tau441 ^{T212/217A+S214A}	GGCCCTGCCGGCACCGCCTACAC
	3'-tau441 ^{T212/217A+S214A}	GGTGCACGACTACGGCTACCCG
	5'-tau441 ^{T212/217/220A+S214A}	GGCACCGCCTGCACGTGAACCGAAAAAAG
	3'-tau441 ^{T212/217/220A+S214A}	GGCAGGGCCGGTGCACGA
	5'-tau441 ^{S412/413A}	GAGTAATGTTGCGGCAACCGGCAGCATTGATATGGTTGATAGCC
	3'-tau441 ^{S412/413A}	AGATGACGCGGGCTGGTA
	5'-tau441 ^{S412/413/416A+T414A}	CGCAATTGATATGGTTGATAGCCC
	3'-tau441 ^{S412/413/416A+T414A}	CCTGCTGCCGCAACATTACTION
	5'-tau441 ^{S409/412/413/416A+T414A}	GCGTCATCTGGCCAATGTTGCGGCAGCAG
	3'-tau441 ^{S409/412/413/416A+T414A}	GGGCTGGTATCGCCGCTC

A: Adenine, C: Cytosine, for: Forward, G: Guanine, T: Thymine

Table 14 continued: Sequences of primers and oligonucleotides used for cloning procedures.

	Designation	Primer sequence (5' → 3')
Generation of APP fragments	5'-APP695 ¹⁻²⁶⁷ (N-APP)	AGCAACCGAATAAACCACCAGCATTG
	3'-APP695 ¹⁻²⁶⁷ (N-APP)	TCTTCATACGGTTCTTCTG
	5'-APP695 ²⁶⁸⁻⁶¹² (E2) (A)	TCATCAGAAATAAGTTTCTTTGCAGAAGATGTTGG
	3'-APP695 ²⁶⁸⁻⁶¹² (E2) (A)	TGCACTTCATAACCGCTATC
	5'-APP695 ²⁶⁸⁻⁶¹² (E2) (B)	CGTACCACCAGCATTGCAA
	3'-APP695 ²⁶⁸⁻⁶¹² (E2) (B)	GGATCCGCGACCCATTTG
	5'-APP695 ⁶¹³⁻⁶⁹⁵ (APP-C)	GAACAGAATTATAGTGATGATGTGC
3'-APP695 ⁶¹³⁻⁶⁹⁵ (APP-C)	GGATCCGCGACCCATTTG	
Generation of CK1δ NanoBit® constructs	5'-pBiT-C-CK1δ (plasmid)	cgtgcaccgaTCTGGCTCGAGCGGTGGT
	3'-pBiT-C-CK1δ (plasmid)	tcagctccatATTCCCCTGAGCTCCCCTTAG
	5'-pBiT-C-CK1δ (insert)	tcaggggaatATGGAGCTGAGAGTCGGG
	3'-pBiT-C-CK1δ (insert)	tcgagccagaTCGGTGACGACAGACTG
	5'-pBiT-N-CK1δ (plasmid)	gcaccgatgaTCAGTCTAAGCTAGCAGATCTTC
	3'-pBiT-N-CK1δ (plasmid)	ctctcagctcATTCCCCTGAGCTCCACC
	5'-pBiT-N-CK1δ (insert)	tcaggggaatGAGCTGAGAGTCGGGAAC
3'-pBiT-N-CK1δ (insert)	cttagactgaTCATCGGTGCACGACAGAC	
Generation of tau441 NanoBit® constructs	5'-pBiT-C-tau441 (plasmid)	gcagggtttgTCTGGCTCGAGCGGTGGT
	3'-pBiT-C-tau441 (plasmid)	gctcagccatATTCCCCTGAGCTCCCCTTAG
	5'-pBiT-C-tau441 (insert)	tcaggggaatATGGCTGAGCCCCGCCAG
	3'-pBiT-C-tau441 (insert)	tcgagccagaCAAACCTGCTTGCCAGG
	5'-pBiT-N-tau441 (plasmid)	ggggttggtgaTCAGTCTAAGCTAGCAGATCTTC
	3'-pBiT-N-tau441 (plasmid)	ggggctcagcATTCCCCTGAGCTCCACC
	5'-pBiT-N-tau441 (insert)	tcaggggaatGCTGAGCCCCGCCAGGAG
3'-pBiT-N-tau441 (insert)	cttagactgaTCACAAACCTGCTTGCCAG	
Generation of APP695 NanoBit® constructs	5'-pBiT-C-APP695 (plasmid)	tcaggggaatATGCTGCCGGTTTGGCA
	3'-pBiT-C-APP695 (plasmid)	tcgagccagaGTTCTGCATCTGCTCAAAGAACTTGAG
	5'-pBiT-C-APP695 (insert)	gatgcagaacTCTGGCTCGAGCGGTGGT
	3'-pBiT-C-APP695 (insert)	cgggcagcatATTCCCCTGAGCTCCCCTTAG
	5'-pBiT-N-APP695 (plasmid)	tcaggggaatCTGCCGGTTTGGCACTG
	3'-pBiT-N-APP695 (plasmid)	cttagactgaTCAGTTCTGCATCTGCTCAAAGAAC
	5'-pBiT-N-APP695 (insert)	gcagaactgaTCAGTCTAAGCTAGCAGATCTTC
3'-pBiT-N-APP695 (insert)	aaccgggcagATTCCCCTGAGCTCCACC	

A: Adenine, C: Cytosine, for: Forward, G: Guanine, T: Thymine

Table 15: Sequences of primers used for sequencing.

	Designation	Primer sequence (5' → 3')
Sequencing primers	5'-T7 promoter	TAATACGACTCACTATAGGG
	3'-tau441 (A)	GGTTCTTCGCTACCATCTTC
	3'-tau441 (B)	CAGATCAGGCATCGGAACC
	3'-T7 terminator	GCTAGTTATTGCTCAGCGG
	5'-pBiT-C	GCTTGGCAATCCGGTACTG
	3'-pBiT-C	GACCCTCCACCTCCGCTC
	5'-pBiT-N	GAGCGGAGGTGGAGGCTC
	3'-pBiT-N	CCGACTCTAGAAGATCTGCTAGC

A: Adenine, C: Cytosine, for: Forward, G: Guanine, T: Thymine

2.1.11 Software, databases and online tools

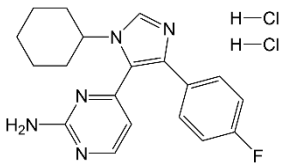
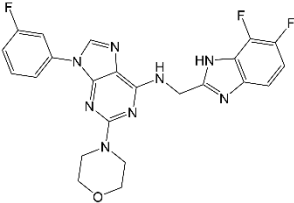
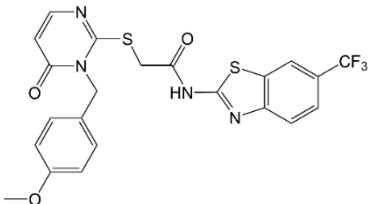
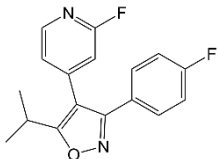
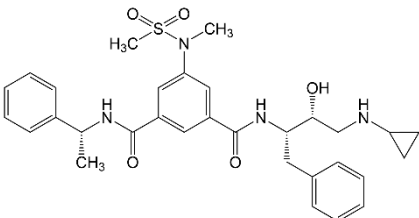
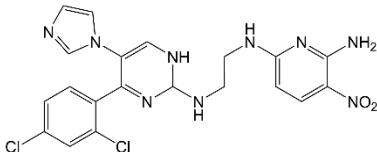
Table 16: Software, databases and online tools.

Term	Software/URL/source
Bio-1D Version 15.08b	Vilber Lourmat, Collégien, France
BLAST®	https://blast.ncbi.nlm.nih.gov/Blast.cgi by National Center for Biotechnology Information (NCBI) (USA)
cellSens Dimensions 2.3 (Build 18,987)	Olympus Europa, Hamburg, Germany
GraphPad Prism 8	GraphPad, San Diego, CA, USA
ICE, Version 1.0.8.1	Berthold Technologies, Bad Wildbad, Germany
ImageJ 1.48v	Wayne Rasband, National Institutes of Health, Bethesda, MD, USA
MaxQuant software suite v.1.6.7.0	Max-Planck-Gesellschaft, Munich, Germany
NEBaseChanger® (version 1.3.3)	New England Biolabs Inc., Ipswich, NY, USA
NEBuilder® Assembly Tool (version 2.6.1)	New England Biolabs Inc., Ipswich, NY, USA
Prism 8	GraphPad, San Diego, CA, USA
PyMOL 2.4	Schroedinger Inc., New York, NY, USA
R (version 4.2.0)	R Foundation for Statistical Computing, Vienna, Austria
R package “colocr”	[5]
R package “imager”	[26]
RStudio (version 2022.02.2)	RStudio PBC, Boston, MA, USA
Scansite 4.1.0	Michael B. Yaffe Laboratory, Koch Institute, MIT, Cambridge, MA, USA
UNICORN 5.31	GE Healthcare Life Sciences, Chicago, IL, USA
UniProt	UniProt Consortium [337]

2.1.12 Inhibitors

Commercially available or published kinase inhibitor, which were used in this study, are shown in Table 17. All inhibitors were stored as 10 mM stocks in DMSO at -20 °C.

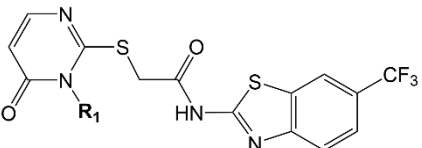
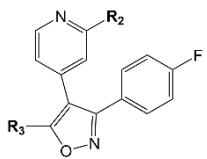
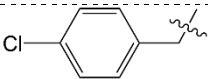
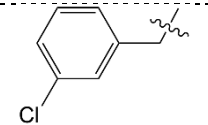
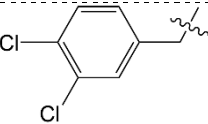
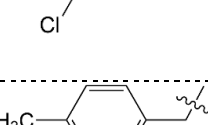
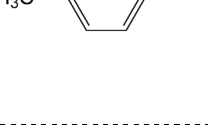
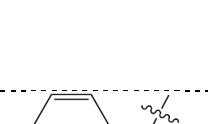
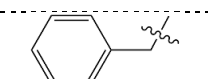
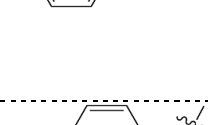
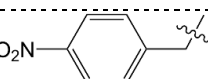
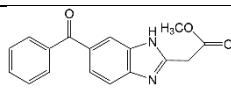
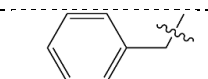
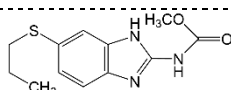
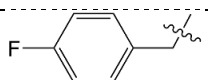
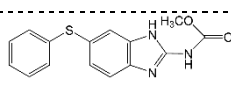
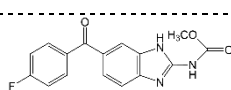
Table 17: Commercially available or published inhibitors used in this study.

Inhibitor/ class	Structure	MW	Target (IC ₅₀)	Ref.
PF-670462		410 g/mol	CK1δ (13 nM), CK1ε (90 nM)	[353]
SR-3029		481 g/mol	CK1δ (44 nM), CK1ε (260 nM)	[32]
Liu-20		507 g/mol	CK1δ (86 nM), CK1ε (723 nM)	[212]
Peifer-1		282 g/mol	p38α (450 nM), CK1δ (230 nM)	[262]
β-secretase inhibitor IV		579 g/mol	BACE1 (15 nM), BACE2 (230 nM)	[87, 318]
CHIR-98014		487 g/mol	GSK3α (650 nM), GSK3β (580 nM)	[281]

BACE1/2: β-site APP cleaving enzyme 1/2, GSK3α/β: Glycogen synthase kinase-3α/β, MW: Molecular weight.

The inhibitors, which were screened for their ability to inhibit CK1 activity were designed, synthesized and provided by Prof. Dr. Christian Peifer (Christian-Albrecht University of Kiel, Kiel Germany; IWP-derived compounds as well as benzimidazole derivatives) and Dr. Andreas Luxenburger (Victoria University of Wellington, Wellington, New Zealand; isoxazole derivatives) (Table 18).

Table 18: Overview of the tested compounds. Tested compounds include IWP-derived inhibitors, benzimidazole derivatives and isoxazole derivatives. *MW*: Molecular weight, *TFA*: Trifluoroacetic acid.

IWP-derived compounds			Isoxazole derivatives		
Name	Structure	MW	Name	Structure	MW
382		265 g/mol	391 (39 in [104])		336 g/mol
383		299 g/mol	392 (+)-48 in [104])		471 g/mol
384		313 g/mol	393 (-)-48 in [104])		471 g/mol
385		490 g/mol	394 (-)-34 in [104])		453 g/mol
386		544 g/mol	395 (+)-34 in [104])		453 g/mol
387		476 g/mol	402 (49 in [104])		300 g/mol
388		521 g/mol	Mebendazole		395 g/mol
389		521 g/mol	Albendazole		265 g/mol
390		494 g/mol	Fenbendazole		299 g/mol
			Flubendazole		313 g/mol

2.1.13 CK1δ-derived peptide library

The CK1δ-derived peptide library contains peptides that were generated out of the aa sequences of human CK1δ (TV1) (Table 19). Each CK1δ-derived peptide consists of 15 aa in length with five aa at each end overlapping with the previous and the next peptides. Each peptide is tagged with biotin at the N-terminal end, which is separated from the CK1δ-specific sequence by a four aa spacer (SGSG). Peptides were synthesized by Dr. Hubert Kalbacher (Interfaculty Institute of Biochemistry, University of Tübingen, Tübingen, Germany), Nico Preising (Core Facility Functional Peptidomics, Ulm University, Ulm, Germany), Synpeptide Co., Ltd (Shanghai Shi, China) and Biomatik (Kitchener, ON, Canada). All synthesized peptides were > 95 % pure as determined by analytical reversed phase high-performance liquid chromatography. Peptides were stored in DMSO at – 20 °C.

Table 19: CK1δ-derived peptide library with corresponding aa sequence.

Peptide	Peptide sequence	Peptide	Peptide sequence
δ-1	Biotin-SGSG- MELRV GNRYR LGRKI	δ-211	Biotin-SGSG- LPWQG LKAAT KRQKY
δ-11	Biotin-SGSG- LGRKI GSGSF GDIYL	δ-221	Biotin-SGSG- KRQKY ERISE KKMST
δ-21	Biotin-SGSG- GDIYL GTDIA AGEEV	δ-231	Biotin-SGSG- KKMST PIEVL CKGYP
δ-31	Biotin-SGSG- AGEEV AIKLE CVKTK	δ-241	Biotin-SGSG- CKGYP SEFAT YLNFC
δ-41	Biotin-SGSG- CVKTK HPQLH IESKI	δ-251	Biotin-SGSG- YLNFC RSLRF DDKPD
δ-51	Biotin-SGSG- IESKI YKMMQ GGVGI	δ-261	Biotin-SGSG- DDKPD YSYLR QLFRN
δ-61	Biotin-SGSG- GGVGI PTIRW CGAEG	δ-271	Biotin-SGSG- QLFRN LFHRQ GFSYD
δ-71	Biotin-SGSG- CGAEG DYNVM VMELL	δ-281	Biotin-SGSG- GFSYD YVFDW NMLKF
δ-81	Biotin-SGSG- VMELL GPSLE DLFNF	δ-291	Biotin-SGSG- NMLKF GASRA ADDAE
δ-91	Biotin-SGSG- DLFNF CSRKF SLKTV	δ-301	Biotin-SGSG- ADDAE RERRD REERL
δ-101	Biotin-SGSG- SLKTV LLLAD QMISR	δ-311	Biotin-SGSG- REERL RHSRN PATRG
δ-111	Biotin-SGSG- QMISR IEYIH SKNFI	δ-321	Biotin-SGSG- PATRG LPSTA SGRLR
δ-121	Biotin-SGSG- SKNFI HRDVK PDNFL	δ-331	Biotin-SGSG- SGRLR GTQEV APPTP
δ-131	Biotin-SGSG- PDNFL MGLGK KGNLV	δ-341	Biotin-SGSG- APPTP LTPTS HTANT
δ-141	Biotin-SGSG- KGNLV YIIDF GLAKK	δ-351	Biotin-SGSG- HTANT SPRPV SGMER
δ-151	Biotin-SGSG- GLAKK YRDAR THQHI	δ-361	Biotin-SGSG- SGMER ERKVS MRLHR
δ-161	Biotin-SGSG- THQHI PYREN KNLTG	δ-371	Biotin-SGSG- MRLHR GAPVN ISSSD
δ-171	Biotin-SGSG- KNLTG TARYA SINTH	δ-381	Biotin-SGSG- ISSSD LTGRQ DTSRM
δ-181	Biotin-SGSG- SINTH LGIEQ SRRDD	δ-391a	Biotin-SGSG- DTSRM STSQN SIPFE
δ-191	Biotin-SGSG- SRRDD LESLG YVLMY	δ-391b	Biotin-SGSG- MSTSQ NSIPF EHHGK
δ-201	Biotin-SGSG- YVLMY FNLGS LPWQG		

2.2 Molecular biological methods

2.2.1 Primer design

All primers were designed using NEBaseChanger[®] (version 1.3.3) for site-directed mutagenesis or NEBuilder[®] Assembly Tool (version 2.6.1) for Gibson Assembly reaction. Designed primers are shown in Table 14.

2.2.2 Site-directed mutagenesis

For the substitution and deletion of aa, the Q5[®] Site-Directed Mutagenesis Kit (see chapter 2.1.3) was used. Reactions were performed according to manufacturer's instructions. The inverse polymerase chain reaction (iPCR) was set up using primers shown in table 14. A total volume of 25 μ L PCR reaction mix included 12.5 μ L Q5 Hot Start High-Fidelity 2x Master Mix, 1.25 μ L 10 μ M forward primer, 1.25 μ L 10 μ M reverse primer, 1 μ L template DNA (10 ng/ μ L) and 9 μ L nuclease-free water. Amplification was performed using cycling conditions as shown in table 20 and checked via agarose gel electrophoresis (chapter 2.2.4).

Table 20: PCR cycling conditions according to Q5[®] Site-Directed Mutagenesis Kit.

Step	Temperature	Time/cycles	
initial denaturation	98 °C	30 s	
denaturation	98 °C	10 s	30 cycles
annealing	50 – 72 °C (depending on the primer pair)	30 s	
extension	72 °C	3 min	
final extension	72 °C	2 min	
hold	4 °C		

Afterwards, 1 μ L of the iPCR product was incubated with 5 μ L 2x KLD reaction buffer, 1 μ L 1x KLD enzyme mix and 3 μ L nuclease-free water for 5 min at RT. Ligated product was transformed in *E. coli* (see chapter 2.3.2). Successful introduction of substitution or deletion was checked via PCR and agarose gel electrophoresis (chapter 2.2.4) or sequencing (chapter 2.2.6).

2.2.3 Gibson Assembly®

2.2.3.1 iPCR and DpnI digestion

All iPCR reactions were performed in a total reaction volume of 50 µL including 3 µL DNA template (10 ng/µL), 10 µL 5x HF-PCR buffer, 5 µL 5 µM forward primer, 5 µL 5 µM reverse primer, 1 µL 10 mM dNTPs, 0.5 µL Phusion® High-Fidelity DNA polymerase (2 U/µL) and 22.5 µL dH₂O. Reactions were mixed and centrifugated briefly. Cycling conditions are shown in Table 21. Successful amplification was verified with agarose gel electrophoresis (see chapter 2.2.4).

Table 21: PCR cycling conditions with Phusion® High-Fidelity DNA polymerase for DNA amplification.

Step	Temperature	Time	
initial denaturation	98 °C	2 min	
denaturation	98 °C	15 s	30 cycles
annealing	50 – 72 °C (depending on the primer pair)	30 s	
extension	72 °C	4.5 min	
final extension	72 °C	10 min	
hold	4 °C		

In order to improve cloning efficiency, iPCR products were incubated with the restriction enzyme *DpnI*. Therefore, 10 µL PCR product were mixed with 1 µL *DpnI* (20 U/µL) and 1 µL CutSmart® buffer and incubated at 37 °C for 1.5 h. The enzyme reaction was stopped by incubation at 80 °C for 20 min. Finally, the reaction mix was used for plasmid ligation (see the following chapter).

2.2.3.2 Ligation via Gibson Assembly®

Gibson Assembly® reaction was performed according to manufacturer's instructions. The reaction was performed in a total volume of 20 µL including 0.02 to 0.5 pmol total amount of plasmid fragments (insert and backbone) and 10 µL 2x Gibson Assembly® Master Mix in dH₂O at 50 °C for 15 min. For clone selection, 5 µL Gibson Assembly® reaction mix was used for bacterial transformation (see chapter 2.3.2).

2.2.4 Agarose gel electrophoresis

PCR products from iPCR (chapter 2.2.2 and 2.2.3) or control PCR (chapter 2.2.5) were analyzed using agarose gel electrophoresis. For separation, 1 % (w/v) agarose gel (in 1x TAE buffer composed of 40 mM Tris-HCl, 20 mM acetic acid, 1 mM EDTA in dH₂O) containing 5 µL Midori Green was used. Samples were loaded with 6x loading dye. Additionally, 5 µL GeneRuler™ 1 kb DNA Ladder was used as MW standard. Electrophoresis was performed in 1x TAE buffer at 120 V for 30 min. Detection of PCR products was performed under UV light using the Fusion FX imaging system.

2.2.5 Control PCR

Prior to DNA sequencing, purified plasmids obtained by small-scale preparation (chapter 2.3.2.1) were checked via PCR and agarose gel electrophoresis. All PCR reactions were performed in a total reaction volume of 25 µL including 4 µL DNA template (10 ng/µL), 2.5 µL 10x PCR buffer, 2.5 µL 1 µM forward primer, 2.5 µL 1 µM reverse primer, 2.5 µL 2.5 mM dNTPs, 0.2 µL taq DNA Polymerase (2 U/µL) and 10.8 µL dH₂O. Reactions were mixed and centrifugated briefly. Cycling conditions are shown in Table 22. Successful amplification was verified with agarose gel electrophoresis.

Table 22: PCR cycling conditions with taq DNA polymerase for DNA amplification.

Step	Temperature	Time	
initial denaturation	95 °C	3 min	
denaturation	95 °C	30 s	30 cycles
annealing	50 – 72 °C (depending on the primer pair)	30 s	
extension	72 °C	2 min	
final extension	72 °C	5 min	
hold	4 °C		

2.2.6 DNA sequencing

Purified DNA samples obtained by large-scale preparation (chapter 2.3.2) were sequenced to confirm mutagenesis via next-generation sequencing using the Mix2Seq Kit from Eurofins. Sequencing results were aligned to corresponding reference sequence using nucleotide-nucleotide basic local alignment search tool

(BLAST[®]) hosted by the National Center for Biotechnology Information [251]. Plasmids were stored at - 20 °C for later use.

2.3 Bacteria methods

2.3.1 Preparation of chemically competent *Escherichia coli*

For the preparation of chemically competent cells, 5 mL LB medium were inoculated with *E. coli* and incubated at 37 °C overnight. The next day, 500 mL LB medium were mixed with the overnight culture and incubated at 37 °C and 120 rpm to an optical density at 600 nm (OD₆₀₀) of 0.4 AU to 0.6 AU. Afterwards, the culture was incubated on ice for 20 min. The cells were centrifuged for 10 min at 3,220 g at 4 °C and the cell pellet was resuspended in 100 mM CaCl₂ solution. The cell suspension was incubated on ice for 1 h and subsequently centrifuged at 3,220 g and 4 °C for 5 min. The cell pellet was resuspended in 5 mL ice cold 85 mM CaCl₂ solution supplemented with 15 % glycerol. Cell suspension was distributed in 50 µL aliquots and stored at -80 °C for later use.

2.3.2 Transformation, amplification, and plasmid isolation

Transformation into chemically competent *E. coli* was performed for clone selection, plasmid amplification and recombinant protein expression. Therefore, 50 µL chemically competent *E. coli* Subcloning Efficiency[™] DH5α (cloning strain) or *E. coli* SHuffle[®] T7 Express or *E. coli* SoluBL21[™] (expression strains) were mixed with plasmid DNA and incubated on ice for 30 min. Afterwards, cells were heat shocked at 42 °C for 45 s followed by incubation on ice for 2 min. Subsequently, 200 µL LB medium (see Table 8) were added and the cell suspension was incubated at 37 °C and 300 rpm for 1 h. Finally, the transformation mix was plated onto agar plates (1.5 % Bacto[™] agar in LB medium with 25 µg/mL kanamycin or 100 µg/mL ampicillin) and incubated at 37 °C overnight.

2.3.2.1 Small-scale preparation of plasmid DNA

A single bacteria colony was inoculated in 3 mL LB medium (containing 25 µg/mL kanamycin or 100 µg/mL ampicillin). Bacteria were incubated at 37 °C and 120 rpm overnight. The next day, 2 mL of the culture was centrifuged at 4 °C and 16,000 g for 10 min and the pellet was resuspended in 200 µL resuspension buffer. Cell lysis

was performed by adding 200 μ L lysis buffer and incubating at RT for 5 min after mixing briefly. Cell lysis was stopped by adding 200 μ L of prechilled neutralization solution. Cell suspension was incubated on ice for 10 min and centrifuged at 4 $^{\circ}$ C and 16,000 g for 10 min. The supernatant was mixed with 600 μ L isopropanol and centrifuged at 4 $^{\circ}$ C and 16,000 g for 10 min. Precipitated DNA was washed with 100 μ L 70 % ethanol and centrifuged at 16,000 g for 5 min. The washed pellet was air dried and resuspended in 20 μ L dH₂O. Purified DNA was further used for control PCR (see chapter 2.2.5).

Resuspension buffer:	50 mM Tris-HCl (pH 8.0), 10 mM EDTA, 100 μ g/mL RNase A in dH ₂ O
Lysis buffer:	1 % (w/v) SDS in 0.2 M sodium hydroxide solution
Neutralization solution:	3 M potassium acetate (pH 5.5)

EDTA: Ethylenediaminetetraacetic acid, SDS: Sodium dodecyl sulfate

2.3.2.2 Large-scale preparation of plasmid DNA

For large-scale preparation of plasmid DNA a single bacteria colony was inoculated in 50 mL LB medium (containing 25 μ g/mL kanamycin or 100 μ g/mL ampicillin) and incubated at 37 $^{\circ}$ C and 120 rpm overnight. The next day, bacteria were harvested by centrifugation at 4 $^{\circ}$ C and 3,220 g for 15 min. For plasmid preparation the QIAfilter Plasmid Kit was used according to manufacturer's instructions. The purified plasmid was further used for DNA sequencing (see chapter 2.2.6).

2.3.3 Bacterial expression of recombinant proteins

For the production of 6xHis-tagged proteins, plasmid pET28a(+) was used, which encodes for T7 promotor, T7 terminator, kanamycin resistance (*kan*), N-terminal 6xHis-tag and a thrombin cleavage site (Figure 11(A)). Glutathione-S transferase (GST)-tagged proteins were encoded on pGEX-6P-3, which carries the genes for ampicillin resistance (*amp*), Lac repressor (*lacI*) and the taq promotor (Figure 11(B)). The protein expression of both plasmids was induced by the addition of isopropyl β -D-1-thiogalactopyranoside (IPTG). All plasmids were synthesized by Biomatik (see Table 11).

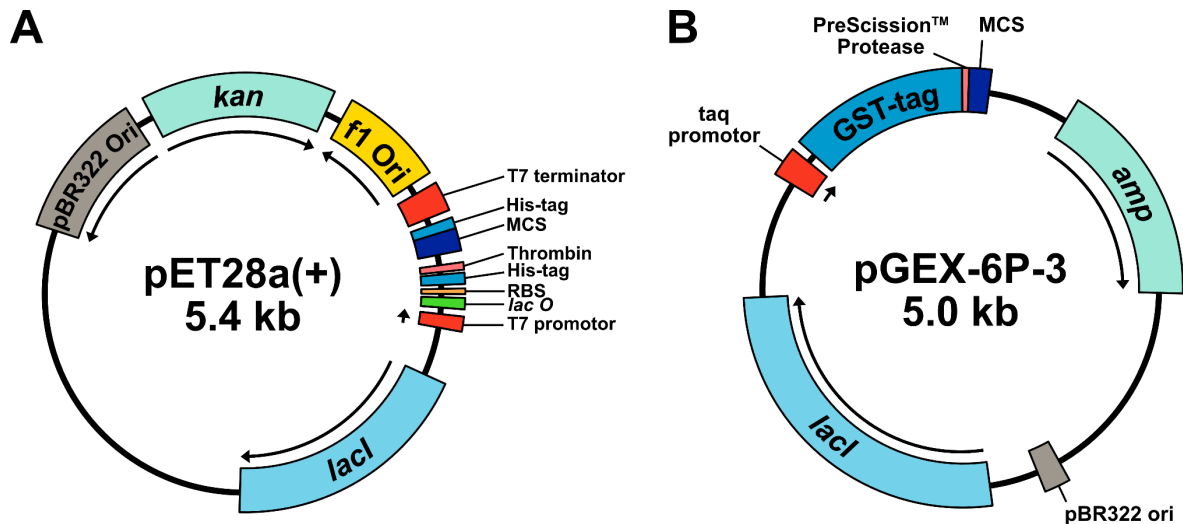


Figure 11: Plasmids for the expression of 6xHis- and GST-tagged proteins. (A) The pET28a(+) vector encodes for T7 promoter, T7 terminator, Lac repressor (*lacI*), resistance gene against kanamycin (*kan*) thrombin cleavage site and the N-terminal 6xHis-tag. **(B)** The pGEX-6P-3 vector carries *lacI* (encoding for the Lac repressor), *taq* promoter, glutathione-S-transferase (GST)-tag and the resistance gene against ampicillin (*amp*). Genes on both plasmids encode for pBR322 origin (origin of replication). *GST*: Glutathione-S transferase, *MCS*: Multiple cloning site, *RBS*: Ribosome binding site.

2.3.3.1 Bacterial expression of 6xHis-APP695 fragments, 6xHis-tau441 and 6xHis-tau383 fusion proteins

For protein expression of 6xHis-APP695 fragments and 6xHis-tau441 proteins, *E. coli* SHuffle® T7 Express containing the plasmid of interest was inoculated in 50 mL LB medium with kanamycin (25 µg/mL) and 2.5 % glucose. Bacteria were incubated at 37 °C and 120 rpm overnight. The following day, the culture was diluted to an OD₆₀₀ of 0.3 AU in 450 mL LB medium with kanamycin (12.5 µg/mL) and 5 % glucose using baffled flasks. Protein expression was induced at an OD₆₀₀ of 0.6 to 0.8 AU with 1 mM (6xHis-tau441 and 6xHis-tau383 proteins) or 2 mM (6xHis-APP695 fragments) IPTG. After 2 to 3 h bacteria were harvested by centrifugation at 4 °C and 3 220 g for 10 min. Cell pellet was stored at -80 °C for later use.

2.3.3.2 Bacterial expression of GST-CK1 and 6xHis-CK1 fusion proteins

For protein expression of GST-CK1 and 6xHis-CK1 fusion proteins, *E. coli* SoluBL21™ were inoculated in 50 mL LB medium with ampicillin (100 µg/mL) or kanamycin (25 µg/mL) and incubated at 37 °C and 120 rpm overnight. The next day, the culture was diluted to an OD₆₀₀ of 0.3 AU in 450 mL LB medium with ampicillin (100 µg/mL) or kanamycin (25 µg/mL). Protein expression was induced at an OD₆₀₀ of 0.6 to 0.8 AU with 1 mM IPTG and bacteria were incubated at 18 °C for 18 h.

Bacteria were harvested by centrifugation at 4 °C and 3,220 g for 10 min and the pellet was stored at -80 °C for later use.

2.3.4 Purification of N-terminal 6xHis-tagged fusion proteins

The use of pET28a(+) encoding for a 6xHis-tagged fusion protein allowed the protein purification via immobilized metal affinity chromatography (IMAC). Purification was performed with either TALON® IMAC beads (see chapter 2.3.4.1) or using a fast protein liquid chromatography (FPLC) purification system (see chapter 2.3.4.2 for soluble proteins or chapter 2.3.4.3 for insoluble proteins). Prior to protein purification, the cell pellet containing the expressed proteins were frozen and thawed three times for freeze-thaw-lyse. The bacteria pellet was resuspended in 10 mL of the respective lysis buffer (see chapter 2.3.4.1, 2.3.4.2 and 2.3.4.3), transferred into a Sorvall tube and incubated for 30 min on ice. After cell lysis, 10 mL lysis buffer were added, and the cell suspension was sonicated for 1 min using the Sonifier 250 to destroy bacterial DNA. After sonication, the cell suspension was centrifuged for 20 min at 15,500 g and 4 °C. For purification of tau proteins, the supernatant was boiled for 10 min at 95 °C. After cooling, the suspension was centrifuged for 10 min 15,500 g at 4 °C.

2.3.4.1 Batch purification of soluble 6xHis-tagged proteins

For batch purification, cleared supernatant was mixed with 800 µL TALON® IMAC resin (50 % (v/v) in PBS) and incubated for 2 h at 4 °C and 25 rpm. After centrifugation for 2 min at 3,220 g, TALON® IMAC beads were washed three times with 1 mL washing buffer. Specific bound proteins were eluted stepwise with 600 µL, 300 µL and 150 µL elution buffer after an incubation time of 20 min, 10 min and 5 min at 4 °C and 25 rpm. As a final step, protein solution (except 6xHis-CK1 isoforms) was dialyzed using PD-10 desalting columns and dialysis solution according to the manufacturer's instructions. Purified protein was adjusted to 10 % glycerol and stored at -80 °C for later use.

Lysis buffer	50 mM sodium phosphate buffer (pH 7.0), 350 mM NaCl, 10 % glycerol, 0.5 % NP-40, 15 mM imidazole, 1 mM benzamidine, 0.25 µg/mL aprotinin, 10 mg lysozyme in dH ₂ O
Washing buffer	50 mM sodium phosphate buffer (pH 7.0), 350 mM NaCl, 10 % glycerol, 15 mM imidazole, 1 mM benzamidine, 0.25 µg/mL aprotinin in dH ₂ O
Elution buffer	50 mM sodium phosphate buffer (pH 7.0), 100 mM NaCl, 350 mM imidazole in dH ₂ O
Dialysis solution	50 mM sodium phosphate buffer (pH 7.0), 100 mM NaCl in dH ₂ O

NP-40: Nonidet-P 40

2.3.4.2 Purification of soluble 6xHis-tagged proteins with automated FPLC

For purification via automated FPLC the cOmplete™ His-Tag purification column was equilibrated manually with 10 column volumes of lysis buffer using the infusion syringe pump Perfusor Secura FT. The cleared sample was filtered and loaded onto the column with a volumetric flow rate of 0.5 mL/min. The loaded column and buffers were connected to the FPLC purification system (Ettan™ LC) and the alarm pressure was set on 1 MPa. The column was washed with lysis buffer until the absorption at 280 nm (UV₂₈₀) reached the baseline followed by ultraviolet (UV) autozero for setting the UV signal to 0 AU. To remove unbound protein, the column was washed with a gradient of lysis buffer and washing buffer within 30 min. Thereafter, the UV signal was set to 0 AU and samples were eluted with a gradient of washing and elution buffer within 3 min. During the elution, 250 µL of the eluted proteins were fractionated into 96-well and protein containing fractions were pooled. As a final step, protein solution (except 6xHis-CK1 isoforms) was dialyzed using PD-10 desalting columns and dialysis solution according to the manufacturer's instructions. Purified protein was adjusted to 10 % glycerol and stored at -80 °C for later use.

Lysis buffer/ (Pump A1)	50 mM sodium phosphate buffer (pH 8.0), 150 mM NaCl, 10 mM imidazole, 1 mM benzamidine, 0.25 µg/mL aprotinin, 10 mg lysozyme in dH ₂ O
Washing buffer/ (Pump B1)	50 mM sodium phosphate buffer (pH 8.0), 1000 mM NaCl, 10 mM imidazole, 1 mM benzamidine, 0.25 µg/mL aprotinin in dH ₂ O
Elution buffer/ (Pump A2)	50 mM sodium phosphate buffer (pH 8.0), 500 mM imidazole, 0.25 µg/mL aprotinin in dH ₂ O
Dialysis solution	50 mM sodium phosphate buffer (pH 7.0), 100 mM NaCl in dH ₂ O

2.3.4.3 Purification of insoluble 6xHis-tagged proteins with automated FPLC

For batch purification of insoluble 6xHis-tagged proteins, the cell pellet was washed twice in 10 mL washing buffer 1 followed by a third washing step in 10 mL washing

buffer 2. Afterwards, the insoluble protein was solubilized and boiled in 10 mL equilibration buffer followed by centrifugation at 15,500 g and 4 °C for 30 min. For purification via automated FPLC the cOmplete™ His-Tag purification column was equilibrated manually with 10 column volumes of equilibration buffer using the infusion syringe pump Perfusor Secura FT. The supernatant was filtered and loaded onto the column with a volumetric flow rate of 0.5 mL/min. The loaded column as well as lysis buffer U, washing buffer and elution buffer were connected to the FPLC purification system (Ettan™ LC) and the alarm pressure was set on 1 MPa. The column was washed with equilibration buffer until UV_{280} reached the baseline followed by UV autozero for setting the UV signal to 0 AU. For on-column refolding, urea was removed with a gradient of equilibration and lysis buffer within 960 min and a flow rate of 0.1 mL/min. The refolded protein was eluted with a gradient of lysis and elution buffer within 3 min and a flow rate of 0.5 mL/min. During the elution, 250 μ L of the eluted proteins were fractionated into 96-well and protein containing fractions were pooled. As a final step, buffer exchange and protein concentration were performed as described in chapter 2.3.6. Purified protein was adjusted to 10 % glycerol and stored at -80 °C for later use.

Lysis buffer U	50 mM sodium phosphate buffer (pH 8.0), 150 mM NaCl, 10 mM imidazole, 1 mM benzamidine, 0.25 μ g/mL aprotinin, 0.1 % SDS, 0.5 % glycerol, 10 mg lysozyme in dH ₂ O
Washing buffer 1	50 mM sodium phosphate buffer (pH 8.0), 2 M urea, 2 % Triton-X 100, 0.1 % SDS, 0.5 % glycerol in dH ₂ O
Washing buffer 2	50 mM sodium phosphate buffer (pH 8.0), 0.1 % SDS, 0.5 % glycerol in dH ₂ O
Equilibration buffer	50 mM sodium phosphate buffer (pH 8.0), 8 M urea, 1000 mM NaCl, 10 mM imidazole, 1 mM benzamidine, 0.25 μ g/mL aprotinin, 0.1 % SDS, 0.5 % glycerol in dH ₂ O
Elution buffer	50 mM sodium phosphate buffer (pH 8.0), 100 mM NaCl, 250 mM imidazole, 0.25 μ g/mL aprotinin, 0.1 % SDS, 0.5 % glycerol in dH ₂ O

SDS: Sodium dodecyl sulfate

2.3.5 Purification of GST-tagged fusion proteins

The use of pGEX-6P-3 encoding for a GST-tagged fusion protein allowed the protein purification via affinity chromatography. Purification was performed with either Glutathione Sepharose® beads (see chapter 2.3.5.1) or using the FPLC purification system (see chapter 2.3.5.2). Prior to protein purification, the cell pellet containing the expressed proteins were frozen and thawed three times for freeze-thaw-lyse. The bacteria pellet was resuspended in 10 mL of the respective lysis buffer (see

chapter 2.3.5.1 and 2.3.5.2), transferred into a Sorvall tube and incubated for 30 min on ice. After cell lysis, 10 mL lysis buffer were added, and the cell suspension was sonicated for 1 min using the Sonifier 250 to destroy bacterial DNA. After sonication, the cell suspension was centrifuged for 20 min at 15,500 g and 4 °C.

2.3.5.1 Batch purification

For batch purification of GST-tagged proteins, samples were mixed with 600 µL Glutathione Sepharose® (50 % (v/v) in PBS) and incubated rotating at 4 °C overnight. The following day, the suspension was centrifuged for 2 min at 3,220 g and 4 °C. Beads were washed with 1 mL washing buffer 1 and centrifuged for 1 min at 16,000 g and 4 °C. The washing step was repeated two times with washing buffer 1 and two times with washing buffer 2. Specific bound proteins were eluted stepwise with 600 µL, 300 µL and 150 µL elution buffer after an incubation time of 20 min, 10 min and 5 min at 4 °C and 25 rpm. In the final step, protein solution (except GST-CK1 isoforms) was dialyzed using PD-10 desalting columns and dialysis solution according to the manufacturer's instructions. Purified protein was adjusted to 10 % glycerol and stored at -80 °C for later use.

Lysis buffer	20 mM Tris-HCl (pH 7.6), 150 mM NaCl, 0.5 % NP-40, 10 % glycerine, 1 mM EDTA, 1 mM EGTA, 1 mM benzamidine, 0.25 µg/mL aprotinin, 1 mM DTT, 10 mg lysozyme in dH ₂ O
Washing buffer 1	20 mM Tris-HCl (pH 7.6), 330 mM NaCl, 0.5 % NP-40, 10 % glycerine, 1 mM EDTA, 1 mM EGTA, 1 mM benzamidine, 0.25 µg/mL aprotinin, 1 mM DTT in dH ₂ O
Washing buffer 2	20 mM Tris-HCl (pH 7.6), 50 mM NaCl, 10 % glycerine, 1 mM EDTA, 0.25 µg/mL aprotinin in dH ₂ O
Elution buffer	50 mM Tris-HCl (pH 7.0), 1 mM EDTA, 0.25 µg/mL aprotinin, reduced glutathione in dH ₂ O
Dialysis solution	50 mM Tris-HCl (pH 7.0), 1 mM EDTA in dH ₂ O

DTT: Dithiothreitol, EDTA: Ethylenediaminetetraacetic acid, EGTA: Ethylene glycol tetraacetic acid, NP-40: Nonidet-P 40

2.3.5.2 Purification with automated FPLC

For purification via automated FPLC the GSTrap™ FF column was equilibrated manually with 10 column volumes of lysis buffer using the infusion syringe pump Perfusor Secura FT. The cleared sample was filtered and loaded onto the column with a volumetric flow rate of 0.5 mL/min. The loaded column and buffers were connected to the FPLC purification system (Ettan™ LC) and the alarm pressure was set on 1 MPa. The column was washed with lysis buffer until the absorption at UV₂₈₀

reached the baseline followed by UV autozero for setting the UV signal to 0 AU. To remove unbound protein, the column was washed with lysis buffer until the UV signal reached base line. Thereafter, the UV signal was set to 0 AU and samples were eluted stepwise with elution buffer. During the elution, 250 μ L of the eluted proteins were fractionated into 96-well and protein containing fractions were pooled. As a final step, protein solution (except GST-CK1 isoforms) was dialyzed using PD-10 desalting columns and dialysis solution according to the manufacturer's instructions. Purified protein was adjusted to 10 % glycerol and stored at -80 °C for later use.

Lysis buffer	20 mM Tris-HCl (pH 7.6), 150 mM NaCl, 0.5 % NP-40, 10 % glycerol, 1 mM EDTA, 1 mM EGTA, 1 mM benzamidine, 0.25 μ g/mL aprotinin, 1 mM DTT, 10 mg lysozyme in dH ₂ O
Elution buffer	50 mM Tris-HCl (pH 7.6), 5 mM reduced glutathione, 0.25 μ g/mL aprotinin, 1 mM EDTA in dH ₂ O
Dialysis solution	50 mM Tris-HCl (pH 7.0), 1 mM EDTA in dH ₂ O

DTT: Dithiothreitol, EDTA: Ethylenediaminetetraacetic acid, EGTA: Ethylene glycol tetraacetic acid, NP-40: Nonidet-P 40

2.3.6 Protein concentration

Protein concentration was performed to achieve higher protein amounts of APP695 fragments N-APP and APP-C. Therefore, Amicon Ultra-0.5 mL centrifugal filters were used with a nominal MW limit of 3 kDa. Samples were concentrated according to the specifications provided by the manufacturer with the dialysis solution. After concentration, proteins solutions were adjusted to 10 % glycerol and stored at -80 °C for later use.

Dialysis solution	50 mM sodium phosphate buffer (pH 7.0), 1 mM EDTA in dH ₂ O
--------------------------	--

EDTA: Ethylenediaminetetraacetic acid

2.4 Protein biochemical methods

2.4.1 Cell lysis and quantification of protein concentration

Cells were washed with 20 mM Tris-HCl (pH 7.6) supplemented with 140 mM NaCl. Cell lysis was performed in RIPA lysis buffer supplemented with phosphatase inhibitor cocktail and cOmplete™ protease inhibitor cocktail on ice. After an incubation time of 30 min cell lysates were centrifuged at 16,000 g and 4 °C for

10 min. Concentration of total protein was determined using Pierce™ BCA protein assay kit according to manufacturer's protocol.

RIPA lysis buffer: 50 mM Tris-HCl (pH 7.4), 150 mM NaCl, 0.5 % sodium deoxycholate, 1 % NP-40, 1 mM EDTA, 2 mM PMSF, 2 mM PNT, 1 mM Na₃VO₄, 1 mM NaF in dH₂O

EDTA: Ethylenediaminetetraacetic acid, NP-40: Nonidet-P 40, PMSF: Phenylmethylsulfonyl fluoride, PNT: 1,10-phenanthroline

2.4.2 Resolution of proteins by SDS polyacrylamide gel electrophoresis (SDS-PAGE)

The electrophoretic separation of proteins was performed under denaturing conditions in discontinuous gel electrophoresis. Proteins were separated in SDS-polyacrylamide gels (7.5 % to 12.5 %) composed of an upper gel (stacking gel) and lower gel (separating) gel. Before loading, proteins were mixed with 5x SDS sample buffer and heated to 99 °C for 5 min. Electrophoresis was performed for approximately 1 h at 180 V in 1x running buffer.

Upper gel: 300 mM Tris-HCl (pH 6.6), 4.4 % (w/v) acrylamide, 0.1 % (w/v) APS, 2 % (w/v) SDS, 0.06 % (v/v) TEMED in dH₂O

Lower gel (12.5 %): 300 mM Tris-HCl (pH 8.8), 7.5 – 12.5 % (w/v) acrylamide, 0.6 % (w/v) APS, 2 % (w/v) SDS, 0.2 % (v/v) TEMED in dH₂O

10x running buffer: 250 mM Tris-HCl, 1.9 M glycine, 1 % (w/v) SDS in dH₂O

5x SDS sample buffer: 250 mM Tris-HCl (pH 6.8), 25 % (v/v) β-mercaptoethanol, 50 % (v/v) glycerine, 10 % (w/v) SDS, 0.5 % (w/v) bromophenol blue in dH₂O

APS: Ammonium persulfate, SDS: Sodium dodecyl sulfate, TEMED: N,N,N',N'-tetramethyl ethylenediamine

2.4.3 Coomassie staining and quantification of protein concentration

Proteins separated by SDS-PAGE (see chapter 2.4.2) were stained with Coomassie Brilliant Blue staining solution for 15 min. Subsequently, the stained gels were destained with destaining solution for at least 45 min. For documentation, gels were photographed using the imaging system Fusion FX and the white light conversion screen for colorimetric stained protein gels. For calculation of protein amounts, the software ImageJ was used.

Coomassie Brilliant Blue staining solution: 0.15 % (w/v) Coomassie Brilliant Blue R-250, 45 % (v/v) isopropanol, 10 % (v/v) acetic acid in dH₂O

Destaining solution: 10 % (v/v) isopropanol, 10 % (v/v) acetic acid in dH₂O

2.4.4 Western blotting (immunoblotting)

Cell lysates were separated on SDS gels and transferred to a polyvinylidene fluoride (PVDF) membrane using a wet Western blot system at 60 V for 1 h. After the protein transfer, unspecific binding sites were blocked by incubating the membranes either with 5 % bovine serum albumin (BSA) or 5 % milk in TBST buffer at RT for 1 h. Proteins were detected by incubating membranes with primary antibodies diluted in blocking buffer at 4 °C overnight (see Table 13). After washing the membrane three times in TBST buffer for 10 min, the membrane was incubated with the secondary horseradish-peroxidase (HRP)-conjugated antibody (see Table 13) for 1 h under constant rocking at RT. After three more washing steps, detection was performed using the enhanced chemiluminescence (ECL) solution and the Fusion FX imaging system.

Transfer buffer	25 mM Tris-HCl (pH 8.3), 192 mM glycine in dH ₂ O
TBS buffer	10 mM Tris-HCl (pH 8.0), 150 mM NaCl in dH ₂ O
TBST buffer	0.1 % (v/v) Tween in TBS
ECL solution:	50 % ECL solution A: 100 mM Tris-HCl (pH 8.5), 2.5 mM luminol, 400 μM p-coumaric acid in dH ₂ O 50 % ECL solution B: 100 mM Tris-HCl (pH 8.5), 13 mM H ₂ O ₂ in dH ₂ O

ECL: Enhanced chemiluminescence, TBS: Tris-buffered saline

2.4.5 *In vitro* kinase assay

Generally, *in vitro* kinase assays were performed in a total reaction volume of 15 μL containing the substrate (APP695 fragments, tau or α-casein), the recombinant kinase (GST-tagged CK1 or 6xHis-tagged CK1 isoforms), radioactively labeled [γ -³²P]-ATP (2 μCi per reaction) and 1x kinase buffer. All kinase reactions were started simultaneously by centrifugation, incubated at 30 °C and finally stopped by the addition of 5x SDS sample buffer and boiling at 99 °C for 5 min. Phosphorylated proteins were separated via SDS-PAGE (see chapter 2.4.2) and gels were stained with Coomassie Brilliant Blue and dried. Stained bands containing [³²P]-labeled proteins were identified by autoradiography, excised and phosphate incorporation was quantified by Cherenkov counting.

Kinase buffer (10x):	250 mM Tris-HCl (pH 7.0), 100 μM ATP, 100 mM MgCl ₂ , 1 mM EDTA in dH ₂ O
-----------------------------	---

ATP: Adenosine triphosphate, EDTA: Ethylenediaminetetraacetic acid

For the identification of peptides inhibiting the phosphorylation of APP695 fragments or tau, 2 μM substrate (APP695 fragments or tau), 20 μM CK1 δ -derived peptide (in DMSO) and 10 nM GST-CK1 δ or 70 nM 6xHis-CK1 δ in 1x kinase buffer were incubated at 30 °C for 30 min. For control, same reactions were performed using 2 μM α -casein. Data were normalized to DMSO controls and statistical analysis (see chapter 2.9) were performed using GraphPad Prism 8.

Prior to the characterization of new CK1 δ -specific SMIs, standard conditions were established according to the following chapters.

2.4.5.1 Establishment of the standard conditions to determine IC_{50} values of SMIs

The potencies of SMIs targeting various enzymes are usually compared by their IC_{50} values. However, the comparability of IC_{50} values can be limited due to different reaction set-ups. To overcome this problem, the enzyme-specific inhibitor constant (K_i) was determined, which is a parameter independent of the experimental set-up and universally comparable. To determine comparative values, such as IC_{50} and K_i , important basics of enzyme kinetics had to be considered. These included the determination of the initial velocity (V_{init}) region of the enzyme reaction and the determination of the Michaelis constant (K_m) of ATP and K_i under previously determined V_{init} conditions (Figure 12).

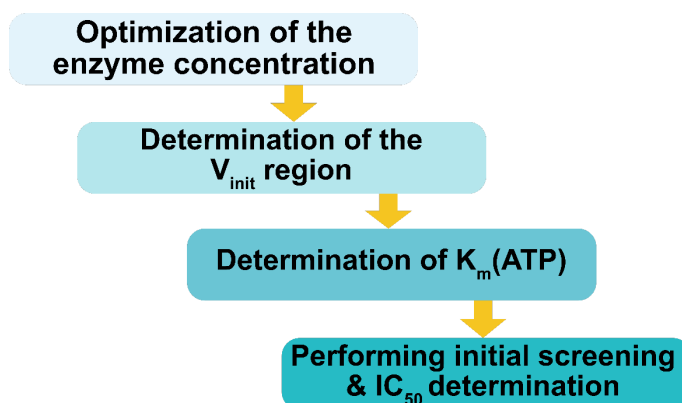


Figure 12: Workflow for the establishment of standard conditions for *in vitro* kinase assays using SMIs. The workflow consists of four steps resulting in the generation of major parameters, which are essential to obtain valid IC_{50} values and to calculate K_i values of ATP-competitive inhibitors. The figure was modified from [288], which is licensed under a Creative Commons Attribution 4.0 international license (CC BY 4.0), <https://creativecommons.org/licenses/by/4.0/>. IC_{50} : Half maximal inhibitory concentration, $K_m(ATP)$: Michaelis constant of ATP, V_{init} : Initial velocity.

In the following chapters, the steps to establish standard conditions to determine IC_{50} and K_i values of SMIs are described.

A Determination of V_{init}

V_{init} describes the linear part of the product-over-time progression curve, which is characterized by time-dependent increase in product (phosphorylated substrate) and a constant slope presenting the highest enzyme velocity, which is possible [48]. Determining V_{init} by testing different enzyme concentrations was necessary for correct determination of kinetic parameters. For the determination of V_{init} , *in vitro* kinase reactions were performed with 7, 70 and 335 nM kinase and 10 μ M ATP. Phosphorylation of 2.5 μ M α -casein was monitored within 60 min.

B Determination of K_m under V_{init}

Prior to the calculation of K_i , K_m of ATP ($K_m(\text{ATP})$) has been determined. Therefore, the previously defined conditions of the V_{init} region were used for testing different ATP concentrations in a range from 0.5 to 5 times K_m while maintaining the phosphorylated substrate (α -casein) under saturating conditions. As the value of $K_m(\text{ATP})$ was unknown, the determination of $K_m(\text{ATP})$ was performed in an iterative process, where the range of ATP concentrations were evaluated and re-adjusted. Therefore, dilution series ranging from 0.5 to 100 μ M ATP were prepared with DMSO. In kinase reactions, 2 μ L diluted ATP, 2.5 μ M α -casein and previously determined amounts of GST-tagged CK1 α , CK1 δ or CK1 ϵ were used in a total reaction volume of 15 μ L. Obtained data was used to calculate the kinase velocity (V). Calculated V was plotted over the used ATP concentrations and fitted to the Michaelis-Menten model with GraphPad Prism 8. $K_m(\text{ATP})$ was calculated as the ATP concentration needed to reach half-maximal velocity.

C Initial screening, determination of IC_{50} values and calculation of K_i

The initial screening was performed under established standard conditions with 10 μ M inhibitor and DMSO as control. To determine CK1 isoforms specificity, CK1 isoforms α , δ and ϵ were used as kinases. Data were normalized to DMSO control. Potent inhibitors were further characterized for their IC_{50} values. Therefore, inhibitor concentrations in a range from 0.002 μ M to 10 μ M were tested under established standard conditions. DMSO served as control. Data were normalized to DMSO controls and IC_{50} determination as well as statistical analysis (see chapter 2.9) were performed using GraphPad Prism 8.

After the determination of IC_{50} values under established standard conditions, K_i was calculated according to the Cheng-Prusoff equation [379] (see equation (1)).

$$K_i = \frac{IC_{50}}{\left(\frac{[S]}{K_m(ATP)} + 1\right)} \quad (1)$$

Using ATP competitive inhibitors, the inhibitory constant of competitive inhibitors (K_{ic}) can be calculated if the ATP concentration ($[S]$) used in the IC_{50} determination equals the $K_m(ATP)$ (see equation (2)).

$$[S] = K_m(ATP) \quad (2)$$

Under these conditions, equation (2) can be inserted into equation (1). Then, K_{ic} is defined as half of the tested IC_{50} value (see equation (3)).

$$K_{ic} = \frac{IC_{50}}{2} \quad (3)$$

As consequence, the use of ATP concentrations equal to $K_m(ATP)$ under V_{init} conditions allows direct conversion of the calculated IC_{50} value to enzyme-specific parameter K_{ic} .

2.4.6 Two-dimensional phosphopeptide analysis

In vitro phosphorylated proteins (see chapter 2.4.5) were separated via SDS-PAGE and subsequently transferred onto a PVDF membrane (see chapter 2.4.2 and 2.4.4). Protein bands of interest were detected via autoradiography, excised, and incubated with 5 % (w/v) polyvinylpyrrolidone (in 10 mM acetic acid) at 37 °C for 30 min. Proteins were extensively washed with 50 mM ammonium bicarbonate buffer and afterwards digested with 10 µg TPCK-trypsin supplemented with 10 µg BSA at 37 °C for 7 h. Samples were lyophilized overnight and oxidized with performic acid on ice for 2 h. Oxidation was stopped by the addition of 500 µL dH₂O and samples were lyophilized overnight. The next day, radioactively labeled phosphopeptides were measured via Cherenkov counting and resuspended in pH 3.6 buffer to obtain 3,333 cpm/µL. 3 µL of the resuspended sample were spotted on thin-layer cellulose plates. To track peptide migration, 1 µL marker was applied. Phosphopeptides were separated by electrophoresis at pH 1.9 followed by ascending chromatographic separation in chromatography buffer. Plates were dried and radioactively labeled phosphopeptides were visualized by autoradiography.

Formic acid:	10 % (v/v) H ₂ O ₂ , 90 % (v/v) formic acid
pH 3.6 buffer:	acetic acid/pyridine/dH ₂ O (10:1:289)
pH 1.9 buffer:	formic acid/acetic acid/pyridine/dH ₂ O (60:12.5:2.5:925)
Chromatograph buffer:	n-butanol/acetic acid/pyridine/dH ₂ O (75:15:50:60)
Marker:	5 mg/mL dinitrophenyl-lysine, 1 mg/mL xylene cyanol FF

2.4.7 LC-MS/MS analysis

In vitro phosphorylated tau441 was separated via SDS-PAGE and stained with Coomassie Brilliant Blue staining solution. Mass spectrometric analysis was performed by the Proteome Center at the University of Tübingen in Germany. Separated proteins were digested with trypsin [41], desalted using a C18 StageTips [272] and applied to LC-MS/MS analysis. Mass spectrometric analysis was performed on an Easy-nLC 1200 UHPLC connected to a QExactive HF Orbitrap mass spectrometer [300]. Peptides were eluted by using a segmented gradient and a flow rate of 200 nL/min within 60 min. For fragmentation with HCD, seven most intensive peaks were selected. Obtained data were processed using the MaxQuant software suite v.1.6.7.0 [81] and search for variable modification phosphorylation (serine, threonine and tyrosine) was enabled. The data was searched against human UniProt database (containing 96,817 entries) by using the Andromeda search engine [82]. For the identification of CK1 δ -specific tau phosphorylation sites, phosphorylation sites were not globally normalized to the proteome.

2.4.8 Tau aggregation and Thioflavin S assay

Tau441 was phosphorylated *in vitro* as described in chapter 2.4.5 with 1,000 μ M ATP and 300 nM GST-CK1 δ at 30 °C for 30 min. After the reaction, the reaction mix was cleared by centrifugation for 10 min at full speed and 4 °C. Induction of cross- β structure formation and thus, tau aggregation was performed with 4 μ M phosphorylated and non-phosphorylated tau441 (CTRL) in 100 mM Tris-HCl (pH 6.8) and 150 μ M arachidonic acid solved in ethanol [25, 69]. Tau aggregation was monitored after the addition of Thioflavin S (ThS) by measuring the excitation wavelength at 430 nm and the emission wavelength at 480 nm using a TriStar² LB 942 multimode plate reader at intervals of 1.5 min within a period of 30 min. Obtained data were fit to one-phase association exponential model via GraphPad Prism 8.

2.5 Cell biological methods

2.5.1 Freezing and thawing cells

A vial containing approximately 10^6 cells was thawed at 37 °C and mixed with 9 mL growth medium (see Table 7). Cell suspension was centrifuged at 500 x g for 3 min and the supernatant was removed. Cells were resuspended in fresh growth medium and seeded into culture dish. The next day, medium was exchanged. For freezing cells, sub-confluent cells were washed with 1x PBS and detached with either trypsin-EDTA or Accutase solution. Cell suspension was centrifuged at 500 x g for 3 min. The cell pellet was resuspended in freezing medium (10 % DMSO in growth medium) to attain a concentration of 10^6 cells/mL. Cells were frozen at – 80 °C and stored in liquid nitrogen.

2.5.2 Maintenance of mammalian cell lines

All used cell lines were cultured at 37 °C in a 5 % CO₂ humidified atmosphere.

2.5.2.1 HEK293 and HEK293T

HEK293 and HEK293T cells were maintained in DMEM with 10 % (v/v) FCS and 1 % (v/v) penicillin-streptomycin (Pen/Strep) solution. HEK293(T) cells were passaged as sub-confluent monolayers every two to four days by incubating the cells with trypsin-EDTA solution for 5 min at 37 °C. The reaction was stopped by the addition of growth medium. Cells were diluted and seeded into fresh culture dishes.

2.5.2.2 Human neural progenitor cells (hNPCs)

Immortalized hNPCs (ReNcell[®] VM) were expanded in proliferation medium (see Table 8) on Matrigel-coated flasks or plates. For differentiation, the medium was changed to differentiation medium, which was prepared the same way as the proliferation medium without adding bFGF and EGF. Every three to four days, confluent hNPCs were washed with 1x PBS and incubated with Accutase for 3 min at 37 °C. After detachment, cells were centrifuged at 500 x g for 3 min and the supernatant was removed. Cells were diluted in proliferation medium and seeded into fresh culture dishes.

2.5.3 Generation of the “Alzheimer’s-in-a-dish” cell culture model

The “Alzheimer’s in-a-dish” model is a 3D human neural cell culture system for mimicking AD pathology based on Choi et al. [70] and Kim et al. [181], exhibiting key events in the AD pathogenesis, such as amyloid plaques and NFTs. An overview of the generation of the “Alzheimer’s-in-a-dish” cell culture model is shown in Figure 13.

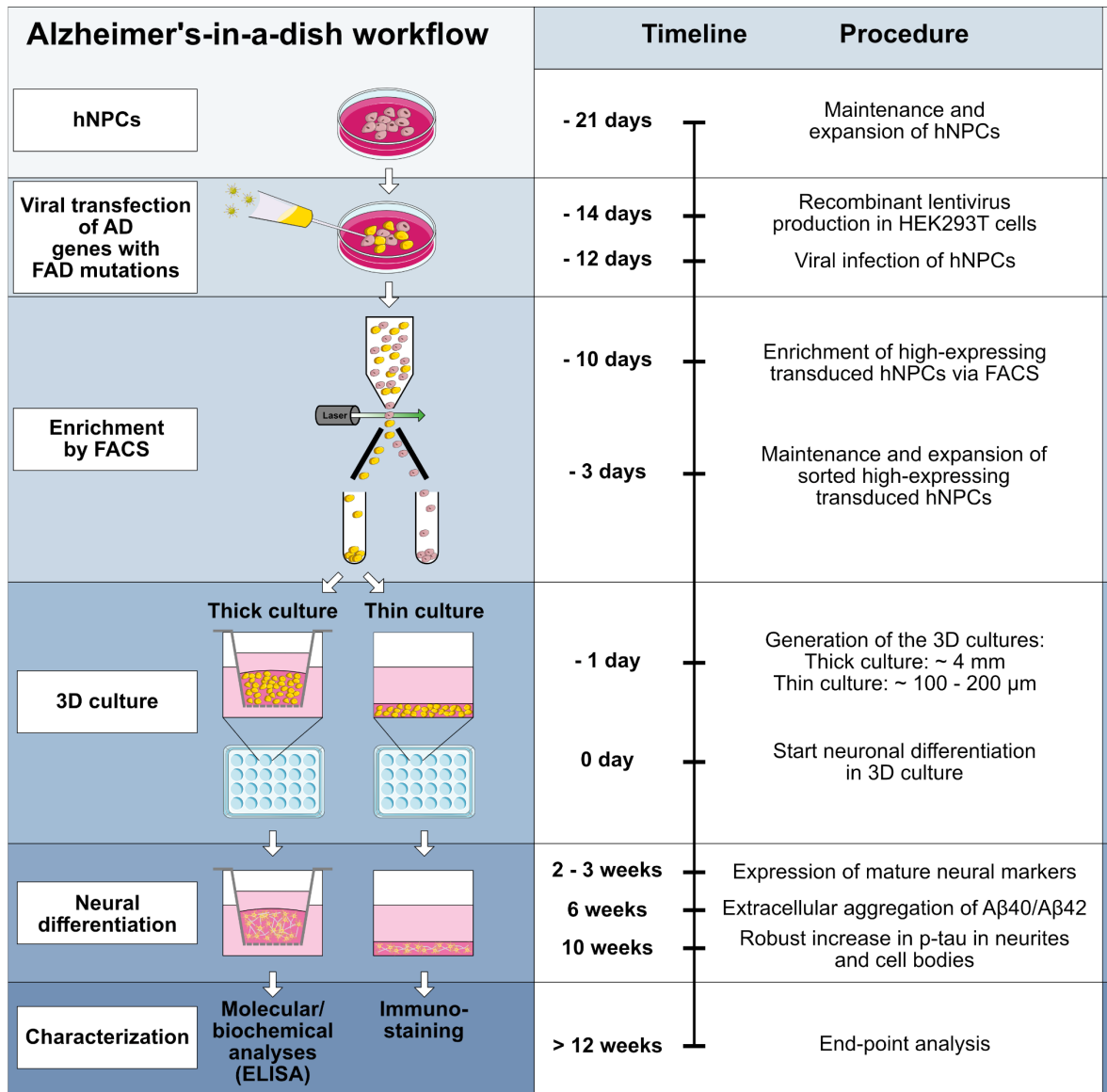


Figure 13: Overview of the generation of the “Alzheimer’s-in-a-dish” cell culture model. The experimental procedure starts with the generation of the hNPC cell line virally transfected with the AD-associated genes APP and PSEN1 with FAD mutations. Positive transfected and highly APP and PSEN1 expressing hNPCs were enriched based on GFP and mCherry signals by fluorescence-activated cell sorting (FACS). On the right side, a timeline of the experimental procedure is shown describing each step of the generation of the “Alzheimer’s-in-a-dish” model. The Alzheimer’s-in-a-dish workflow is based on [70, 181]. AD: Alzheimer’s disease, FACS: Fluorescence activated cell sorting, FAD: Familial Alzheimer’s disease, hNPCs: Human neural progenitor cells.

The cell culture system involves genetically engineered immortalized hNPCs over-expressing mutated FAD genes (APP (K670N/M671L, V717I) and PSEN1 (Δ E9)), resulting in the production of high levels of A β 40, A β 42 and elevated A β 42/A β 40 ratio compared to control hNPCs [71]. The use of 3D cultures embedded in Matrigel closely mimics *in vivo* conditions and inhibits the removal of secreted A β peptides during medium exchange compared to 2D grown cells. Another key aspect of the “Alzheimer’s-in-a-dish” model is the induction of tau pathology without utilizing tau mutations associated with frontotemporal dementia [71].

2.5.3.1 Recombinant lentivirus production with HEK293T cells

For lentiviral production the envelope and packaging vectors pMD2.G and psPAX2, kindly provided by Prof. Dr. Cagatay Günes (from Ulm University), as well as the lentiviral DNA constructs pCSCW-PSEN1(Δ E9)-IRES-mCherry and pCSCW-APPSL-IRES-GFP encoding human PSEN1 (Δ E9) and mCherry or full-length human APP695 bearing a K670N/M671L/V717I mutation (also known as Swedish and London mutation) and GFP, respectively, which were kindly provided by Prof. Dr. Doo Kim (from Massachusetts General Hospital), were used. For lentiviral transfection, 1.8 μ g pSPAX2, 300 ng pMD2.G and 3 μ g pCSCW-PSEN1(Δ E9)-IRES-mCherry or pCSCW-APPSL-IRES-GFP were gently mixed with 30 μ L polyethylenimine and 500 μ L serum-free medium and incubated for 20 min at RT. The transfection solution was added dropwise to 50 % confluent (corresponding approximately to 6×10^6) HEK293T cells in a 10 cm culture. After cells were incubated for 24 h at 37 °C, the transfection solution was exchanged with 5 mL medium containing Pen/Strep and FCS. 48 h after transfection, lentiviral-containing supernatants were collected and stored at 4° C until next day. Additional 5 mL were added and cells were incubated for further 24 h. Virus-harvesting was repeated as described before and supernatants from both days were pooled, filtered and stored at -80 °C for later use.

2.5.3.2 Viral infection of hNPCs

For the generation of hNPCs stably expressing APPSL/GFP and PSEN1(Δ E9)/mCherry, hNPCs were seeded into a 6-well one day in advance so that they reached a confluency of 80 % (approximately 6×10^6 cells) the next day. At 80 % confluency, hNPCs were incubated with 10 μ g/mL polybrene and lentiviral

particles generated by using pCSCW-PSEN1(Δ E9)-IRES-mCherry. After 24 h incubation, cells were washed twice with PBS and covered with fresh proliferation medium. The next day, transduced cells were enriched by using fluorescence activated cell sorting (FACS) (see chapter 2.5.3.3). To generate cells expressing both AD-associated proteins, PSEN1(Δ E9)/mCherry and APPSL/GFP, enriched hNPCs expressing PSEN1(Δ E9)/mCherry were infected again with lentiviral particles generated by using pCSCW-APPSL-IRES-GFP. After 24 h incubation, cells were washed twice with PBS and then supplied with fresh proliferation medium. Transduced cells were again enriched by using FACS.

2.5.3.3 *Enrichment of high-expressing transduced hNPCs via FACS*

For the enrichment of high-expressing transduced hNPCs with FACS, transduced cells were detached as described in chapter 2.5.2. The cell pellet was resuspended in 4 mL PBS. The cell concentration was determined using an automated LUNATM cell counter. Cells were centrifuged, supernatant was removed, and the cells were resuspended in ice-cold sorting medium (see Table 8) to a cell concentration of 10^7 cells/mL. Prior to sorting, cells were singularized using a cell-strainer mesh (70 μ m). Transduced hNPCs were sorted by using a FACSAria cell sorter provided by the Core Facility Cytometry at Ulm University. Cells were sorted by using mCherry and/or GFP channels. Sorted and enriched cells were expanded in proliferation medium.

2.5.4 **Cell metabolic activity assay**

The cytotoxic effects of SMIs and peptides were determined by the cell metabolic activity assay measuring the conversion of MTT to formazan via absorption. For MTT cytotoxicity assays, transduced hNPCs were seeded in Matrigel-coated 96-well plates at a concentration of 5×10^3 cells/mL in differentiation medium. Following 2D differentiation for six days, differentiated cells were treated with 0.1 to 10 μ M of CK1 δ -derived peptides, SMIs or DMSO as control and were incubated for another 24 h. The next day, 10 μ L of a 5 mg/mL MTT solution were added under sterile conditions to each well of the 96-well plates, and the plates were incubated for 4 h under culture conditions. Subsequently, the supernatant was removed and purple formazan crystals, which were generated in metabolically active cells, were

dissolved in 100 μ L of acidic isopropanol per well at RT for 30 min. Color change was measured at 590 nm using a TriStar² LB 942 multimode plate reader.

MTT solution: 5 mg/mL MTT in sterile PBS

Acidic isopropanol: 10 % 1 M hydrochloric acid in isopropanol

MTT: 3-(4,5-dimethylthiazol-2-yl)-2,5-diphenyltetrazolium bromide, PBS: Phosphate-buffered saline

2.5.5 3D cell culture of transduced hNPCs and treatment

For 3D cultivation, transduced and sorted hNPCs were properly resuspended in ice-cold differentiation medium and stored on ice. For thick-layer 3D culture (~ 4 mm thickness), Matrigel was added to the ice-cold cell suspension at a dilution of 1:2 to obtain a final cell concentration of 1×10^7 cells/mL. Afterwards, 300 μ L of the Matrigel/cell suspension were transferred into tissue culture inserts inserted into a 24-well. For thin-layer 3D culture (~ 100 to 200 μ m), the Matrigel/cell suspension was diluted 1:10 with ice-cold differentiation medium to a final cell concentration of 1×10^6 cells/mL and 600 μ L the diluted Matrigel/cell suspension was plated in a 24-well. Cells were incubated at 37 °C overnight. The next day, 0.5 mL fresh differentiation medium per insert and well was added, respectively. Cells were differentiated for six days and treated with peptides or SMIs for up to six or twelve weeks to observe amyloid plaque formation or tau pathology, respectively. Treatment was carried out by incubating the differentiated hNPCs with 1 μ M CK1 δ -derived peptides or 100 nM SMIs and DMSO as solvent control. Compound β -secretase-specific inhibitor IV at a concentration of 10 μ M [202] and GSK3 α/β -specific inhibitor CHIR-98014 at a concentration of 0.1 μ M [281] were used as positive controls to modulate APP metabolism and tau hyperphosphorylation, respectively. Media was exchanged every second to third day. After the treatment, media were discarded, and Matrigel/cell pellets were stored at -80 °C for later use (see chapter 2.5.5.3).

2.5.5.1 Monitoring of cell viability

The status of the 3D culture viability was constantly monitored by a performing lactate dehydrogenase (LDH) release assay for the exclusion of cytotoxic effects caused by the respective treatment. Therefore, samples were collected every second to third day and processed according to manufacturer's instructions. Fluorescence signals were measured by using a Tecan Spark 10M microplate

reader. Results were calculated as a fold change of cytotoxicity of the untreated control at 2 days.

2.5.5.2 Quantitative analysis of A β levels

After treating differentiated hNPCs, which were grown in thick-layer 3D, levels of A β ₁₋₄₂ were measured by Quantikine[®] human A β (aa 1 to 42) enzyme-linked immunosorbent assay (ELISA) according to manufacturer's instructions. Samples were collected after treatment and diluted with a dilution factor of 2 prior to use in the ELISA by using dilution buffer, which was provided by the manufacturer. Absorption was measured using a Tecan Spark 10M microplate reader. Results were normalized to untreated control.

2.5.5.3 Sarkosyl extraction of thick-layer 3D culture

For the extraction of sarkosyl-soluble fractions (SSF) and sarkosyl-insoluble fractions (SISF), Matrigel/cell pellets (from chapter 2.5.3) were thawed on ice for 10 min. 100 μ L 2x TBS extraction buffer were added, and Matrigel/cell pellet was homogenized using a rotor-driven homogenizer. Afterwards, the suspension was sonicated for 10 min at 4 °C using a sonic water bath. Samples were mixed with an equal volume of 2x RIPA extraction buffer and homogenized using the rotor-driven homogenizer on ice. Samples were incubated on ice for 15 min and sonicated twice for 5 min each. Matrigel/cell suspension was centrifuged at 10,000 x g for 5 min at 4 °C and supernatant was transferred into a fresh tube. 80 μ L 1x RIPA extraction buffer was added and pellets were resuspended and sonicated. The suspension was centrifuged at 10,000 x g for 5 min at 4 °C and supernatants were pooled. 100 μ L of 20 % sarkosyl solution was added to the supernatant and incubated at RT for 60 min in a rotary mixer. The suspension was centrifuged at 150,000 x g for 1 h at 4 °C. Supernatants were transferred into fresh reaction tubes and protein concentration of the SSF was measured (see chapter 2.4.1). Pellets were washed briefly with 100 μ L 2x RIPA buffer and three times with 500 μ L PBS. Pellets were resuspended in 1x SDS sample buffer supplemented with 10 M urea (SISF). Samples were heated at 95 °C for 5 min and stored at -80 °C for later use.

10x TBS/EDTA buffer	383 mM Tris-HCl (pH 7.4), 1.5 M NaCl, 1 mM EDTA in dH ₂ O
2x TBS extraction buffer	75 mM Tris-HCl (pH 7.4), 300 mM NaCl, 10 mM NaVO ₃ , 10 mM NaF, 2 mM PNT, 2 mM PMSF, two tablets of protease inhibitor cocktail, one tablet of phosphatase inhibitor cocktail in dH ₂ O
2x RIPA extraction buffer	0.5 % (w/v) sodium deoxycholate, 0.04 % (v/v) NP-40, 10 mM NaVO ₃ , 10 mM NaF, 2 mM PNT, 2 mM PMSF, two tablets of protease inhibitor cocktail, one tablet of phosphatase inhibitor cocktail in 1x TBS/EDTA buffer

EDTA: Ethylenediaminetetraacetic acid, NP-40: Nonidet-P 40, PMSF: Phenylmethylsulfonyl fluoride, PNT: 1,10-phenanthroline, TBS: Tris-buffered saline

2.6 Interaction analysis

2.6.1 Streptavidin-linked interaction assay

APP695 fragments, tau441 or tau383 were coated onto the surfaces of 96-well Nunc MaxiSorp plates at a concentration of 0.01 µg/µL in carbonate coating buffer at 4 °C overnight. The next day, non-specific binding was prevented by incubating the coated proteins with 5 % FCS in PBS. After a washing the proteins with PBST three times, 1 µg of biotinylated CK1δ-derived peptides was added and incubated at RT for 2.5 h with minimal shaking. DMSO served as negative control. Protein-peptide complexes were washed three times with PBST and incubated with HRP-conjugated streptavidin at a dilution factor of 8,000 in 0.5 % FCS in PBS at RT for 2 h under gentle rocking. Thereafter, protein-peptide complexes were washed three times with PBST and incubated with ABTS detection solution at RT for 40 min. Absorption was detected at 405 nm using a TriStar² LB942 multimode plate reader.

Carbonate coating buffer	100 mM carbonate buffer (pH 9.6)
PBST	0.137 M NaCl, 2.7 mM KCl, 10 mM Na ₂ HPO ₄ , 1.8 mM KH ₂ PO ₄ , 0.05 % Tween
ABST	50 mM potassium phosphate buffer (pH 5.7), 5 % ABTS stock solution (1 mg/mL), 0.05 % H ₂ O ₂

ABTS: 2,2'-azino-bis(3-ethylbenzothiazoline-6-sulphonic acid)

2.6.2 Surface plasmon resonance analysis with tau441

Surface plasmon resonance (SPR) analysis was done using a BiacoreTM X100. Prior to protein coupling, the NTA sensor chip was saturated with nickel by injecting the nickel solution at a flow rate of 10 µL/min. Nickel solution was not injected over the reference surface, which served as negative control. For immobilization, 0.1 µM 6xHis-tagged tau441 were prepared in running buffer and injected over the nickel activated sensor surface with a contact time of 3 min. After capturing the protein,

binding analysis was performed using 50 μM peptides in HBS-EP for 2 min at a flow rate of 5 $\mu\text{L}/\text{min}$. After each binding analysis, sensor chip was regenerated with regeneration buffer for 1 min at a flow rate of 10 $\mu\text{L}/\text{min}$. Data were analyzed using the Biacore™ Insight Evaluation Software. Each sensorgram was corrected for the response obtained in the reference surface and normalized to baseline.

Nickel solution:	0.5 mM NiCl ₂
Running buffer: (HBS-P)	0.01 M HEPES (pH 7.4), 0.15 M NaCl, 0.005 % (v/v) surfactant P20, 10 mM MgCl ₂ in dH ₂ O
Washing buffer: (HBS-EP)	0.01 M HEPES (pH 7.4), 0.15 M NaCl, 0.005 % (v/v) surfactant P20, 10 mM MgCl ₂ , 3 mM EDTA in dH ₂ O
Regeneration buffer:	0.01 M HEPES (pH 7.4), 0.15 M NaCl, 0.005 % (v/v) surfactant P20, 10 mM MgCl ₂ , 350 mM EDTA in dH ₂ O

EDTA: Ethylenediaminetetraacetic acid, HBS: HEPES-buffered saline, HEPES: N-2-hydroxyethylpiperazine-N'-2-ethanesulfonic acid

2.6.3 NanoLuc® binary technology PPI system

To identify CK1 δ -derived peptides, which block the interaction of CK1 δ and APP695 or tau441, the NanoLuc® binary technology (NanoBiT®) PPI system was established according to manufacturer's instructions [246]. Generally, NanoBiT® is a system to detect PPI in live cells and is based on two NanoLuc® luciferase subunits, which are fused to proteins of interest: a large binary technology (LgBiT) and a small binary technology (SmBiT). When the proteins are expressed in the cell and interact, the subunits are brought into close proximity to form an active enzyme that generates a luminescent signal (Figure 14) [246].

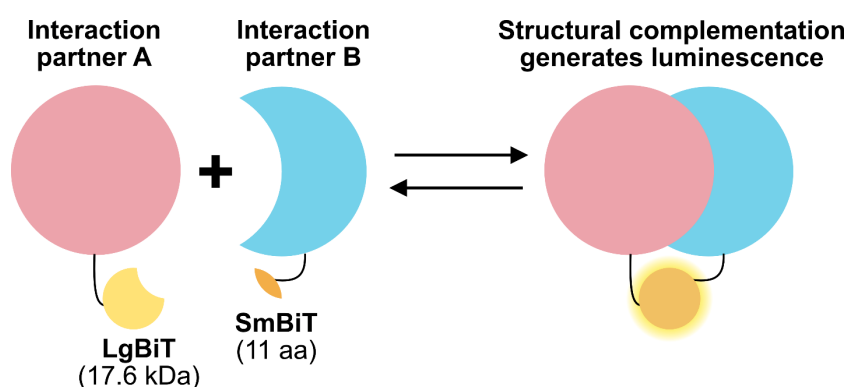


Figure 14: Principle of the NanoBiT® PPI system. For PPI of interest, interaction partner A and B are fused to LgBiT and SmBiT and after transfection expressed in cells. Interaction of both proteins results in structural complementation of LgBiT and SmBiT forming an active enzyme that generates luminescent signals. Figure is based on [246]. *LgBiT*: Large unit of the binary technology, *SmBiT*: Small unit of the binary technology.

2.6.3.1 Establishment of the NanoBiT[®] PPI assay

For the establishment of the NanoBiT[®] PPI assay all construct combinations were generated to define the optimal orientation for fusing CK1δ, APP695 and tau441 to LgBiT or SmBiT resulting in four different expression constructs per protein of interest. Therefore, subunits LgBiT or SmBiT were fused C- or N-terminally to CK1δ, APP695 or tau441 via iPCR and Gibson Assembly[®] (as described in chapter 2.2.3) (see Figure 15). After successful cloning, 100 ng expression constructs were co-transfected into 90 % confluent HEK293 cells via Lipofectamine[™] 3000 according to Figure 15. As negative control, the NanoBiT[®] negative control vector encoding for HaloTag[®]-SmBiT was used, which replaces the SmBiT fusion protein [246]. Transfection and assay efficiency was monitored using NanoBiT[®] positive control vectors encoding for protein kinase cAMP-activated catalytic subunit α (PRKACA) and protein kinase cAMP-dependent type II regulatory subunit α (PRKAR2A) [246]. The next day, NanoBiT[®] PPI luminescence was measured. Therefore, supplied Nano-Glo[®] LCS dilution buffer was equilibrated to ambient temperature and Nano-Glo[®] live cell substrate was mixed. Culture medium was aspirated and replaced with 100 μL DMEM supplemented with 10 % FCS. The mixed Nano-Glo[®] live cell substrate was diluted with a dilution factor of 20 and 25 μL were added to each well. Luminescence was measured immediately after adding the Nano-Glo[®] Live Cell Reagent at RT for 2 h using a TriStar² LB942 multimode plate reader.

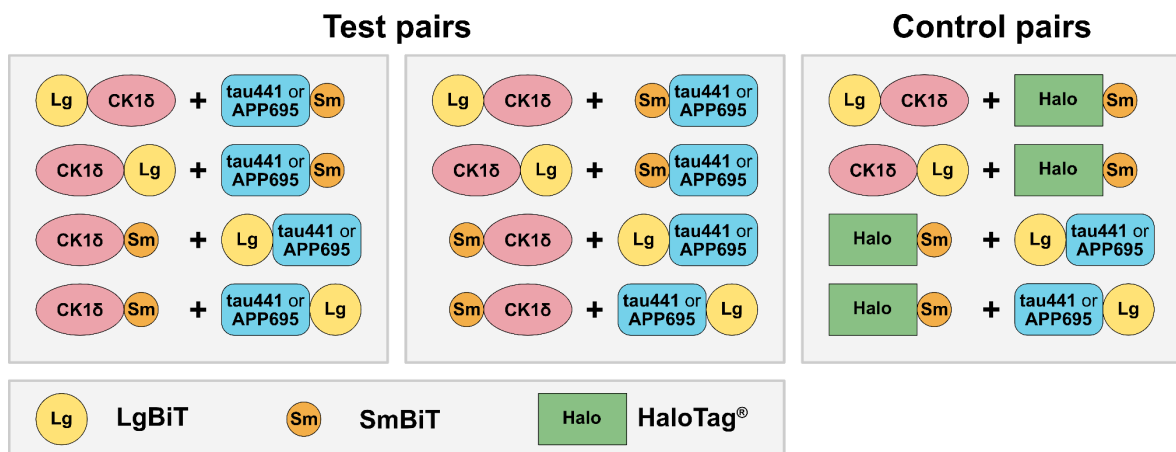


Figure 15: Establishment of the NanoBiT[®] PPI system. Subunits LgBiT or SmBiT were fused C- or N-terminally to CK1δ, APP695 or tau441 via iPCR and Gibson Assembly[®]. For transfection, both interaction partners (CK1δ and APP695 or CK1δ and tau441) were co-transfected into HEK293 (test pairs). As control pairs, the NanoBiT[®] negative control vector encoding for HaloTag[®]-SmBiT was used, which replaces the SmBiT fusion protein. APP: Amyloid precursor protein, LgBiT: Large unit of the binary technology, SmBiT: Small unit of the binary technology.

2.6.3.2 *Measuring NanoBiT[®] PPI luminescence in the presence of peptides*

After determining the optimal fusion-tag orientation and combination of expression constructs, CK1 δ -derived peptides were added prior to the addition of the Nano-Glo[®] Live Cell Reagent. Therefore, medium of co-transfected HEK293 cells was aspirated and replaced with fresh DMEM supplemented with 10 % FCS and 10 μ M CK1 δ -derived peptides or DMSO as solvent control. Cells were incubated for 30 min at RT. Afterwards, 25 μ L of the diluted Nano-Glo[®] Live Cell Reagent were added, and luminescence was measured for 2 h at RT using a TriStar² LB942 multimode plate reader. Obtained data were normalized to DMSO.

2.7 Immunohistochemical methods

2.7.1 Immunofluorescence staining of 2D grown cells

After incubation, cells were washed three times with 1x PBS and subsequently fixed with 4 % (v/v) paraformaldehyde in 1x PEM buffer at 4 °C for 20 min. Fixed cells were permeabilized with 0.3 % (v/v) Triton-X 100 in 1x PEM buffer for 5 min at RT. After brief washing with 1x PEM buffer, cells were blocked with 5 % (w/v) BSA in 1x PEM buffer for 30 min at RT. Afterwards, cells were washed three times in 1x PEM buffer and incubated with the first primary antibody at 4 °C overnight or with streptavidin-conjugate (see Table 13) at RT for 30 min. Cells were washed three times with 1x PEM. In case of staining with antibodies, cells were incubated with the secondary antibody (see Table 13) at RT for 40 min and washed three times with 1x PEM buffer. For staining of a second target, cells were again blocked in 5 % BSA in 1x PEM buffer and staining procedure was performed as described before. Washed cells were stained with 0.1 μ g/mL DAPI at RT for 5 min and washed with 1x PEM buffer and dH₂O. Finally, washed cells were sealed with ProLong[™] Glass Antifade Mountant. The next day, fluorescence images were captured with an Olympus IX81 microscope and connected XM10 camera at 10x magnification or the Leica SP8 confocal microscope at 63x magnification. Images were either processed and analyzed with the Olympus software cellSens Dimensions or R and RStudio (see chapter 2.8.2).

PEM buffer

80 mM PIPES (pH 6.8), 1 mM EGTA, 5 mM MgCl₂

2.7.2 Immunofluorescence staining of 3D grown cells

After treatment, cells were washed briefly with 1x PBS and fixed with 4 % (v/v) paraformaldehyde in 1x PEM buffer at 4 °C overnight. Fixed cells were permeabilized with 0.3 % Triton-X 100 in 1x PEM buffer for 1 h at RT. After brief washing with 1x PEM buffer, cells were blocked with 5 % BSA in 1x PEM buffer for 8 h at RT. Afterwards, cells were washed three times in 1x PEM buffer and incubated with the primary antibody (see Table 13) at 4 °C overnight with minimal shaking. Cells were washed five times with 1x PEM buffer and subsequently incubated with the secondary antibody (see Table 13) at RT for 5 h. Cells were washed five times with 1x PEM buffer and sealed with ProLong™ Glass Antifade Mountant. Fluorescence images were captured as described before.

2.8 Computational methods

2.8.1 Peptide localization in CK1δ

To prove whether the identified peptides present potential candidates for specific binding to APP695 or tau, surface maps of CK1δ were generated highlighting localization of identified peptides. The truncated structure of CK1δ from aa 1 to 296 with the protein data bank (PDB) code 6GZM [241] was used as a basis for the surface representation using the graphic visualization tool PyMOL 2.4. The specific binding peptides were colored in blue.

2.8.2 Co-localization analysis via R

Co-localization analysis was performed using R (version 4.2.0) and RStudio (version 2022.02.2). The required packages included “imager” and “colocr” (see Table 16). Three regions of interest (ROI) were chosen in the gray-scale image. Afterwards, the threshold was set to a value of 95. For the evaluation of the co-localization of tau441 and CK1δ, the Mander’s overlap coefficient (MOC) and the Pearson’s correlation coefficient (PCC) were determined according to [5]. MOC describes the fraction of pixels from the Cy5 and FITC channel with values above the background. The co-variance of the pixel intensities from both channels (Cy5 and FITC) is described by PCC.

2.9 Statistical analysis

Results are displayed as the mean of experiments at least performed in triplicates as not stated otherwise. Evaluation and statistical analysis of the results were carried out with GraphPad Prism 8.0. Based on the hypotheses underlying each specific experiments, statistical significance was tested by using the non-parametric Mann-Whitney U test. Differences between the groups are considered statistically significant at $p \leq 0.05$, presented as *.

3 Results

3.1 Characterization of CK1 δ -mediated phosphorylation of tau

A main pathological event in AD is the generation of NFTs derived from hyperphosphorylated and subsequently aggregated tau proteins. Previous studies already reported the critical involvement of PKs including members of the CK1 family that could be linked to the pathogenesis of AD by the hyperphosphorylation of tau [149, 207].

3.1.1 Tau441 is phosphorylated by CK1 δ *in vitro*

By using the software-based approach ScanSite 4.1.0 [252], several putative target sites for CK1-mediated phosphorylation could be identified in the longest tau isoform (tau441) (Figure 16A). The set of recognition sequences and preferences for specific aa residues implemented in these motif-scan algorithms are shown in Figure 16B and Figure 16C.

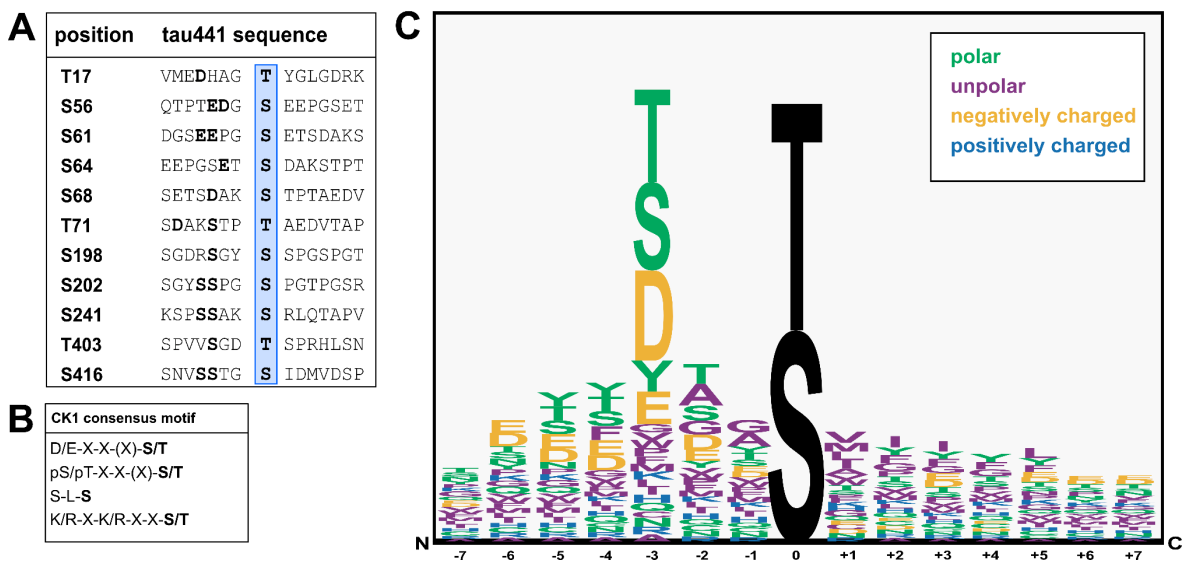


Figure 16: Tau441 contains several putative target sites for CK1. (A) Aa sequences of potential phosphorylation sites specific for CK1 on tau441, which were predicted by the software-based approach ScanSite 4.1.0 at minimum stringency (according to Krismer et al. [188]). (B), (C) Consensus motifs for CK1. The figure was modified from [289], which is licensed under a Creative Commons Attribution 4.0 international license (CC BY 4.0), <https://creativecommons.org/licenses/by/4.0/>. D: Aspartic acid, E: Glutamic acid, K: Lysine, L: Leucine, pS: Phosphorylated serine, pT: Phosphorylated threonine, R: Arginine, S: Serine, T: Threonine, X: Amino acid without any preference.

Initially, LC-MS/MS analysis of CK1 δ -phosphorylated recombinant tau441 was performed to detect whether CK1 δ is capable of phosphorylating tau441. For this

purpose, full-length human N-terminal 6xHis-tagged tau441 was recombinantly expressed in *E. coli*, purified via IMAC and phosphorylated by human recombinant 6xHis-tagged CK1δ *in vitro*. Mass spectrometric analysis revealed 94.1 % and 91.8 % sequence coverage of CK1δ-phosphorylated tau441 and non-phosphorylated tau441, respectively, based on the aa sequence of the longest human tau isoform (tau441, UniProt: P10636-8). Moreover, LC-MS/MS analysis did not discover any phosphorylation of non-phosphorylated tau441. In total, ten different phosphorylation sites, which were targeted by CK1δ, could be identified (Table 23) and, in most instances, precise phosphorylation sites could be detected. A clear assignment was not possible for the aa residues Thr414 and Ser416, which belong to a phosphopeptide sequence that contains four closely spaced potential CK1δ-specific phosphorylation sites Ser412, Ser413, Thr414 and Ser416.

Table 23: Results of LC-MS/MS analysis of phosphorylated tau441. Recombinant tau441 was phosphorylated by CK1δ *in vitro* and analyzed by LC-MS/MS. Identified phosphorylation sites within tau441, phosphorylation probability and measured signal intensity are shown. Detected phosphorylation of the aa residues is indicated with **p** within the modified sequence. The table was modified from [289], which is licensed under a Creative Commons Attribution 4.0 international license (CC BY 4.0), <https://creativecommons.org/licenses/by/4.0/>.

Site position	Probability [%]	Modified sequence	CK1δ intensity	AD association
S198	100	SGY p SSPGSPGTPGSR	1.8*10 ⁸	yes [148, 244]
S214	100	TP p SLPTPPTREPK	3.0*10 ⁷	yes [148, 162]
S289	100	KLDLSNVQ p SK	4.2*10 ⁷	yes [149]
S305	100	HVPGGG p SVQIVYKPVDSLK	3.1*10 ⁹	no
S324	100	CG p SLGNIHHKPGGGQVEVK	2.2*10 ⁷	no
S341	100	p SEKLDLFKDR	3.9*10 ⁷	no
T361	100	IGSLDNI p THVPGGGNK	1.1*10 ⁹	no
T386	100	AK p TDHGAEIVYK	9.5*10 ⁸	no
S416/T414	60.5/34.3	HLSNVSS p TG p SIDMVDSPQLATL ADEVASLAK	5.8*10 ⁷	yes/yes [149]
T427	67.7	HLSNVSS T GSIDMVDSPQLA p TL ADEVASLAK	2.4*10 ⁷	yes [149]

Moreover, five out of ten detected CK1δ-specific phosphorylation sites were located within the MT-binding domain, which has an important role in the interaction of tau with the MT [203] (Figure 17A). Additionally, the identified phosphorylation sites Ser198, Ser214, Ser289, Ser324, Thr361 and Ser416 are located within CK1-specific phospho-primed, acidic or non-canonical consensus motifs (Figure 17B). No typical CK1-specific consensus motif was observed for the detected

phosphorylation sites Ser305, Thr386, Thr414 and Thr427. Interestingly, of the ten phosphorylation sites, which were detected via LC-MS/MS, five were associated to AD in previous studies (including Ser198, Ser214, Ser289, Thr414, Ser416 and Thr427) (Table 23) [148, 149, 162, 244].

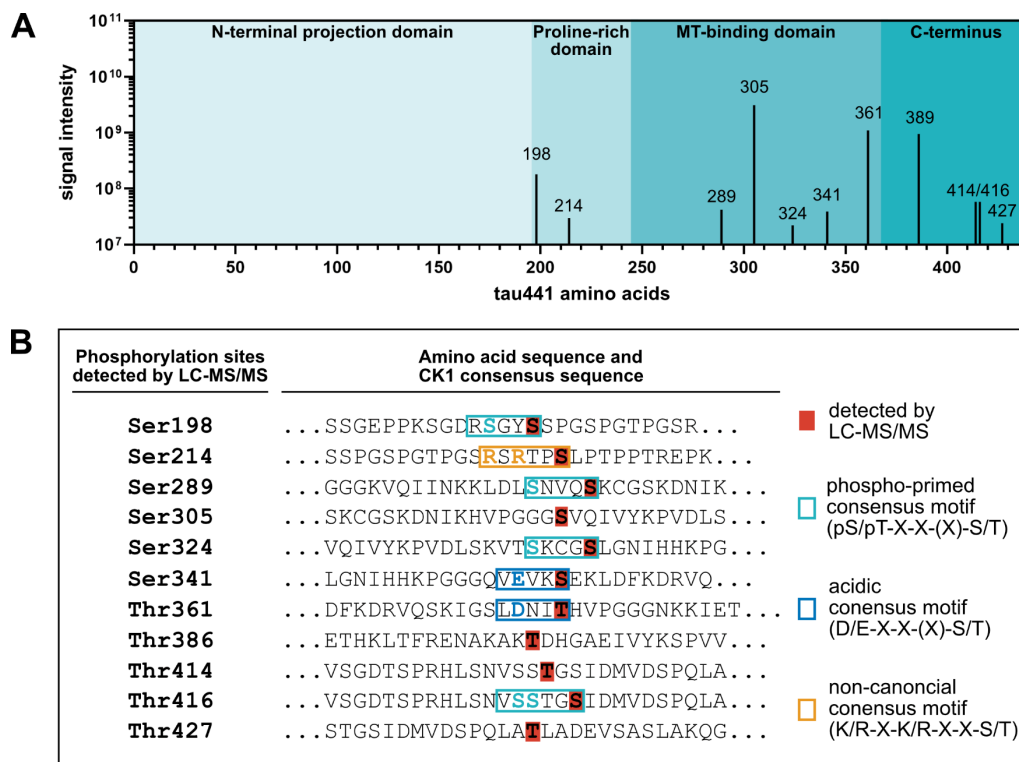


Figure 17: Mass spectrometric analysis of tau441 phosphorylated by CK1δ *in vitro*. Tau441 was recombinantly expressed, purified and used for *in vitro* phosphorylation by CK1δ. *In vitro* phosphorylated tau441 was digested with TPCK-trypsin and analyzed via LC-MS/MS. **(A)** LC-MS/MS analysis detected ten tau441 phosphorylation sites specific for CK1δ. **(B)** Aa sequences of tau441 including the detected phosphorylation sites via LC-MS/MS (covered in red). Phospho-primed, acidic or non-canonical consensus motifs of CK1 are marked in green, blue and orange, respectively. The figure was modified from [289], which is licensed under a Creative Commons Attribution 4.0 international license (CC BY 4.0), <https://creativecommons.org/licenses/by/4.0/>. *D*: Aspartic acid, *E*: Glutamic acid, *K*: Lysine, *pS*: Phosphorylated serine, *pT*: Phosphorylated threonine, *R*: Arginine, *S*: Serine, *T*: Threonine, *X*: Amino acid without any preference.

To validate the results obtained by LC-MS/MS analysis, tau441 fragments were generated according to different tau441 domains including the N-terminal projection domain, proline-rich domain and MT-binding domain/C-terminus (Figure 18). Therefore, the aa sequence of tau441 was split into three shorter protein fragments (tau441¹⁻¹⁵⁵, tau441¹⁵⁶⁻²⁴² and tau441²⁴³⁻⁴⁴¹). Phosphorylation by CK1δ was observed for all fragments indicating that CK1δ-specific phosphorylation sites are located within all tau441 domains. Most intense phosphorylation was detected for fragment tau441¹⁵⁶⁻²⁴², which contained the second most *in silico* predicted CK1-targeted phosphorylation sites on tau441. As shown before, LC-MS/MS analysis

detected most of the phosphorylation sites located on tau441²⁴³⁻⁴⁴¹, which could not be supported by the results obtained from the *in vitro* kinase assay, which measured the transfer of radioactively labeled phosphate to tau441 protein substrate.

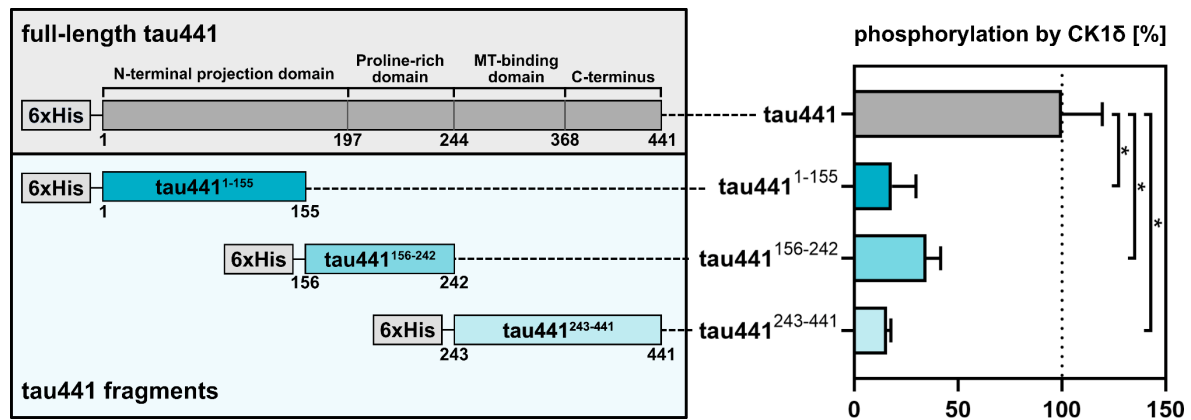


Figure 18: Generation and phosphorylation of tau441 fragments. Tau441 fragments tau441¹⁻¹⁵⁵, tau441¹⁵⁶⁻²⁴² and tau441²⁴³⁻⁴⁴¹ were generated according to different tau441 domains N-terminal projection domain, proline-rich domain and the MT-binding domain/C-terminus. Tau441 and tau441 fragments were phosphorylated *in vitro*. After separation of phosphorylated proteins via SDS-PAGE and Coomassie staining, phosphate incorporation into different tau441 proteins was measured via Cerenkov counting. Experiments were performed in triplicates and data were normalized to full-length tau441. Data is shown as mean values of the results and error bars represent the standard deviation. Statistical significance was tested with the non-parametric Mann-Whitney U test. * indicates $p \leq 0.05$. The figure was modified from [289], which is licensed under a Creative Commons Attribution 4.0 international license (CC BY 4.0), <https://creativecommons.org/licenses/by/4.0/>. MT: Microtubule.

After having obtained the results from LC-MS/MS analysis and *in vitro* kinase assays, another approach based on two-dimensional phosphopeptide analysis was carried out to support the results obtained from the previous experiments. Due to technical limitations, full separation of the protein bands of tau441 as well as tau441¹⁻¹⁵⁵ and CK1δ was not possible by using SDS-PAGE. By performing phosphopeptide analysis with CK1δ, phosphopeptides, which were more significant for the autophosphorylated kinase were clearly detected and excluded from the evaluation of tau441 and tau441¹⁻¹⁵⁵ phosphopeptide analysis (Figure 19A). The autoradiograph of tau441¹⁻¹⁵⁵ showed two major phosphopeptides (peptides 1 and 2) and one additional phosphopeptide, which cannot be assigned to full-length tau441 (peptide I) (Figure 19B). The phosphorylation pattern of tau441¹⁵⁶⁻²⁴² showed one major full-length tau441-associated phosphopeptide (peptide 4) and two additional phosphopeptides, which are exclusively assignable to the phosphorylated fragment (peptides II and III) (Figure 19C). Most major peptide signals that can be assigned to full-length tau441 were detectable in the autoradiograph of tau441²⁴³⁻⁴⁴¹ (peptide 5 to 9) (Figure 19D).

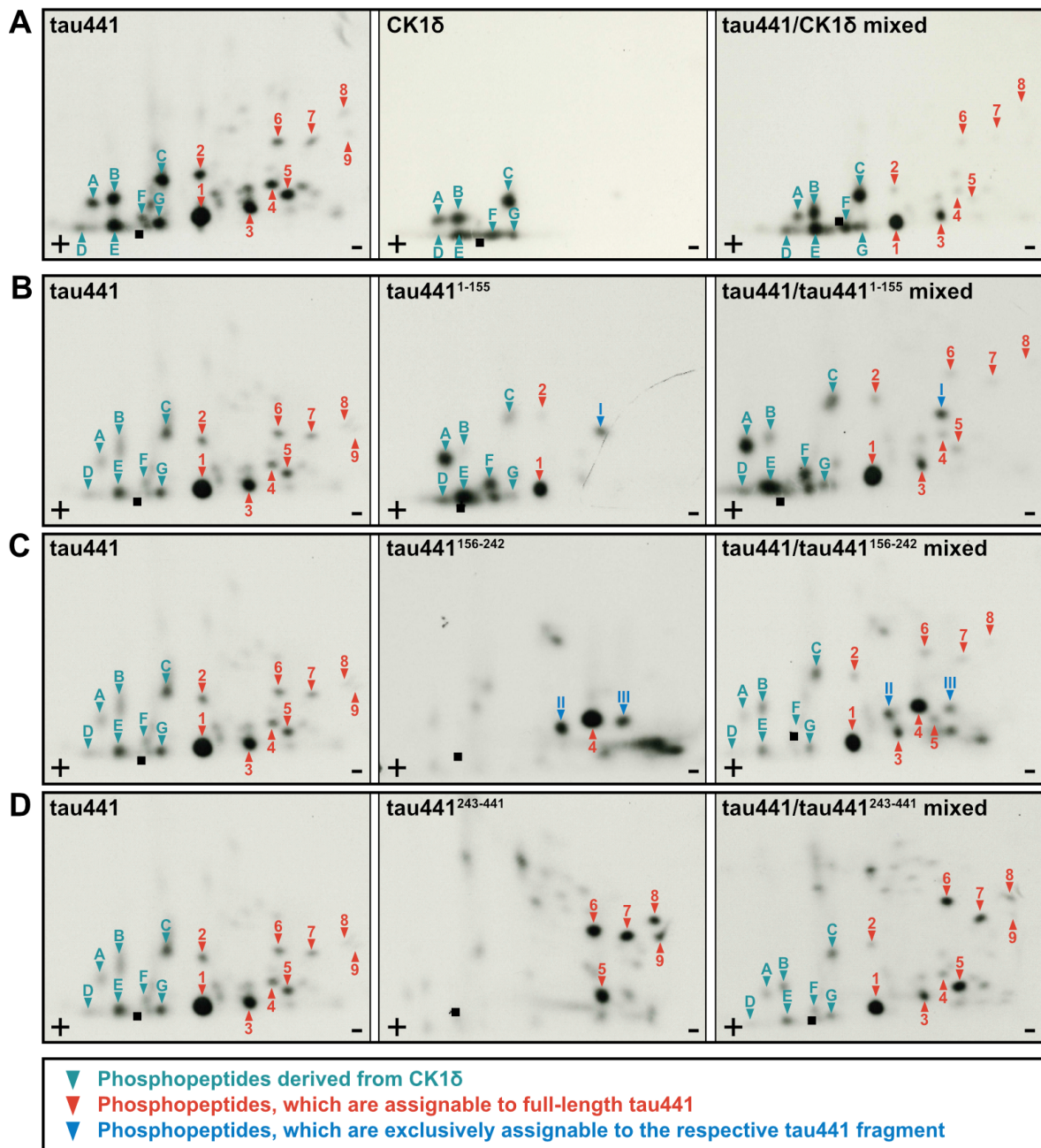


Figure 19: Phosphopeptide analysis of tau441 fragments. (A) Two-dimensional phosphopeptide analysis of autophosphorylated CK1δ and tau441 phosphorylated by CK1δ. Letters indicate phosphorylated peptides that correspond to autophosphorylated CK1δ (marked in green). Full-length tau441 and tau441 fragments (B) tau441¹⁻¹⁵⁵, (C) tau441¹⁵⁶⁻²⁴² and (D) tau441²⁴³⁻⁴⁴¹ were phosphorylated by CK1δ *in vitro* and analyzed via two-dimensional phosphopeptide analysis. Arabic numbers indicate major phosphopeptides, which can be assigned to full-length tau441 (marked in red). Phosphorylated peptides that are exclusively phosphorylated in the respective tau441 fragment are indicated with roman numerals (marked in blue). The figure was modified from [289], which is licensed under a Creative Commons Attribution 4.0 international license (CC BY 4.0), <https://creativecommons.org/licenses/by/4.0/>. +: Anode, -: Cathode, ■: Loading point.

In sum, combined results from *in silico* prediction, LC-MS/MS analysis and classical biochemical approaches indicate that CK1δ phosphorylates tau441 at many different phosphorylation sites *in vitro*. The distribution of *in silico* predicted CK1-

targeted tau441 phosphorylation sites could be supported by the results obtained by the *in vitro* kinase assays, especially for tau fragments tau441¹⁵⁶⁻²⁴² and tau441²⁴³⁻⁴⁴¹ (Figure 20). In contrast to these results, data received from LC-MS/MS analysis clearly supported the results of two-dimensional phosphopeptide analysis indicating a contrary pattern of distribution.

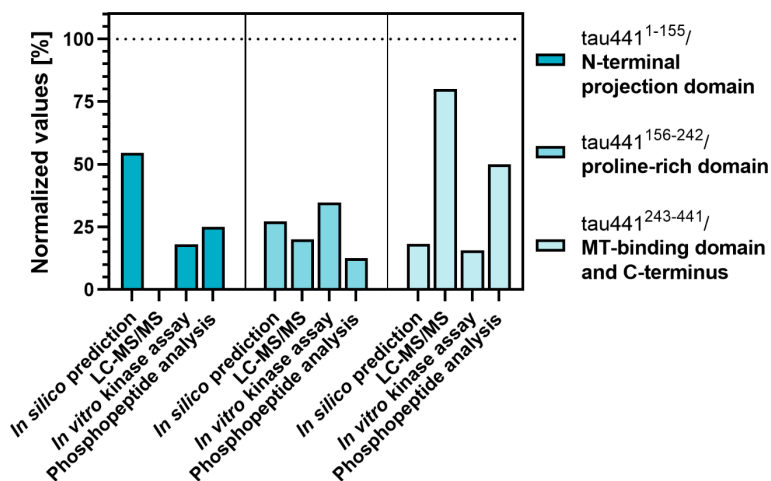


Figure 20: Summary of the data obtained from *in silico* prediction, mass spectrometric analysis and biochemical approaches. Amount of the detected CK1-specific phosphorylation sites from *in silico* prediction via ScanSite 4.1.0 at minimum stringency [188], LC-MS/MS analysis and the amount of phosphopeptides detected by phosphopeptide analysis were normalized to the whole amount of phosphorylated residues or phosphopeptides identified by the respective method. Data obtained by the *in vitro* kinase assay was normalized to full-length tau441 and is shown as mean values of the experiments conducted in triplicates. The figure was modified from [289], which is licensed under a Creative Commons Attribution 4.0 international license (CC BY 4.0), <https://creativecommons.org/licenses/by/4.0/>. MT: Microtubule.

From these results, it can be deduced that most CK1 δ -specific tau441 phosphorylation sites are located within its MT-binding as well as C-terminal domain, which are both located on fragment tau441²⁴³⁻⁴⁴¹. To validate the results described in this chapter, *in vitro* kinase assays and phosphopeptide analysis were performed with tau441 phosphomutants and cell-based assays were carried out, which are shown in the following chapter.

3.1.2 CK1 δ targets AD-associated phosphorylation sites on tau441

To verify potential AD-associated CK1 δ -specific tau phosphorylation sites predicted by the consensus sequences via ScanSite 4.1.0 or detected by LC-MS/MS analysis, six tau441 phosphomutants were designed and generated via site-directed mutagenesis (chapter 2.2.2). Equimolar amounts of recombinantly expressed and purified wild type (wt) tau441 and tau441 phosphomutants were phosphorylated by CK1 δ *in vitro* by using radioactively labeled [γ -³²P]-ATP and phosphate incorporation

was quantified via Cherenkov counting. Mutation of serine and threonine to alanine at residues Ser198/Ser199/Ser202/Thr205 and Ser422/Thr427 led to minor reduction of CK1 δ -specific phosphorylation to 65 % and 58 % compared to naïve tau441 (wt) (Figure 21). However, a major reduction in phosphorylation was observed for Ser68/Thr69/Thr71, Thr212/Ser214/Thr217/Thr220, Ser289 and Ser409/Ser412/Ser413/Thr414/Ser416 with 18 %, 16 % 39 % and 22 % rest activity compared to wt tau441.

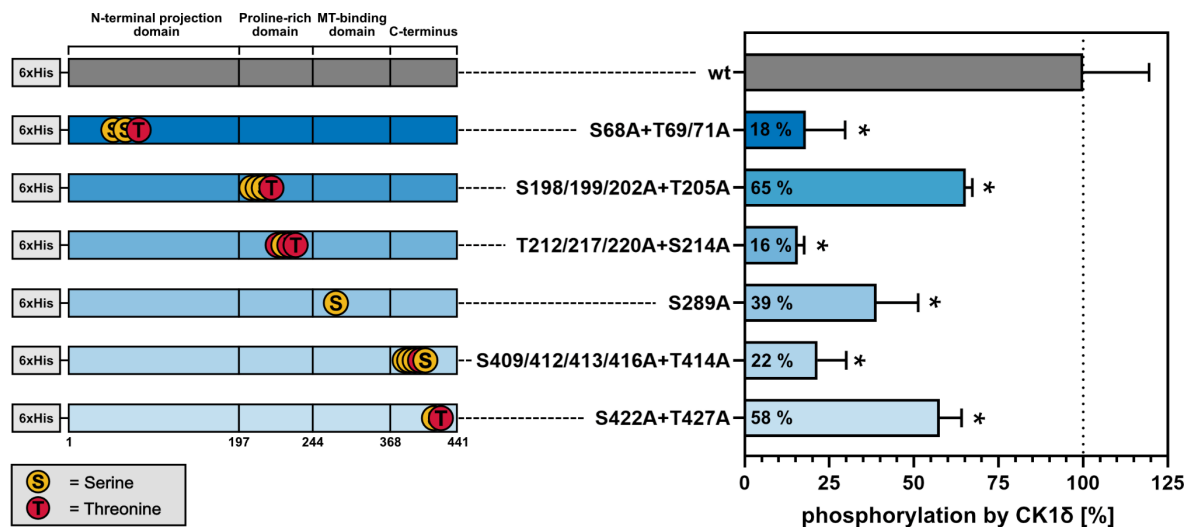


Figure 21: Generation and phosphorylation of tau441 phosphomutants. Tau441 phosphomutants were selected and generated via site-directed mutagenesis (left side of the figure) according to the positions of the predicted CK1 phosphorylation sites (via ScanSite 4.1.0) or the detection via LC-MS/MS analysis. Naïve tau441 (wt) and tau441 phosphomutants were phosphorylated by CK1 δ *in vitro*. Phosphate incorporation was quantified and normalized to wt tau441. Experiments were performed in triplicates. Results are shown as mean values and error bars represent the standard deviation. Differences in means were tested for statistical significance by using the non-parametric Mann-Whitney U test. * indicates $p \leq 0.05$. The figure was modified from [289], which is licensed under a Creative Commons Attribution 4.0 international license (CC BY 4.0), <https://creativecommons.org/licenses/by/4.0/>. A: Alanine, MT: Microtubule, S: Serine, T: Threonine, wt: Wild type.

To validate these results, phosphopeptide analysis using wt tau441 and corresponding phosphomutants tau441^{S68A+T69A+T71A}, tau441^{S198A+S199A+S202A+T205A}, tau441^{T212A+S214A+T217A+T220A}, tau441^{S289A}, tau441^{S409A+S412A+S413A+T414A+S416A} and tau441^{S422A+T427A} was performed (Figure 22). As expected from the *in silico* approach, the two-dimensional phosphopeptide analysis of tau441^{S68A+T69A+T71A} lacks one phosphopeptide (peptide 2) that most likely includes the aa residues Ala68, Ala69 and Ala71 (Figure 22A). In addition, phosphorylation pattern of the phosphopeptide analysis of tau441^{S289A} showed differences concerning phosphopeptides 7 and 9 compared to control. The shift of phosphorylation intensities from peptide 7 to 9, most likely due to the aa exchange from Ser289 to

Ala289, leads to the conclusion that Ser289 is phosphorylated by CK1 δ *in vitro* (Figure 22B). However, phosphopeptide analysis shows that not only Ser289 is phosphorylated on this phosphopeptide by CK1 δ , which is why it can still be detected despite the aa exchange. Phosphopeptide analysis of phosphomutants tau441^{S198A+S199A+S202A+T205A}, tau441^{T212A+S214A+T217A+T220A}, tau441^{S422A+T427A} and tau441^{S409A+S412A+S413A+T414A+S416A} did not show any striking and clear changes in the phosphorylation pattern (Figure 22C-F). Accordingly, no additional information was obtained for these phosphomutants using this experimental approach.

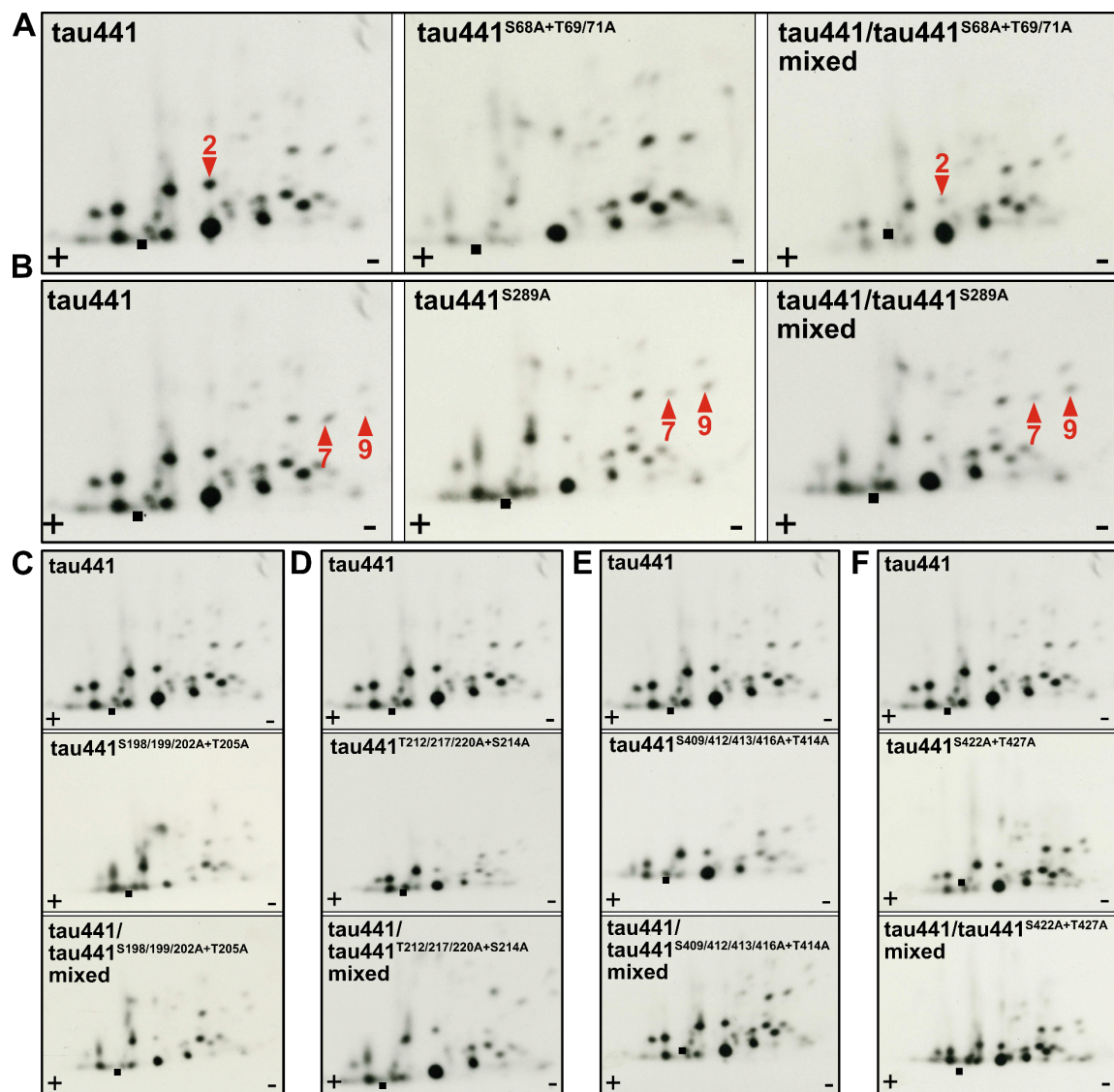


Figure 22: Phosphopeptide analysis of tau441 phosphomutants. Two-dimensional phosphopeptide analysis of CK1 δ -phosphorylated tau441 phosphomutants (A) tau441^{S68A+T69A+T71A}, (B) tau441^{S289A}, (C) tau441^{S198A+S199A+S202A+T205A}, (D) tau441^{T212A+S214A+T217A+T220A}, (E) tau441^{S409A+S412A+S413A+T414A+S416A} and (F) tau441^{S422A+T427A}. Positions of arrows indicate changes in phosphorylation patterns or loss of a major phosphopeptide (marked in red). Phosphopeptide analysis with mixed samples verifies the identity of marked phosphopeptides. The figure was modified from [289], which is licensed under a Creative Commons Attribution 4.0 international license (CC BY 4.0), <https://creativecommons.org/licenses/by/4.0/>. +: Anode, -: Cathode, ■: Loading point.

To investigate whether CK1 δ modulates tau phosphorylation in living neurons, transduced hNPCs were differentiated for two weeks and treated with the CK1 δ -specific inhibitor PF-670462 or DMSO as solvent control for 24 h. After treatment, cells were lysed and site-specific phosphorylation of tau was detected via Western blot using phospho-specific tau antibodies targeting AD-associated aa residues p-Ser202/p-Thr205, p-Ser214 or p-Ser416 (Figure 23A). The treatment of transduced and differentiated hNPCs with PF-670462 for 24 h did not affect the expression of tau generally (Figure 23B). However, tau phosphorylation in neuronal cells, which were treated with PF-670462, was significantly decreased at Ser214 supporting the results obtained by LC-MS/MS analysis and *in vitro* kinase assay, both of which already indicated CK1 δ -mediated phosphorylation of Ser214 *in vitro*. Tau phosphorylation at Ser202/Thr205 and Ser416 was not significantly affected by the CK1 δ -specific inhibition by PF-670462 (Figure 23C-E).

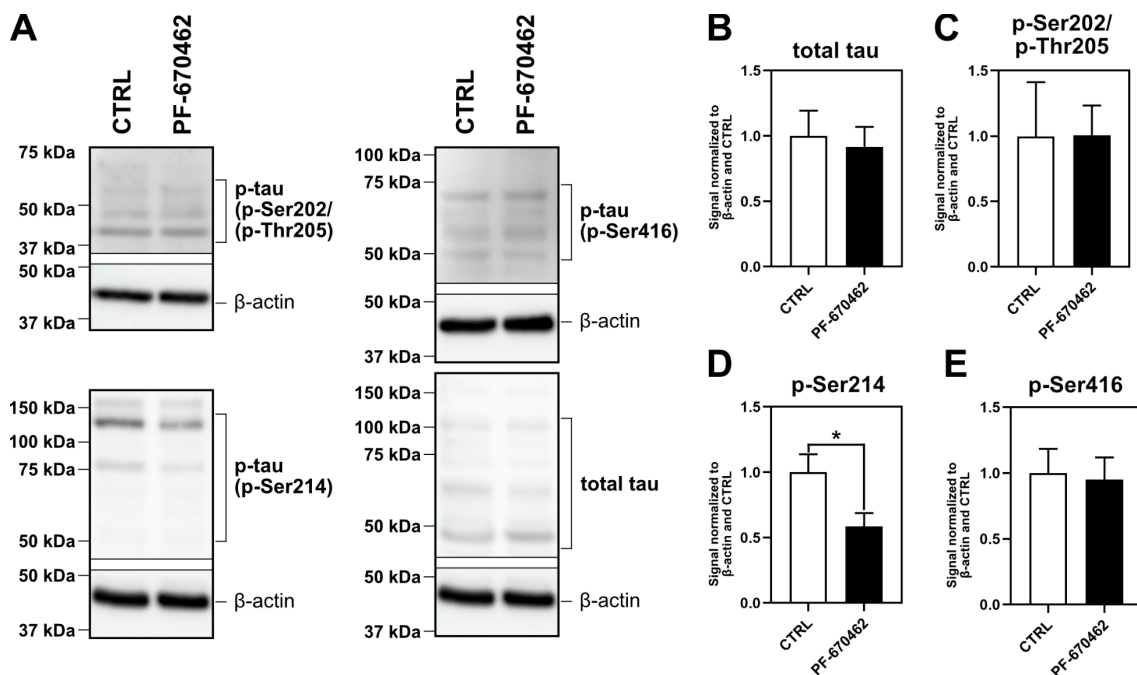


Figure 23: Identification of CK1 δ -specific tau phosphorylation sites in neuronal cells via Western blot analysis. Transduced and differentiated hNPCs were treated with 1 μ M CK1 δ -specific inhibitor PF-670462 or DMSO as solvent control (CTRL). **(A)** Tau phosphorylation at specific aa residues was detected by Western blot using antibodies targeting total tau or tau at p-Ser202/p-Thr205, p-Ser214 and p-Ser416, respectively. β -actin was used for loading control. **(B-E)** Western blot signal intensities from (A) were quantified via ImageJ and normalized to β -actin and CTRL. Experiments were performed in triplicates. Results are shown as mean values and error bars represent the standard deviation. Differences in means were tested for statistical significance by using the non-parametric Mann-Whitney U test. * indicates $p \leq 0.05$. The figure was modified from [289], which is licensed under a Creative Commons Attribution 4.0 international license (CC BY 4.0), <https://creativecommons.org/licenses/by/4.0/>.

In summary, data obtained by *in silico* prediction, LC-MS/MS analysis, biochemical approaches (including *in vitro* kinase assays and phosphopeptide analysis) and Western blot analysis with lysates of neuronal cells treated with a CK1 δ -specific inhibitor and phospho-specific tau targeting antibodies provide evidence that CK1 δ is able to phosphorylate AD-associated sites on tau. An overview of AD-associated phosphorylation sites on tau targeted by CK1 δ is shown in Table 24.

Table 24: AD-associated tau phosphorylation sites targeted by CK1 δ . Results were obtained from different methods and different sources of tau including *in silico* prediction (with tau441), LC-MS/MS analysis (with recombinantly produced tau441), *in vitro* kinase assay and two-dimensional phospho-peptide analysis (with recombinantly produced tau441) and Western blot analysis (with endogenous tau). Phosphorylation sites marked with “minor” showed only a slight reduction in phosphorylation due to the aa exchange. The table was modified from [289], which is licensed under a Creative Commons Attribution 4.0 international license (CC BY 4.0), <https://creativecommons.org/licenses/by/4.0/>.

	Ser68	Thr69	Thr71	Ser198	Ser199	Ser202	Thr205	Thr212	Ser214	Thr217	Thr220	Ser289	Thr403	Ser409	Ser412	Ser413	Thr414	Ser416	Ser422	Thr427
<i>In silico</i> prediction	✓		✓	✓		✓							✓					✓		
LC-MS/MS analysis				✓					✓			✓					✓	✓		✓
<i>In vitro</i> kinase assay		✓*			✓*	(minor)			✓*			✓	x			✓*				✓*
Phospho-peptide analysis		✓*										✓	x							
Western blot	x	x	x	x	x			x	✓	x	x	x	x	x	x	x	x	x	x	x

✓: Identified phosphorylation site targeted by CK1 δ , ✓*: Identified phosphorylation site targeted by CK1 δ within a tau441 phosphomutant, which includes multiple aa changes, x: not performed.

3.1.3 CK1 δ co-localizes with tau in neuronal cells

Further, it was investigated whether CK1 δ and tau are co-locating in human neuronal cells that were derived from hNPCs. The expression of CK1 δ and tau was visualized in neuronal cells by double immunofluorescence staining and confocal microscopy (Figure 24A). Control staining with secondary antibodies only is shown in Figure 24B. Additionally, neuronal differentiation level was determined by immunofluorescence staining of the neuron-specific expression marker MAP2, which is shown in Figure 24C and Figure 24D. As depicted in Figure 24A, immunofluorescence staining of both proteins revealed a variety of subcellular localizations. Additionally, a clear staining pattern for CK1 δ as well as tau was especially observed in the cell body and around the nuclei.

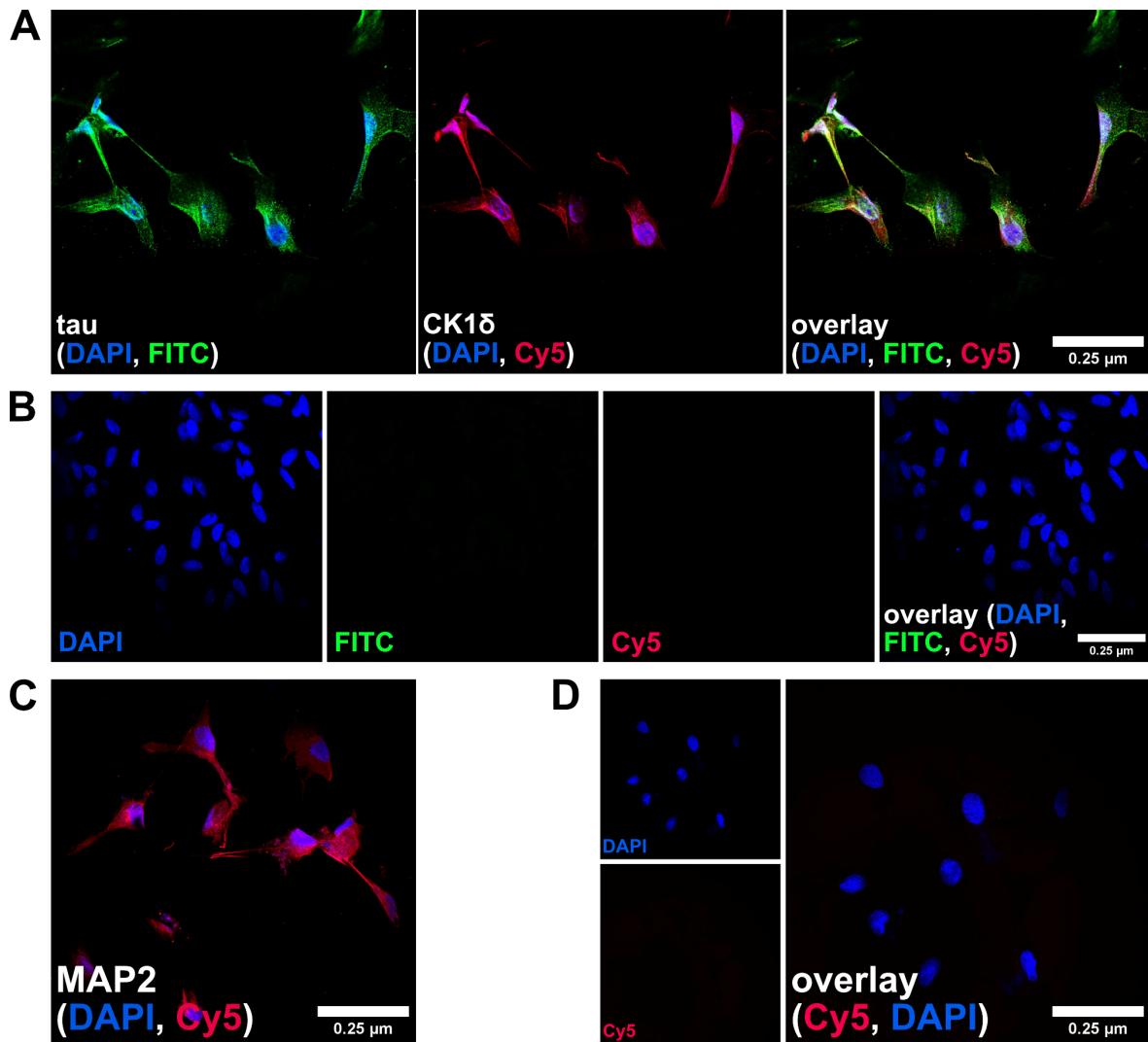


Figure 24: Immunofluorescence staining of CK1δ and tau in neuronal cells. hNPCs were differentiated for two weeks, fixed and stained with DAPI (nuclei, in blue) as well as **(A)** anti-CK1δ goat antibody with Alexa Fluor 647 anti-goat antibody (CK1δ in red/Cy5) and anti-tau mouse antibody with DyLight 488 anti-mouse antibody (tau in green/FITC). **(C)** Neuronal differentiation level was evaluated by staining the neuron-specific marker MAP2. Representative images of stained negative controls in which primary antibodies **(B)** anti-tau antibody and anti-CK1δ antibody or **(D)** anti-MAP2 antibody were omitted, are shown. Images were taken at x63 magnification with the Leica SP8 confocal microscope. The figure was modified from [289], which is licensed under a Creative Commons Attribution 4.0 international license (CC BY 4.0), <https://creativecommons.org/licenses/by/4.0/>. MAP: Microtubule-associated protein, Scale bar: 0.25 μm.

To quantify the subcellular co-localization of CK1δ with tau, the analysis of MOC and PCC was performed using R (Figure 25). Therefore, at least five overlays were processed and analyzed via R according to Ahmed et al. [5]. In detail, merged images (Figure 25A) were converted to low-resolution images (pixel set) and three ROIs were selected per image (Figure 25B, C). According to the pixel set of the selected ROIs raw pixel intensities (Figure 25D) and density of the pixel values (Figure 25E) for Cy5 and FITC channels were generated. Based on these, MOC

and PCC were determined. Co-localization analyzes of five images resulted in a MOC of 87 % and a PCC of 75 % (0.75) for the overlay of endogenous CK1 δ (Cy5) with endogenous tau (FITC) (Figure 25F) that indicate a strong intracellular co-localization of CK1 δ and tau in differentiated neuronal cells.

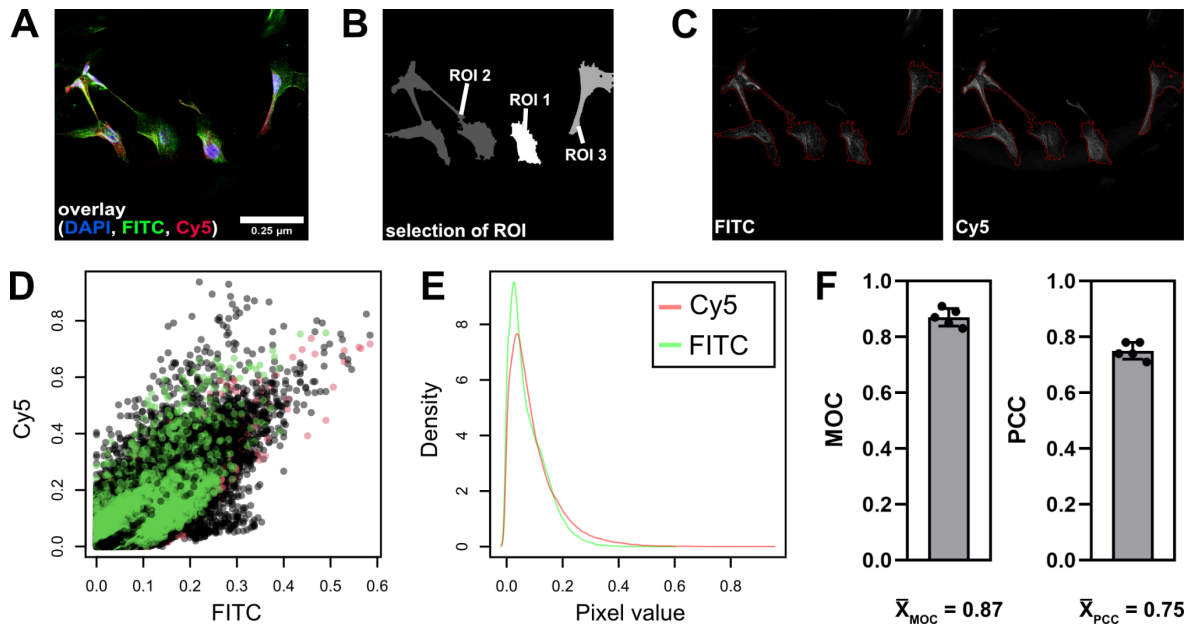


Figure 25: Co-localization analysis of CK1 δ and tau. (A) hNPCs were differentiated for two weeks, fixed and stained with DAPI (nuclei, in blue), anti-CK1 δ goat antibody with Alexa Fluor 647 anti-goat antibody (CK1 δ in red/Cy5) and anti-tau mouse antibody with DyLight 488 anti-mouse antibody (tau in green/FITC). (B, C) Images were merged, processed and analyzed via R according to Ahmed et al. [5]. (B) Merged image was processed to low-resolution image (pixel set) with three selected ROIs. (C) Three selected ROIs were highlighted within both channels with a red line. (D) Raw pixel intensities of FITC (in green) and Cy5 (in red) from three selected ROIs. Overlay is depicted in black. (E) Density of the pixel values of FITC (in green) and Cy5 (in red) from summarized ROIs. (F) Resulting analysis of MOC and PCC according to Ahmed et al. [5] with five images ($n = 5$). Results of MOC and PCC are given as mean and standard deviation is represented as error bars. The figure was modified from [289], which is licensed under a Creative Commons Attribution 4.0 international license (CC BY 4.0), <https://creativecommons.org/licenses/by/4.0/>. MOC: Mander's overlap coefficient, PCC: Pearson's correlation coefficient, ROI: Region of interest.

3.1.4 CK1 δ -mediated phosphorylation has an impact on tau441 aggregation

Hyperphosphorylation of tau by several kinases leads to the aggregation of tau into PHF resulting in NFT formation causing neuronal cell death in AD. Therefore, it was investigated whether CK1 δ enhances tau aggregation by phosphorylating tau at phosphorylation sites, which are associated to AD.

Tau aggregation assay was conducted using non-phosphorylated tau441 and *in vitro* CK1 δ -phosphorylated tau441 (p-tau441). For the measurement of tau aggregation, ThS assay was used and tau aggregation was monitored at 480 nm. As negative control, standard reaction mix without protein was used. As shown in

Figure 26A, the formation of tau aggregation was strongly influenced by the phosphorylation of CK1 δ . CK1 δ -mediated phosphorylation highly increased the formation of tau441 aggregates that correlates with an increased plateau value of 165,001 RFU compared to non-phosphorylated tau441 with 112,145 RFU (Figure 26B). The influence of CK1 δ -mediated phosphorylation on tau aggregation is additionally expressed by the decreased half-time of the aggregation kinetics of p-tau441 (1.38 min) compared to non-phosphorylated tau441 (3.43 min), which correlates with an increased aggregation velocity of the phosphorylated tau441.

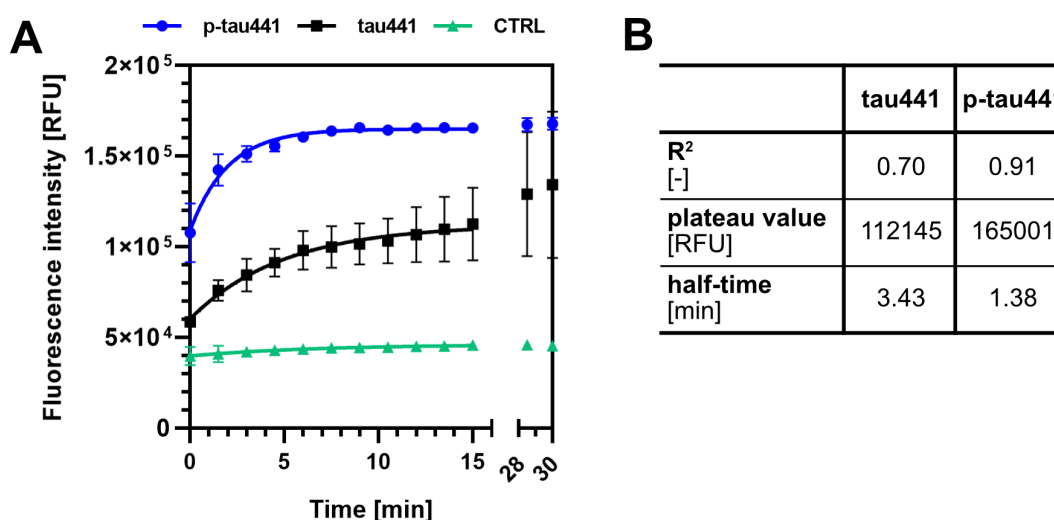


Figure 26: Phosphorylation of tau441 by CK1 δ is linked to tau aggregation. (A) Tau aggregation assay was performed with non-phosphorylated tau441 (tau441) and *in vitro* CK1 δ -phosphorylated tau441 (p-tau441). Control reaction (CTRL) was conducted with standard reaction mix without protein. Tau441 aggregation was measured by adding ThS and measuring at 480 nm. Results are given as mean and standard deviation is represented as error bars. Data within the first 15 min were fit to one-phase association exponential model. (B) For quantitative evaluation of tau aggregation, amount of formed aggregates (plateau value in [RFU]) and velocity of aggregation (half-time in [min]) were calculated. The figure was modified from [289], which is licensed under a Creative Commons Attribution 4.0 international license (CC BY 4.0), <https://creativecommons.org/licenses/by/4.0/>. CTRL: Control reaction, p-tau441: CK1 δ -phosphorylated tau441, RFU: Relative fluorescence units, tau441: Non-phosphorylated tau441.

3.2 Identification of new CK1 δ -specific compounds for the treatment of AD

Several studies and the results shown in chapter 3.1 have demonstrated a possible role of CK1 δ in the development of AD by influencing the metabolism of APP favoring the production of A β peptides and amyloid plaques [204, 352] as well as by the hyperphosphorylation of tau protein leading to its aggregation [149, 182, 218]. Based on these experimental findings, CK1 δ could represent an interesting target for therapeutic intervention in the development of AD.

Initially, three sets of potential CK1 δ -specific inhibitors including benzimidazole derivatives, IWP-derived compounds, and isoxazole derivatives were tested for their potency and selectivity. Prior to inhibitor testing, standard conditions (involving several kinetic parameters) for the *in vitro* kinase assay were established. After CK1 δ -specific inhibitors were found, they were tested for their toxicity in a cell-based system and for their biological effect in the well-described “Alzheimer’s-in-a-dish” model by simulating APP and tau pathology in neuronal cells.

3.2.1 Establishment of standard conditions for *in vitro* kinase assays

For the evaluation of new CK1 δ -specific SMIs, IC₅₀ values were determined and used for the comparison of the inhibitors’ potency. Due to major differences in experimental set-ups, the IC₅₀ values derived from different studies conducted by different working groups considerably lack comparability. To circumvent this problem, kinase-specific standard conditions were determined prior to the determination of IC₅₀ values. In the following, the establishment of standard conditions (V_{init} region) and determination of enzyme-specific parameters ($K_m(\text{ATP})$) that affect the determination of IC₅₀ values are shown for GST-CK1 α , GST-CK1 δ and GST-CK1 ϵ .

3.2.1.1 Determination of adequate kinase concentrations

As an IC₅₀ value describes the concentration of an inhibitor, which is required to reduce the enzyme activity by 50 %, the determination of an IC₅₀ value strongly depends on the used enzyme amount. To minimize the IC₅₀ detection limit, the lowest possible kinase concentration sufficient to detect signal intensities was determined.

For the evaluation of the lowest possible kinase concentration, time-dependent phosphorylation of the CK1-specific substrate α -casein by GST-CK1 α , GST-CK1 δ or GST-CK1 ϵ was quantified and the signal-to-noise (S/N) ratio was calculated (Figure 27). S/N ratio greater than 10 was assumed as a robust signal derived from the kinase phosphorylation [74]. The calculation of S/N ratio clearly showed that GST-CK1 δ at a concentration of 7 nM and a reaction time of 2 min was already sufficient as the S/N ratio was greater than 10. However, for GST-CK1 α and GST-CK1 ϵ a S/N ratio greater than 10 could only be reached at concentrations of 30 nM

and 7 nM and a reaction time of 10 min, when the calculated S/N ratios were 14 (GST-CK1 α) and 12 (GST-CK1 ϵ), respectively.

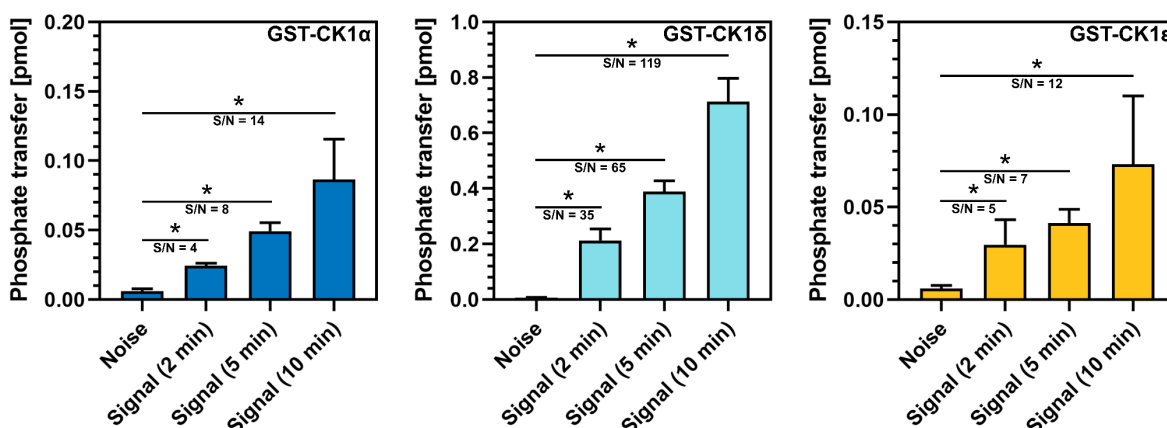


Figure 27: Calculation of the S/N ratio. CK1-specific substrate α -casein was phosphorylated by GST-CK1 α (30 nM), GST-CK1 δ (7 nM) and GST-CK1 ϵ (7 nM). Phosphorylation of 2.5 μ M α -casein was quantified, and S/N ratio was calculated. Experiments were performed in triplicates. Results are shown as mean values and error bars represent the standard deviation. Differences in means were tested for statistical significance by using the non-parametric Mann-Whitney U test. * indicates $p \leq 0.05$. S/N: Signal-to-noise.

3.2.1.2 Determination of the V_{init} region

In the next step, the V_{init} region for GST-CK1 α , GST-CK1 δ or GST-CK1 ϵ was determined by detecting the time-dependent phosphorylation of α -casein in the presence of 10 μ M ATP (corresponding to 150 pmol per reaction) (Figure 28A). Determining V_{init} by testing different enzyme concentrations was necessary for correct determination of kinetic parameters such as $K_m(\text{ATP})$ (see chapter 2.4.5.1). Additionally, the corresponding time-dependent autophosphorylation of GST-CK1 α , GST-CK1 δ and GST-CK1 ϵ was quantified by measuring phosphate incorporation into the respective kinase (Figure 28A, autophosphorylation).

Time-dependent phosphorylation of the CK1-specific substrate α -casein and the autophosphorylation of the GST-tagged kinase showed a typical time-conversion curve, which started with a linear region (maximal V_{init}) and reached a plateau at later time points (> 45 min). Additionally, proportional autophosphorylation of all kinases showed an increase with increasing substrate phosphorylation making up about 10 % of the total phosphorylation. To determine the V_{init} region, a linear regression analysis was conducted for each kinase. Thereby, the number of included data-points of the product-over-time progression curve was decreased

stepwise until the coefficient of determination (R^2) reached the maximum value (Figure 28B and Table 25).

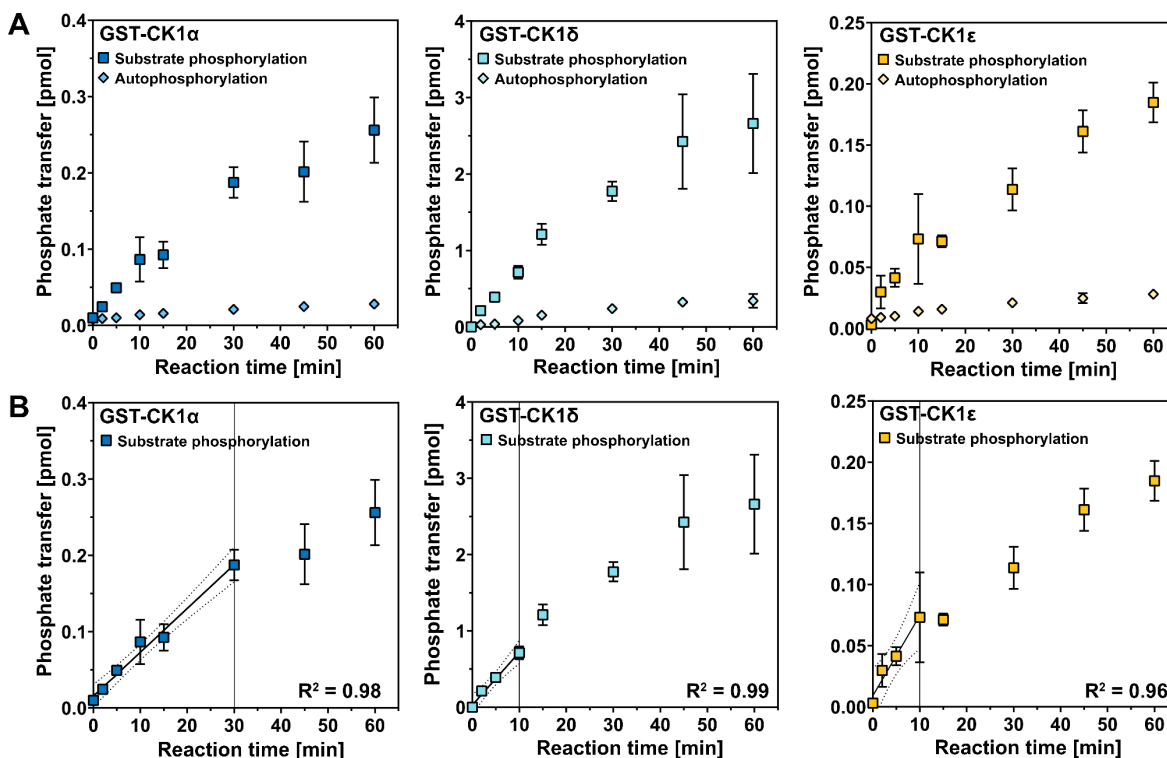


Figure 28: Determination of the V_{init} region of GST-tagged CK1. Time-dependent phosphate transfer from $[\gamma\text{-}^{32}\text{P}]\text{-ATP}$ to the substrate (α -casein) was catalyzed by human recombinant GST-CK1 α , GST-CK1 δ or GST-CK1 ϵ in the presence of DMSO. **(A)** Product-over-time progression for substrate phosphorylation of GST-CK1 α , GST-CK1 δ or GST-CK1 ϵ . Time-dependent autophosphorylation of GST-CK1 α , GST-CK1 δ and GST-CK1 ϵ has been measured and is presented similar to data shown for substrate phosphorylation. **(B)** Determination of V_{init} in the linear region. For the definition of the maximum coefficient of determination (R^2), linear regression analysis was performed with a stepwise decrease in the number of measured time points of the product-over-time progression curve. Linear regression of the determined V_{init} region includes R^2 value and confidence bands at 95 %. Results are shown as mean values and error bars represent the standard deviation. The figure was modified from [288], which is licensed under a Creative Commons Attribution 4.0 international license (CC BY 4.0), <https://creativecommons.org/licenses/by/4.0/>. R^2 : Coefficient of determination.

Linear regression analysis indicated for GST-CK1 δ and GST-CK1 ϵ an optimal time range of 10 min (CK1 δ : $R^2 = 0.99$, CK1 ϵ : $R^2 = 0.96$), respectively (Table 25). With regard to curve progression and the high standard deviation of phosphate transfer after 10 min, an optimal time range of 30 min ($R^2 = 0.98$) was selected for GST-CK1 α .

According to this data, determination of $K_m(\text{ATP})$ and subsequent determination of IC_{50} values using GST-CK1 α and GST-CK1 δ were performed with an enzyme concentration of 30 nM and 7 nM within a reaction time of 30 min and 10 min,

respectively. Due to activity loss during storage, the concentration of GST-CK1 ϵ was increased from 7 nM to 70 nM and was used within a reaction time of 10 min.

Table 25: Determination of V_{init} region for GST-tagged CK1 α , CK1 δ and CK1 ϵ . Linear regression was performed to determine the maximal R^2 value. Analyzed data points of the product-over-time progression curve were decreased stepwise. The table was modified from [288], which is licensed under a Creative Commons Attribution 4.0 international license (CC BY 4.0), <https://creativecommons.org/licenses/by/4.0/>.

Time range [min]	n	R^2		
		GST-CK1 α	GST-CK1 δ	GST-CK1 ϵ
0 - 60	8	0.96	0.92	0.96
0 - 45	7	0.94	0.97	0.95
0 - 30	6	0.98	0.96	0.90
0 - 15	5	0.94	0.99	0.86
0 - 10	4	0.99	0.99	0.96
Optimal reaction time [min]		30	10	10

n: Sample size, R^2 : Coefficient of determination.

3.2.1.3 Determination of K_m within V_{init}

Generally, $K_m(\text{ATP})$ is defined as the ATP concentration at which half of the maximal velocity (V_{max}) is achieved. To determine $K_m(\text{ATP})$ for GST-CK1 α , GST-CK1 δ and GST-CK1 ϵ , Michaelis-Menten kinetic analysis was conducted under defined V_{init} using different ATP concentrations in a range from 0.5 μM to 100 μM (Figure 29).

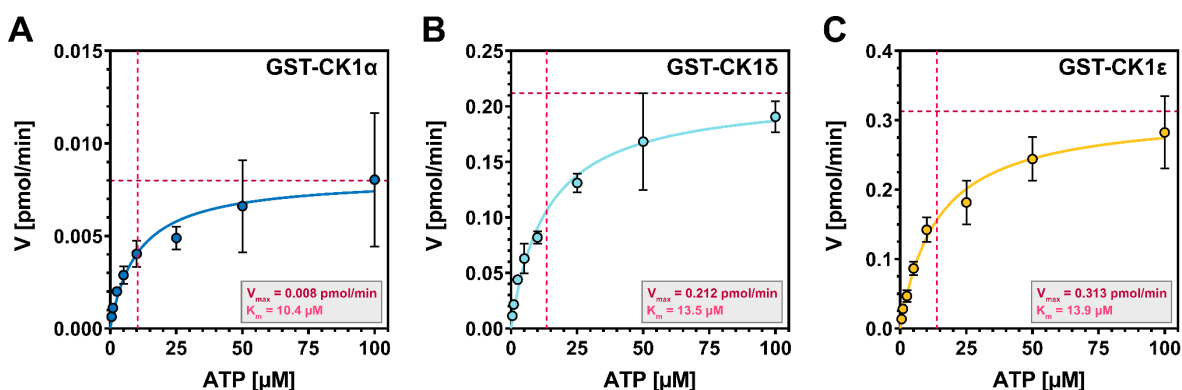


Figure 29: Michaelis-Menten kinetics of GST-tagged CK1 α , CK1 δ and CK1 ϵ . Michaelis-Menten kinetics for (A) GST-CK1 α , (B) GST-CK1 δ and (C) GST-CK1 ϵ was performed in the presence of increasing ATP concentrations. For the determination of V_{init} in [pmol/min], different ATP concentrations in a range from 0.5 to 100 μM were tested. $K_m(\text{ATP})$ is defined as the ATP concentration at which half of V_{max} is achieved. The figure was modified from [288], which is licensed under a Creative Commons Attribution 4.0 international license (CC BY 4.0), <https://creativecommons.org/licenses/by/4.0/>. $K_m(\text{ATP})$: Michaelis constant for ATP, V_{max} : Maximal velocity.

According to the Michaelis-Menten kinetic, the determined V_{max} of GST-CK1 α , GST-CK1 δ and GST-CK1 ϵ were 0.008 pmol/min, 0.212 pmol/min and 0.313 pmol/min.

The calculated $K_m(\text{ATP})$ of GST-CK1 α , GST-CK1 δ and GST-CK1 ϵ were 10.4 μM , 13.5 μM and 13.9 μM , respectively.

After having determined $K_m(\text{ATP})$ for all kinases, the transformation of IC_{50} values to K_i could be simplified according to the Cheng-Prusoff equation, which was explained in chapter 2.4.5.1. With the aim to determine IC_{50} (and K_i) values, ATP concentrations equivalent to the defined $K_m(\text{ATP})$ were used in the following experiments. All parameters of the established standard condition, which were used in the following, are shown in Table 26.

Table 26: Summary of the established standard conditions for the determination of IC_{50} values. Established standard conditions for GST-CK1 α , GST-CK1 δ and GST-CK1 ϵ include kinase concentration in [nM], reaction time in [min], $K_m(\text{ATP})$ in [μM] and V_{max} in [pmol/min]. Standard error of $K_m(\text{ATP})$ and V_{max} is represented as \pm .

		GST-CK1 α	GST-CK1 δ	GST-CK1 ϵ
Kinase concentration	[nM]	30	7	70
Reaction time	[min]	30	10	10
$K_m(\text{ATP})$	[μM]	10.4 \pm 3.8	13.5 \pm 2.3	13.9 \pm 2.4
V_{max}	[pmol/min]	0.008 \pm 0.001	0.212 \pm 0.012	0.313 \pm 0.017

$K_m(\text{ATP})$: Michaelis constant for ATP, V_{max} : Maximal velocity.

3.2.2 Biological activity of tested compounds *in vitro*

Initially, all compounds were screened in *in vitro* kinase assays at a concentration of 10 μM under established standard conditions for their inhibitory potency and selectivity among wild type GST-tagged CK1 isoforms (GST-CK1 α , GST-CK1 δ and GST-CK1 ϵ). Tested compounds include benzimidazole derivatives (chapter 3.2.2.1), IWP-derived inhibitors (chapter 3.2.2.2) and isoxazole derivatives (chapter 3.2.2.3).

For the comparison of inhibitory potency and isoform selectivity, a potent and ATP-competitive CK1 δ - and CK1 ϵ -specific purine scaffold inhibitor SR-3029 was used in all experiments [32]. Compounds that showed a low residual kinase activity at 10 μM were further used to determine IC_{50} values.

3.2.2.1 Initial screening and IC_{50} determination of benzimidazole derivatives

The set of benzimidazole derivatives is an important drug class in pharmaceutical industry and widely used for the treatment of various diseases. Regarding CK1 inhibition, benzimidazole-based inhibitors have already proven strong inhibitory potency and selectivity towards CK1 isoforms [37, 122].

In the initial screening, benzimidazole derivatives were tested at a concentration of 10 μM with GST-CK1 α , GST-CK1 δ and GST-CK1 ϵ (Figure 30). Unfortunately, none of the tested benzimidazole derivatives inhibited CK1 α and CK1 δ activity more than 50 %. Fenbendazole could significantly reduce CK1 δ and CK1 ϵ activity, which was nevertheless not enough to perform IC₅₀ determination.

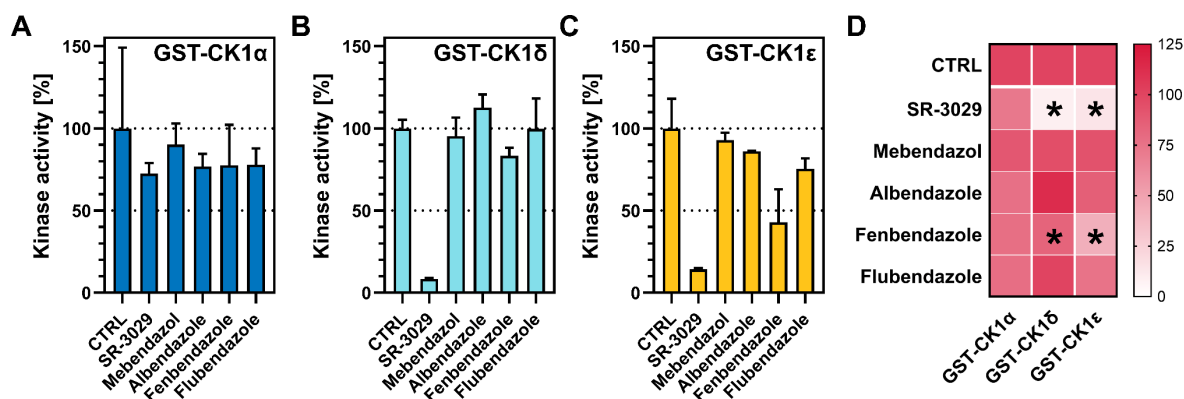


Figure 30: Initial screening of benzimidazole derivatives. Benzimidazole derivatives were screened at a concentration of 10 μM with (A) GST-CK1 α , (B) GST-CK1 δ and (C) GST-CK1 ϵ . Inhibitor SR-3029 was used as positive control. Phosphate incorporation was quantified and normalized to DMSO as solvent control (CTRL). Experiments were performed in triplicates. Results are shown as mean values and error bars represent the standard deviation. (D) Heatmap of the results shown in (A), (B) and (C). Differences in means were tested for statistical significance by using the non-parametric Mann-Whitney U test. * indicates $p \leq 0.05$.

3.2.2.2 Initial screening and IC₅₀ determination of IWP-derived compounds

As benzimidazole derivatives and IWPs share high structural similarities, IWPs were assumed to have high selectivity and potency against CK1 isoforms, which was proven in several studies [122, 212]. When the benzene ring from the earlier characterized ATP-competitive compound Liu-20 was modified, a new series of molecules was obtained that could potentially increase the inhibitory potency and selectivity towards CK1 isoforms. The new series of IWP-derived compounds was kindly provided by our cooperation partner Prof. Dr. Christian Peifer (from Christian-Albrechts-University of Kiel in Germany) and initially tested for their biological activity against GST-CK1 α , GST-CK1 δ and GST-CK1 ϵ at a concentration of 10 μM (Figure 31). For the comparison of structural changes in terms of inhibitory potency and selectivity in this inhibitor set, the potent and selective IWP-related inhibitor Liu-20 was used as control inhibitor [212].

In the initial screening, all tested compounds (382 to 390) strongly inhibited kinase activity of CK1 δ and CK1 ϵ (Figure 31B and C), while activity of CK1 α was not

affected. This observation was not the case for 386, which significantly reduced activity of CK1 α to less than 50 % (Figure 31A and D). At a concentration of 10 μ M all tested IWP-derived compounds (except inhibitor 386) were comparable to Liu-20 in terms of inhibitory potency and selectivity.

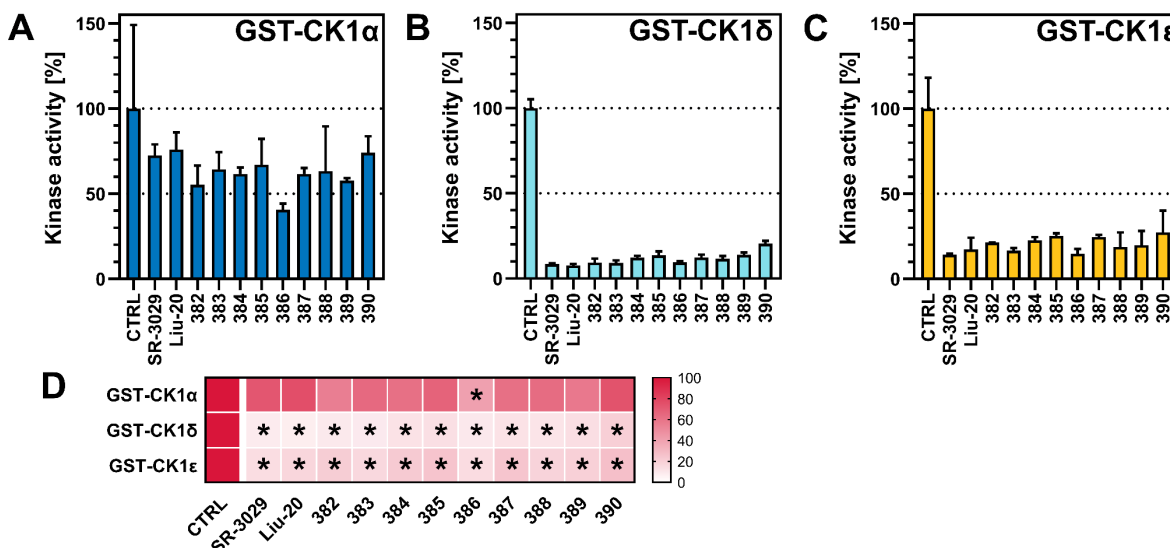


Figure 31: Initial screening of IWP-derived compounds. IWP-derived compounds were screened at a concentration of 10 μ M with (A) GST-CK1 α , (B) GST-CK1 δ and (C) GST-CK1 ϵ . Inhibitors SR-3029 and Liu-20 were used as positive controls. Phosphate incorporation was quantified and normalized to DMSO as solvent control (CTRL). Experiments were performed in triplicates. Results are shown as mean values and error bars represent the standard deviation. (D) Heatmap of the results shown in (A), (B) and (C). Differences in means were tested for statistical significance by using the non-parametric Mann-Whitney U test. * indicates $p \leq 0.05$.

Because all IWP-derived compounds significantly reduced the residual kinase activity to less than 50 %, IC₅₀ values for CK1 δ and CK1 ϵ were determined for all IWP-derived compounds. Determined IC₅₀ and calculated K_{ic} values for all IWP-derived compounds tested with CK1 δ and CK1 ϵ are shown in Table 27.

Table 27: IC₅₀ determination of IWP-derived compounds. IC₅₀ and K_{ic} values of IWP-derived compounds for GST-CK1 α , GST-CK1 δ and GST-CK1 ϵ . IC₅₀ determination was performed in triplicates.

Inhibitor	IC ₅₀ value [nM]/K _{ic} value [nM]			IC ₅₀ (CK1 δ /CK1 ϵ) ratio
	GST-CK1 α	GST-CK1 δ	GST-CK1 ϵ	
SR-3029	> 10,000	354/177	2,210/1,105	6
Liu-20	> 10,000	403/202	2,743/1,372	7
382	> 10,000	342/171	382/191	1
383	> 10,000	118/59	1,416/708	12
384	> 10,000	135/68	1,857/929	14
385	> 10,000	572/286	699/350	1
386	nd	385/193	2,486/1,243	7
387	> 10,000	969/485	432/216	2 (CK1 ϵ /CK1 δ)
388	> 10,000	638/319	185/93	4 (CK1 ϵ /CK1 δ)
389	> 10,000	671/336	309/155	2 (CK1 ϵ /CK1 δ)
390	> 10,000	1,500/750	nd	-

nd: Not determined.

Most potent and CK1 δ -selective IWP-derived compounds 383 and 384 are shown in Figure 32A and B, respectively. The results of IC₅₀ determination of the less potent and CK1 δ -selective IWP-derived compounds 382 and 385 to 390 are shown in Supplementary Figure 1. Additionally, IC₅₀ values were determined for both control inhibitors Liu-20 and SR-3029 (Figure 32C and D).

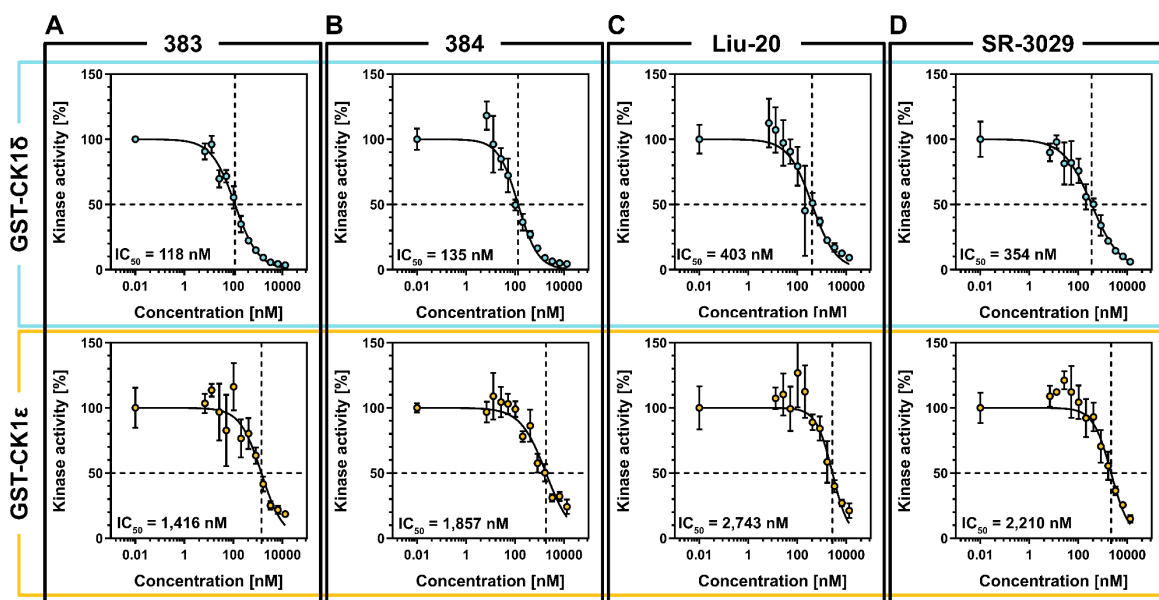


Figure 32: IC₅₀ determination of the most potent IWP-derived compounds. IC₅₀ determination was performed with GST-CK1 δ and GST-CK1 ϵ for the most potent IWP-derived compounds (A) 383 and (B) 384 as well as (C) Liu-20 and (D) SR-3029 as positive controls. Phosphate incorporation was quantified and normalized to DMSO as solvent control. Experiments were performed in triplicates. Results are shown as mean values and error bars represent the standard deviation. Data were fit to sigmoidal dose-response curve using GraphPad Prism 8.

Among the set of tested IWP-derived compounds, inhibitor 383 showed the strongest effect with an IC_{50} value of 118 nM for CK1 δ . Additionally, IC_{50} value for CK1 ϵ was 12 times higher with 1,416 nM compared to CK1 δ indicating high CK1 δ -isoform selectivity. CK1 δ -isoform selectivity could be exceeded by IWP-derived compound 384 with an IC_{50} value of 135 nM for CK1 δ and 1,857 nM for CK1 ϵ . Compared to the determined IC_{50} values of Liu-20 for CK1 δ (403 nM) and CK1 ϵ (2,743 nM) and SR-3029 for CK1 δ (354 nM) and CK1 ϵ (2,210 nM), both inhibitors, 383 and 384, showed higher potency towards both kinases and higher selectivity towards CK1 δ . Additionally, inhibitor 386 showed a potent, but non-selective inhibition towards CK1 δ and CK1 ϵ in the initial screenings at 10 μ M. However, according to the determined IC_{50} values, inhibitor 386 showed a high CK1 δ isoform selectivity compared to CK1 ϵ , which was shown to be very similar to the determined IC_{50} values of Liu-20. Interestingly, inhibitors 387, 388 and 389 were more specific for CK1 ϵ than for CK1 δ .

3.2.2.3 Initial screening and IC_{50} determination of isoxazole derivatives

Recently, several isoxazole-based inhibitors has been reported as potent CK1 δ -specific inhibitors [224, 262]. The inhibitor Pfeifer-1 (3,4-diaryl-isoxazole 1) was identified as a potent dual inhibitor of p38 α MAPK1 and CK1 δ [262]. Pfeifer-1 was selected as lead structure for the development of optimized ATP-competitive CK1 δ inhibitors. To enhance its selectivity towards CK1 isoforms, chiral iminosugars were attached that resulted in the set of isoxazole derivatives, which were developed, synthesized and kindly provided by Dr. Andreas Luxenburger and colleagues.

In the initial screening, isoxazole derivatives were tested at a concentration of 10 μ M with GST-CK1 α , GST-CK1 δ and GST-CK1 ϵ (Figure 33). Compounds 392 to 394 and 402 significantly inhibited CK1 δ and CK1 ϵ activity, while CK1 α was not affected. Contrarily to that, compound 395 significantly inhibited all CK1 isoforms (Figure 33). Compound 391, which is linked to an amino alcohol, did not show any noticeable inhibitory activity towards all CK1 isoforms.

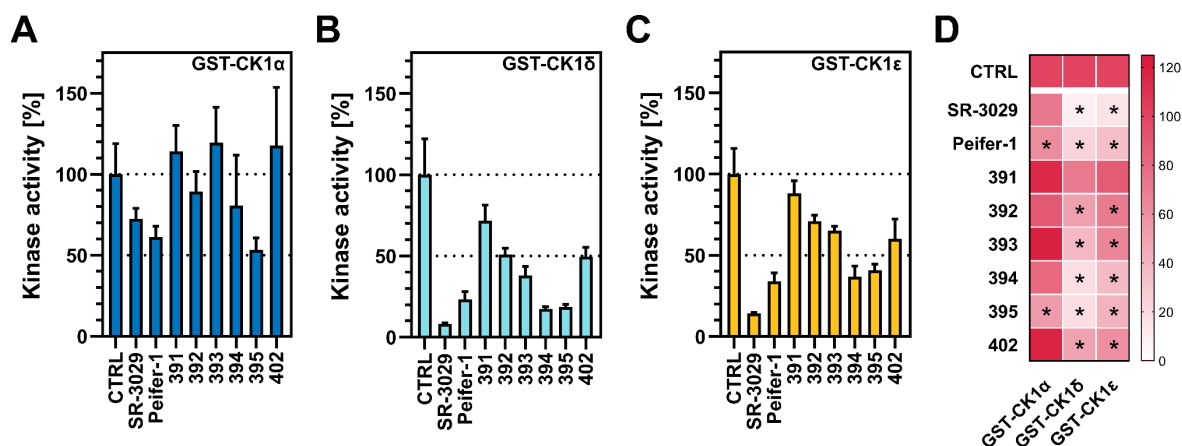


Figure 33: Initial screening of isoxazole derivatives. Isoxazole derivatives were screened at a concentration of 10 μ M with **(A)** GST-CK1 α , **(B)** GST-CK1 δ and **(C)** GST-CK1 ϵ . Inhibitors SR-3029 and Peifer-1 were used as positive controls. Phosphate incorporation was quantified and normalized to DMSO as solvent control (CTRL). Experiments were performed in triplicates. Results are shown as mean values and error bars represent the standard deviation. **(D)** Heatmap of the results shown in (A), (B) and (C). Differences in means were tested for statistical significance by using the non-parametric Mann-Whitney U test. * indicates $p \leq 0.05$. The figure was modified from [104], which is licensed under a Creative Commons Attribution 4.0 international license (CC BY 4.0), <https://creativecommons.org/licenses/by/4.0/>.

Because compound 394 and 395 significantly reduced the residual kinase activity of CK1 δ and CK1 ϵ to less than 50 %, IC₅₀ values for both kinases were determined for these compounds (Figure 34). Results of IC₅₀ determination of compound 393 with CK1 δ is shown in Supplementary Figure 2. Determined IC₅₀ and calculated K_{ic} values for the tested isoxazole derivatives tested with GST-CK1 δ and GST-CK1 ϵ are shown in Table 28.

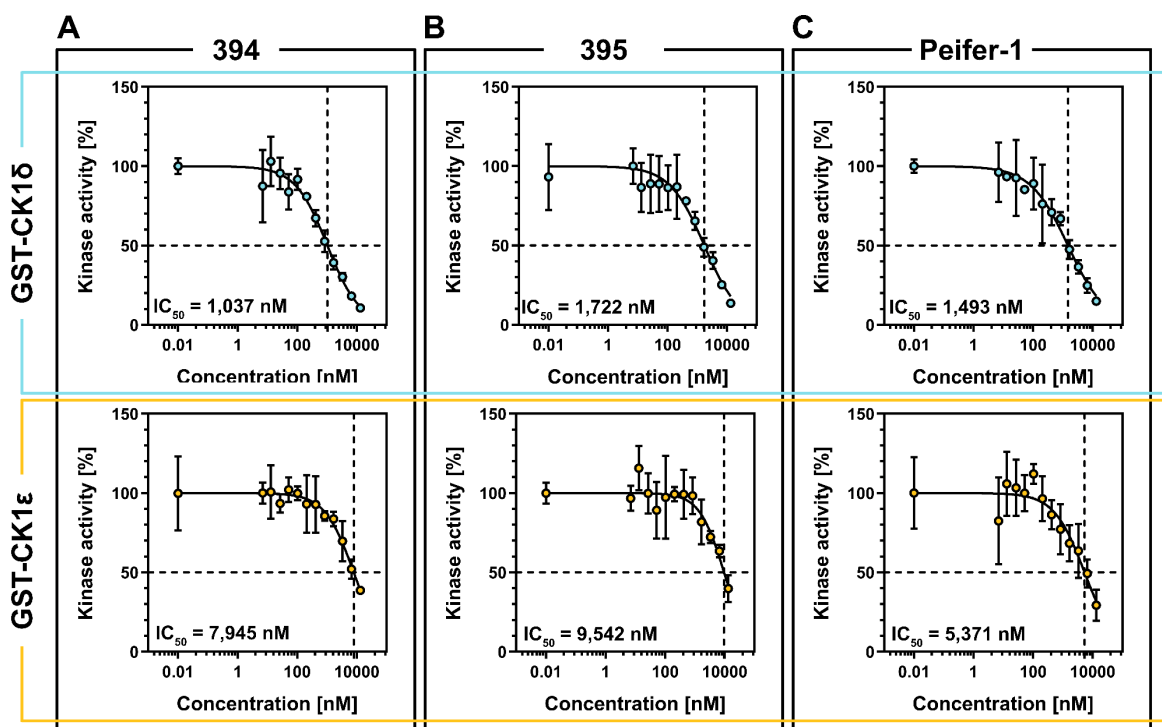


Figure 34: IC₅₀ determination of the most potent isoxazole derivatives. IC₅₀ determination was performed with GST-CK1 δ and GST-CK1 ϵ for the most potent isoxazole derivatives (**A**) 394, (**B**) 395 and (**C**) Peifer-1 as positive control. Phosphate incorporation was quantified and normalized to DMSO as solvent control. Experiments were performed in triplicates. Results are shown as mean values and error bars represent the standard deviation. Data were fit to sigmoidal dose-response curve using GraphPad Prism 8.

Among all tested compounds, compound 394 (bearing a 3*S*,4*R*-configured iminosugar) was identified as the most potent inhibitor with an IC₅₀ value of 1,037 nM (for CK1 δ) and 7,945 nM (for CK1 ϵ) (Figure 34A). Additionally, compound 394 had better inhibitory activity toward CK1 δ than the lead structure Peifer-1 with an IC₅₀ value of 1,496 nM for CK1 δ and 5,731 nM for CK1 ϵ . Moreover, compound 394 was twice as selective as the lead structure Peifer-1. Comparing both enantiomers (394 and 395) with each other, 395 proved to be slightly less active with an IC₅₀ value of 1,722 nM for CK1 δ and less selective towards both CK1 isoforms. Both 2-fluoropyridinyl analogs 393 and 392 were less active compared to their non-fluorinated analogs 394 and 395. However, according to the outcome of the configuration of 394 and 395, compound 393 (bearing the 3*S*,4*R*-configured iminosugar) proved to be more active towards CK1 δ compared to its enantiomer 392.

Table 28: IC₅₀ determination of isoxazole derivatives. IC₅₀ and K_{ic} values of isoxazole derivatives for GST-CK1 α , GST-CK1 δ and GST-CK1 ϵ . IC₅₀ determination was performed in triplicates.

Inhibitor	IC ₅₀ value [nM]/K _{ic} value [nM]			IC ₅₀ (CK1 δ /CK1 ϵ) ratio
	GST-CK1 α	GST-CK1 δ	GST-CK1 ϵ	
SR-3029	> 10,000	354/177	2,210/1,105	6
Peifer-1	> 10,000	1,493/747	5,371/2,686	4
391	> 10,000	> 10,000	> 10,000	-
392	Enantiomers	> 10,000	> 10,000	-
393		3,418/1,709	> 10,000	> 3
394	Enantiomers	> 10,000	1,037/519	7,945/3,973
395		> 10,000	1,722/861	9,542/4,771
402	> 10,000	> 10,000	> 10,000	-

3.2.3 Toxicity of compounds in cell culture

As IWP-derived compounds 383 and 384 as well as isoxazole derivative 394 have proven their inhibitory potency and selectivity towards CK1 δ *in vitro*, this set of inhibitors and their respective control inhibitors (Liu-20, Peifer-1 and SR-3029) were further characterized for their cytotoxic effects and maximal applicable dose for further experiments. As the CK1 δ -specific and potent inhibitor PF-670462 has already proven its potential to inhibit tau phosphorylation significantly (see chapter 3.1.2), it has additionally been selected for the following experiments.

Cytotoxic effects of the selected CK1 δ -specific inhibitors were identified by using transduced hNPCs, which were differentiated to glial cells and neurons for six days. After this time period, cells were treated with 383, 384, 394 and the respective control compounds Liu-20, Peifer-1, SR-3029 and PF-670462 at several concentrations (0.1, 0.5, 1, 5 and 10 μ M) for 24 h. Cell viability after the treatment was determined by using a cell metabolic assay measuring the conversion of MTT to formazan via absorption. Obtained data was normalized to DMSO (corresponding to 0 μ M), which served as solvent control. Results are shown in Figure 35.

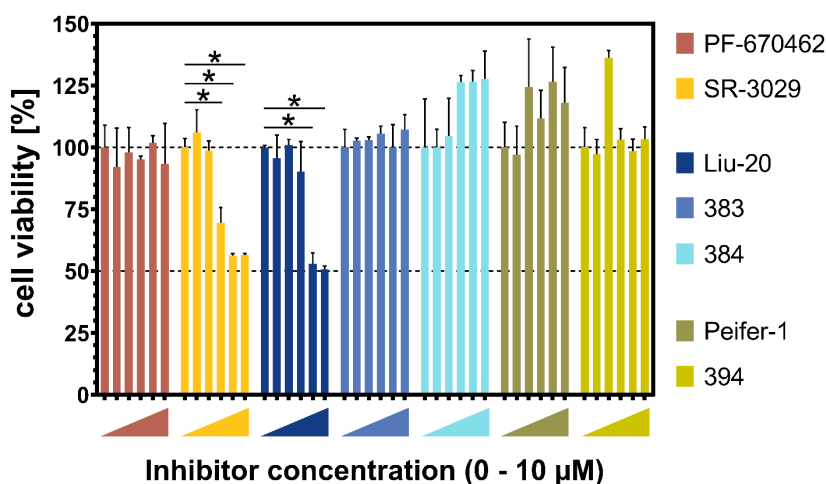


Figure 35: Neuronal cell toxicity of CK1δ-specific inhibitors. Transduced hNPCs were differentiated for six days and treated with 0.1, 0.5, 1, 5 and 10 μM CK1δ-specific inhibitors and DMSO as solvent control for 24 h. The next day, mitochondrial activity (corresponding to cell viability) was tested by using MTT solution. Conversion of MTT to formazan was quantified using a multimode plate reader. Data was normalized to DMSO. Experiments were performed in triplicates. Results are shown as mean values and error bars represent the standard deviation. Differences in means were tested for statistical significance by using the non-parametric Mann-Whitney U test. * indicates $p \leq 0.05$.

Most of the tested inhibitors did not affect cell viability in the analyzed concentration range between 0.1 μM and 10 μM. However, inhibitor SR-3029 and Liu-20 significantly reduced cell viability at a concentration of 1 μM (SR-3029) and 5 μM (Liu-20). With a view to preserve the CK1δ-specific inhibitors' therapeutic potential, while keeping cyto-toxic effects and thus inhibitor concentration as low as possible, and for reasons of comparability, all inhibitors were used at the same concentration of 0.1 μM for long-term experiments.

3.2.4 Biological effect of CK1δ-specific inhibitors in the “Alzheimer’s-in-a-dish” model

For the investigation of the therapeutic effects of CK1δ-specific inhibitors, the “Alzheimer’s-in-a-dish” model system was used. The “Alzheimer’s-in-a-dish” model was established by viral transduction of hNPCs with mutant forms APPSL and PSEN1ΔE9, which are relevant in early-onset FAD [181]. As a consequence, transduced hNPCs secrete high levels of Aβ peptides and the formation of amyloid plaques as well as tau hyperphosphorylation and aggregation can be observed in 3D cultures after at least six weeks (amyloid plaques) and 10 weeks (tau hyperphosphorylation and aggregation) of differentiation and cell maintenance, respectively [181].

With the aim to investigate the biological effects of the set of selected CK1 δ -specific inhibitors PF-670462, SR-3029, Liu-20, 383, 384, Peifer-1 and 394 on A β pathology as well as tau hyperphosphorylation and aggregation, thin- and thick-layer 3D cultures of transduced hNPCs were generated. After six days of differentiation, cells were treated with 0.1 μ M CK1 δ -specific inhibitors, 10 μ M β -secretase-specific inhibitor IV [202] and 0.1 μ M GSK3 α / β -specific inhibitor CHIR-98014 [281] as positive control for a total maintenance period of six weeks (for amyloid plaque formation) or twelve weeks (for tau hyperphosphorylation and aggregation). The treatment with DMSO was used as solvent control.

Cell viability of the 3D cultures was representatively tested by monitoring the thick-layer 3D cultures routinely via the LDH release assay during the treatment period (Figure 36A). Routinely monitoring of the cell viability detected no substantial changes in cell viability corresponding to the treatment with CK1 δ -specific inhibitors or DMSO as control. Increased LDH release was observed after the first two days of treatment and maintenance, which was probably a cellular reaction to changed growth conditions related to changes in media composition. The effect of DMSO on cell viability could be excluded as LDH release of control cells was similarly increased. Control treatment with the 100-fold higher concentrated β -secretase inhibitor IV compared to CK1 δ -specific inhibitors did not lead to increased LDH release during the entire observation period. However, treatment with 0.1 μ M CHIR-98014 led to continuous reduction of cell viability during the treatment of twelve weeks (Figure 36A). Therefore, control samples of cells treated with CHIR-98014 were excluded from the experimental set-up.

To investigate the influence of CK1 δ -specific inhibitors on APP processing, cells grown in thick-layer 3D cultures, which were treated with CK1 δ -specific inhibitors, β -secretase inhibitor IV as positive control or DMSO as solvent control for six weeks, were used for the quantification of secreted A β levels within the growth media by ELISA specifically detecting A β ₁₋₄₂ (Figure 36B). By comparing the A β release of naïve differentiated hNPCs (wt) with viral transduced hNPCs, it was clearly demonstrated that the viral transduction of hNPCs with mutant forms APPSL and PSEN1 Δ E9 had a drastic effect on A β production and APP processing indicating a successful establishment of the “Alzheimer’s-in-a-dish” model.

Regarding inhibitor treatment, the treatment of transduced cells with the positive control β -secretase inhibitor IV dramatically decreased $A\beta$ levels as expected. Decreased $A\beta$ levels were also observed after the treatment with the CK1 δ -specific inhibitor SR-3029. However, decreased levels of $A\beta$ peptides were probably caused by toxic properties of SR-3029 resulting in cell death, which was visualized by immuno-fluorescence staining (Figure 36C). Unfortunately, treatment with other CK1 δ -specific inhibitors had no significant influence on $A\beta$ release compared to DMSO (CTRL). Nevertheless, slightly decreased $A\beta$ levels were observed for Peifer-1 and 394.

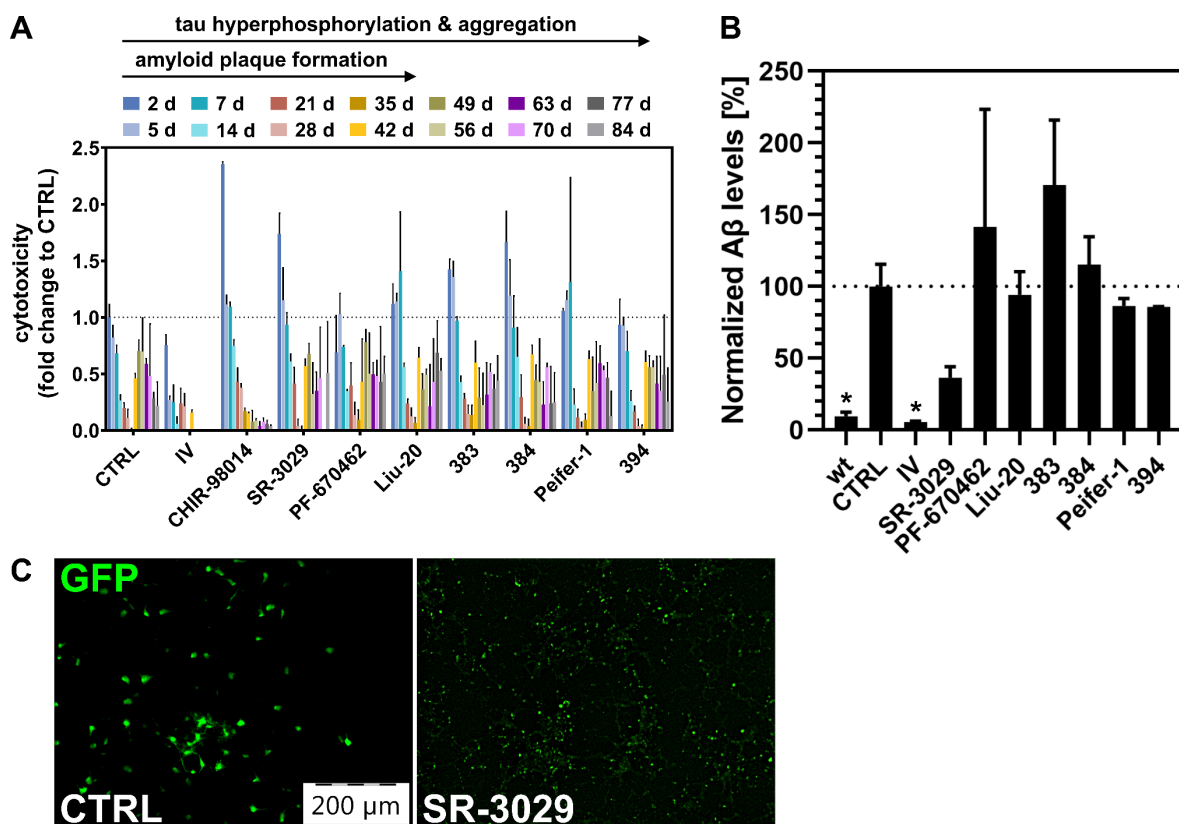


Figure 36: Effect of CK1 δ -specific inhibitors on $A\beta$ processing. (A) Effect of CK1 δ -specific inhibitors on cell viability of the 3D cell culture was monitored routinely via LDH release assay during the treatment of 42 d (for the observation of amyloid plaque formation) or 84 d (to detect tau pathology). Cell viability is shown as fold change to the value, which was determined for cell culture treated with DMSO (CTRL) after 2 d. **(B)** $A\beta$ release of transduced and differentiated hNPCs grown in thick 3D cultures was quantified using $A\beta$ -ELISA detecting $A\beta_{1-42}$ in the media after the treatment with CK1 δ -specific inhibitors, β -secretase inhibitor IV or DMSO as control (CTRL) for 42 d. Results were normalized to $A\beta$ release of cells treated with DMSO. Differences in means were tested for statistical significance by using the non-parametric one-sided Mann-Whitney U test. * indicates $p \leq 0.05$. **(C)** Thin-layer 3D cultures of transduced and differentiated cells after treating the cells with 0.1 μ M SR-3029 or DMSO (CTRL) as vehicle control. GFP signal results from the transduction of the lentiviral construct coding for APPSL-IRES-GFP. Images were taken at 10x magnification with an epifluorescence Olympus IX81 microscope. IV: β -secretase inhibitor IV, wt: Naïve differentiated hNPCs.

Further, it was investigated if the treatment with CK1 δ -specific inhibitors has an impact on tau hyperphosphorylation and aggregation. To analyze the phosphorylation of tau levels after treatment with CK1 δ -specific inhibitors or DMSO as solvent control, Western blot analysis with antibodies against total tau and p-tau (p-Ser214) were performed with lysates of the thick-layer 3D culture. Therefore, proteins were extracted using the detergent sarkosyl. Tau proteins, which were not soluble in the presence of sarkosyl (SISF) are assumed to be associated to PHF by showing the same structural and antigenic properties [191, 304, 364]. Western blot analysis of SSF and SISF are shown in Figure 37A and Figure 37B, respectively.

Changes in the phosphorylation patterns and signal intensities of p-tau (p-Ser214) within the SSF were detectable after the treatment with PF-670462, Liu-20 and 384 compared to CTRL (Figure 37A). Phosphorylation pattern of total tau showed more pronounced changes especially after the treatment with Liu-20, 384 and 394, but less with PF-670462. This diversity of high-MW tau bands most likely indicates different stages of tau phosphorylation.

Treatment with PF-670462 showed dramatic decrease in the phosphorylation of Ser214 and slight changes in the phosphorylation pattern compared to CTRL within the SISF, while the other inhibitors had no influence on phosphorylation at Ser214 (Figure 37B). Contrarily, the high-MW total tau bands were detected only after the treatment with PF-670462, 394 and DMSO in the SISF suggesting the presence of sarkosyl-insoluble tau aggregates. Reduced sarkosyl-insoluble tau aggregates were observed after the treatment with Liu-20, 383, 384 and Peifer-1.

Based on these experiments, immunofluorescence staining of tau was performed with fixed cells after the treatment with PF-670462, Liu-20 and 384 to visualize tau aggregates (Figure 37C). Signal, which resulted from tau staining (Cy5/red) was normalized to recombinantly expressed GFP and DMSO as solvent control (Figure 37D). Tau staining could especially be observed in neurites and neuronal cell bodies of the cells treated with DMSO. Treatment with PF-670462, Liu-20 and 384 dramatically decreased tau-staining. Significant differences in the tau staining were observed for PF-670462 and 384 compared to GFP and DMSO as control (Figure 37D). Nevertheless, due to the use of tau-antibody recognizing all tau proteins and not exclusively PHF-tau, caution should be exercised to directly connect total tau staining to tau aggregation.

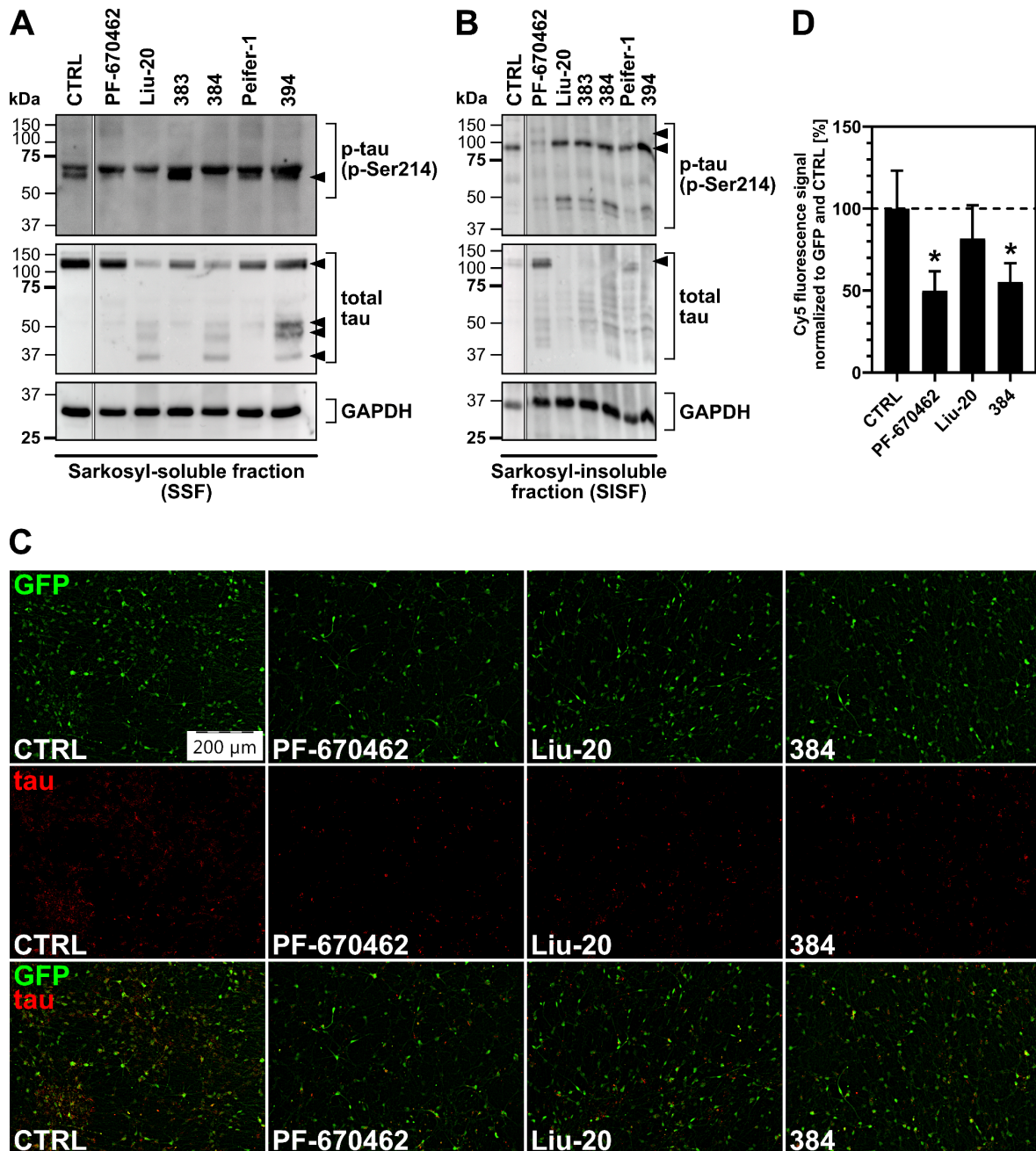


Figure 37: Effect of CK1 δ -specific inhibitors on tau phosphorylation and aggregation. (A/B) Transduced and differentiated cells were treated with CK1 δ -derived peptides for 84 h. After the treatment (A) SSF and (B) SISF were isolated and Western blot analysis were performed with anti-tau-p-Ser214, anti-tau or anti-GAPDH antibody, respectively. (C) Thin-layer 3D cultures of transduced and differentiated cells were stained with anti-tau antibody/anti-mouse antibody (Cy5/red) after treating the cells with 0.1 μM PF-670462, Liu-20, 384 or DMSO (CTRL) as vehicle control. GFP signal results from the transduction of the lentiviral construct coding for APPSL-IRES-GFP. Images were taken at 10x magnification with an epifluorescence Olympus IX81 microscope. (D) Fluorescence intensities from (C) were quantified using ImageJ. Cy5 fluorescence signal was normalized to GFP fluorescence signal. Experiments were performed in triplicates and are shown as mean values. Error bars represent the standard deviation. Differences in means were tested for statistical significance by using the non-parametric one-sided Mann-Whitney U test. * indicates $p \leq 0.05$. Scale bar: 200 μm .

3.3 Identification of CK1 δ -derived peptides modulating AD pathology

Previous studies already reported the critical involvement of PKs including members of CK1, such as CK1 δ , that could be linked to the pathogenesis of AD through the modulation of APP metabolism [204, 352] and the hyperphosphorylation of tau [149, 182, 218]. Although CK1-specific inhibitors have already proven to reduce A β production [325] and phosphorylation of tau-Ser214, most often they inhibit the activity of CK1-isoforms in general. As CK1 isoforms are essential for many cellular processes, also in healthy tissue, a general inhibition of certain CK1 isoforms might induce side effects. To bypass these circumstances, alternatives focusing on specific intervention of the kinase-substrate interaction are of particular interest. Therefore, the aim of the following chapter was to identify CK1 δ -derived peptides that specifically interfere with and prevent the interaction of CK1 δ and the target proteins APP695 or tau without directly inhibiting the kinase activity in general.

Initially, the CK1 δ -derived peptides library (as introduced in chapter 2.1.13) was tested for the interaction with APP695 and tau, and the ability to inhibit the CK1 δ -mediated phosphorylation. Afterwards, selected CK1 δ -derived peptides had to demonstrate their non-cytotoxic effects, cell entry ability and beneficial biological effect on the pathogenesis of AD that was investigated in the established cell culture model for AD.

3.3.1 CK1 δ -derived peptides bind to APP695 fragments and inhibit their CK1 δ -mediated phosphorylation

With the aim to identify peptides, which specifically block the interaction between CK1 δ and APP695, interaction analyses were performed. To perform peptide-protein interaction analysis *in vitro*, high amounts of recombinant protein were necessary. Unfortunately, biotechnological approaches failed to produce recombinant full-length APP695. Thus, with the aim to facilitate recombinant production of APP695, APP695 protein fragments were generated according to Figure 38.

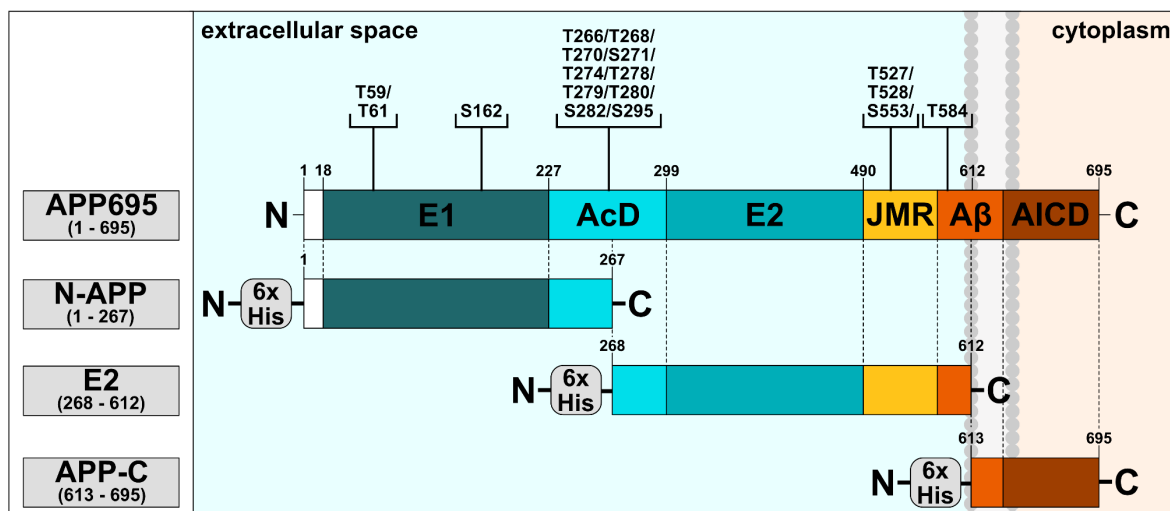


Figure 38: Generation of APP695 fragments to facilitate the protein production. Domain structure of full-length human APP695 including the E1-domain, AcD, E2-domain, JMR, A β and the AICD. Plasmid encoding for full-length human APP695 was used to generate APP695 fragments N-APP (aa 1 to 267), E2 (aa 268 to 612) and APP-C (613 to 695) via iPCR. Potential phosphorylation sites for CK1 on APP695 were predicted by the software-based approach ScanSite 4.1.0 at minimum stringency (according to Krismer et al. [188]) and are presented in brackets. *AcD*: Acidic domain, *AICD*: APP intracellular domain, *JMR*: Juxtamembrane region

For this approach, the protein sequence of APP695 was divided into smaller protein fragments, each of them includes certain domains of the full-length APP695 resulting in the generation of N-APP (aa 1 to 267), E2 (aa 268 to 612) and APP-C (613 to 695). A reduced MW and changes in physicochemical properties were supposed to facilitate production of the respective recombinant fragment in bacterial cultures. All APP695 fragments were generated by iPCR-mediated introduction of deletion or point mutations into the expression vector encoding for the codon-optimized full-length APP695.

To identify CK1 δ -derived peptides, which specifically interact with APP695 fragments, a streptavidin-linked interaction assay was performed using the CK1 δ -derived library (see chapter 2.6.1). In initial screenings, peptides interacting with APP695 fragments N-APP, E2 and APP-C were identified (Supplementary Figure 3). To confirm the results obtained in the initial screenings, CK1 δ -derived peptides, which showed significant binding to the tested APP695 fragments were further tested for their specific binding by comparing their binding to wells coated with APP695 fragments to uncoated wells (Figure 39).

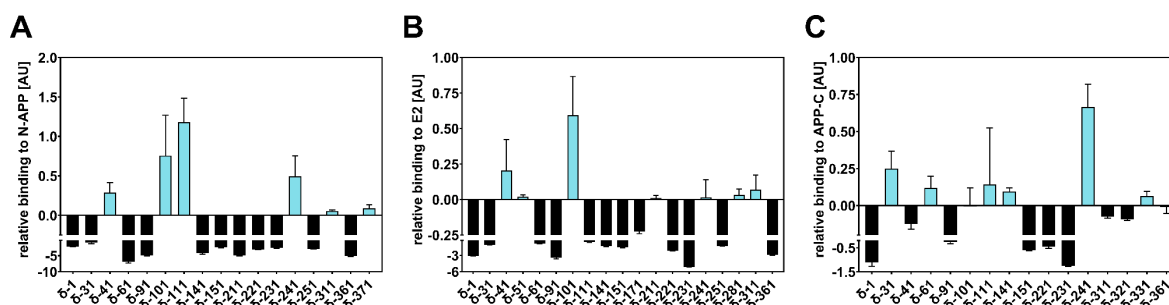


Figure 39: Identification of CK1 δ -derived peptides, which specifically bind to APP695 fragments. CK1 δ -derived peptides, which specifically bind to APP695 fragments (A) N-APP, (B) E2 or (C) APP-C were detected via streptavidin-linked interaction assay. Specific binding of CK1 δ -derived peptides to the respective APP695 fragment is shown in comparison with nonspecific binding to uncoated wells. Experiments were performed in triplicates. Results are shown as mean values and error bars represent the standard deviation. The figure was modified from [286], which is licensed under a Creative Commons Attribution 4.0 international license (CC BY 4.0), <https://creativecommons.org/licenses/by/4.0/>.

According to the data obtained from the streptavidin-linked interaction assay, peptides δ -41, δ -101, δ -111, δ -241, δ -311 and δ -371 interacted specifically with N-APP (Figure 39A). Among them, δ -311 and δ -371 showed weakest interaction with N-APP. According to the comparison of E2-coated to uncoated wells, CK1 δ -derived peptides δ -41, δ -51, δ -101, δ -211, δ -251, δ -281 and δ -311 were able to specifically interact with E2 (Figure 39B). Considering all CK1 δ -derived peptides interacting with E2, δ -41 and δ -101 showed the strongest interaction. Additionally, peptides δ -31, δ -61, δ -111, δ -141, δ -241 and δ -331 interacted specifically with APP-C. Strongest peptide-protein interaction was observed for δ -31 and δ -241. Among all tested peptides, δ -41, δ -101 and δ -241 demonstrated the strongest binding to the respective APP695 fragment.

Subsequent to the analysis of peptide-protein interactions via streptavidin-linked interaction assay, a set of selected CK1 δ -derived peptides, which showed binding abilities to APP695 fragments, were tested for their inhibitory ability. Therefore, *in vitro* kinase assays were performed with APP695 fragments N-APP, E2 and APP-C, which were used as substrates in equimolar amounts, and 6xHis-CK1 δ as kinase. Within the *in vitro* kinase assay, 20 μ M of the selected CK1 δ -derived peptides were utilized as potential peptide-based inhibitors, which compete with CK1 δ for the binding of APP695 fragments, leading to reduced phosphorylation of these fragments by CK1 δ .

Prior to the experimental approach, which tested the selected set of CK1 δ -derived peptides for inhibitory abilities, *in vitro* kinase assays have been performed to

demonstrate robust phosphorylation of the APP695 fragments (Figure 40A). By using the software-based approach ScanSite 4.1.0 [252], several putative phosphorylation sites for CK1-mediated phosphorylation could already be predicted in APP695 and are mostly located within the fragment E2 (see Figure 38). Results of the *in vitro* kinase assay with N-APP and E2 showed strong phosphorylation of both protein substrates by CK1 δ . As expected from the *in silico* analysis, no or only weak phosphorylation could be detected for APP695 fragment APP-C compared to N-APP and E2. However, detection of CK1 δ autophosphorylation confirms proper experimental conditions and kinase activity.

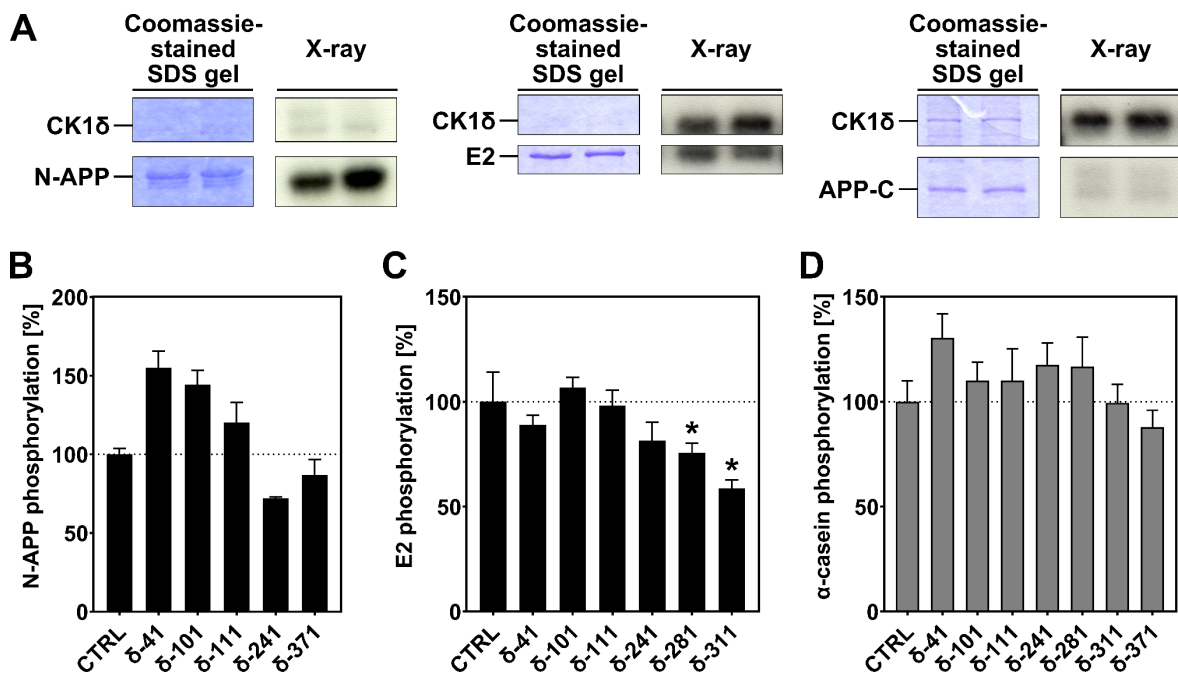


Figure 40: Effect of CK1 δ -derived peptides on CK1 δ -mediated phosphorylation of APP695 fragments. (A) CK1 δ -mediated phosphorylation of APP695 fragments. APP695 fragments N-APP, E2 and APP-C were phosphorylated by CK1 δ *in vitro*, separated via SDS-PAGE and visualized by Coomassie staining. Phosphorylation of the proteins and kinase autophosphorylation was visualized by autoradiography (X-ray). *In vitro* kinase assays were carried out with 20 μ M CK1 δ -derived peptides using 6xHis-CK1 δ as kinase. Phosphate incorporation was quantified and normalized to DMSO as solvent control (CTRL). Reactions were performed with recombinant (B) N-APP, (C) E2 or (D) α -casein as control. Experiments were performed in triplicates. Results are shown as mean values and error bars represent the standard deviation. Differences in means were tested for statistical significance by using the non-parametric one-sided Mann-Whitney U test. * indicates $p \leq 0.05$. The figure was modified from [286], which is licensed under a Creative Commons Attribution 4.0 international license (CC BY 4.0), <https://creativecommons.org/licenses/by/4.0/>.

For the evaluation of the inhibitory abilities of the selected set of positive binding CK1 δ -derived peptides to the APP695 fragments, *in vitro* kinase assays were carried out with 20 μ M CK1 δ -derived peptide or DMSO as solvent control. *In vitro* kinase reactions using N-APP as substrate indicated that peptide δ -241 reduces

phosphorylation of N-APP (Figure 40B). Phosphorylation of E2 was markedly reduced in the presence of CK1 δ -derived peptides δ -281 and δ -311 (Figure 40C). The inhibitory abilities of the other CK1 δ -derived peptides δ -371 for N-APP as well as δ -41, δ -101, δ -111 and δ -241 were less remarkable. Interestingly, an increase in phosphorylation was observed for CK1 δ -derived peptides δ -41 and δ -101 for N-APP. Control reactions proving that inhibition of CK1 δ -mediated phosphorylation of APP695 fragments is substrate-specific, was performed using the prototypic and CK1-specific substrate α -casein (Figure 40D). Among the tested peptides no significant inhibition of CK1 δ -mediated phosphorylation of α -casein could be detected, except for δ -371, which slightly reduced the phosphorylation of α -casein. In summary, control reactions indicated that the inhibitory abilities are specific for N-APP and/or E2. As previously described, no or only weak phosphorylation could be observed for APP695 fragment APP-C, when it was phosphorylated with CK1 δ . Based on this, inhibitory abilities of CK1 δ -derived peptides have not been tested for APP-C including the transmembrane and C-terminal domain of APP695.

As a means to further characterize whether the identified peptides block the interaction of APP695 and CK1 δ , the NanoBiT[®] PPI system was established. With the NanoBiT[®] system, APP695-CK1 δ interactions were detected in live cells based on two subunits, which were fused to APP695 and CK1 δ . When both proteins with the subunits were expressed and interact, subunits were brought into close proximity to form an active enzyme that produced a luminescent signal after the addition of the Nano-Glo[®] Live Cell Reagent (see chapter 2.6.3). With the NanoBiT[®] system, selected CK1 δ -derived peptides should prove their ability to disturb the interaction between APP695 and CK1 δ .

For the establishment of appropriate conditions for the NanoBiT[®] APP695-CK1 δ interaction system eight different orientations of APP695 and CK1 δ fused to LgBiT and SmBiT C- or N-terminally were generated via iPCR and Gibson-Assembly. After successful generation, eight different combinations were co-transfected into HEK293 cells, incubated for 24 h and tested for their ability to interact by adding the Nano-Glo[®] Live Cell Reagent. The eight different combinations showed an increasing signal after adding the substrate, although the height and shape of the curve strongly varied between the combinations (Figure 41). Figure 41A shows the combinations with LgBiT fused to CK1 δ N- or C-terminally (indicated as Lg-N-CK1 δ

or Lg-C-CK1 δ) and SmBiT fused to APP695 N- or C-terminally (indicated as Sm-N-APP695 or Sm-C-APP695). Results of the interaction of APP695 fused to LgBiT N- or C-terminally (indicated as Lg-N-APP695 or Lg-C-APP695) and CK1 δ fused to SmBiT N- or C-terminally (indicated as Sm-N-CK1 δ or Sm-C-CK1 δ) are shown in Figure 41B. As recommended by the manufacturer, HaloTag[®] fused to SmBiT (Sm-Halo) co-expressed with the respective LgBiT fused CK1 δ or APP695 served as negative control. Specific protein interaction should result in higher levels of luminescence than LgBiT fusion protein, which was co-expressed with HaloTag[®]-SmBiT.

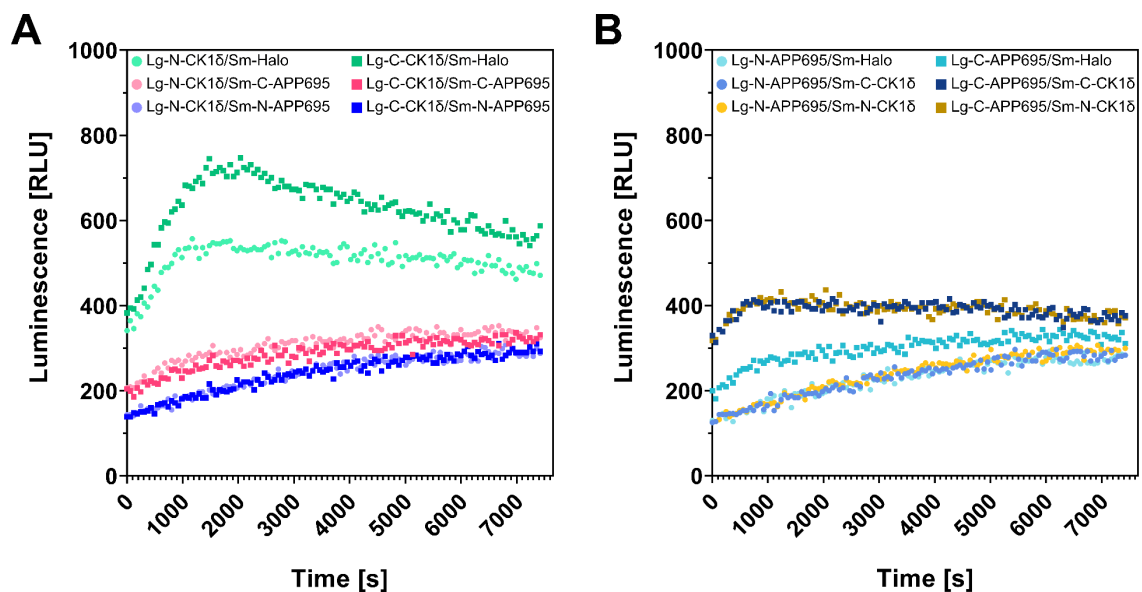


Figure 41: Establishment of the NanoBiT[®] APP695-CK1 δ interaction system. (A)/(B) Screening for optimal orientations of the CK1 δ and APP695 pair. Following transient co-transfection of HEK293 cells with the APP695-CK1 δ pair, the Nano-Glo[®] Live Cell Reagent was added and the luminescence signal was measured continuously at RT for 2 h. For control reactions, LgBiT was fused to CK1 δ or APP695 and SmBiT was fused to HaloTag[®]. **(A)** LgBiT fused to CK1 δ and SmBiT fused to APP695 in various orientations. **(B)** LgBiT fused to APP695 and SmBiT fused to CK1 δ in various orientations. *Lg*: LgBiT, *Sm*: SmBiT.

Comparing the combinations of LgBiT fused to CK1 δ and the respective counterparts, SmBiT fused to APP695 (Sm-C-APP695 or Sm-N-APP695) or SmBiT fused to HaloTag[®] as control (Sm-Halo), control reaction composed of LgBiT-CK1 δ and Sm-HaloTag[®] showed the highest signal intensities among all combinations indicating non-specific binding of LgBiT-CK1 δ to SmBiT-APP695 (Figure 41A). APP695 fused to LgBiT C-terminally (Lg-C-APP695) interacting with CK1 δ fused to SmBiT N- and C-terminally (Sm-N-CK1 δ and Sm-C-CK1 δ) resulted in two times higher signal intensities compared to the respective control (indicated as ■ in Figure 41B). APP695 fused to LgBiT N-terminally (Lg-N-APP695) did not result in any

difference between APP695-CK1 δ and the control APP695-HaloTag[®]. (indicated as • in Figure 41B). However, two times higher signal intensities of APP695-CK1 δ interaction compared to APP695-HaloTag[®] control was considered not specific enough for following experiments.

3.3.2 CK1 δ -derived peptides bind to tau and inhibit its CK1 δ -mediated phosphorylation

After performing experiments with APP695 and APP695 fragments, interaction analysis with tau and CK1 δ -derived peptides were performed. To identify CK1 δ -derived peptides, which specifically interact with tau, the aforementioned streptavidin-linked interaction assay was performed using the CK1 δ -derived library (see chapter 2.1.13) and two different tau isoforms, tau441 and tau383. Both isoforms differ in the number of N-terminal extension domains (N). Tau isoforms with 4R, such as tau441 and tau383, were described to lead to greater neurodegeneration and elevation of 4R tau isoforms was tightly connected to tauopathies [12, 249]. The difference between tau441 and tau383 is shown in Figure 42.

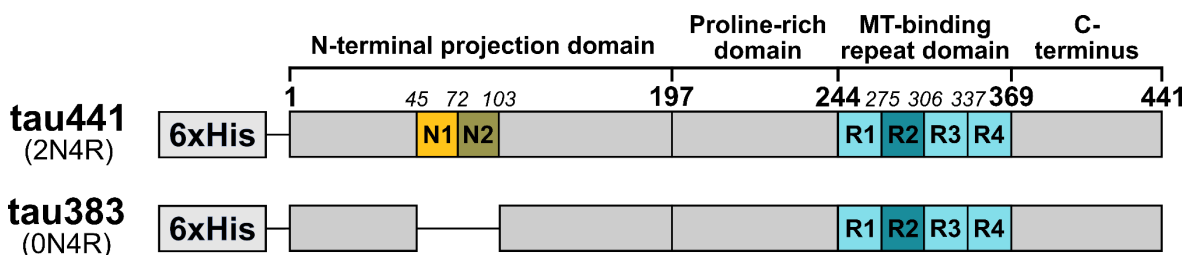


Figure 42: Domain structure of tau441 and tau383. Schematic overview of tau isoforms, tau441 and tau383, highlighting the N-terminal extension domains (N) and repeats (R), which are located within the MT-binding domain. Figure was modified from [311], which is licensed under a Creative Commons Attribution 4.0 international license (CC BY 4.0), <https://creativecommons.org/licenses/by/4.0/>. *MT: Microtubule*.

In initial screenings, peptides interacting with tau441 or tau383 were identified (Supplementary Figure 4). To confirm the results obtained in the initial screenings, CK1 δ -derived peptides, which showed significant binding to the tested tau isoforms, were further tested for their specific binding by comparing their binding to tau441- or tau383-coated wells to uncoated wells (Figure 43). In comparison of tau441-coated to uncoated wells, peptides δ -71, δ -101, δ -111, δ -241 and δ -281 were identified as specific tau441-binding peptides (Figure 43A). According to the comparison of tau383-coated to uncoated wells, peptides δ -71, δ -101, δ -201, δ -241,

δ -281 and δ -381 were able to specifically interact with tau383 (Figure 43B). Among them, δ -101 and δ -381 were identified as the strongest tau383-interacting peptides. Unlike APP695 fragments, tau441 could be purified in sufficient quality and quantity. Therefore, the results obtained by streptavidin-linked interaction assay could be verified by testing a small selection of promising peptides for their interaction abilities with tau441 via SPR (Figure 43C). For this approach, recombinantly produced 6xHis-tau441 was immobilized to a NTA sensor chip and binding of CK1 δ -derived peptides were detected by SPR analysis. As peptide δ -11 was a non-binding tau441 peptide in the streptavidin-linked interaction assay, it served as negative control in SPR. Although this measurement did not include all peptides, which were tested in streptavidin-linked interaction assay, peptides δ -71, δ -111 and δ -241 could be confirmed as specific tau441-binding peptides. In addition to that, also peptides δ -31, δ -311, δ -331 and δ -361 were observed to interact with tau441. In contrast to the streptavidin-linked interaction assay, δ -281 was observed as a non-specific binding peptide.

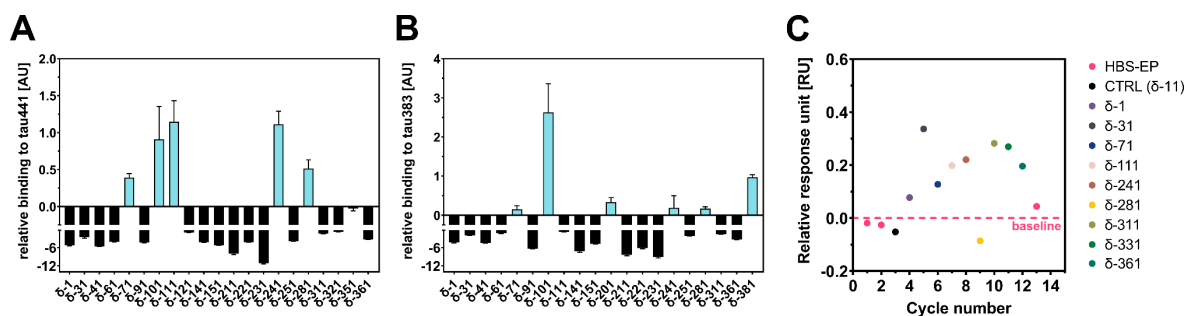


Figure 43: Identification of CK1 δ -derived peptides, which specifically bind to tau. CK1 δ -derived peptides, which specifically bind to (A) tau441 or (B) tau383 were detected via streptavidin-linked interaction assay. Specific binding of CK1 δ -derived peptides to tau441 or tau383 is shown relative to unspecific binding to uncoated wells. Experiments were performed in triplicates. Results are shown as mean values and error bars represent the standard deviation. (C) Interaction analysis with SPR. His-tagged tau441 was immobilized to the surface of a Biacore™ NTA sensor chip and interaction between CK1 δ -derived peptides (applied in 50 μ M concentration) and immobilized tau441 was detected by SPR analysis using a Biacore™ X100 instrument. HBS-EP: HEPES-buffered saline with EDTA and surfactant P20 as additives.

For the purpose to identify CK1 δ -derived peptides inhibiting CK1 δ -mediated phosphorylation of tau441 and tau383, the set of tau441- and tau383-interacting peptides were further tested in *in vitro* kinase assay reactions. Results of CK1 δ -derived peptides inhibiting CK1 δ -mediated phosphorylation of tau441, tau383 and α -casein as control substrate are shown in Figure 44.

As described before, *in vitro* kinase reactions were performed with 20 μ M CK1 δ -derived peptides or DMSO as solvent control. Most significant inhibition of CK1 δ -mediated phosphorylation of tau441 was detected for peptides δ -31, δ -71, δ -101, δ -241 and δ -281. Except peptide δ -241, all peptides reduced tau441 phosphorylation by more than 50 % (Figure 44A). For CK1 δ -mediated phosphorylation of tau383 no significant inhibitory effects could be determined (Figure 44B). For all CK1 δ -derived peptides that have proven significant inhibition of CK1 δ -mediated phosphorylation of tau441, no inhibitory effects on α -casein phosphorylation could be observed, thereby demonstrating inhibitory effects specific for tau441 phosphorylation (Figure 44C).

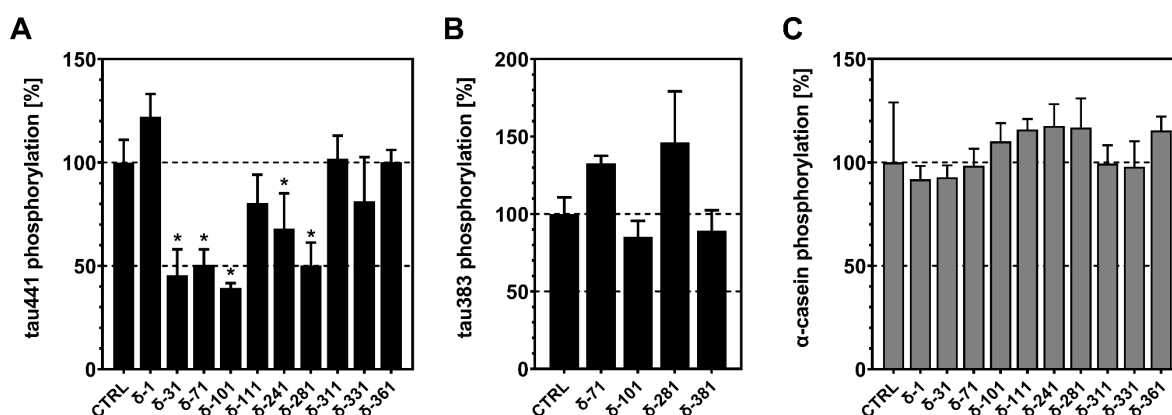


Figure 44: Effect of CK1 δ -derived peptides on CK1 δ -mediated tau phosphorylation. *In vitro* kinase assays were carried out with 20 μ M CK1 δ -derived peptides using 6xHis-CK1 δ as kinase. Phosphate incorporation was quantified and normalized to DMSO as solvent control (CTRL). Reactions were performed with recombinant (A) 6xHis-tau441, (B) 6xHis-tau383 or (C) α -casein as control. Experiments were performed in triplicates. Results are shown as mean values and error bars represent the standard deviation. Differences in means were tested for statistical significance by using the non-parametric Mann-Whitney U test. * indicates $p \leq 0.05$.

According to chapter 3.3.1, for the establishment of appropriate conditions for the NanoBiT[®] tau441-CK1 δ interaction system eight different orientations of CK1 δ and tau441 fused to LgBiT and SmBiT C- or N-terminally were generated, transfected and tested for their ability to interact. Eight tested combinations showed an increase in the signal after adding the Nano-Glo[®] Live Cell Reagent, although the signal intensity and shape varied between the tested combinations (Figure 45). Results of the interaction of LgBiT fused to CK1 δ N- or C-terminally (indicated as Lg-N-CK1 δ or Lg-C-CK1 δ) and SmBiT fused to tau441 N- or C-terminally (indicated as Sm-N-tau441 or Sm-C-tau441) is shown in Figure 45A. Reverse combination consisting of LgBiT fused to tau441 N- or C-terminally (indicated as Lg-N-tau441 and Lg-C-tau441) and SmBiT fused to CK1 δ N- or C-terminally (indicated as

Sm-N-CK1 δ or Sm-C-CK1 δ) are shown in Figure 45B. As already explained in chapter 3.3.1, HaloTag[®] fused to SmBiT (Sm-Halo) co-expressed with the respective LgBiT fused CK1 δ or tau441 served as negative control.

As shown in Figure 45A, all combinations with LgBiT fused to CK1 δ including SmBiT fused to tau441 or HaloTag[®] showed weak signal intensities. Comparing the combinations of LgBiT fused to tau441 and the respective counterparts (SmBiT fused to CK1 δ or SmBiT fused to HaloTag[®]), the combination Lg-N-tau441/Sm-N-CK1 δ had the highest signal intensity (Figure 45B). Based on the characteristic shaped sigmoidal kinetic curve and the signal intensity of Lg-N-tau441/Sm-N-CK1 δ , which was three times higher compared to control combination, Lg-N-tau441/Sm-N-CK1 δ was considered specific enough with caution and, therefore, selected for the following experiments.

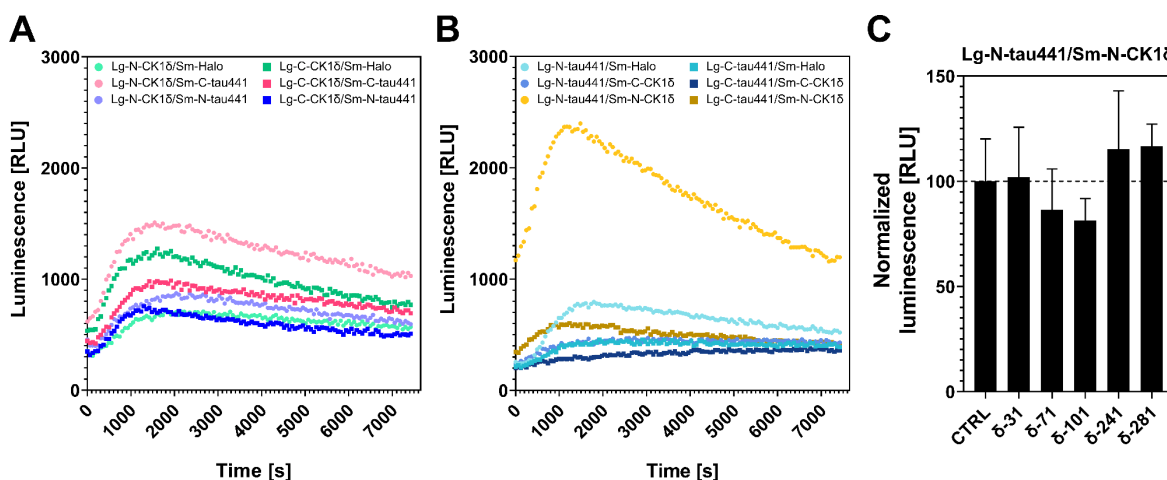


Figure 45: Identification of CK1 δ -derived peptides blocking the interaction of tau441 and CK1 δ by using NanoBiT[®]. (A)/(B) Screening for optimal orientations of the CK1 δ and tau441 pair. Following transient co-transfection of HEK293 cells with the CK1 δ /tau441 pair, the Nano-Glo[®] Live Cell Reagent was added and the luminescence signal was measured continuously at RT for 2 h. For control reactions, LgBiT was fused to CK1 δ or tau441 and SmBiT was fused to Halo. (A) LgBiT fused to CK1 δ and SmBiT fused to tau441 in various orientations. (B) LgBiT fused to tau441 and SmBiT fused to CK1 δ in various orientations. (C) After co-transfecting the cells with LgBiT-N-tau441 (Lg-N-tau441) and SmBiT-N-CK1 δ (Sm-N-CK1 δ), 10 μ M CK1 δ -derived peptides or DMSO as solvent control (CTRL) were added and incubated for 30 min. Nano-Glo[®] Live Cell Reagent was added and 15 min after addition, luminescence signal was measured using a multimode microplate reader. Results are shown as mean values and error bars represent the standard deviation. Differences in means were tested for statistical significance by using the non-parametric Mann-Whitney U test. *Lg*: LgBiT, *Sm*: SmBiT.

With the established NanoBiT[®] system including the combination Lg-N-tau441/Sm-N-CK1 δ , the set of inhibitory CK1 δ -derived peptides were tested for their ability to disturb the interaction between tau441 and CK1 δ in living HEK293 cells. Therefore, after co-transfection of the combination of Lg-N-tau441/Sm-N-CK1 δ , 10 μ M CK1 δ -

derived peptides or DMSO as solvent control were added and incubated for 30 min. Luminescence signal was measured 15 min after adding the Nano-Glo[®] Live Cell Reagent (Figure 45C). No decrease in luminescence signals were observed for CK1 δ -derived peptides δ -31, δ -241 and δ -281. However, the addition of δ -71 and δ -101 slightly reduced luminescence signal indicating potential disturbing effects.

3.3.3 Peptide localization confirms potential CK1 δ interaction sites

In order to assess whether the identified interacting and phosphorylation-inhibiting CK1 δ -derived peptides originate from potential kinase interacting domains, surface diagrams of CK1 δ were generated that highlight the localization of identified CK1 δ -derived peptides in the full-length CK1 δ protein structure. For this approach, the localization of the sequences of CK1 δ -derived peptides δ -31, δ -41, δ -71, δ -101, δ -111, δ -241 and δ -281 was visualized in the 3D cartoon and surface representation of CK1 δ (Figure 46). Generally, the C-terminal domain of CK1 δ cannot be illustrated due to its intrinsically disordered structure. For this reason, localization of the CK1 δ -derived peptides δ -311 and δ -371, which are located within the C-terminal domain, could not be visualized.

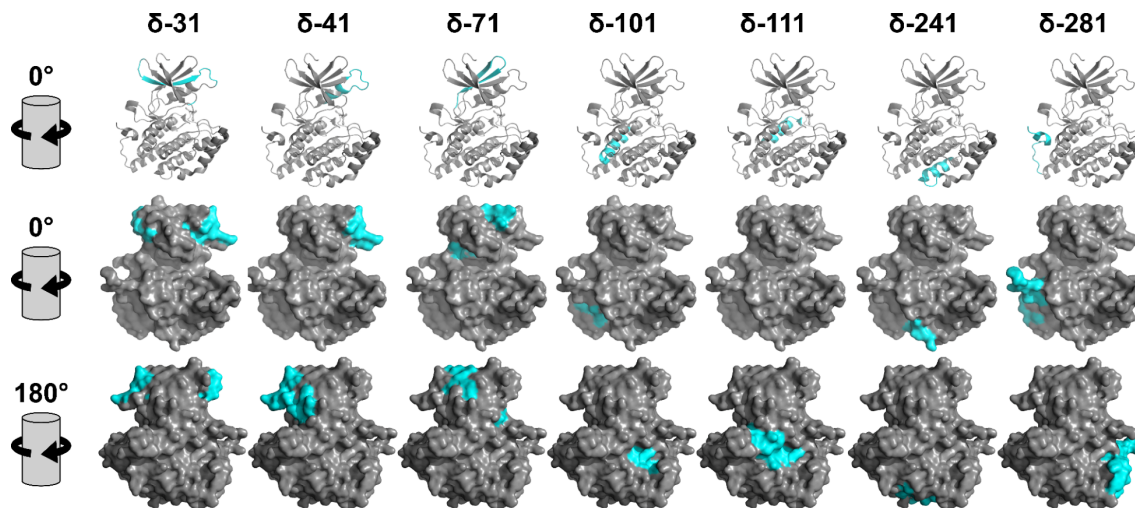


Figure 46: Localization of APP695/tau-interacting and -inhibiting CK1 δ -derived peptides in CK1 δ protein structure. The molecular structure of truncated CK1 δ encompassing aa 1 to 295 (PDB entry 6GZM) is represented as cartoon and surface diagram. Both representations show the localization of CK1 δ -derived peptides δ -31, δ -41, δ -71, δ -101, δ -111, δ -241 and δ -281. Since there is no structural data of the C-terminal domain of CK1 δ available, peptides δ -311 and δ -371 cannot be displayed. Shown peptides are highlighted in blue. Figures were created with the structure visualization software PyMOL. Protein structure of CK1 δ is displayed in original view (shown as 0°) and after rotation by 180°. The figure was modified from [286], which is licensed under a Creative Commons Attribution 4.0 international license (CC BY 4.0), <https://creativecommons.org/licenses/by/4.0/>.

As shown in Figure 46, most parts of the displayed CK1 δ -derived peptides were well exposed to the surface of the CK1 δ protein structure. Good accessibility of residues and, thus, direct contact between interaction partners is a necessary pre-condition for phosphorylation events. Therefore, peptides derived from protein regions within CK1 δ , which are well exposed, could also be involved in mediating binding mechanisms of full-length CK1 δ to interaction partners such as APP695 or tau under physiological conditions.

3.3.4 CK1 δ -derived peptides successfully enter neuronal cells without inducing cytotoxic effects

After it was proven that several CK1 δ -derived peptides block the interaction between CK1 δ and APP695 and/or tau and decrease their phosphorylation, which was shown via biochemical approaches *in vitro*, the identified CK1 δ -derived peptides were tested for their cytotoxic and cell-penetrating properties and, thus, their therapeutic potential.

First, cytotoxic effects of the selected CK1 δ -derived peptides were identified by using transduced hNPCs, which were differentiated to glial cells and neurons for six days. After this time period, cells were treated with CK1 δ -derived peptides at several concentrations (0.1, 0.5, 1, 5 and 10 μ M) for 24 h. Conversion of MTT to formazan was quantified using a multimode plate reader. Obtained data was normalized to DMSO (0 μ M), which served as solvent control. Results are shown in Figure 47.

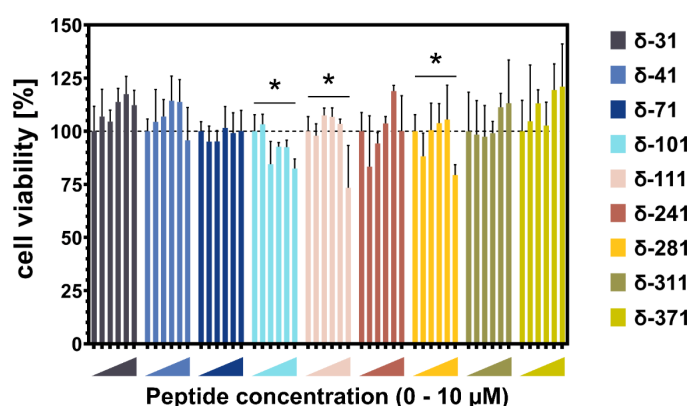


Figure 47: Neuronal cell toxicity of CK1 δ -derived peptides. Transduced hNPCs were differentiated for six days and treated with 0.1, 0.5, 1, 5 and 10 μ M CK1 δ -derived peptides and DMSO as solvent control for 24 h. The next day, mitochondrial activity (corresponding to cell viability) was tested by using MTT solution. Conversion of MTT to formazan was quantified using a multimode plate reader. Data was normalized to DMSO. Experiments were performed in triplicates. Results are shown as mean values and error bars represent the standard deviation. Differences in means were tested for statistical significance by using the non-parametric Mann-Whitney U test. * indicates $p \leq 0.05$.

Most of the tested CK1 δ -derived peptides showed no unspecific cytotoxic effects in the analyzed peptide concentration range between 0.1 μ M and 10 μ M. Peptides δ -101, δ -111 and δ -281 significantly reduced cell viability at a concentration of 10 μ M. However, lower peptide concentrations had no effect on the cell viability. With a view to preserve the CK1 δ -derived peptides' therapeutic potential, while keeping cytotoxic effects and thus peptide concentration as low as possible, a peptide concentration of 1 μ M was selected for further long-term treatments of 3D cultures.

Prior to the determination of peptide-mediated biological effects on cellular AD-associated functions, such as APP metabolism and tau hyperphosphorylation, cell-penetrating properties of the CK1 δ -derived peptides were investigated. For this experiment, naïve hNPCs were differentiated for six days and afterwards being treated with 1 μ M of the selected CK1 δ -derived peptide for 24 h. After the treatment, cells were fixed and stained with DAPI (to visualize the cell nuclei), anti- β -III-tubulin-antibody/DyLight 488 anti-mouse antibody (in green) to visualize the neuronal MT network, and streptavidin-TRITC (in red) to visualize biotinylated CK1 δ -derived peptides (Figure 48A). For the quantification of the peptide uptake, cells and peptide accumulations were counted and the peptide uptake ratio was calculated as the number of counted peptide accumulations per cell (Figure 48B).

Strong fluorescence staining of peptide accumulations could be observed for peptides δ -111, δ -281 and δ -371. Numerous accumulations could also be detected for δ -31, although fluorescence staining intensity of peptide accumulations was very weak. However, the presence of peptides indicate that these CK1 δ -derived peptides successfully entered the cell. Among all peptides the highest peptide uptake ratio could be calculated for δ -281 with 0.24 that demonstrates that the peptide enters 24 % of all analyzed cells. Compared to the peptides mentioned before, peptide-specific fluorescence staining was weak for δ -241 and δ -311. No peptide-specific staining could be detected for δ -41, δ -71 and δ -101. Following the confirmation of cell entry abilities, CK1 δ -derived peptides were tested with regard to their therapeutic potential in the cell-based "Alzheimer's-in-a-dish" model system published by Kim and colleagues [70, 181].

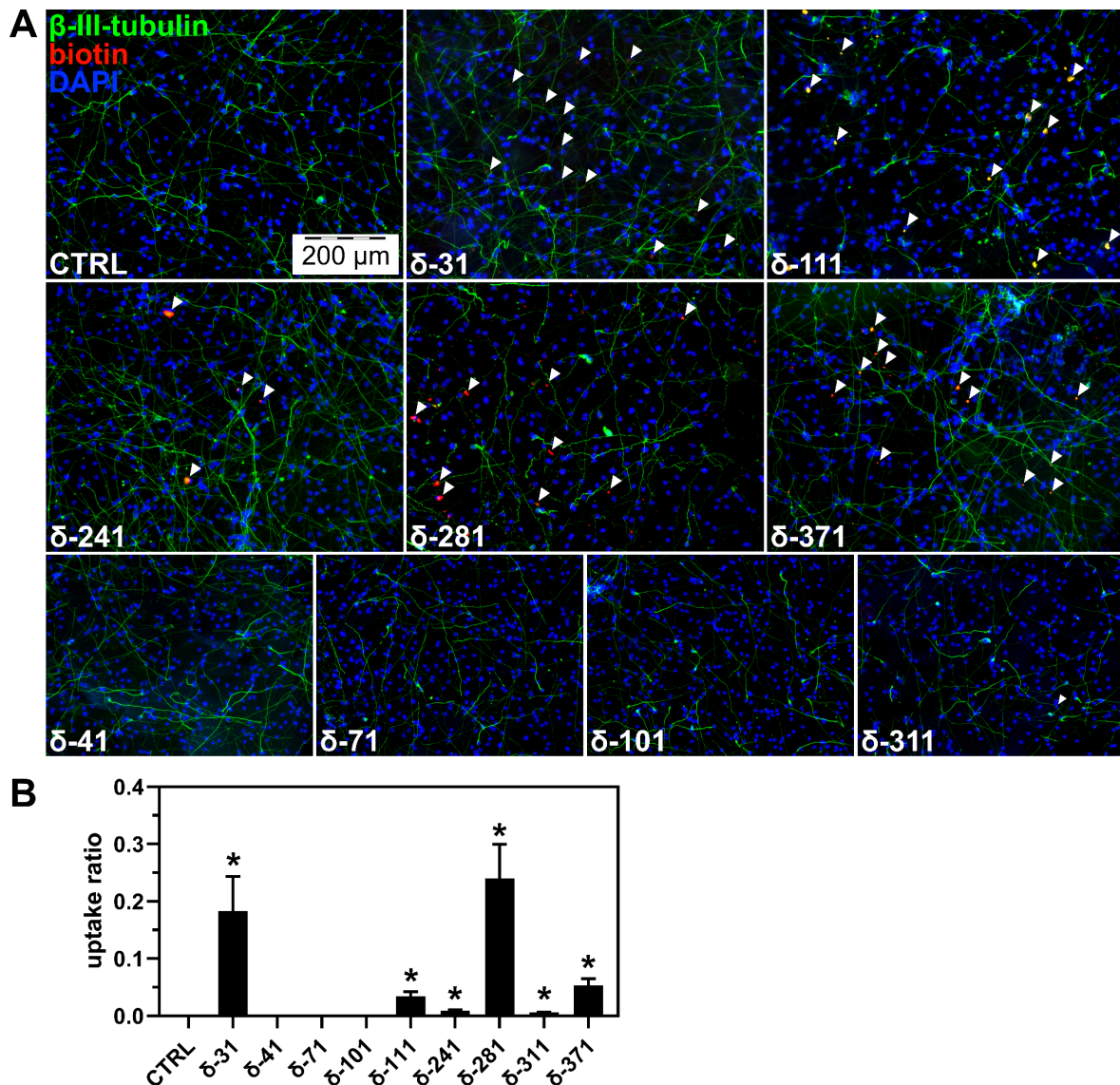


Figure 48: Cell entry of CK1 δ -derived peptides into living neuronal cells. (A) Naive hNPCs were differentiated for six days and incubated with 1 μ M biotinylated CK1 δ -derived peptides for 24 h. Differentiated cells were fixed and stained with DAPI (in blue) to visualize the cell nuclei, anti- β -III-tubulin-antibody/DyLight 488 anti-mouse antibody (in green) to visualize the neuronal MT network, and streptavidin-TRITC (in red) to visualize biotinylated CK1 δ -derived peptides. Images were taken at 10x magnification with an epifluorescence Olympus IX81 microscope. White arrows indicate peptide accumulations. *Scale bar: 200 μ m.* **(B)** Quantification of peptide uptake was performed by counting cells and peptide accumulations. Uptake ratio was calculated as the number of counted peptide accumulations per cell. Experiments were performed in triplicates. Differences in means were tested for statistical significance by using the non-parametric Mann-Whitney U test. * indicates $p \leq 0.05$. The figure was modified from [286], which is licensed under a Creative Commons Attribution 4.0 international license (CC BY 4.0), <https://creativecommons.org/licenses/by/4.0/>.

3.3.5 Biological effect of CK1 δ -derived peptides in the “Alzheimer’s-in-a-dish” model

To investigate the therapeutic effect of CK1 δ -derived peptides on AD pathology that have proven interaction with APP695 fragments and/or tau, inhibitory effects and cell entry abilities, the “Alzheimer’s-in-a-dish” model system was used. As described before, hNPCs, which were transduced with APPSL and PSEN1 Δ E9, secrete high

levels of A β peptides leading to the formation of amyloid plaques, and show tau hyperphosphorylation and aggregation in 3D cultures after at least six or ten weeks of differentiation and cell maintenance, respectively [181].

3.3.5.1 Treatment with CK1 δ -derived peptides results in lower A β levels and reduced formation of amyloid plaques

With the aim to characterize the biological effect of the set of selected CK1 δ -derived peptides (δ -41, δ -101, δ -111, δ -241, δ -281, δ -311 and δ -371) on A β release and amyloid plaque formation, 3D cultures of transduced hNPCs were generated. After six days of differentiation, cells were treated with 1 μ M of the set of selected CK1 δ -derived peptides, 10 μ M β -secretase inhibitor IV as positive control or DMSO as solvent control for a total maintenance period of six weeks. Cell viability of the thick-layer 3D cultures was routinely tested by LDH release assay during the treatment period (Figure 49A). Routinely monitoring of the cell viability detected no substantial changes in cell viability corresponding to the treatment with CK1 δ -derived peptides or DMSO as control. As for the treatment with CK1 δ -specific inhibitors, increased LDH release was detected after the first two days of treatment and maintenance, which was associated to changed growth conditions and not influence of DMSO.

After six weeks of treatment with CK1 δ -derived peptides, β -secretase inhibitor IV as positive control or DMSO as solvent control, secreted A β levels were quantified by ELISA within the growth media from thick-layer 3D cultures (Figure 49B). According to the results obtained from the quantitative ELISA, A β levels secreted by cells, which were treated with CK1 δ -derived peptide δ -41, δ -101 and δ -371, were significantly reduced compared to untreated cells (CTRL). A β levels of cells treated with the 10-fold higher concentrated positive control β -secretase inhibitor IV were reduced by approximately 94 %.

To characterize CK1 δ -derived peptides δ -41, δ -101 and δ -371 not only for their ability to inhibit A β secretion, but also to inhibit amyloid plaque formation, thin-layer 3D cultures were stained with an anti-A β antibody to visualize formed amyloid plaques (Figure 49C). Immunofluorescence staining was performed with thin-layer grown transduced hNPCs, which were treated for at least six weeks with CK1 δ -derived peptides or DMSO as solvent control. The GFP signal, which was expressed

within the whole cell, was a product from successful transduction with the lentiviral construct coding for APPSL-IRES-GFP.

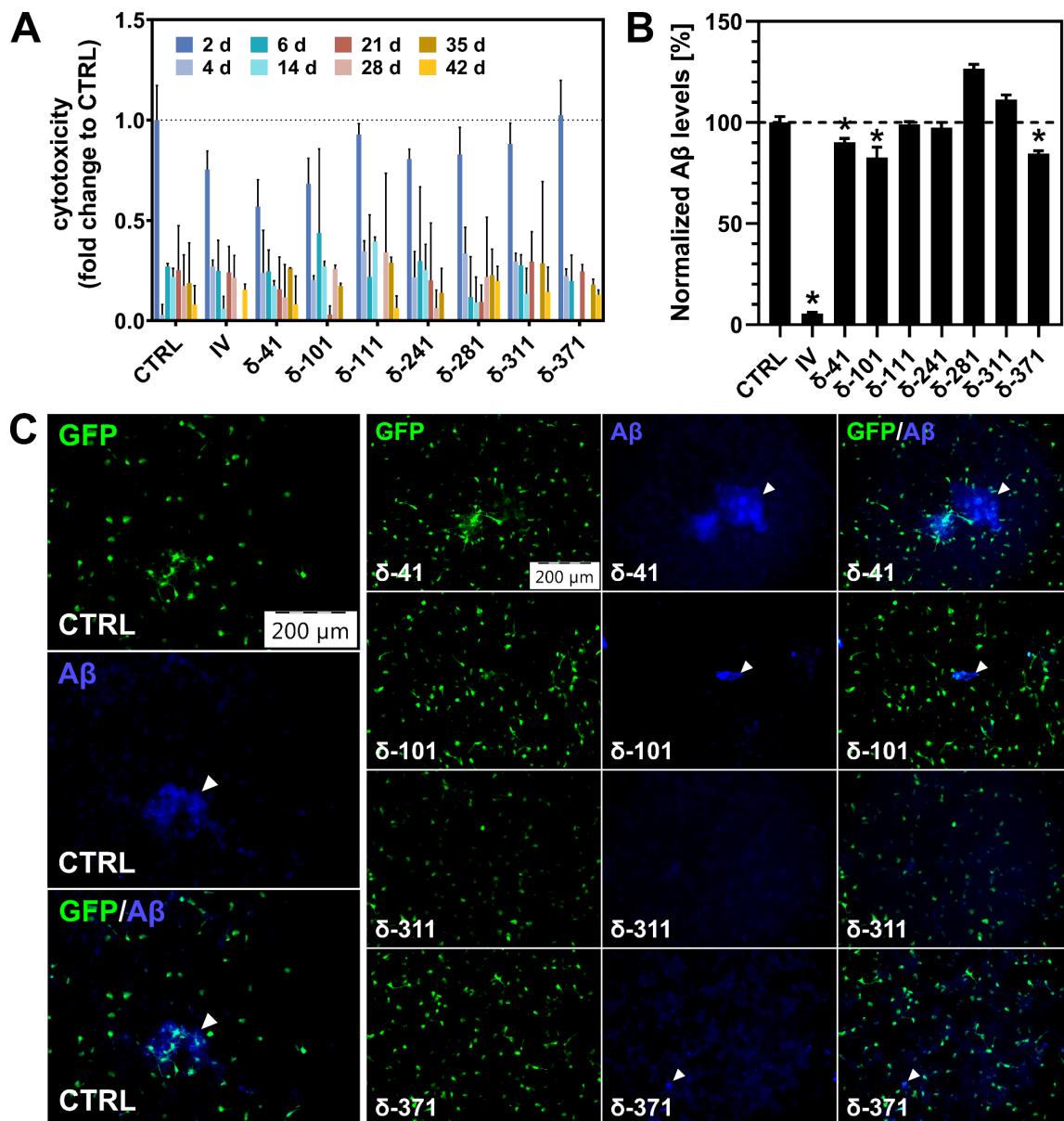


Figure 49: Effect of CK1δ-derived peptides on Aβ processing and amyloid plaque formation. (A) Effect of CK1δ-derived peptides on cell viability of the 3D cell culture was monitored routinely via LDH release assay during the treatment of 42 d. Cell viability is shown as fold change to the value, which was determined for cell culture treated with DMSO (CTRL) after 2 d. (B) Aβ release of transduced and differentiated hNPCs grown in thick 3D cultures was quantified using Aβ-ELISA detecting Aβ₁₋₄₂ in the media after the treatment with CK1δ-derived peptides or DMSO as control (CTRL) for 42 d. Results were normalized to Aβ release of cells treated with DMSO. (C) Immunofluorescence staining of transduced and differentiated hNPCs grown in thin 3D cultures after the treatment with CK1δ-derived peptides or DMSO as control (CTRL) for 42 d. GFP signal results from the transduction of the lentiviral construct coding for APPSL-IRES-GFP. Amyloid plaques were stained with an anti-Aβ antibody. Images were taken at 10x magnification with an epifluorescence Olympus IX81 microscope. White arrows indicate amyloid plaques. Experiments were performed in triplicates. Differences in means were tested for statistical significance by using the non-parametric Mann-Whitney U test. * indicates $p \leq 0.05$. The figure was modified from [286], which is licensed under a Creative Commons Attribution 4.0 international license (CC BY 4.0), <https://creativecommons.org/licenses/by/4.0/>. Scale bar: 200 μm. IV: β-secretase inhibitor IV.

As shown in Figure 49C, amyloid plaque formation was still present in thin-layer grown hNPCs treated with δ -41. However, plaque formation was substantially reduced, and size of visible plaques was decreased for cells treated with δ -101 and δ -371. Although δ -311 did not reduce A β secretion quantitatively, plaque formation was not visible in the immunofluorescence staining of cells treated with δ -311.

3.3.5.2 Treatment with CK1 δ -derived peptides reduced tau phosphorylation

The biological effect of CK1 δ -derived peptides that have proven to interact with tau and inhibit its phosphorylation (δ -31, δ -71, δ -101, δ -241 and δ -281), was tested in the “Alzheimer’s-in-a-dish” model. Therefore, thin- and thick-layer 3D cultures of transduced and differentiated hNPCs were treated with 1 μ M selected CK1 δ -derived peptides or DMSO as solvent control for total maintenance period of twelve weeks.

During the treatment period, changes in cell viability of thick-layer 3D cultures was routinely tested by LDH release assay (Figure 50A). As already described for peptides interacting with APP, routinely monitoring of the cell viability detected no substantial changes in cell viability corresponding to the treatment with CK1 δ -derived peptides or DMSO as control, not even after prolonged treatment period of twelve weeks.

The biological effect of CK1 δ -derived peptides on tau hyperphosphorylation was investigated by Western blot analysis with antibodies against total tau and p-tau (p-Ser214) using protein lysates from the SSF and SISF both obtained from the thick-layer 3D culture after twelve weeks of maintenance and treatment. Results of the Western blot analysis of SSF and SISF are shown in Figure 50B and Figure 50D, respectively.

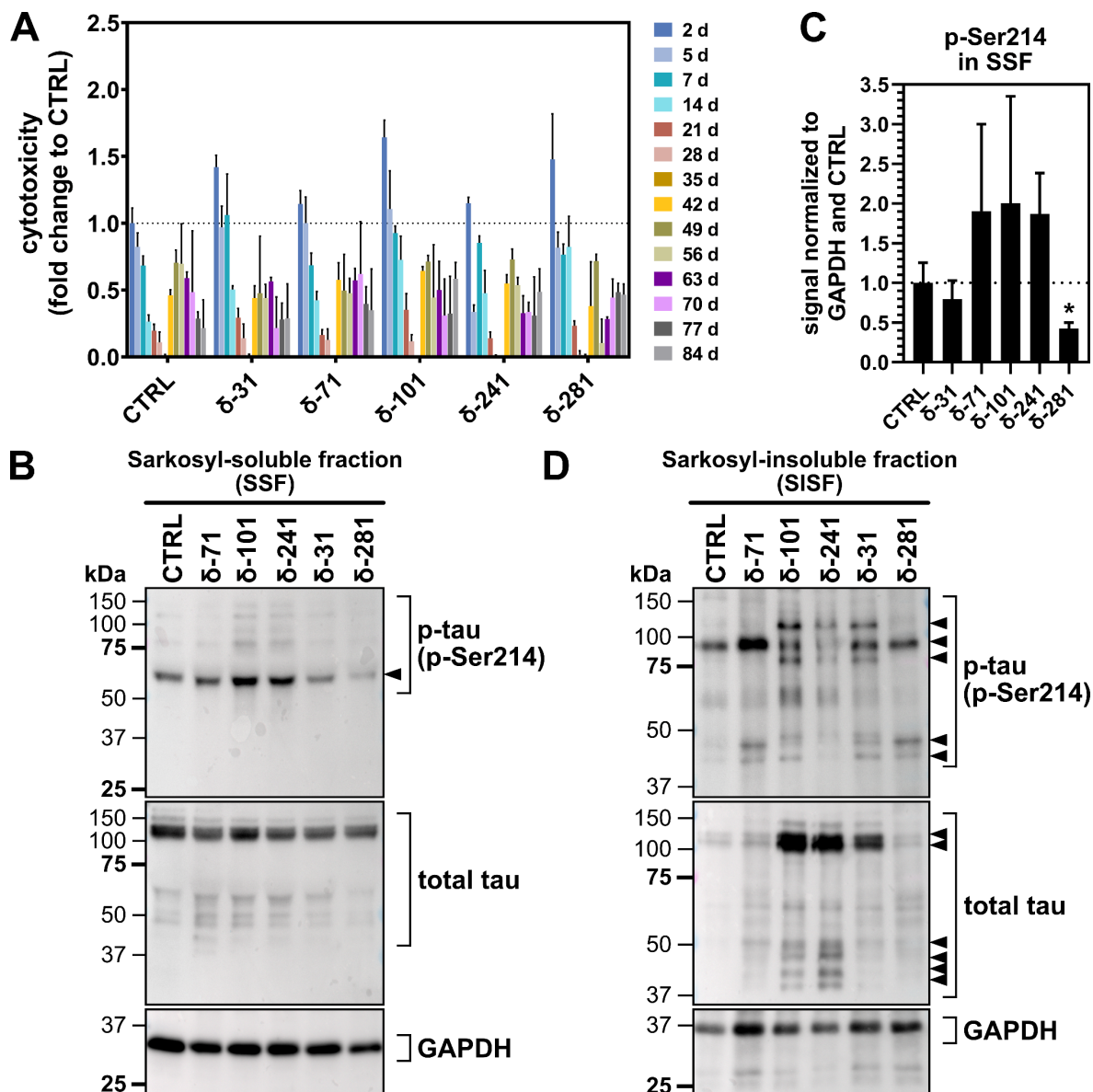


Figure 50: Effect of CK1 δ -derived peptides on tau phosphorylation. (A) Effect of 1 μ M CK1 δ -derived peptides on cell viability of the 3D cell culture was monitored routinely via LDH release assay during the treatment of 84 d. Cell viability is shown as fold change to the value, which was determined for cells treated with DMSO (CTRL) after 2 d. After 84 d, **(B)** SSF and **(D)** SISF were isolated and Western blot analysis were performed with anti-tau-p-Ser214, anti-tau or anti-GAPDH antibody, respectively. **(C)** Western blot signal intensities from tau-p-Ser214 within the SSF were quantified via ImageJ and normalized to GAPDH and CTRL. Experiments were performed in triplicates. Results are shown as mean values and error bars represent the standard deviation. Differences in means were tested for statistical significance by using the non-parametric Mann-Whitney U test. * indicates $p \leq 0.05$. Scale bar: 200 μ m. SISF: Sarkosyl-insoluble fraction, SSF: Sarkosyl-soluble fraction.

Western blot analysis of SSF with anti-tau-p-Ser214 antibody revealed significantly decreased phosphorylation of Ser214 after the treatment with δ -281 (Figure 50C). Slightly decreased phosphorylation of Ser214 was observed after the treatment with δ -31. Peptides δ -71, δ -101 and δ -241 did not reduce phosphorylation of Ser214. In general, the expressed protein amount and phosphorylation pattern of tau within the SSF was not drastically affected by the treatment with CK1 δ -derived peptides.

In the SISF, Western blot analysis of p-tau (p-Ser214) showed alterations in the phosphorylation pattern after the treatment with δ -31, δ -101 and δ -241, but not δ -281 (Figure 50D). As mentioned before, the variety of high-MW total tau bands most likely indicates different stages of tau phosphorylation. Additionally, an increase in total tau levels in SISF was detected after the treatment with δ -31, δ -101 and δ -241 indicating an increase in sarkosyl-insoluble tau aggregates. A lower amount of tau in the SISF was found after the treatment with δ -281.

To further investigate the properties of δ -281 on the inhibition of tau aggregation, thin-layer grown 3D cultures were stained with an anti-tau antibody to visualize formed tau aggregates (Figure 51). Even though peptide δ -31 altered the tau phosphorylation pattern in the SISF, it appeared to have a promising inhibitory effect on tau-Ser214 phosphorylation, which therefore was further investigated. Peptide δ -101 was chosen as control, as it was one of the peptides that increased phosphorylation of Ser214 and caused changes in the phosphorylation pattern and an increase of total tau levels in the SISF. Signal, which was obtained from tau staining (Cy5/red), was quantified and normalized to recombinantly expressed GFP and DMSO as solvent control (Figure 51B).

As expected from the previous results, immunofluorescence staining of tau revealed a significant decrease of tau staining after the treatment with δ -281 indicating a potential inhibitory effect for tau aggregation. Additionally, slightly decreased tau staining was observed for δ -31. Contrarily, but in line with the previous findings, peptide δ -101 drastically increased the presence of tau in the thin-layer 3D culture. Nevertheless, the results must be interpreted with caution, since a total-tau antibody was used that recognizes all tau proteins and not exclusively PHF-tau.

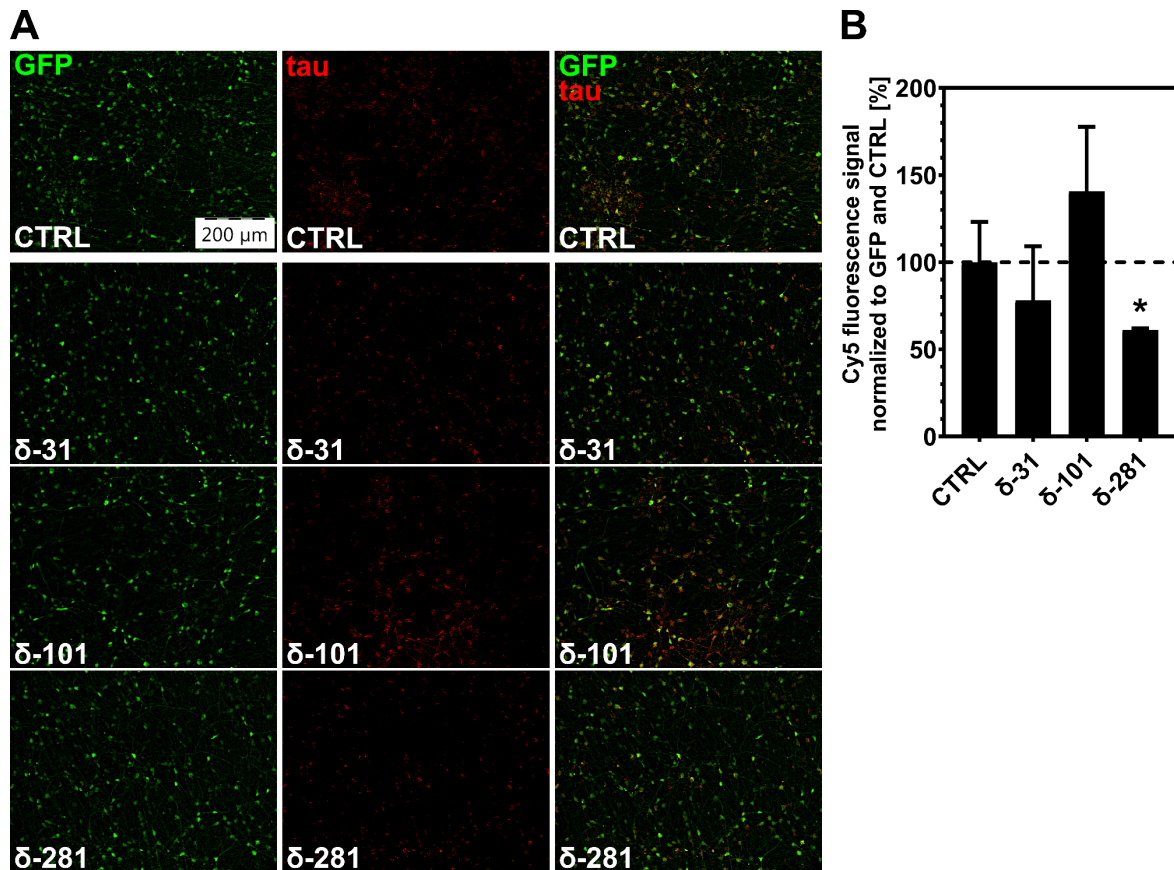


Figure 51: Effect of CK1δ-derived peptides on tau aggregation. (A) Thin-layer 3D cultures of transduced and differentiated hNPCs were stained with anti-tau antibody/anti-mouse antibody (Cy5/red) after treating the cells with 1 μM CK1δ-derived peptides or DMSO (CTRL) as vehicle control. GFP signal results from the transduction of the lentiviral construct coding for APPSL-IRES-GFP. Images were taken at 10x magnification with an epifluorescence Olympus IX81 microscope. (B) Fluorescence intensities from (A) were quantified using ImageJ. Cy5 fluorescence signal was normalized to GFP fluorescence signal. Experiments were performed in triplicates. Results are shown as mean values and error bars represent the standard deviation. Differences in means were tested for statistical significance by using the non-parametric one-sided Mann-Whitney U test. * indicates $p \leq 0.05$. Scale bar: 200 μm.

4 Discussion

Dysregulation of CK1 in physiological processes has been linked to phosphorylation events of key proteins, among them, APP and tau, which are implicated in the development of AD. Since CK1 δ seems to be involved in APP processing and tau hyperphosphorylation, it represents an interesting point for therapeutic intervention, either by targeting CK1 δ in general via SMIs or modulating the interaction of CK1 δ and its interaction partners APP or tau, which are main drivers of the formation of amyloid plaques and NFTs in the development of AD.

4.1 CK1 δ is a potential target for tau-mediated phosphorylation

A main pathological hallmark in the development of AD is the generation of NFTs originating from multiple phosphorylated and aggregated tau proteins, which are the products of various kinases. It is widely known that a wide range of kinases including CK1 δ have been associated to the phosphorylation of tau. However, the involvement of CK1 δ in the tau pathology is poorly understood and findings are mainly based on *in vitro* data. The present study provides evidence that (i) tau441 is phosphorylated by CK1 δ *in vitro*, (ii) CK1 δ targets AD-associated phosphorylation sites on tau441 including Ser214, (iii) CK1 δ co-localizes with tau in neuronal cells, and (iv) CK1 δ -mediated phosphorylation has an impact on tau441 aggregation. These findings will be discussed within the following chapter.

Primarily, site-specific phosphorylation of the tau isoform tau441 was predicted for CK1 canonical consensus sequences using ScanSite 4.1.0 detecting ten potential phosphorylation sites. Partially covering results were obtained by LC-MS/MS analysis revealing ten potential CK1 δ -specific phosphorylation sites. The majority of phosphorylation sites, which were detected by LC-MS/MS, were recently discovered by Hanger et al. [147]. LC-MS/MS analysis of this study identified two additional phosphorylation sites, Ser324 and Thr427 that have not been detected so far. However, the results of the LC-MS/MS analysis cannot confirm the CK1 δ -targeted phosphorylation of Thr17, Ser46, Thr50, Thr95, Thr101, Thr102, Ser113, Ser131, Thr149, Thr169, Ser184, Ser208, Ser210, Thr212, Ser237, Ser238, Ser241, Ser258, Ser262, Thr263, Ser285, Ser341, Ser352, Ser356, Thr361, Thr373, Ser412, Ser413, Ser433, and Ser435, which were recently detected via LC-MS/MS

analysis [147]. The results of classical biochemical approaches (e.g. *in vitro* kinase assay, two-dimensional phosphopeptide analysis) showed that CK1 δ prefers to phosphorylate tau441 especially within the proline-rich domain (aa 197 to 244) as well as the MT-binding and C-terminal domain (aa 244 to 441). These results are supported by the findings of several other studies, proving that most of the detected AD-associated phosphorylation sites can be found within the central (aa 172 to 251) and the C-terminal region (aa 368 to 441) [214, 250, 293]. Due to better accessibility and the elimination of some phosphorylation sites in the respective tau fragments, minor phosphorylation sites might be more likely to be phosphorylated by CK1 δ , which explains the appearance of new peptides within the tau fragments compared with full-length tau.

Combined results of the *in silico* prediction and LC-MS/MS analysis revealed that CK1 δ specifically phosphorylates tau441 phosphorylation sites Ser68, Thr71, Ser198, Ser214, Ser289, Thr414 or Ser416 and Thr427, which are associated to AD [148, 149, 162, 244]. Biochemical approaches and Western blot analysis using phospho-specific antibodies and cell lysates obtained after the treatment with CK1 δ -specific inhibitor PF-670462 were used to verify these results. Results, which were obtained by the variety of different methods, demonstrated that not all *in silico* predicted phosphorylation sites, which are represented by the implemented CK1-specific consensus sequences [188], are phosphorylated by CK1 δ *in vitro*. In addition, some of the CK1 δ -targeted phosphorylation sites identified by LC-MS/MS analysis could not be verified in other *in vitro* experiments (such as Ser198, Ser202 and Thr427) and vice versa. Results obtained from *in vitro* kinase assays verified that AD-associated tau441 phosphorylation sites Ser68 and/or Thr71 as well as Ser289 are targeted by CK1 δ . Although Ser68 and Thr71 were not found by LC-MS/MS analysis, both biochemical approaches (*in vitro* kinase assay and phosphopeptide analysis) identified these sites as CK1 δ -specific emphasizing the potential of biochemical methods. A reason for the failure to detect these phosphorylation sites by LC-MS/MS analysis could be based on difficulties in separation, reduced peptide lengths or the loss of phosphate groups during sample preparation [216, 316, 339]. Differences between the phosphopeptide analysis and *in vitro* kinase assay is probably caused by technical limitations regarding sample preparation prior to phosphopeptide separation. For preparation of samples, on-

membrane digestion with TPKC-trypsin was chosen that nevertheless had clear advantages over in-gel digestion such as better tryptic digestion efficiency due to easier protein accessibility [223]. However, even with this method some (phospho-) peptides might be lost, which can be explained by peptide precipitation or protein residues cross-linked to unpolymerized acrylamide that interfere with tryptic digestion and eventually lead to inefficient membrane detachment and insufficient tryptic peptide digestion [223]. Phosphorylated Thr414/Ser416 were predicted *in silico* and detected experimentally via LC-MS/MS analysis and *in vitro* kinase assays. However, phosphorylation of Ser416 could not be confirmed by Western blot analysis of lysates derived from neuronal cells suggesting no physiological relevance for the phosphorylation by CK1 δ . Contrarily, significant physiological relevance of CK1 δ -mediated phosphorylation was demonstrated for Ser214. Several studies already highlighted that the combination of results gained from different methods is crucial to reliably prove the phosphorylation of specific aa residues [38, 98, 159, 238, 239]. Considering the results from all performed methods, Ser68/Thr71, Ser214 and Ser289 seem to be phosphorylated by CK1 δ .

In this work, the tau aa residues Ser68 and Thr71 were firstly described as novel identified CK1 δ -specific phosphorylation sites that are highly associated to the prevalent tau pathogenesis in AD. In previous studies, comprehensive LC-MS/MS analysis detected phosphorylated Ser68 and Thr71 in brain tissue, which was isolated from patients with AD [149]. So far, just a few kinases have been described to phosphorylate Thr69 or Thr71, among them GSK3 [147] and AMP-activated PK [333]. Interestingly, phosphorylation of Thr71 was detected after combining GSK3 β and CK1 δ pointing towards a potential priming function of CK1 δ for GSK3 β [149]. Hyperphosphorylated tau in formed PHFs was described to contain several double-site phosphorylation motifs, such as Thr212/Ser214, which is known to be a specific marker for AD [192]. Additionally, phosphorylation of Ser68 and Thr71 as well as Thr212 and Ser214 is absent in biopsy-originated normal tau [230]. Of special interest is the phosphorylation of Ser214, as its phosphorylation alone potentially leads to decreased affinity of tau for MTs and increases the disruption of MT-binding [162]. Phosphorylation of Ser214 was shown to be mediated by Akt [192], PKA [149, 385], CDK5, GSK3 and CK1 δ [147, 149]. Among the detected CK1 δ -specific phosphorylation sites, Ser289 is positioned within the MT-binding domain of tau,

which is important for its MT-binding property. Phosphorylation events within the MT-binding domain were connected to conformational changes of tau and its detachment from the MTs [33, 214]. Other kinases, which are associated to the phosphorylation of Ser289, are GSK3 [147], Chk1 and Chk2 [236].

Additionally, double immunofluorescence staining provides evidence that endogenous CK1 δ co-localizes with tau in differentiated neuronal cells. Co-localization is essential for the interaction of both proteins resulting in subsequent phosphorylation. The results support the hypothesis that CK1 δ is involved in the modulation of tau, which is further substantiated by the findings that CK1 is active in a physiological environment in neuronal cells and that increased expression of CK1 δ in AD brains was probably causing severe disruptions of tau-MT binding [125, 149, 376].

CK1 δ is able to phosphorylate tau at AD-associated residues *in vitro* as well as *in cellulo* and to co-localizes with endogenous tau in neuronal cells. Additionally, it has been reported that its expression is up-regulated in brain tissue derived from patients suffering from AD [125]. To directly show the functional effect of CK1 δ -mediated tau phosphorylation on its aggregation, well-described *in vitro* tau aggregation assays with pre- and non-phosphorylated tau441 were performed. By using this experimental set-up, a remarkable difference in the aggregation kinetics of pre- and non-phosphorylated tau441 was observed. The velocity of aggregation as well as the amount of formed aggregates of pre-phosphorylated tau441 were highly increased compared to non-phosphorylated tau441. In aggregated PHF-tau several aa were detected to be phosphorylated including aa within the N-terminal domain (Ser68, Ser69, Thr71, Ser184 and Ser185), the proline-rich domain (Ser202, Thr205, Ser208, Ser210, Thr212, Ser214, Thr231 and Ser235), the MT-binding domain (Ser235, Ser258, Ser262 and Ser289) and the C-terminus (Thr403, Ser412, Thr414, Ser416, Ser422, Thr427, Ser433 and Ser435) [100, 149, 243, 367, 385]. In the present study, several PHF-tau-associated phosphorylation sites were predicted to be phosphorylated by CK1 via ScanSite 4.1.0 (including Ser68, Thr71, Ser198, Ser202, Thr403 and Ser289) or detected experimentally (including Ser68, Thr71, Ser214 and Ser289). In addition to CK1 δ , other kinases such as Fyn and TTBK1 have also been associated with tau aggregation [45, 368]. Overexpression of TTBK1 in a bi-transgenic P301L tau mutant mouse model promoted the

phosphorylation of tau residues Ser202/T205, Ser262/Ser356, Ser396/Ser404 and Ser422 that enhanced the accumulation of tau aggregates [368]. TTBK1 as a neuron-specific kinase is known to regulate tau phosphorylation. Of note, TTBK1 shares high homology and similar characteristics with CK1 δ , which is the reason why both kinases belong to the CK1 family according to the phylogenetic tree of human kinases [208].

Altogether, the comprehensive characterization of CK1 δ -mediated tau phosphorylation (see Figure 52) and the evidence of a functional effect of CK1 δ on tau aggregation presented in this study as well as the existing data published in recent studies point towards a potential role of CK1 δ in AD tauopathy and disease progression. On that basis, CK1 δ represents an interesting point for therapeutic intervention, which can be realized through the general inhibition of CK1 δ via CK1 δ -specific SMIs, or alternatively, the intervention of CK1 δ activity at the level of CK1 δ -substrate interactions via low MW peptides derived from the CK1 δ aa sequence.

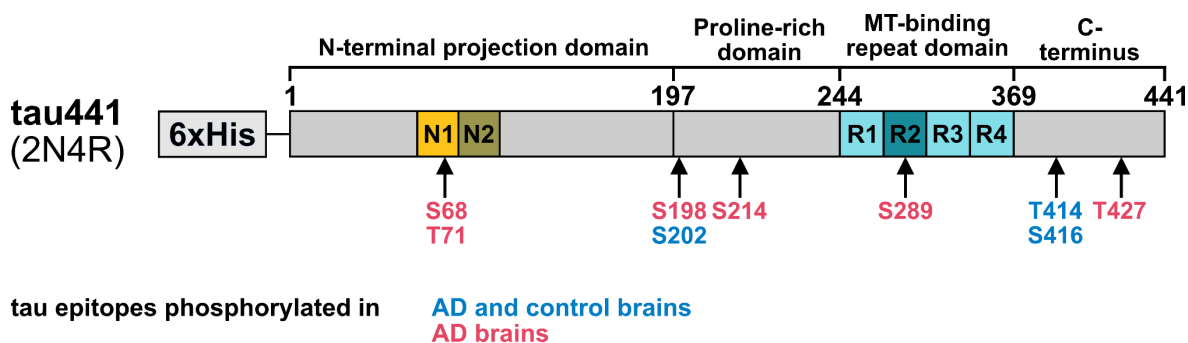


Figure 52: Overview of potential CK1 δ -specific tau phosphorylation sites. Phosphorylation sites on tau441 were predicted *in silico* or identified experimentally. Shown are CK1 δ -specific tau441 phosphorylation sites that have been predicted or identified by at least two methods. Blue: Tau441 aa residues that were found to be phosphorylated in AD and control brains. Red: Tau441 aa residues that were found to be phosphorylated only in AD brains. The figure was modified from [311] and [289], which are licensed under a Creative Commons Attribution 4.0 international license (CC BY 4.0), <https://creativecommons.org/licenses/by/4.0/>.

4.2 Identification of new CK1 δ -specific compounds for the treatment of AD

Various studies indicated a possible involvement of CK1 δ in AD pathogenesis by influencing the APP metabolism and favoring the A β production as well as formation of amyloid plaques [204, 352]. Based on the experimental findings of this study, which are supported by recently published data, CK1 δ was shown to be involved in the hyperphosphorylation of tau leading to its aggregation [149, 182, 218]. Based

on this involvement, CK1 δ represents an interesting therapeutic target for the treatment of AD. Initially, three sets of potential CK1 δ -specific inhibitors including benzimidazole derivatives, IWP-derived compounds and isoxazole derivatives were tested for their potency, selectivity and biological effect. Within this chapter, results regarding the (i) establishment of standard conditions for *in vitro* kinase assays, (ii) biological activity of tested compounds *in vitro* (iii) toxicity of compounds in cell culture and (iv) biological effects of CK1 δ -specific inhibitors in the “Alzheimer’s-in-a-dish” model will be discussed.

In order to evaluate and compare the potency and selectivity of newly developed SMIs, IC₅₀ values are commonly determined. Nevertheless, the comparison of different values described in literature is difficult, because experimental approaches used for the determination of inhibitory effects lack comparability due to insufficient normalization, different experimental readout parameters or the huge number of experimental approaches. To achieve more universal comparability between the *in vitro* characterization of SMIs, standard conditions were established for GST-tagged CK1 α , CK1 δ and CK1 ϵ including the determination of the V_{init} region and $K_m(\text{ATP})$ within V_{init} . A thorough determination of V_{init} as well as the use of ATP concentrations equal to $K_m(\text{ATP})$ allow the conversion of obtained IC₅₀ values for ATP competitive inhibitors into K_{ic} , a variable specific for each enzyme and inhibitor that is independent of the experimental approach and universally comparable. When comparing IC₅₀ data obtained in this study, the determined IC₅₀ values for SR-3029 (354 nM), Liu-20 (403 nM) and Peifer-1 (1,493 nM) for CK1 δ differed drastically from the previously published IC₅₀ values of 44 nM for SR-3029 [32], 86 nM for Liu-20 [212] and 230 nM for Peifer-1 [262] and CK1 δ . Five to eight times lower IC₅₀ values might arise, because V_{init} has not been defined properly or arbitrary ATP concentrations were used within the experimental set-ups [32, 212, 262]. To ensure comparability of the values describing inhibitor potency between different enzymes and inhibitors, inhibitors should be tested at ATP concentrations equal to $K_m(\text{ATP})$ and thus, K_i values should be determined and stated by default. In this study, only compounds derived from ATP-competitive inhibitors were used, for which K_{ic} can easily be determined. Nevertheless, comparison with the literature is difficult, because only a few values for K_i are mentioned, which is why IC₅₀ values are discussed in the following.

Due to their ability of binding various target sites, benzimidazole-derivatives are an important class in pharmaceutical industry for the treatment of various diseases including cancer [9, 154, 276], hypertension [193], viral infections [329, 330] and parasitosis [8, 93]. Furthermore, benzimidazole-derivatives were identified to be an attractive scaffold for the development of inhibitors against several PKs including the families of TK [373], CDK [110], CK2 [301], aurora kinase [1], polo-like kinase [200] and CK1 [37, 280]. From the set of CK1 δ -targeting already published benzimidazole-derived inhibitors, Bischof-5 was identified as a highly potent and selective CK1 δ -specific inhibitor with an IC₅₀ value of 22 nM [37]. Due to structural similarities, the approved and commercially available benzimidazole-derivatives mebendazole, albendazole, fenbendazole and flubendazole, which are widely used as antiparasitic drugs, because of to their anthelmintic properties (e.g. for the treatment of echinococcosis [279]), were tested for their potency and selectivity against CK1 δ . Unfortunately, none of the tested benzimidazole-derivatives sufficiently reduced CK1 activity, thus indicating that structural similarities between the tested benzimidazole-derivatives and Bischof-5 were not sufficient to exert an effect on CK1 activity. Consequently, the set of benzimidazole-derivatives was not tested further.

IWP-derived compounds belong to the class of SMIs that specifically block porcupine, a member of the membrane-bound O-acyltransferase family, which is involved in the catalysis of the palmitoylation of Wnt ligands and thereby essential for Wnt secretion and signaling [62, 356]. On that basis, IWP-derived compounds are interesting as pharmacological tools inhibiting the Wnt pathway. As IWPs and benzimidazole derivatives share high structural similarities, IWPs were assumed to have high selectivity and potency against CK1 isoforms. After they have previously proven their selectivity and potency against specific CK1 isoforms, IWP-derived compounds have been chosen as an interesting starting point toward further optimization steps [122, 212]. Based on the data, which was previously published, Liu-20 was selected as lead structure to be used to develop inhibitors that are more potent and CK1 isoform-selective by modifying functional groups, which were attached to the benzene ring. To test their potency and selectivity against different CK1 isoforms (CK1 α , CK1 δ and CK1 ϵ), the set of newly developed IWP-derived inhibitors were tested at 10 μ M *in vitro*. The initial screening showed remarkably

isoform-selective differences, whereas all compounds exhibited increased selectivity towards CK1 δ . Especially compounds 383 and 384 demonstrated increased selectivity towards CK1 δ which could be confirmed by the determination of IC₅₀ values for CK1 δ and CK1 ϵ leading to IC₅₀ (CK1 δ /CK1 ϵ) ratios of 12 and 14, respectively. 383 and 384 as well as 382, which was not as selective as its enantiomer 383, were more potent compared to their non-chlorinated analogs indicating an essential role of chlorine in the specific CK1 δ -inhibitor interaction. IC₅₀ values of 383 and 384 were determined at 118 nM and 135 nM, respectively, thereby representing interesting inhibitors for further investigations in a cell-based system.

Compound Peifer-1, as a representative of the isoxazole-derivatives, was identified as a potent dual inhibitor of CK1 δ (IC₅₀ value of 230 nM) and p38 α MAPK1 (IC₅₀ value of 450 nM) [262]. Further optimization approaches led to Peifer-2 with reduced potency towards p38 α , while preserving high potency against CK1 δ (IC₅₀ (CK1 δ): 33 nM, IC₅₀ (p38 α): 2.5 μ M, IC₅₀ ratio (CK1 δ /p38 α): 0.013) [262]. Unfortunately, both inhibitors exhibited reduced chemical stability, which negatively influences the usage *in vitro* and *in vivo*. Further developments led to the conclusion that the presence of the water network facilitates binding interactions between the ATP ribose pocket and kinase ligand [146, 224]. By using these water-mediated interactions for the optimization of CK1 δ -isoform selective inhibitors, the extensions of the central pharmacophore toward interaction with the ribose pocket was investigated. Therefore, lead structure Peifer-1 was modified with chiral iminosugar scaffolds at the isoxazole core. The iminosugar-modified analogs were tested for their potency and selectivity against different CK1 forms at 10 μ M *in vitro*. Compound 394 bearing a 3S,4R-configured iminosugar, was identified as the most potent inhibitor among the set of isoxazole derivatives. Additionally, inhibitor 394 was more selective toward CK1 δ than the original lead compound Peifer-1, which indicates that the insertion of the additional iminosugar enhances binding interactions within the ATP binding pocket. However, its enantiomer 395 bearing a 3R,4S-configured iminosugar was less selective with an increased IC₅₀ value of 1.72 μ M and a reduced IC₅₀ ratio (CK1 δ /CK1 ϵ) of 6 indicating that the enantiomeric configuration of the iminosugar was involved in less suitable binding interactions. Compared to 394 and 395, both fluorinated inhibitors 392 and 393 were less active,

which is probably a result of the weakening of hydrogen bridges between the hinge region of CK1 δ and pyridine due to electronegative effects caused by the addition of the 2-fluoro substituent. Interestingly, consistent with the results obtained for 394 and 395, compound 393 substituted with the 3S,4R-configured iminosugar exerted better activity toward CK1 δ compared to its enantiomeric compound 392. Generally, isoxazole derivatives seemed to be less potent and less selective compared to IWP-derived compounds. Nevertheless, compound 394 as a representative of the isoxazole derivatives with good potency and high selectivity towards CK1 δ was chosen for further investigations in the “Alzheimer’s-in-a-dish” model.

Although IWP-derived compounds 383 and 384 as well as isoxazole derivative 394 have proven their inhibitory potential *in vitro*, obtained results were successfully complemented by the biological effects observed in subsequently performed cell-based experiments. Prior to the investigation of biological effects on AD-like phenotypes by using the “Alzheimer’s-in-a-dish” model, inhibitor-induced cytotoxic effects of CK1 δ -specific inhibitors and their respective controls were determined using differentiated hNPCs. With the aim to identify cytotoxic effects and define maximal applicable inhibitor doses for further experiment, cell viability assays were performed. Consistent with recently published data showing a low nanomolar EC₅₀ value of 86 nM for SR-3029 and human melanoma cell line A375 [32] and a low micromolar EC₅₀ value of 3 μ M for Liu-20 and human colorectal cancer cell line SW620 [212], cytotoxic effects were observed for SR-3029 and Liu-20 at a concentration of 1 μ M and 5 μ M, respectively. Inhibitors PF-670462, 383, 384, Peifer-1 and 394 induced no cytotoxic effects on neuronal cells indicating either highly substrate-selective effects or poor membrane permeability due to physicochemical properties including hydrophilicity and negatively charged compounds (such as carboxylic acids, sulfonates or phosphates) [233, 348].

Finally, therapeutic effects of CK1 δ -specific inhibitors were investigated using the “Alzheimer’s-in-a-dish” cell culture model, which was used to simulate AD typical phenotypes including tau and A β pathology within a 3D human differentiated neural cell culture system [71, 181]. To establish the 3D cell culture system, an immortalized hNPC cell line was transduced with lentiviral vectors encoding mutated PSEN1 (Δ E9) and mutated APP695 (with the Swedish and London mutation), which are both linked to early-onset forms of FAD. High levels of mutant PSEN1 and

APP695 expressing hNPCs were then seeded in thin- and thick-layer 3D cultures and differentiated by removing growth-factors. The “Alzheimer’s-in-a-dish” 3D model has many advantages over conventional 2D cell culture systems as it supports neuronal differentiation, the formation of neuronal networks and it mimics the *in vivo* environment very closely. Using the “Alzheimer’s-in-a-dish” model, extracellular A β aggregation was visible after six weeks of maintenance, whereas robust tau phosphorylation in cell bodies and neurites as well as tau pathology could be detected after ten to 14 weeks of maintenance [71, 181].

With the aim to investigate the biological effect of CK1 δ -specific inhibitors PF-670462, SR-3029, Liu-20, 383, 384, Peifer-1 and 394 on A β pathology, thin- and thick-layer 3D cultures of transduced hNPCs were treated for six weeks with the respective CK1 δ -specific inhibitor and a β -secretase-specific inhibitor (IV) as control. Although routinely monitoring of the thick-layer 3D culture treated with SR-3029 showed no alterations in the cell viability measured via LDH release, immunofluorescence staining clearly demonstrated that permanent treatment with SR-3029 at concentration of 0.1 μ M led to cell death after six weeks indicating potential severe off-target effects against several other kinases, which was already reported for CDK4, MYLK4 and FLT3 [32]. Additionally, cell toxic effects after the treatment period were probably caused by its strong dual-inhibitory properties against both CK1 isoforms, CK1 δ and CK1 ϵ (IC₅₀ (CK1 δ): 44 nM and IC₅₀ (CK1 ϵ): 260 nM). Although inhibitor PF-670462 has similarly strong dual-specific effects (IC₅₀ (CK1 δ): 13 nM, IC₅₀ (CK1 ϵ): 90 nM [353]), it did not exhibit any cytotoxic effects. This supports the assumption that effects observed for SR-3029 are due to targeting of other kinases. Due to the observed cytotoxic effects and lower amount of living cells, it is not surprising that A β levels were drastically reduced compared to solvent control. Unfortunately, none of the tested CK1 δ -specific inhibitors had a significant effect on A β levels, and thus, no further analyses were performed concerning APP metabolism. With these results, a previously published study demonstrating that PF-670462 reduced A β and amyloid plaque size could not be confirmed with that experimental set-up [325]. However, adjustments in dosage and treating periods could be beneficial for the treatment of A β pathology with CK1 δ -specific inhibitors.

Because tau hyperphosphorylation and aggregation in the “Alzheimer’s-in-a-dish” cell culture model become obvious after ten weeks of maintenance, the established thick- and thin-layer 3D cultures were treated for twelve weeks with the selected CK1 δ -specific inhibitors except SR-3029 due to reasons, which were discussed before. Total tau and phosphorylated tau at residue Ser214, as one of the major CK1 δ -targeted and AD-associated tau phosphorylation sites, were investigated in the SSF and SISF of thick-layer grown cells treated with the respective CK1 δ -specific inhibitors. SSF and SISF were isolated in the presence of the ionic detergent sarkosyl, which has been demonstrated to solubilize most of the natively folded tau in the brain while preserving misfolded tau aggregates showing same structural and antigenic properties as PHFs [136, 191, 304, 364]. In accordance with the findings described in chapter 3.1, phosphorylation of Ser214 in SSF as well as the SISF was reduced after the treatment with PF-670462. Reduction of p-Ser214 in the SSF was also observed for Liu-20 and its derivative 384 indicating that common structural features lead to similar biological effects. Further supporting this assumption, considerable changes in the phosphorylation pattern were detected for Liu-20 and 384. Within the SISF, a decrease in total tau was shown for inhibitor Liu-20, 383, 384 and 394, whereas PF-670462 and Peifer-1 had no inhibitory effect on tau aggregation. Decrease of p-Ser214 and changes in the tau phosphorylation pattern within the SSF as well as a decrease in aggregated tau indicate that Liu-20 and its further developed analog 384 have a positive influence on tau pathology. In order to substantiate these findings, immunofluorescence staining of tau was performed with fixed thin-layer grown cells after the treatment with Liu-20, 384 and PF-670462. Generally, tau staining was especially observed in neurites and the neuronal cell bodies which is in line with the observation made by Choi and colleagues [70]. Additionally, treatment with 384 as well as PF-670462 led to significantly decreased tau staining probably correlating with tau aggregation. However, as discussed before, due to the use of tau-antibody recognizing all tau proteins and not exclusively PHF-tau, caution should be exercised to directly connect total tau staining to tau aggregation. In accordance with the results obtained from the Western blot analysis of SSF and SISF, especially 384 and to a lesser extent Liu-20, seem to have a beneficial effect on tau pathology. However, further efforts should be made to investigate potential off-target effects, which might be involved in the

beneficial therapeutic effect on tau pathology. Off-target effects directly affecting tau phosphorylating kinases would not be unlikely, as tau can be phosphorylated by a variety of kinases including structurally related kinases such as TTBK1 [298] or more distantly related kinases such as GSK3 β [317] and CDK5 [307].

4.3 Identification of CK1 δ -derived peptides modulating AD pathology

As an alternative to SMIs, a novel therapeutic approach using CK1 δ -derived peptides was investigated. These peptide therapeutics, which were used to target kinase-mediated functions, were intended to interfere with the interaction motif for the kinase located within the substrate. As a beneficial consequence, the ideal peptide only influences the effect of kinase activity towards the specific interaction partner [109]. The present study demonstrates that (i) CK1 δ -derived peptides specifically disturb the interaction between CK1 δ and APP695 and/or tau *in vitro* and inhibit their phosphorylation, respectively, (ii) enter neuronal cells without inducing cytotoxic effects and (iii) show significant therapeutic effects in the “Alzheimer’s-in-a-dish” model.

Streptavidin-linked (and SPR-based) interaction analyses were carried out to define dominant motifs, which are involved in mediating the interaction of CK1 δ with APP695 (fragments) as well as tau441 and tau383. By using streptavidin-linked interaction analysis and APP695 fragments (N-APP, E2 and APP-C), a set of seven APP695 fragment-binding peptides were identified including δ -41, δ -101, δ -111, δ -241, δ -281, δ -311 and δ -371. Combined results of the streptavidin-linked interaction assay and SPR, a set of eleven tau441- and tau383-binding peptides was obtained including δ -1, δ -31, δ -71, δ -101, δ -111, δ -241, δ -281, δ -311, δ -331, δ -361 and δ -381. The interaction potential of these identified peptides and the ability to competitively block the interaction of CK1 δ with both target proteins APP695 (fragments) and tau have been further analyzed by *in vitro* phosphorylation experiments. After testing the set of seven CK1 δ -derived peptides interacting with APP695 fragments, six peptides (δ -41, δ -111, δ -241, δ -281, δ -311 and δ -371) reduced phosphorylation of N-APP or E2. Nevertheless, these peptide-mediated effects are not as drastic as those being caused by well-described SMIs and failed to decrease phosphorylation by more than 28 % (as detected for peptide δ -241 and

phosphorylation of N-APP) and 41 % (as detected for peptide δ -311 and phosphorylation of E2). Among the set of eleven CK1 δ -derived peptides interacting with tau441 and tau383, only five peptides have clearly been identified to significantly reduce phosphorylation of tau441, but none of the tau383-interacting peptides inhibited the phosphorylation of tau383. This observation is probably due to the absence of both N-terminal extension domains (N1 and N2) between the aa 45 and 103, which harbor the potential phosphorylation sites Ser68 and Thr71. Since both potential phosphorylation sites are missing in tau383, their phosphorylation by CK1 δ cannot be prevented by tau383-interacting peptides.

Comparable to APP695 targeting peptides, the peptide-mediated effects on tau phosphorylation are not as substantial as the inhibition induced by SMIs and led to a reduction of only 42 % (as observed for peptide δ -101 and tau441). Most current and well-described CK1 δ -specific SMIs with IC₅₀ values within the sub-micromolar range showed more potent effects on CK1 δ phosphorylation than it was detected for the CK1 δ -derived peptides at the used concentrations [369]. With IC₅₀ values of 118 nM and 135 nM for CK1 δ , inhibitors 383 and 384 would induce more potent effects on CK1 δ at the selected concentration. However, the major advantage of the tested CK1 δ -derived peptides was the remarkable substrate-selective inhibition of APP695 (or rather N-APP and E2) and tau441 phosphorylation, since no effect on CK1 δ -mediated α -casein phosphorylation was observed for most peptides. The superior selectivity of CK1 δ -derived peptides, which cannot be achieved by SMIs due to their mode of action, has already been indicated in a previous study investigating the effect of CK1 δ -mediated phosphorylation on α -tubulin [190].

For fragment APP-C, which is located C-terminally within APP695 and encompassing the TMD as well as AICD of APP695, only weak CK1 δ -mediated phosphorylation could be measured. Although APP695 was shown to be generally phosphorylated by ectoprotein-CK1 and CK1 δ during biosynthesis and cellular trafficking, its membrane-located domain (TMD) is hidden in the phospholipid bilayer and thus, can possibly not be reached by PKs [64, 352]. In addition, within the purification process, the highly hydrophobic TMD is probably masked by hydrophobic molecules, which was necessary to be included in the procedure to simplify isolation of insoluble proteins but might simultaneously prevent *in vitro* phosphorylation by CK1 δ [315]. As it can be deduced from the performed

biochemical approaches, CK1 δ -mediated phosphorylation of the TMD within APP695 seems not to be relevant. Vice versa, these findings demonstrate that major CK1 δ -specific phosphorylation sites are located within the APP695 fragments N-APP and E2. This observation is further supported by ScanSite-based search for phosphorylation sites showing that most potential CK1-specific phosphorylation sites are located in the AcD within aa 266 to 295. Additionally, a previous study detected CK1-specific phosphorylation sites within the aa 181 to 224 of APP695 [252, 352].

The respective aa sequences of CK1 δ -derived peptides interacting with target proteins APP695 or tau were generally expected to be derived from the CK1 δ surface, thereby imitating the actual kinase-substrate interaction motifs. As expected, most of the identified interacting CK1 δ -derived peptides are localized on the protein surface of CK1 δ . However, peptide δ -241, which demonstrated a remarkable binding to APP695 fragments N-APP and APP-C as well as tau441 and tau383, occupies only a small surface compared to the other peptides. As a consequence, the area of the corresponding protein surface of each CK1 δ -derived peptide does not necessarily correlate with the findings obtained by interaction analyses, indicating that the peptide binding affinity is generally more important for its specific peptide-protein interaction. Moreover, peptide sequences that demonstrated a robust interaction with APP695 fragments and/or tau, may also be found within regions distant to the active site of CK1 δ . This assumption is supported by the observation that binding sequences for CK1 may be distinct from CK1-specific phosphorylation sequences, which may also be separated within the substrate protein [51].

Although all presented results were generated *in vitro* by using recombinant artificial fragments of APP695 and tau, obtained data were successfully complemented by the biological effects observed in following performed cell culture experiments. Before investigating biological effects on AD-like phenotypes, cell entry abilities and peptide-induced cytotoxic effects of CK1 δ -derived peptides were investigated using differentiated hNPCs. In accordance with their highly substrate-selective effect detected by *in vitro* kinase reactions, CK1 δ -derived peptides induced no cytotoxic effects on neuronal cells. This result indicates that the treatment with CK1 δ -derived peptides induce no general inhibition of CK1 δ kinase activity and no other targets

were affected whose inhibition may lead to severe off-target effects. The ability to enter differentiated hNPCs could be demonstrated for most of the peptides. The plasma membrane, which represents the final barrier, has to be penetrated by therapeutic agents to enter the cell and as discussed before, permeability of hydrophilic SMIs and low MW drugs is usually poor [233, 348]. Poor membrane permeability due to physicochemical properties combined with a short period of incubation could be the reason why the CK1 δ -tau441 interaction was blocked only slightly in the experimental approach using NanoBiT[®]. Because cellular uptake mechanisms such as active transport, endocytosis, and simple or facilitated diffusion are often insufficient, external or artificial delivery systems such as antibodies, liposomes, nanoparticles or cell-penetrating peptides could be used to enhance delivery and cellular uptake of peptides [296, 326, 381]. Nevertheless, at least for CK1 δ -derived peptides δ -31, δ -111, δ -281 and δ -371 used in the experimental set-up, an extensive ability to enter differentiated hNPCs could be demonstrated without the use of further delivery techniques or modifications on peptide sequence.

Finally, biological effects of CK1 δ -derived peptides were tested using the “Alzheimer’s-in-a-dish” model, which was used to simulate the AD typical phenotypes including A β as well as tau pathology based on a 3D cell culture system using transduced hNPCs [71, 181]. Since extracellular amyloid plaques composed of A β aggregates become detectable after six weeks of maintenance, the established thin- and thick-layer 3D cultures were treated for six weeks with the respective CK1 δ -derived peptides and the β -secretase-specific inhibitor IV, which served as control. Moderate cell entry abilities were detected for peptide δ -311, and, subsequently, strong effects on the A β production and amyloid plaque formation were observed. However, reduced A β levels did not necessarily correlate with the results of cell entry experiments. Although A β levels were significantly decreased after the treatment with δ -41, δ -101 and δ -311, cell entry abilities were most obvious for CK1 δ -derived peptides δ -111, δ -281 and δ -371. As peptides are generally susceptible to fast degradation and no significant peptide-specific immunofluorescence staining could be detected for δ -41 and δ -101, although the peptides led to significant effects on APP metabolism, both peptides might be taken up intracellularly, but are then rapidly metabolized [266]. As an alternative, the biotin,

which is tagged N-terminally to the peptides, could be masked after binding to APP leading to reduced or absent staining with TRITC-conjugated streptavidin. Peptide-mediated effects after the treatment with δ -41 on A β levels and formation of amyloid plaques were rather minor, whereas the peptide-mediated effect of δ -101 was sufficient to reduce A β levels and plaque formation remarkably. Nevertheless, generation of A β peptides was only reduced by 13 % as detected for peptide δ -101. For tau hyperphosphorylation and aggregation, thin- and thick-layer 3D cultures were treated for twelve weeks with the respective CK1 δ -derived peptides. After isolating SSF and SISF from thick-layer grown cells, Western blot analysis was performed with antibodies against tau-p-Ser214, total tau and GAPDH. In accordance with good cell entry abilities, decrease of p-Ser214 within the SSF was detected after the treatment with δ -31 and δ -281, while total tau was not affected. Peptides δ -71, δ -101 and δ -241 did not affect phosphorylation of Ser214. However, changes in the phosphorylation pattern of tau were observed in the SISF for δ -31, δ -101 and δ -241, but not for δ -281. Changes in the phosphorylation pattern detected by antibody against p-Ser214 caused by peptides δ -31, δ -101 and δ -241 seem to be related to drastic increase of total tau levels in the SISF indicating that those peptides promote formation of tau aggregates. Unfortunately, a clear beneficial effect of δ -281 on the formation of tau aggregates could not be shown via Western blot. Nevertheless, to confirm the results obtained by Western blot, CK1 δ -derived peptides δ -31 and δ -281 were further investigated for their ability to inhibit tau aggregation. Therefore, thin-layer 3D cultures were stained with an anti-tau antibody to visualize formed tau aggregates. Interestingly, peptide δ -101 causing changes in the phosphorylation pattern and tau aggregation was shown to drastically increase the presence of tau in the thin-layer 3D culture indicating a promoting effect on tau aggregation, while inhibiting A β secretion and plaque formation. The abilities of promoting tau aggregation could be a result of physicochemical properties regarding the ability to form aggregates under suitable conditions including solvent, pH conditions and temperature [143, 169, 387]. Small peptides or peptide aggregates could trigger the formation of bigger tau aggregates. A hexapeptide derived from the R3 domain of the tau protein was already shown to induce tau aggregation [321]. In contrast to these observations, presence of tau within the thin-layer 3D culture was

(significantly) decreased after the treatment with δ -31 and δ -281 supporting the beneficial properties on tau pathology of those peptides.

4.4 Conclusion

The inhibitors Liu-20, and especially, PF-670462 and 384 have shown positive effects on the development of tau pathology. Compared to small peptide drugs, SMIs are known to have distinct advantages including good membrane penetration ability, possibility for oral administration and low production costs combined with low sale prices [163]. However, their small molecule size, which is responsible for these advantageous properties, also leads to poor inhibition of large surface interactions including PPI and low specificity towards a specific target compared to peptide drugs. By inhibiting multiple off-targets, undesirable cell toxic effects are often observed after the treatment with SMIs [113, 271, 345], which was probably the case for SR-3029 and Liu-20 at high concentrations. To reduce off-target effects of SMI, which are often a result of pathway cross-talks and non-specific interactions, a focus on the selectivity of an inhibitor during development is needed. Since many kinases are multi-domain proteins, the specific destruction of a kinase could be more effective than only inhibiting its catalytic activity. This principle is applied in the development of specific inhibitors that induce the ubiquitylation-mediated protein degradation of specific proteins in the context of PROTAC (proteolysis-targeting chimeras) technology [79]. The PROTAC technology has already been successfully demonstrated and approved for lenalidomide in leukemia, which induces the ubiquitination and degradation of CK1 α [79, 189].

Regarding CK1 δ -derived peptides modulating AD pathology, peptide δ -101 was shown to be a potent therapeutically active peptide that demonstrated superior binding to APP695 fragments. Together with other promising CK1 δ -derived peptides like δ -311, it might present a good starting point for the development of novel therapeutic approaches for the treatment of AD by influencing APP metabolism. However, clearly more convincing was the effect of CK1 δ -derived peptides on tau hyperphosphorylation (and aggregation). Peptides δ -31 and δ -281 presented potent therapeutically active peptides with inhibiting effects on the phosphorylation of Ser214-tau (and tau aggregation). The effect on A β levels and amyloid plaque formation as well as tau hyperphosphorylation and aggregation

could possibly be potentiated by combining two or more peptides, since each CK1 δ -derived peptide potentially blocks a different located interaction site for CK1 δ on APP695 or tau. Therefore, effects induced by simultaneous treatment with different CK1 δ -derived peptides could lead in more distinct additive or synergistic effects. For example, a combination of δ -101 and δ -311 or δ -31 and δ -281 could reduce A β levels or tau hyperphosphorylation, respectively.

In contrast to SMIs, the unique physicochemical and physiological properties of peptide-based inhibitors including their sufficiently large size, allows peptides to act as highly specific and potent inhibitors of PPIs [268], which has been shown for most of CK1 δ -derived peptides that blocked the phosphorylation of APP695 fragments or tau, but had no effect on α -casein phosphorylation. Nevertheless, there are two major drawbacks that hinder the use of peptide drugs in therapeutic approaches, their poor *in vivo* stability and their weak membrane (and BBB) permeability. Membrane impermeability and/or *in vivo* degradation have been shown for peptides δ -41, δ -71 and δ -101 rendering them almost useless for therapeutic use. These intrinsic disadvantages of peptide-based drugs present huge challenges in peptide drug development regarding peptide drug design, optimization and application form [355]. Nevertheless, some progress has already been made in this direction and could also be useful for the CK1 δ -derived peptides tested here. For the improvement of *in vivo* stability several modifications could be tested, for example PEGylation of peptides [171, 343] or peptide backbone modifications that includes the substitution of L-aa in D-aa [360, 361], the incorporation of β -aa [61] and the insertion of methyl-aa [57, 355, 361]. As described before, membrane permeability could be enhanced by the use of lysosomes, nanoparticles, polymeric micelles and dendrimers [102, 355]. However, due to their artificial nature, they lack the ability to penetrate the BBB, which can be overcome by using conjugated cell-penetrating peptides or BBB shuttle peptides, such as , penetratin [206], SynB [290, 291] or angiopep-2 [59].

Overall, the presented and discussed data, obtained by using the “Alzheimer’s-in-a-dish” model, clearly showed that CK1 δ represents an interesting target for therapeutic intervention in the development of AD, either through the use of CK1 δ -specific SMIs and the consequent inhibition of CK1 δ in general or, alternatively, through CK1 δ -derived peptides that disrupt the interaction of CK1 δ with its AD-

associated interaction partner. Both strategies provide promising starting points for further research and development of novel potent and/or highly selective small-molecule or peptide based-inhibitors as highly innovative and novel pharmacological approaches for the treatment of AD.

5 Summary

Alzheimer's disease (AD) is a multifactorial neurodegenerative disease first described in 1906 by the pathologist Alois Alzheimer. Amyloid plaques and intracellular neurofibrillary tangles (NFTs) are widely accepted and have been extensively described as hallmarks of AD. The presence and distribution of amyloid plaques, NFTs and synaptic degeneration correlate with the course and degree of cognitive decline. Remarkably, both histopathological hallmarks, amyloid plaques and NFTs, are related to phosphorylation events. More precisely, amyloid plaques are composed of A β peptides, whose production is modulated by the phosphorylation of amyloid precursor protein (APP) mediated by kinases, whereas NFTs are a result of hyperphosphorylation events of tau. Even though several studies proposed that the family of casein kinase (CK)1 is involved in the pathogenesis of AD, so far, not much is known about CK1 δ -specific phosphorylation of AD-associated key proteins like APP and tau.

As reported, members of the CK1 family are critically involved in the pathogenesis of AD, especially by the hyperphosphorylation of tau. Precise effects and mechanisms of CK1 δ -mediated tau phosphorylation are only weakly understood. In the first part of the study recombinantly produced tau441 was phosphorylated by CK1 δ *in vitro* and analyzed via mass spectrometry resulting in ten potential phosphorylation sites. Among them, five potential phosphorylation sites are known to be associated with AD. To verify these results, several biochemical approaches (such as *in vitro* kinase assay and two-dimensional phosphopeptide analysis) were carried out with generated tau441 phosphomutants. By using these biochemical approaches, the AD-associated phosphorylation sites Ser68/Thr71 and Ser289 were confirmed as targets for CK1 δ . To confirm the biochemical approaches, the "Alzheimer's-in-a-dish" model was established by viral transduction of human neural progenitor cells (hNPCs) with mutant forms APP and presenilin, which are relevant in early-onset familial AD. Treatment of transduced and differentiated hNPCs with the CK1 δ -specific inhibitor PF-670462 and following Western blot analysis detected Ser214 as CK1 δ -targeted physiological relevant phosphorylation site. By using an *in vitro* tau aggregation assay, a possible role of CK1 δ -mediated phosphorylation on tau aggregation could be demonstrated. These results provide evidence that

CK1 δ represents an interesting point for therapeutic intervention in the development of AD, which was further investigated through the inhibition of CK1 δ in general (via CK1 δ -specific inhibitors) or alternatively, the intervention of CK1 δ activity at the level of CK1 δ -substrate interactions via CK1 δ -derived peptides.

Since the majority of previously developed CK1 inhibitors do not selectively inhibit CK1 isoforms, further chemical improvements are being sought to achieve greater selectivity (and potency). In cooperation with external partners, further developed compounds including benzimidazole derivatives, inhibitors of Wnt production (IWP)-derived compounds and isoxazole derivatives were tested for their selectivity and potency towards CK1 δ under established standard conditions. Highly selective and potent inhibitors (383, 384 and 394) and their related lead structures were tested for their cytotoxic effects and for their biological effect in the complex “Alzheimer’s-in-a-dish” model mimicking AD pathology. According to the results obtained from the “Alzheimer’s-in-a-dish” model the IWP-related compound 384 and to a lesser extent the chemically related inhibitor Liu-20 seem to have a beneficial effect on tau pathology, but not A β pathology. However, potential off-target effects, which might be involved in the beneficial therapeutic effect on tau pathology, have to be investigated.

As an alternative to CK1 δ -specific inhibitors probably exerting off-target effects, a novel therapeutic approach using CK1 δ -derived peptides was investigated. Initially, CK1 δ -derived peptides manipulating the protein-protein interaction of CK1 δ and APP and/or tau were characterized by interaction and phosphorylation analysis *in vitro* (via streptavidin-linked assays, surface plasmon resonance and *in vitro* kinase assays). The set of selected peptides subsequently demonstrated their potential to enter neuronal cells without inducing cytotoxic effects. For at least four of the identified CK1 δ -derived peptides, reduced A β levels and amyloid plaque formation (δ -101 and δ -311) or reduced tau hyperphosphorylation and aggregation (δ -31 and δ -281) could be successfully demonstrated in the complex “Alzheimer’s-in-a-dish” model mimicking AD pathology.

Consequently, the results obtained in this study provide an interesting starting point for further development and optimization steps of novel potent and/or highly selective small-molecule or peptide based-inhibitors as highly innovative and novel pharmacological tools for the treatment of AD.

6 References

- [1] Abd El-All, A. S., Magd-El-Din, A. A., Ragab, F. A. F., ElHefnawi, M., Abdalla, M. M., Galal, S. A., and El-Rashedy, A. A. 2015. New benzimidazoles and their antitumor effects with Aurora A kinase and KSP inhibitory activities. *Archiv der Pharmazie* 348, 7, 475–486.
- [2] Abraham, R. T. 2004. PI 3-kinase related kinases: 'big' players in stress-induced signaling pathways. *DNA repair* 3, 8-9, 883–887.
- [3] 2022. *Addgene: AAVS1 CAG rtTA3 TauWT 2N4R-EGFP*. <https://www.addgene.org/132389/>. Accessed 6 September 2022.
- [4] Adler, P., Mayne, J., Walker, K., Ning, Z., and Figeys, D. 2019. Therapeutic Targeting of Casein Kinase 1 δ/ϵ in an Alzheimer's Disease Mouse Model. *Journal of proteome research* 18, 9, 3383–3393.
- [5] Ahmed, M., Lai, T. H., and Kim, D. R. 2019. colocr: an R package for conducting co-localization analysis on fluorescence microscopy images. *PeerJ* 7, e7255.
- [6] Alappat, E. C., Feig, C., Boyerinas, B., Volkland, J., Samuels, M., Murmann, A. E., Thorburn, A., Kidd, V. J., Slaughter, C. A., Osborn, S. L., Winoto, A., Tang, W.-J., and Peter, M. E. 2005. Phosphorylation of FADD at serine 194 by CK1 α regulates its nonapoptotic activities. *Molecular cell* 19, 3, 321–332.
- [7] Alappat, E. C., Volkland, J., and Peter, M. E. 2003. Cell cycle effects by C-FADD depend on its C-terminal phosphorylation site. *The Journal of biological chemistry* 278, 43, 41585–41588.
- [8] Albanese, G., Venturi, C., and Galbiati, G. 2001. Treatment of larva migrans cutanea (creeping eruption): a comparison between albendazole and traditional therapy. *International journal of dermatology* 40, 1, 67–71.
- [9] Alpan, A. S., Zencir, S., Zupkó, I., Coban, G., Réthy, B., Gunes, H. S., and Topcu, Z. 2009. Biological activity of bis-benzimidazole derivatives on DNA topoisomerase I and HeLa, MCF7 and A431 cells. *Journal of enzyme inhibition and medicinal chemistry* 24, 3, 844–849.
- [10] Amanchy, R., Kandasamy, K., Mathivanan, S., Periaswamy, B., Reddy, R., Yoon, W.-H., Joore, J., Beer, M. A., Cope, L., and Pandey, A. 2011. Identification of Novel Phosphorylation Motifs Through an Integrative Computational and Experimental Analysis of the Human Phosphoproteome. *Journal of proteomics & bioinformatics* 4, 2, 22–35.
- [11] Amit, S., Hatzubai, A., Birman, Y., Andersen, J. S., Ben-Shushan, E., Mann, M., Ben-Neriah, Y., and Alkalay, I. 2002. Axin-mediated CKI phosphorylation of beta-catenin at Ser 45: a molecular switch for the Wnt pathway. *Genes & development* 16, 9, 1066–1076.
- [12] Andreadis, A. 2005. Tau gene alternative splicing: expression patterns, regulation and modulation of function in normal brain and neurodegenerative diseases. *Biochimica et biophysica acta* 1739, 2-3, 91–103.
- [13] Aplin, A. E., Gibb, G. M., Jacobsen, J. S., Gallo, J. M., and Anderton, B. H. 1996. In vitro phosphorylation of the cytoplasmic domain of the amyloid precursor protein by glycogen synthase kinase-3 β . *Journal of neurochemistry* 67, 2, 699–707.
- [14] Arai, T., Hasegawa, M., Akiyama, H., Ikeda, K., Nonaka, T., Mori, H., Mann, D., Tsuchiya, K., Yoshida, M., Hashizume, Y., and Oda, T. 2006. TDP-43 is a component of ubiquitin-positive tau-negative inclusions in frontotemporal lobar degeneration and amyotrophic lateral sclerosis. *Biochemical and biophysical research communications* 351, 3, 602–611.
- [15] Arey, R. and McClung, C. A. 2012. An inhibitor of casein kinase 1 ϵ/δ partially normalizes the manic-like behaviors of the Clock Δ 19 mouse. *Behavioural pharmacology* 23, 4, 392–396.
- [16] Arkin, M. R. and Whitty, A. 2009. The road less traveled: modulating signal transduction enzymes by inhibiting their protein-protein interactions. *Current opinion in chemical biology* 13, 3, 284–290.
- [17] Avendaño, C. and Menéndez, J. C. 2008. Drugs That Inhibit Signalling Pathways for Tumor Cell Growth and Proliferation. In *Medicinal Chemistry of Anticancer Drugs*. Elsevier, 251–305. DOI=10.1016/B978-0-444-52824-7.00009-3.
- [18] Avila, J. 2009. The tau code. *Frontiers in aging neuroscience* 1, 1.
- [19] Avila, J., Lucas, J. J., Perez, M., and Hernandez, F. 2004. Role of tau protein in both physiological and pathological conditions. *Physiological reviews* 84, 2, 361–384.

- [20] Baeshen, M. N., Al-Hejin, A. M., Bora, R. S., Ahmed, M. M. M., Ramadan, H. A. I., Saini, K. S., Baeshen, N. A., and Redwan, E. M. 2015. Production of Biopharmaceuticals in *E. coli*: Current Scenario and Future Perspectives. *Journal of microbiology and biotechnology* 25, 7, 953–962.
- [21] Baier, A. and Szyszka, R. 2022. CK2 and protein kinases of the CK1 superfamily as targets for neurodegenerative disorders. *Frontiers in molecular biosciences* 9, 916063.
- [22] Bao, Y., Hata, Y., Ikeda, M., and Withanage, K. 2011. Mammalian Hippo pathway: from development to cancer and beyond. *Journal of biochemistry* 149, 4, 361–379.
- [23] Barbagallo, A. P. M., Wang, Z., Zheng, H., and D'Adamio, L. 2011. The intracellular threonine of amyloid precursor protein that is essential for docking of Pin1 is dispensable for developmental function. *PloS one* 6, 3, e18006.
- [24] Barbier, P., Zejneli, O., Martinho, M., Lasorsa, A., Belle, V., Smet-Nocca, C., Tsvetkov, P. O., Devred, F., and Landrieu, I. 2019. Role of Tau as a Microtubule-Associated Protein: Structural and Functional Aspects. *Frontiers in aging neuroscience* 11, 204.
- [25] Barghorn, S., Biernat, J., and Mandelkow, E. 2005. Purification of recombinant tau protein and preparation of Alzheimer-paired helical filaments in vitro. *Methods in molecular biology (Clifton, N.J.)* 299, 35–51.
- [26] Barthelmé, S. and Tschumperlé, D. 2019. imager: an R package for image processing based on CImg. *JOSS* 4, 38, 1012.
- [27] Bayliss, R., Sardon, T., Vernos, I., and Conti, E. 2003. Structural basis of Aurora-A activation by TPX2 at the mitotic spindle. *Molecular cell* 12, 4, 851–862.
- [28] Behrend, L., Milne, D. M., Stöter, M., Deppert, W., Campbell, L. E., Meek, D. W., and Knippschild, U. 2000. IC261, a specific inhibitor of the protein kinases casein kinase 1-delta and -epsilon, triggers the mitotic checkpoint and induces p53-dependent postmitotic effects. *Oncogene* 19, 47, 5303–5313.
- [29] Behrend, L., Stöter, M., Kurth, M., Rutter, G., Heukeshoven, J., Deppert, W., and Knippschild, U. 2000. Interaction of casein kinase 1 delta (CK1delta) with post-Golgi structures, microtubules and the spindle apparatus. *European journal of cell biology* 79, 4, 240–251.
- [30] Benek, O., Hroch, L., Aitken, L., Gunn-Moore, F., Vinklarova, L., Kuca, K., Perez, D. I., Perez, C., Martinez, A., Fisar, Z., and Musilek, K. 2018. 1-(Benzodthiazol-2-yl)-3-phenylureas as dual inhibitors of casein kinase 1 and ABAD enzymes for treatment of neurodegenerative disorders. *Journal of enzyme inhibition and medicinal chemistry* 33, 1, 665–670.
- [31] Beyaert, R., Vanhaesebroeck, B., Declercq, W., van Lint, J., Vandenabele, P., Agostinis, P., Vandenheede, J. R., and Fiers, W. 1995. Casein kinase-1 phosphorylates the p75 tumor necrosis factor receptor and negatively regulates tumor necrosis factor signaling for apoptosis. *The Journal of biological chemistry* 270, 40, 23293–23299.
- [32] Bibian, M., Rahaim, R. J., Choi, J. Y., Noguchi, Y., Schürer, S., Chen, W., Nakanishi, S., Licht, K., Rosenberg, L. H., Li, L., Feng, Y., Cameron, M. D., Duckett, D. R., Cleveland, J. L., and Roush, W. R. 2013. Development of highly selective casein kinase 1 δ /1 ϵ (CK1 δ / ϵ) inhibitors with potent antiproliferative properties. *Bioorganic & medicinal chemistry letters* 23, 15, 4374–4380.
- [33] Biernat, J., Gustke, N., Drewes, G., Mandelkow, E. M., and Mandelkow, E. 1993. Phosphorylation of Ser262 strongly reduces binding of tau to microtubules: distinction between PHF-like immunoreactivity and microtubule binding. *Neuron* 11, 1, 153–163.
- [34] Biernat, J. and Mandelkow, E. M. 1999. The development of cell processes induced by tau protein requires phosphorylation of serine 262 and 356 in the repeat domain and is inhibited by phosphorylation in the proline-rich domains. *Molecular biology of the cell* 10, 3, 727–740.
- [35] Bingham, E. W. and Farrel, H. M. 1974. Casein kinase from the Golgi apparatus of lactating mammary gland. *The Journal of biological chemistry* 249, 11, 3647–3651.
- [36] Bioukar, E. B., Marricco, N. C., Zuo, D., and Larose, L. 1999. Serine phosphorylation of the ligand-activated beta-platelet-derived growth factor receptor by casein kinase I-gamma2 inhibits the receptor's autophosphorylating activity. *The Journal of biological chemistry* 274, 30, 21457–21463.
- [37] Bischof, J., Leban, J., Zaja, M., Grothey, A., Radunsky, B., Othersen, O., Strobl, S., Vitt, D., and Knippschild, U. 2012. 2-Benzamido-N-(1H-benzodimidazol-2-yl)thiazole-4-carboxamide derivatives as potent inhibitors of CK1 δ / ϵ . *Amino acids* 43, 4, 1577–1591.

- [38] Bischof, J., Randoll, S.-J., Süßner, N., Henne-Bruns, D., Pinna, L. A., and Knippschild, U. 2013. CK1 δ kinase activity is modulated by Chk1-mediated phosphorylation. *PloS one* 8, 7, e68803.
- [39] Blume, J. von, Knippschild, U., Dequiedt, F., Giamas, G., Beck, A., Auer, A., van Lint, J., Adler, G., and Seufferlein, T. 2007. Phosphorylation at Ser244 by CK1 determines nuclear localization and substrate targeting of PKD2. *The EMBO journal* 26, 22, 4619–4633.
- [40] Bogoyevitch, M. A., Barr, R. K., and Ketterman, A. J. 2005. Peptide inhibitors of protein kinases-discovery, characterisation and use. *Biochimica et biophysica acta* 1754, 1-2, 79–99.
- [41] Borchert, N., Dieterich, C., Krug, K., Schütz, W., Jung, S., Nordheim, A., Sommer, R. J., and Macek, B. 2010. Proteogenomics of *Pristionchus pacificus* reveals distinct proteome structure of nematode models. *Genome research* 20, 6, 837–846.
- [42] Bowman, B. M., Sebolt, K. A., Hoff, B. A., Boes, J. L., Daniels, D. L., Heist, K. A., Galbán, C. J., Patel, R. M., Zhang, J., Beer, D. G., Ross, B. D., Rehemtulla, A., and Galbán, S. 2015. Phosphorylation of FADD by the kinase CK1 α promotes KRASG12D-induced lung cancer. *Science signaling* 8, 361, ra9.
- [43] Boyce, J. J. and Shea, T. B. 1997. Phosphorylation events mediated by protein kinase C alpha and epsilon participate in regulation of tau steady-state levels and generation of certain "Alzheimer-like" phospho-epitopes. *International journal of developmental neuroscience : the official journal of the International Society for Developmental Neuroscience* 15, 3, 295–307.
- [44] Bozatzki, P. and Sapkota, G. P. 2018. The FAM83 family of proteins: from pseudo-PLDs to anchors for CK1 isoforms. *Biochemical Society transactions* 46, 3, 761–771.
- [45] Briner, A., Götz, J., and Polanco, J. C. 2020. Fyn Kinase Controls Tau Aggregation In Vivo. *Cell reports* 32, 7, 108045.
- [46] Brockman, J. L., Gross, S. D., Sussman, M. R., and Anderson, R. A. 1992. Cell cycle-dependent localization of casein kinase I to mitotic spindles. *Proceedings of the National Academy of Sciences of the United States of America* 89, 20, 9454–9458.
- [47] Brockschmidt, C., Hirner, H., Huber, N., Eismann, T., Hillenbrand, A., Giamas, G., Radunsky, B., Ammerpohl, O., Bohm, B., Henne-Bruns, D., Kalthoff, H., Leithäuser, F., Trauzold, A., and Knippschild, U. 2008. Anti-apoptotic and growth-stimulatory functions of CK1 delta and epsilon in ductal adenocarcinoma of the pancreas are inhibited by IC261 in vitro and in vivo. *Gut* 57, 6, 799–806.
- [48] Brooks, H. B., Geeganage, S., Kahl, S. D., Montrose, C., Sittampalam, S., Smith, M. C., and Weidner, J. R. 2004. *Assay Guidance Manual. Basics of Enzymatic Assays for HTS*, Bethesda (MD).
- [49] Bryja, V., Schulte, G., Rawal, N., Grahn, A., and Arenas, E. 2007. Wnt-5a induces Dishevelled phosphorylation and dopaminergic differentiation via a CK1-dependent mechanism. *Journal of cell science* 120, Pt 4, 586–595.
- [50] Budini, M., Jacob, G., Jedlicki, A., Pérez, C., Allende, C. C., and Allende, J. E. 2009. Autophosphorylation of carboxy-terminal residues inhibits the activity of protein kinase CK1 α . *Journal of cellular biochemistry* 106, 3, 399–408.
- [51] Bustos, V. H., Ferrarese, A., Venerando, A., Marin, O., Allende, J. E., and Pinna, L. A. 2006. The first armadillo repeat is involved in the recognition and regulation of beta-catenin phosphorylation by protein kinase CK1. *Proceedings of the National Academy of Sciences of the United States of America* 103, 52, 19725–19730.
- [52] Cadigan, K. M. and Nusse, R. 1997. Wnt signaling: a common theme in animal development. *Genes & development* 11, 24, 3286–3305.
- [53] Caporaso, G. L., Gandy, S. E., Buxbaum, J. D., Ramabhadran, T. V., and Greengard, P. 1992. Protein phosphorylation regulates secretion of Alzheimer beta/A4 amyloid precursor protein. *Proceedings of the National Academy of Sciences of the United States of America* 89, 7, 3055–3059.
- [54] Cegielska, A., Gietzen, K. F., Rivers, A., and Virshup, D. M. 1998. Autoinhibition of casein kinase I epsilon (CKI epsilon) is relieved by protein phosphatases and limited proteolysis. *The Journal of biological chemistry* 273, 3, 1357–1364.
- [55] Chaffey, N. 2003. Alberts, B., Johnson, A., Lewis, J., Raff, M., Roberts, K. and Walter, P. *Molecular biology of the cell*. 4th edn. *Annals of Botany* 91, 3, 401.

- [56] Chan, K. Y., Alonso-Nuñez, M., Grallert, A., Tanaka, K., Connolly, Y., Smith, D. L., and Hagan, I. M. 2017. Dialogue between centrosomal entrance and exit scaffold pathways regulates mitotic commitment. *The Journal of cell biology* 216, 9, 2795–2812.
- [57] Chatterjee, J., Rechenmacher, F., and Kessler, H. 2013. N-methylation of peptides and proteins: an important element for modulating biological functions. *Angewandte Chemie (International ed. in English)* 52, 1, 254–269.
- [58] Chauhan, A., Chauhan, V. P., Murakami, N., Brockerhoff, H., and Wisniewski, H. M. 1993. Amyloid beta-protein stimulates casein kinase I and casein kinase II activities. *Brain research* 629, 1, 47–52.
- [59] Ché, C., Yang, G., Thiot, C., Lacoste, M.-C., Currie, J.-C., Demeule, M., Régina, A., Bêliveau, R., and Castaigne, J.-P. 2010. New Angiopep-modified doxorubicin (ANG1007) and etoposide (ANG1009) chemotherapeutics with increased brain penetration. *Journal of medicinal chemistry* 53, 7, 2814–2824.
- [60] Chellappa, S., Kushekhar, K., Munthe, L. A., Tjønnfjord, G. E., Aandahl, E. M., Okkenhaug, K., and Taskén, K. 2019. The PI3K p110 δ Isoform Inhibitor Idelalisib Preferentially Inhibits Human Regulatory T Cell Function. *Journal of immunology (Baltimore, Md. : 1950)* 202, 5, 1397–1405.
- [61] Cheloha, R. W., Watanabe, T., Dean, T., Gellman, S. H., and Gardella, T. J. 2016. Backbone Modification of a Parathyroid Hormone Receptor-1 Antagonist/Inverse Agonist. *ACS chemical biology* 11, 10, 2752–2762.
- [62] Chen, B., Dodge, M. E., Tang, W., Lu, J., Ma, Z., Fan, C.-W., Wei, S., Hao, W., Kilgore, J., Williams, N. S., Roth, M. G., Amatruda, J. F., Chen, C., and Lum, L. 2009. Small molecule-mediated disruption of Wnt-dependent signaling in tissue regeneration and cancer. *Nature chemical biology* 5, 2, 100–107.
- [63] Chen, C., Gu, J., Basurto-Islas, G., Jin, N., Wu, F., Gong, C.-X., Iqbal, K., and Liu, F. 2017. Up-regulation of casein kinase 1 ϵ is involved in tau pathogenesis in Alzheimer's disease. *Scientific reports* 7, 1, 13478.
- [64] Chen, G.-F., Xu, T.-H., Yan, Y., Zhou, Y.-R., Jiang, Y., Melcher, K., and Xu, H. E. 2017. Amyloid beta: structure, biology and structure-based therapeutic development. *Acta pharmacologica Sinica* 38, 9, 1205–1235.
- [65] Chen, H., Ma, H., Inuzuka, H., Diao, J., Lan, F., Shi, Y. G., Wei, W., and Shi, Y. 2013. DNA damage regulates UHRF1 stability via the SCF(β -TrCP) E3 ligase. *Molecular and cellular biology* 33, 6, 1139–1148.
- [66] Cheong, J. K. and Virshup, D. M. 2011. Casein kinase 1: Complexity in the family. *The international journal of biochemistry & cell biology* 43, 4, 465–469.
- [67] Chergui, K., Svenningsson, P., and Greengard, P. 2005. Physiological role for casein kinase 1 in glutamatergic synaptic transmission. *The Journal of neuroscience : the official journal of the Society for Neuroscience* 25, 28, 6601–6609.
- [68] Chijiwa, T., Hagiwara, M., and Hidaka, H. 1989. A newly synthesized selective casein kinase I inhibitor, N-(2-aminoethyl)-5-chloroisoquinoline-8-sulfonamide, and affinity purification of casein kinase I from bovine testis. *The Journal of biological chemistry* 264, 9, 4924–4927.
- [69] Chirita, C. N., Congdon, E. E., Yin, H., and Kuret, J. 2005. Triggers of full-length tau aggregation: a role for partially folded intermediates. *Biochemistry* 44, 15, 5862–5872.
- [70] Choi, S. H., Kim, Y. H., Hebisch, M., Sliwinski, C., Lee, S., D'Avanzo, C., Chen, H., Hooli, B., Asselin, C., Muffat, J., Klee, J. B., Zhang, C., Wainger, B. J., Peitz, M., Kovacs, D. M., Wolf, C. J., Wagner, S. L., Tanzi, R. E., and Kim, D. Y. 2014. A three-dimensional human neural cell culture model of Alzheimer's disease. *Nature* 515, 7526, 274–278.
- [71] Choi, S. H., Kim, Y. H., Quinti, L., Tanzi, R. E., and Kim, D. Y. 2016. 3D culture models of Alzheimer's disease: a road map to a "cure-in-a-dish". *Molecular neurodegeneration* 11, 1, 75.
- [72] Choksi, D. K., Roy, B., Chatterjee, S., Yusuff, T., Bakhoun, M. F., Sengupta, U., Ambegaokar, S., Kayed, R., and Jackson, G. R. 2014. TDP-43 Phosphorylation by casein kinase I ϵ promotes oligomerization and enhances toxicity in vivo. *Human molecular genetics* 23, 4, 1025–1035.
- [73] Christmann, J. L. and Dahmus, M. E. 1981. Phosphorylation of rat ascites tumor non-histone chromatin proteins. Differential phosphorylation by two cyclic nucleotide-independent protein kinases and comparison to in vivo phosphorylation. *The Journal of biological chemistry* 256, 7, 3326–3331.

- [74] Chung, D.-H., Moore, B. P., Matharu, D. S., Golden, J. E., Maddox, C., Rasmussen, L., Sosa, M. I., Ananthan, S., White, E. L., Jia, F., Jonsson, C. B., and Severson, W. E. 2013. A cell based high-throughput screening approach for the discovery of new inhibitors of respiratory syncytial virus. *Virology journal* 10, 19.
- [75] Clevers, H. 2006. Wnt/beta-catenin signaling in development and disease. *Cell* 127, 3, 469–480.
- [76] Cobb, M. H. and Rosen, O. M. 1983. Description of a protein kinase derived from insulin-treated 3T3-L1 cells that catalyzes the phosphorylation of ribosomal protein S6 and casein. *The Journal of biological chemistry* 258, 20, 12472–12481.
- [77] Cohen, P. 2000. The regulation of protein function by multisite phosphorylation—a 25 year update. *Trends in biochemical sciences* 25, 12, 596–601.
- [78] Cohen, P. 2002. The origins of protein phosphorylation. *Nature cell biology* 4, 5, E127-30.
- [79] Cohen, P., Cross, D., and Jänne, P. A. 2021. Kinase drug discovery 20 years after imatinib: progress and future directions. *Nature reviews. Drug discovery* 20, 7, 551–569.
- [80] Corder, E. H., Saunders, A. M., Strittmatter, W. J., Schmechel, D. E., Gaskell, P. C., Small, G. W., Roses, A. D., Haines, J. L., and Pericak-Vance, M. A. 1993. Gene dose of apolipoprotein E type 4 allele and the risk of Alzheimer's disease in late onset families. *Science (New York, N.Y.)* 261, 5123, 921–923.
- [81] Cox, J. and Mann, M. 2008. MaxQuant enables high peptide identification rates, individualized p.p.b.-range mass accuracies and proteome-wide protein quantification. *Nature biotechnology* 26, 12, 1367–1372.
- [82] Cox, J., Neuhauser, N., Michalski, A., Scheltema, R. A., Olsen, J. V., and Mann, M. 2011. Andromeda: a peptide search engine integrated into the MaxQuant environment. *Journal of proteome research* 10, 4, 1794–1805.
- [83] Cozza, G. and Pinna, L. A. 2016. Casein kinases as potential therapeutic targets. *Expert opinion on therapeutic targets* 20, 3, 319–340.
- [84] Cruciat, C.-M. 2014. Casein kinase 1 and Wnt/ β -catenin signaling. *Current opinion in cell biology* 31, 46–55.
- [85] Cruciat, C.-M., Dolde, C., Groot, R. E. A. de, Ohkawara, B., Reinhard, C., Korswagen, H. C., and Niehrs, C. 2013. RNA helicase DDX3 is a regulatory subunit of casein kinase 1 in Wnt- β -catenin signaling. *Science (New York, N.Y.)* 339, 6126, 1436–1441.
- [86] Cunningham, P. S., Ahern, S. A., Smith, L. C., da Silva Santos, C. S., Wager, T. T., and Bechtold, D. A. 2016. Targeting of the circadian clock via CK1 δ/ϵ to improve glucose homeostasis in obesity. *Scientific reports* 6, 29983.
- [87] Czvitkovich, S., Duller, S., Mathiesen, E., Lorenzoni, K., Imbimbo, B. P., Hutter-Paier, B., Windisch, M., and Wronski, R. 2011. Comparison of pharmacological modulation of APP metabolism in primary chicken telencephalic neurons and in a human neuroglioma cell line. *Journal of molecular neuroscience : MN* 43, 3, 257–267.
- [88] Da Cruz e Silva, E. F. and Da Cruz e Silva, O. A. B. 2003. Protein phosphorylation and APP metabolism. *Neurochemical research* 28, 10, 1553–1561.
- [89] Dahmus, M. E. 1981. Purification and properties of calf thymus casein kinases I and II. *The Journal of biological chemistry* 256, 7, 3319–3325.
- [90] Darnay, B. G., Singh, S., and Aggarwal, B. B. 1997. The p80 TNF receptor-associated kinase (p80TRAK) associates with residues 354-397 of the p80 cytoplasmic domain: similarity to casein kinase. *FEBS letters* 406, 1-2, 101–105.
- [91] Davidson, G., Wu, W., Shen, J., Bilic, J., Fenger, U., Stannek, P., Glinka, A., and Niehrs, C. 2005. Casein kinase 1 γ couples Wnt receptor activation to cytoplasmic signal transduction. *Nature* 438, 7069, 867–872.
- [92] Davies, C. A., Mann, D. M., Sumpter, P. Q., and Yates, P. O. 1987. A quantitative morphometric analysis of the neuronal and synaptic content of the frontal and temporal cortex in patients with Alzheimer's disease. *Journal of the neurological sciences* 78, 2, 151–164.
- [93] Davila-Gutierrez, C. E., Vasquez, C., Trujillo-Hernandez, B., and Huerta, M. 2002. Nitazoxanide compared with quinamide and mebendazole in the treatment of helminthic infections and intestinal protozoa in children. *The American journal of tropical medicine and hygiene* 66, 3, 251–254.

- [94] Del Alonso, A. C., Mederlyova, A., Novak, M., Grundke-Iqbal, I., and Iqbal, K. 2004. Promotion of hyperphosphorylation by frontotemporal dementia tau mutations. *The Journal of biological chemistry* 279, 33, 34873–34881.
- [95] Del Alonso, A. C., Zaidi, T., Novak, M., Barra, H. S., Grundke-Iqbal, I., and Iqbal, K. 2001. Interaction of tau isoforms with Alzheimer's disease abnormally hyperphosphorylated tau and in vitro phosphorylation into the disease-like protein. *The Journal of biological chemistry* 276, 41, 37967–37973.
- [96] Del Valle-Pérez, B., Arqués, O., Vinyoles, M., Herreros, A. G. de, and Duñach, M. 2011. Coordinated action of CK1 isoforms in canonical Wnt signaling. *Molecular and cellular biology* 31, 14, 2877–2888.
- [97] Deng, C., Lipstein, M. R., Scotto, L., Jirau Serrano, X. O., Mangone, M. A., Li, S., Vendome, J., Hao, Y., Xu, X., Deng, S.-X., Realubit, R. B., Tatonetti, N. P., Karan, C., Lentzsch, S., Fruman, D. A., Honig, B., Landry, D. W., and O'Connor, O. A. 2017. Silencing c-Myc translation as a therapeutic strategy through targeting PI3K δ and CK1 ϵ in hematological malignancies. *Blood* 129, 1, 88–99.
- [98] Dephoure, N., Gould, K. L., Gygi, S. P., and Kellogg, D. R. 2013. Mapping and analysis of phosphorylation sites: a quick guide for cell biologists. *Molecular biology of the cell* 24, 5, 535–542.
- [99] Desagher, S., Osen-Sand, A., Montessuit, S., Magnenat, E., Vilbois, F., Hochmann, A., Journot, L., Antonsson, B., and Martinou, J. C. 2001. Phosphorylation of bid by casein kinases I and II regulates its cleavage by caspase 8. *Molecular cell* 8, 3, 601–611.
- [100] Despres, C., Byrne, C., Qi, H., Cantrelle, F.-X., Huvent, I., Chambraud, B., Baulieu, E.-E., Jacquot, Y., Landrieu, I., Lippens, G., and Smet-Nocca, C. 2017. Identification of the Tau phosphorylation pattern that drives its aggregation. *Proceedings of the National Academy of Sciences of the United States of America* 114, 34, 9080–9085.
- [101] Dhillon, S. and Keam, S. J. 2021. Umbralisib: First Approval. *Drugs* 81, 7, 857–866.
- [102] Din, F. U., Aman, W., Ullah, I., Qureshi, O. S., Mustapha, O., Shafique, S., and Zeb, A. 2017. Effective use of nanocarriers as drug delivery systems for the treatment of selected tumors. *International journal of nanomedicine* 12, 7291–7309.
- [103] Dolde, C., Bischof, J., Grüter, S., Montada, A., Halekotte, J., Peifer, C., Kalbacher, H., Baumann, U., Knippschild, U., and Suter, B. 2018. A CK1 FRET biosensor reveals that DDX3X is an essential activator of CK1 ϵ . *Journal of cell science* 131, 1.
- [104] Drathen, T. von, Ure, E. M., Kirschner, S., Roth, A., Meier, L., Woolhouse, A. D., Cameron, S. A., Knippschild, U., Peifer, C., and Luxenburger, A. 2022. C5-Iminosugar modification of casein kinase 1 δ lead 3-(4-fluorophenyl)-5-isopropyl-4-(pyridin-4-yl)isoxazole promotes enhanced inhibitor affinity and selectivity. *Archiv der Pharmazie* 355, 5, e2100497.
- [105] Drennan, D. and Ryazanov, A. G. 2004. Alpha-kinases: analysis of the family and comparison with conventional protein kinases. *Progress in biophysics and molecular biology* 85, 1, 1–32.
- [106] Drewes, G., Ebneith, A., and Mandelkow, E. M. 1998. MAPs, MARKs and microtubule dynamics. *Trends in biochemical sciences* 23, 8, 307–311.
- [107] Drewes, G., Lichtenberg-Kraag, B., Döring, F., Mandelkow, E. M., Biernat, J., Goris, J., Dorée, M., and Mandelkow, E. 1992. Mitogen activated protein (MAP) kinase transforms tau protein into an Alzheimer-like state. *The EMBO journal* 11, 6, 2131–2138.
- [108] Drewes, G., Trinczek, B., Illenberger, S., Biernat, J., Schmitt-Ulms, G., Meyer, H. E., Mandelkow, E. M., and Mandelkow, E. 1995. Microtubule-associated protein/microtubule affinity-regulating kinase (p110mark). A novel protein kinase that regulates tau-microtubule interactions and dynamic instability by phosphorylation at the Alzheimer-specific site serine 262. *The Journal of biological chemistry* 270, 13, 7679–7688.
- [109] Eldar-Finkelman, H. and Eisenstein, M. 2009. Peptide inhibitors targeting protein kinases. *Current pharmaceutical design* 15, 21, 2463–2470.
- [110] Eldehna, W. M., El Hassab, M. A., Abo-Ashour, M. F., Al-Warhi, T., Elaasser, M. M., Safwat, N. A., Suliman, H., Ahmed, M. F., Al-Rashood, S. T., Abdel-Aziz, H. A., and El-Haggar, R. 2021. Development of isatin-thiazolo3,2-abenzimidazole hybrids as novel CDK2 inhibitors with potent in vitro apoptotic anti-proliferative activity: Synthesis, biological and molecular dynamics investigations. *Bioorganic chemistry* 110, 104748.

- [111] Elmore, S. 2007. Apoptosis: a review of programmed cell death. *Toxicologic pathology* 35, 4, 495–516.
- [112] Eng, G. W. L., Edison, and Virshup, D. M. 2017. Site-specific phosphorylation of casein kinase 1 δ (CK1 δ) regulates its activity towards the circadian regulator PER2. *PloS one* 12, 5, e0177834.
- [113] Escudier, B., Worden, F., and Kudo, M. 2019. Sorafenib: key lessons from over 10 years of experience. *Expert review of anticancer therapy* 19, 2, 177–189.
- [114] Flaherty, D. B., Soria, J. P., Tomasiewicz, H. G., and Wood, J. G. 2000. Phosphorylation of human tau protein by microtubule-associated kinases: GSK3 β and cdk5 are key participants. *Journal of neuroscience research* 62, 3, 463–472.
- [115] Flajolet, M., He, G., Heiman, M., Lin, A., Nairn, A. C., and Greengard, P. 2007. Regulation of Alzheimer's disease amyloid-beta formation by casein kinase I. *Proceedings of the National Academy of Sciences of the United States of America* 104, 10, 4159–4164.
- [116] Flotow, H., Graves, P. R., Wang, A. Q., Fiol, C. J., Roeske, R. W., and Roach, P. J. 1990. Phosphate groups as substrate determinants for casein kinase I action. *The Journal of biological chemistry* 265, 24, 14264–14269.
- [117] Fu, Z., Chakraborti, T., Morse, S., Bennett, G. S., and Shaw, G. 2001. Four casein kinase I isoforms are differentially partitioned between nucleus and cytoplasm. *Experimental cell research* 269, 2, 275–286.
- [118] Fulcher, L. J., Bozatz, P., Tachie-Menson, T., Wu, K. Z. L., Cummins, T. D., Bufton, J. C., Pinkas, D. M., Dunbar, K., Shrestha, S., Wood, N. T., Weidlich, S., Macartney, T. J., Varghese, J., Gourlay, R., Campbell, D. G., Dingwell, K. S., Smith, J. C., Bullock, A. N., and Sapkota, G. P. 2018. The DUF1669 domain of FAM83 family proteins anchor casein kinase 1 isoforms. *Science signaling* 11, 531.
- [119] Gandy, S. 2010. Testing the amyloid hypothesis of Alzheimer's disease in vivo. *The Lancet. Neurology* 9, 4, 333–335.
- [120] Gandy, S. E., Caporaso, G. L., Buxbaum, J. D., Cruz Silva, O. de, Iverfeldt, K., Nordstedt, C., Suzuki, T., Czernik, A. J., Nairn, A. C., and Greengard, P. 1993. Protein phosphorylation regulates relative utilization of processing pathways for Alzheimer beta/A4 amyloid precursor protein. *Annals of the New York Academy of Sciences* 695, 117–121.
- [121] Gao, Z.-H., Seeling, J. M., Hill, V., Yochum, A., and Virshup, D. M. 2002. Casein kinase I phosphorylates and destabilizes the beta-catenin degradation complex. *Proceedings of the National Academy of Sciences of the United States of America* 99, 3, 1182–1187.
- [122] García-Reyes, B., Witt, L., Jansen, B., Karasu, E., Gehring, T., Leban, J., Henne-Bruns, D., Pichlo, C., Brunstein, E., Baumann, U., Wesseler, F., Rathmer, B., Schade, D., Peifer, C., and Knippschild, U. 2018. Discovery of Inhibitor of Wnt Production 2 (IWP-2) and Related Compounds As Selective ATP-Competitive Inhibitors of Casein Kinase 1 (CK1) δ/ϵ . *Journal of medicinal chemistry* 61, 9, 4087–4102.
- [123] Gärtner, F., Gihring, A., Roth, A., Bischof, J., Xu, P., Elad, L., Wabitsch, M., Burster, T., and Knippschild, U. 2021. Obesity Prolongs the Inflammatory Response in Mice After Severe Trauma and Attenuates the Splenic Response to the Inflammatory Reflex. *Frontiers in immunology* 12, 745132.
- [124] Gavrin, L. K. and Saiah, E. 2013. Approaches to discover non-ATP site kinase inhibitors. *Med. Chem. Commun.* 4, 1, 41–51.
- [125] Ghoshal, N., Smiley, J. F., DeMaggio, A. J., Hoekstra, M. F., Cochran, E. J., Binder, L. I., and Kuret, J. 1999. A new molecular link between the fibrillar and granulovacuolar lesions of Alzheimer's disease. *The American journal of pathology* 155, 4, 1163–1172.
- [126] Giamas, G., Castellano, L., Feng, Q., Knippschild, U., Jacob, J., Thomas, R. S., Coombes, R. C., Smith, C. L., Jiao, L. R., and Stebbing, J. 2009. CK1delta modulates the transcriptional activity of ERalpha via AIB1 in an estrogen-dependent manner and regulates ERalpha-AIB1 interactions. *Nucleic acids research* 37, 9, 3110–3123.
- [127] Giamas, G., Hirner, H., Shoshiashvili, L., Grothey, A., Gessert, S., Kühl, M., Henne-Bruns, D., Vorgias, C. E., and Knippschild, U. 2007. Phosphorylation of CK1delta: identification of Ser370 as the major phosphorylation site targeted by PKA in vitro and in vivo. *The Biochemical journal* 406, 3, 389–398.

- [128] Gietzen, K. F. and Virshup, D. M. 1999. Identification of inhibitory autophosphorylation sites in casein kinase I epsilon. *The Journal of biological chemistry* 274, 45, 32063–32070.
- [129] Gillespie, S. L., Golde, T. E., and Younkin, S. G. 1992. Secretory processing of the Alzheimer amyloid beta/A4 protein precursor is increased by protein phosphorylation. *Biochemical and biophysical research communications* 187, 3, 1285–1290.
- [130] Goate, A., Chartier-Harlin, M. C., Mullan, M., Brown, J., Crawford, F., Fidani, L., Giuffra, L., Haynes, A., Irving, N., and James, L. 1991. Segregation of a missense mutation in the amyloid precursor protein gene with familial Alzheimer's disease. *Nature* 349, 6311, 704–706.
- [131] Goedert, M., Spillantini, M. G., Jakes, R., Rutherford, D., and Crowther, R. A. 1989. Multiple isoforms of human microtubule-associated protein tau: sequences and localization in neurofibrillary tangles of Alzheimer's disease. *Neuron* 3, 4, 519–526.
- [132] Gołaszewska, A., Bik, W., Motyl, T., and Orzechowski, A. 2019. Bridging the Gap between Alzheimer's Disease and Alzheimer's-like Diseases in Animals. *International journal of molecular sciences* 20, 7.
- [133] Gonzales, M. L., Mellman, D. L., and Anderson, R. A. 2008. CKIalpha is associated with and phosphorylates star-PAP and is also required for expression of select star-PAP target messenger RNAs. *The Journal of biological chemistry* 283, 18, 12665–12673.
- [134] Good, M. C., Zalatan, J. G., and Lim, W. A. 2011. Scaffold proteins: hubs for controlling the flow of cellular information. *Science (New York, N.Y.)* 332, 6030, 680–686.
- [135] Götz, J., Gladbach, A., Pennanen, L., van Eersel, J., Schild, A., Della David, and Ittner, L. M. 2010. Animal models reveal role for tau phosphorylation in human disease. *Biochimica et biophysica acta* 1802, 10, 860–871.
- [136] Gozal, Y. M., Duong, D. M., Gearing, M., Cheng, D., Hanfelt, J. J., Funderburk, C., Peng, J., Lah, J. J., and Levey, A. I. 2009. Proteomics analysis reveals novel components in the detergent-insoluble subproteome in Alzheimer's disease. *Journal of proteome research* 8, 11, 5069–5079.
- [137] Graves, P. R. and Roach, P. J. 1995. Role of COOH-terminal phosphorylation in the regulation of casein kinase I delta. *The Journal of biological chemistry* 270, 37, 21689–21694.
- [138] Greer, Y. E., Gao, B., Yang, Y., Nussenzweig, A., and Rubin, J. S. 2017. Lack of Casein Kinase 1 Delta Promotes Genomic Instability - The Accumulation of DNA Damage and Down-Regulation of Checkpoint Kinase 1. *PLoS one* 12, 1, e0170903.
- [139] Greer, Y. E., Westlake, C. J., Gao, B., Bharti, K., Shiba, Y., Xavier, C. P., Pazour, G. J., Yang, Y., and Rubin, J. S. 2014. Casein kinase 1δ functions at the centrosome and Golgi to promote ciliogenesis. *Molecular biology of the cell* 25, 10, 1629–1640.
- [140] Gross, S. D., Hoffman, D. P., Fisette, P. L., Baas, P., and Anderson, R. A. 1995. A phosphatidylinositol 4,5-bisphosphate-sensitive casein kinase I alpha associates with synaptic vesicles and phosphorylates a subset of vesicle proteins. *The Journal of cell biology* 130, 3, 711–724.
- [141] Grozav, A. G., Chikamori, K., Kozuki, T., Grabowski, D. R., Bukowski, R. M., Willard, B., Kinter, M., Andersen, A. H., Ganapathi, R., and Ganapathi, M. K. 2009. Casein kinase I delta/epsilon phosphorylates topoisomerase IIalpha at serine-1106 and modulates DNA cleavage activity. *Nucleic acids research* 37, 2, 382–392.
- [142] Gu, L., Fullam, A., Brennan, R., and Schröder, M. 2013. Human DEAD box helicase 3 couples IκB kinase ε to interferon regulatory factor 3 activation. *Molecular and cellular biology* 33, 10, 2004–2015.
- [143] Guijarro, J. I., Sunde, M., Jones, J. A., Campbell, I. D., and Dobson, C. M. 1998. Amyloid fibril formation by an SH3 domain. *Proceedings of the National Academy of Sciences of the United States of America* 95, 8, 4224–4228.
- [144] Guillozet, A. L., Weintraub, S., Mash, D. C., and Mesulam, M. M. 2003. Neurofibrillary tangles, amyloid, and memory in aging and mild cognitive impairment. *Archives of neurology* 60, 5, 729–736.
- [145] Haas, D. W. and Hagedorn, C. H. 1991. Casein kinase I phosphorylates the 25-kDa mRNA cap-binding protein. *Archives of biochemistry and biophysics* 284, 1, 84–89.
- [146] Halekotte, J., Witt, L., Ianes, C., Krüger, M., Bührmann, M., Rauh, D., Pichlo, C., Brunstein, E., Luxenburger, A., Baumann, U., Knippschild, U., Bischof, J., and Peifer, C. 2017. Optimized

- 4,5-Diarylimidazoles as Potent/Selective Inhibitors of Protein Kinase CK1 δ and Their Structural Relation to p38 α MAPK. *Molecules (Basel, Switzerland)* 22, 4.
- [147] Hanger, D. P., Anderton, B. H., and Noble, W. 2009. Tau phosphorylation: the therapeutic challenge for neurodegenerative disease. *Trends in molecular medicine* 15, 3, 112–119.
- [148] Hanger, D. P., Betts, J. C., Loviny, T. L., Blackstock, W. P., and Anderton, B. H. 1998. New phosphorylation sites identified in hyperphosphorylated tau (paired helical filament-tau) from Alzheimer's disease brain using nanoelectrospray mass spectrometry. *Journal of neurochemistry* 71, 6, 2465–2476.
- [149] Hanger, D. P., Byers, H. L., Wray, S., Leung, K.-Y., Saxton, M. J., Seereeram, A., Reynolds, C. H., Ward, M. A., and Anderton, B. H. 2007. Novel phosphorylation sites in tau from Alzheimer brain support a role for casein kinase 1 in disease pathogenesis. *The Journal of biological chemistry* 282, 32, 23645–23654.
- [150] Harnoš, J., Ryneš, J., Víšková, P., Foldynová-Trantírková, S., Bajard-Ešner, L., Trantírek, L., and Bryja, V. 2018. Analysis of binding interfaces of the human scaffold protein AXIN1 by peptide microarrays. *The Journal of biological chemistry* 293, 42, 16337–16347.
- [151] Haroutunian, V., Hoffman, L. B., and Beeri, M. S. 2009. Is there a neuropathology difference between mild cognitive impairment and dementia? *Dialogues in clinical neuroscience* 11, 2, 171–179.
- [152] Head, E., Powell, D., Gold, B. T., and Schmitt, F. A. 2012. Alzheimer's Disease in Down Syndrome. *European journal of neurodegenerative disease* 1, 3, 353–364.
- [153] Herbert, C., Schieborr, U., Saxena, K., Juraszek, J., Smet, F. de, Alcouffe, C., Bianciotto, M., Saladino, G., Sibrac, D., Kudlinzki, D., Sreeramulu, S., Brown, A., Rigon, P., Herault, J.-P., Lassalle, G., Blundell, T. L., Rousseau, F., Gils, A., Schymkowitz, J., Tompa, P., Herbert, J.-M., Carmeliet, P., Gervasio, F. L., Schwalbe, H., and Bono, F. 2013. Molecular mechanism of SSR128129E, an extracellularly acting, small-molecule, allosteric inhibitor of FGF receptor signaling. *Cancer cell* 23, 4, 489–501.
- [154] Holden, H. E., Crider, P. A., and Wahrenberg, M. G. 1980. Mitotic arrest by benzimidazole analogs in human lymphocyte cultures. *Environmental mutagenesis* 2, 1, 67–73.
- [155] Honaker, Y. and Piwnica-Worms, H. 2010. Casein kinase 1 functions as both penultimate and ultimate kinase in regulating Cdc25A destruction. *Oncogene* 29, 23, 3324–3334.
- [156] Hornbeck, P. V., Zhang, B., Murray, B., Kornhauser, J. M., Latham, V., and Skrzypek, E. 2015. PhosphoSitePlus, 2014: mutations, PTMs and recalibrations. *Nucleic acids research* 43, Database issue, D512–20.
- [157] Huart, A.-S., MacLaine, N. J., Narayan, V., and Hupp, T. R. 2012. Exploiting the MDM2-CK1 α protein-protein interface to develop novel biologics that induce UBL-kinase-modification and inhibit cell growth. *PLoS one* 7, 8, e43391.
- [158] Hunter, T. 1991. Protein kinase classification. *Methods in enzymology* 200, 3–37.
- [159] Ianes, C., Xu, P., Werz, N., Meng, Z., Henne-Bruns, D., Bischof, J., and Knippschild, U. 2016. CK1 δ activity is modulated by CDK2/E- and CDK5/p35-mediated phosphorylation. *Amino acids* 48, 2, 579–592.
- [160] Iijima, K., Ando, K., Takeda, S., Satoh, Y., Seki, T., Itohara, S., Greengard, P., Kirino, Y., Nairn, A. C., and Suzuki, T. 2000. Neuron-specific phosphorylation of Alzheimer's beta-amyloid precursor protein by cyclin-dependent kinase 5. *Journal of neurochemistry* 75, 3, 1085–1091.
- [161] Ikeda, K., Zhapparova, O., Brodsky, I., Semenova, I., Tirnauer, J. S., Zaliapin, I., and Rodionov, V. 2011. CK1 activates minus-end-directed transport of membrane organelles along microtubules. *Molecular biology of the cell* 22, 8, 1321–1329.
- [162] Illenberger, S., Zheng-Fischhöfer, Q., Preuss, U., Stamer, K., Baumann, K., Trinczek, B., Biernat, J., Godemann, R., Mandelkow, E. M., and Mandelkow, E. 1998. The endogenous and cell cycle-dependent phosphorylation of tau protein in living cells: implications for Alzheimer's disease. *Molecular biology of the cell* 9, 6, 1495–1512.
- [163] Imai, K. and Takaoka, A. 2006. Comparing antibody and small-molecule therapies for cancer. *Nature reviews. Cancer* 6, 9, 714–727.
- [164] Ingham, P. W. and McMahon, A. P. 2001. Hedgehog signaling in animal development: paradigms and principles. *Genes & development* 15, 23, 3059–3087.

- [165] Ishiguro, T., Tanaka, K., Sakuno, T., and Watanabe, Y. 2010. Shugoshin-PP2A counteracts casein-kinase-1-dependent cleavage of Rec8 by separase. *Nature cell biology* 12, 5, 500–506.
- [166] Izeradjene, K., Douglas, L., Delaney, A. B., and Houghton, J. A. 2004. Casein kinase I attenuates tumor necrosis factor-related apoptosis-inducing ligand-induced apoptosis by regulating the recruitment of fas-associated death domain and procaspase-8 to the death-inducing signaling complex. *Cancer research* 64, 21, 8036–8044.
- [167] Jakob-Roetne, R. and Jacobsen, H. 2009. Alzheimer's disease: from pathology to therapeutic approaches. *Angewandte Chemie (International ed. in English)* 48, 17, 3030–3059.
- [168] Janovská, P., Normant, E., Miskin, H., and Bryja, V. 2020. Targeting Casein Kinase 1 (CK1) in Hematological Cancers. *International journal of molecular sciences* 21, 23.
- [169] Jarrett, J. T. and Lansbury, P. T. 1992. Amyloid fibril formation requires a chemically discriminating nucleation event: studies of an amyloidogenic sequence from the bacterial protein OsmB. *Biochemistry* 31, 49, 12345–12352.
- [170] Jesse, S., Steinacker, P., Lehnert, S., Gillardon, F., Hengerer, B., and Otto, M. 2009. Neurochemical approaches in the laboratory diagnosis of Parkinson and Parkinson dementia syndromes: a review. *CNS Neuroscience & Therapeutics* 15, 2, 157–182.
- [171] Jevsevar, S., Kunstelj, M., and Porekar, V. G. 2010. PEGylation of therapeutic proteins. *Biotechnology journal* 5, 1, 113–128.
- [172] Johnson, A. E., Chen, J.-S., and Gould, K. L. 2013. CK1 is required for a mitotic checkpoint that delays cytokinesis. *Current biology : CB* 23, 19, 1920–1926.
- [173] Johnson, T. K. and Soellner, M. B. 2016. Bivalent Inhibitors of c-Src Tyrosine Kinase That Bind a Regulatory Domain. *Bioconjugate chemistry* 27, 7, 1745–1749.
- [174] Kametani, F., Nonaka, T., Suzuki, T., Arai, T., Dohmae, N., Akiyama, H., and Hasegawa, M. 2009. Identification of casein kinase-1 phosphorylation sites on TDP-43. *Biochemical and biophysical research communications* 382, 2, 405–409.
- [175] Kanev, G. K., Graaf, C. de, Esch, I. J. P. de, Leurs, R., Würdinger, T., Westerman, B. A., and Kooistra, A. J. 2019. The Landscape of Atypical and Eukaryotic Protein Kinases. *Trends in pharmacological sciences* 40, 11, 818–832.
- [176] Kani, S., Oishi, I., Yamamoto, H., Yoda, A., Suzuki, H., Nomachi, A., Iozumi, K., Nishita, M., Kikuchi, A., Takumi, T., and Minami, Y. 2004. The receptor tyrosine kinase Ror2 associates with and is activated by casein kinase I ϵ . *The Journal of biological chemistry* 279, 48, 50102–50109.
- [177] Kaucká, M., Plevová, K., Pavlová, S., Janovská, P., Mishra, A., Verner, J., Procházková, J., Krejčí, P., Kotasková, J., Ovesná, P., Tichý, B., Brychtová, Y., Doubek, M., Kozubík, A., Mayer, J., Pospíšilová, S., and Bryja, V. 2013. The planar cell polarity pathway drives pathogenesis of chronic lymphocytic leukemia by the regulation of B-lymphocyte migration. *Cancer research* 73, 5, 1491–1501.
- [178] Kawakami, F., Suzuki, K., and Ohtsuki, K. 2008. A novel consensus phosphorylation motif in sulfatide- and cholesterol-3-sulfate-binding protein substrates for CK1 in vitro. *Biological & pharmaceutical bulletin* 31, 2, 193–200.
- [179] Kholodenko, B. N., Hancock, J. F., and Kolch, W. 2010. Signalling ballet in space and time. *Nature reviews. Molecular cell biology* 11, 6, 414–426.
- [180] Kim, S.-K., Park, H.-J., Hong, H. S., Baik, E. J., Jung, M. W., and Mook-Jung, I. 2006. ERK1/2 is an endogenous negative regulator of the gamma-secretase activity. *FASEB journal : official publication of the Federation of American Societies for Experimental Biology* 20, 1, 157–159.
- [181] Kim, Y. H., Choi, S. H., D'Avanzo, C., Hebisch, M., Sliwinski, C., Bylykbashi, E., Washicosky, K. J., Klee, J. B., Brüstle, O., Tanzi, R. E., and Kim, D. Y. 2015. A 3D human neural cell culture system for modeling Alzheimer's disease. *Nature protocols* 10, 7, 985–1006.
- [182] Kimura, T., Ishiguro, K., and Hisanaga, S.-I. 2014. Physiological and pathological phosphorylation of tau by Cdk5. *Frontiers in molecular neuroscience* 7, 65.
- [183] Klaus, A. and Birchmeier, W. 2008. Wnt signalling and its impact on development and cancer. *Nature reviews. Cancer* 8, 5, 387–398.

- [184] Knippschild, U., Gocht, A., Wolff, S., Huber, N., Löhler, J., and Stöter, M. 2005. The casein kinase 1 family: participation in multiple cellular processes in eukaryotes. *Cellular signalling* 17, 6, 675–689.
- [185] Knippschild, U., Krüger, M., Richter, J., Xu, P., García-Reyes, B., Peifer, C., Halekotte, J., Bakulev, V., and Bischof, J. 2014. The CK1 Family: Contribution to Cellular Stress Response and Its Role in Carcinogenesis. *Frontiers in oncology* 4, 96.
- [186] Knippschild, U., Milne, D. M., Campbell, L. E., DeMaggio, A. J., Christenson, E., Hoekstra, M. F., and Meek, D. W. 1997. p53 is phosphorylated in vitro and in vivo by the delta and epsilon isoforms of casein kinase 1 and enhances the level of casein kinase 1 delta in response to topoisomerase-directed drugs. *Oncogene* 15, 14, 1727–1736.
- [187] Knippschild, U., Wolff, S., Giamas, G., Brockschmidt, C., Wittau, M., Würfl, P. U., Eismann, T., and Stöter, M. 2005. The role of the casein kinase 1 (CK1) family in different signaling pathways linked to cancer development. *Onkologie* 28, 10, 508–514.
- [188] Krismer, K., Bernwinkler, T., and Ehrenberger, T. 2021. *Scan Protein for Motifs - Scansite 4*. <https://scansite4.mit.edu/>. Accessed 13 September 2022.
- [189] Krönke, J., Fink, E. C., Hollenbach, P. W., MacBeth, K. J., Hurst, S. N., Udeshi, N. D., Chamberlain, P. P., Mani, D. R., Man, H. W., Gandhi, A. K., Svinkina, T., Schneider, R. K., McConkey, M., Järås, M., Griffiths, E., Wetzler, M., Bullinger, L., Cathers, B. E., Carr, S. A., Chopra, R., and Ebert, B. L. 2015. Lenalidomide induces ubiquitination and degradation of CK1 α in del(5q) MDS. *Nature* 523, 7559, 183–188.
- [190] Krüger, M., Kalbacher, H., Kastiris, P. L., Bischof, J., Barth, H., Henne-Bruns, D., Vorgias, C., Sarno, S., Pinna, L. A., and Knippschild, U. 2016. New potential peptide therapeutics perturbing CK1 δ/α -tubulin interaction. *Cancer letters* 375, 2, 375–383.
- [191] Ksiezak-Reding, H., Binder, L. I., and Yen, S. H. 1990. Alzheimer disease proteins (A68) share epitopes with tau but show distinct biochemical properties. *Journal of neuroscience research* 25, 3, 420–430.
- [192] Ksiezak-Reding, H., Pyo, H. K., Feinstein, B., and Pasinetti, G. M. 2003. Akt/PKB kinase phosphorylates separately Thr212 and Ser214 of tau protein in vitro. *Biochimica et biophysica acta* 1639, 3, 159–168.
- [193] Kubo, K., Inada, Y., Kohara, Y., Sugiura, Y., Ojima, M., Itoh, K., Furukawa, Y., Nishikawa, K., and Naka, T. 1993. Nonpeptide angiotensin II receptor antagonists. Synthesis and biological activity of benzimidazoles. *Journal of medicinal chemistry* 36, 12, 1772–1784.
- [194] Kukull, W. A., Brenner, D. E., Speck, C. E., Nochlin, D., Bowen, J., McCormick, W., Teri, L., Pfanschmidt, M. L., and Larson, E. B. 1994. Causes of death associated with Alzheimer disease: variation by level of cognitive impairment before death. *Journal of the American Geriatrics Society* 42, 7, 723–726.
- [195] Kulic, L., Walter, J., Multhaup, G., Teplow, D. B., Baumeister, R., Romig, H., Capell, A., Steiner, H., and Haass, C. 2000. Separation of presenilin function in amyloid beta-peptide generation and endoproteolysis of Notch. *Proceedings of the National Academy of Sciences of the United States of America* 97, 11, 5913–5918.
- [196] Kuo, L.-H., Hu, M.-K., Hsu, W.-M., Tung, Y.-T., Wang, B.-J., Tsai, W.-W., Yen, C.-T., and Liao, Y.-F. 2008. Tumor necrosis factor- α -elicited stimulation of gamma-secretase is mediated by c-Jun N-terminal kinase-dependent phosphorylation of presenilin and nicastrin. *Molecular biology of the cell* 19, 10, 4201–4212.
- [197] Kuret, J., Johnson, G. S., Cha, D., Christenson, E. R., DeMaggio, A. J., and Hoekstra, M. F. 1997. Casein kinase 1 is tightly associated with paired-helical filaments isolated from Alzheimer's disease brain. *Journal of neurochemistry* 69, 6, 2506–2515.
- [198] La Rubio de Torre, E., Luzón-Toro, B., Forte-Lago, I., Minguéz-Castellanos, A., Ferrer, I., and Hilfiker, S. 2009. Combined kinase inhibition modulates parkin inactivation. *Human molecular genetics* 18, 5, 809–823.
- [199] Lamba, V. and Ghosh, I. 2012. New directions in targeting protein kinases: focusing upon true allosteric and bivalent inhibitors. *Current pharmaceutical design* 18, 20, 2936–2945.
- [200] Lansing, T. J., McConnell, R. T., Duckett, D. R., Spehar, G. M., Knick, V. B., Hassler, D. F., Noro, N., Furuta, M., Emmitte, K. A., Gilmer, T. M., Mook, R. A., and Cheung, M. 2007. In vitro biological activity of a novel small-molecule inhibitor of polo-like kinase 1. *Molecular cancer therapeutics* 6, 2, 450–459.

- [201] LaRonde-LeBlanc, N. and Wlodawer, A. 2005. A family portrait of the RIO kinases. *The Journal of biological chemistry* 280, 45, 37297–37300.
- [202] Law, B. M., Guest, A. L., Pullen, M. W. J., Perkinson, M. S., and Williams, R. J. 2018. Increased Foxo3a Nuclear Translocation and Activity is an Early Neuronal Response to β -Secretase-Mediated Processing of the Amyloid- β Protein Precursor: Utility of an A β PP-GAL4 Reporter Assay. *Journal of Alzheimer's disease : JAD* 61, 2, 673–688.
- [203] Lee, G., Neve, R. L., and Kosik, K. S. 1989. The microtubule binding domain of tau protein. *Neuron* 2, 6, 1615–1624.
- [204] Lee, M.-S., Kao, S.-C., Lemere, C. A., Xia, W., Tseng, H.-C., Zhou, Y., Neve, R., Ahlijanian, M. K., and Tsai, L.-H. 2003. APP processing is regulated by cytoplasmic phosphorylation. *The Journal of cell biology* 163, 1, 83–95.
- [205] Lee, P. Y., Yeoh, Y., and Low, T. Y. 2022. A recent update on small-molecule kinase inhibitors for targeted cancer therapy and their therapeutic insights from mass spectrometry-based proteomic analysis. *The FEBS journal*.
- [206] Letoha, T., Gaál, S., Somlai, C., Venkei, Z., Glavinas, H., Kusz, E., Duda, E., Czajlik, A., Peták, F., and Penke, B. 2005. Investigation of penetratin peptides. Part 2. In vitro uptake of penetratin and two of its derivatives. *Journal of peptide science : an official publication of the European Peptide Society* 11, 12, 805–811.
- [207] Li, G., Yin, H., and Kuret, J. 2004. Casein kinase 1 delta phosphorylates tau and disrupts its binding to microtubules. *The Journal of biological chemistry* 279, 16, 15938–15945.
- [208] Liachko, N. F., McMillan, P. J., Strovass, T. J., Loomis, E., Greenup, L., Murrell, J. R., Ghetti, B., Raskind, M. A., Montine, T. J., Bird, T. D., Leverenz, J. B., and Kraemer, B. C. 2014. The tau tubulin kinases TTBK1/2 promote accumulation of pathological TDP-43. *PLoS genetics* 10, 12, e1004803.
- [209] Lin, Y.-C., Chen, M.-C., Hsieh, T.-H., Liou, J.-P., and Chen, C.-H. 2020. CK1 δ as a potential therapeutic target to treat bladder cancer. *Aging* 12, 7, 5764–5780.
- [210] Ling, Y., Morgan, K., and Kalsheker, N. 2003. Amyloid precursor protein (APP) and the biology of proteolytic processing: relevance to Alzheimer's disease. *The international journal of biochemistry & cell biology* 35, 11, 1505–1535.
- [211] Liu, C., Li, Y., Semenov, M., Han, C., Baeg, G. H., Tan, Y., Zhang, Z., Lin, X., and He, X. 2002. Control of beta-catenin phosphorylation/degradation by a dual-kinase mechanism. *Cell* 108, 6, 837–847.
- [212] Liu, C., Witt, L., Ianes, C., Bischof, J., Bammert, M.-T., Baier, J., Kirschner, S., Henne-Bruns, D., Xu, P., Kornmann, M., Peifer, C., and Knippschild, U. 2019. Newly Developed CK1-Specific Inhibitors Show Specifically Stronger Effects on CK1 Mutants and Colon Cancer Cell Lines. *International journal of molecular sciences* 20, 24.
- [213] Liu, C.-Y., Zha, Z.-Y., Zhou, X., Zhang, H., Huang, W., Di Zhao, Li, T., Chan, S. W., Lim, C. J., Hong, W., Zhao, S., Xiong, Y., Lei, Q.-Y., and Guan, K.-L. 2010. The hippo tumor pathway promotes TAZ degradation by phosphorylating a phosphodegron and recruiting the SCF{beta}-TrCP E3 ligase. *The Journal of biological chemistry* 285, 48, 37159–37169.
- [214] Liu, F., Li, B., Tung, E.-J., Grundke-Iqbal, I., Iqbal, K., and Gong, C.-X. 2007. Site-specific effects of tau phosphorylation on its microtubule assembly activity and self-aggregation. *The European journal of neuroscience* 26, 12, 3429–3436.
- [215] Liu, J., Carvalho, L. P., Bhattacharya, S., Carbone, C. J., Kumar, K. G. S., Leu, N. A., Yau, P. M., Donald, R. G. K., Weiss, M. J., Baker, D. P., McLaughlin, K. J., Scott, P., and Fuchs, S. Y. 2009. Mammalian casein kinase 1alpha and its leishmanial ortholog regulate stability of IFNAR1 and type I interferon signaling. *Molecular and cellular biology* 29, 24, 6401–6412.
- [216] Liu, S., Zhang, C., Campbell, J. L., Zhang, H., Yeung, K. K.-C., Han, V. K. M., and Lajoie, G. A. 2005. Formation of phosphopeptide-metal ion complexes in liquid chromatography/electrospray mass spectrometry and their influence on phosphopeptide detection. *Rapid communications in mass spectrometry : RCM* 19, 19, 2747–2756.
- [217] Liu, Y. and Gray, N. S. 2006. Rational design of inhibitors that bind to inactive kinase conformations. *Nature chemical biology* 2, 7, 358–364.
- [218] Llorens-Martín, M., Jurado, J., Hernández, F., and Avila, J. 2014. GSK-3 β , a pivotal kinase in Alzheimer disease. *Frontiers in molecular neuroscience* 7, 46.

- [219] Logan, C. Y. and Nusse, R. 2004. The Wnt signaling pathway in development and disease. *Annual review of cell and developmental biology* 20, 781–810.
- [220] Löhler, J., Hirner, H., Schmidt, B., Kramer, K., Fischer, D., Thal, D. R., Leithäuser, F., and Knippschild, U. 2009. Immunohistochemical characterisation of cell-type specific expression of CK1delta in various tissues of young adult BALB/c mice. *PLoS one* 4, 1, e4174.
- [221] Longenecker, K. L., Roach, P. J., and Hurley, T. D. 1996. Three-dimensional structure of mammalian casein kinase I: molecular basis for phosphate recognition. *Journal of molecular biology* 257, 3, 618–631.
- [222] Łukasik, P., Baranowska-Bosiacka, I., Kulczycka, K., and Gutowska, I. 2021. Inhibitors of Cyclin-Dependent Kinases: Types and Their Mechanism of Action. *International journal of molecular sciences* 22, 6.
- [223] Luque-Garcia, J. L. and Neubert, T. A. 2009. On-membrane tryptic digestion of proteins for mass spectrometry analysis. *Methods in molecular biology (Clifton, N.J.)* 536, 331–341.
- [224] Luxenburger, A., Schmidt, D., Ianes, C., Pichlo, C., Krüger, M., Drathen, T. von, Brunstein, E., Gainsford, G. J., Baumann, U., Knippschild, U., and Peifer, C. 2019. Design, Synthesis and Biological Evaluation of Isoxazole-Based CK1 Inhibitors Modified with Chiral Pyrrolidine Scaffolds. *Molecules (Basel, Switzerland)* 24, 5.
- [225] MacDonald, B. T., Tamai, K., and He, X. 2009. Wnt/beta-catenin signaling: components, mechanisms, and diseases. *Developmental cell* 17, 1, 9–26.
- [226] Manning, G., Whyte, D. B., Martinez, R., Hunter, T., and Sudarsanam, S. 2002. The protein kinase complement of the human genome. *Science (New York, N.Y.)* 298, 5600, 1912–1934.
- [227] Marin, O., Bustos, V. H., Cesaro, L., Meggio, F., Pagano, M. A., Antonelli, M., Allende, C. C., Pinna, L. A., and Allende, J. E. 2003. A noncanonical sequence phosphorylated by casein kinase 1 in beta-catenin may play a role in casein kinase 1 targeting of important signaling proteins. *Proceedings of the National Academy of Sciences of the United States of America* 100, 18, 10193–10200.
- [228] Martin, L., Latypova, X., and Terro, F. 2011. Post-translational modifications of tau protein: implications for Alzheimer's disease. *Neurochemistry international* 58, 4, 458–471.
- [229] Mashhoon, N., DeMaggio, A. J., Tereshko, V., Bergmeier, S. C., Egli, M., Hoekstra, M. F., and Kuret, J. 2000. Crystal structure of a conformation-selective casein kinase-1 inhibitor. *The Journal of biological chemistry* 275, 26, 20052–20060.
- [230] Matsuo, E. S., Shin, R. W., Billingsley, M. L., van deVoorde, A., O'Connor, M., Trojanowski, J. Q., and Lee, V. M. 1994. Biopsy-derived adult human brain tau is phosphorylated at many of the same sites as Alzheimer's disease paired helical filament tau. *Neuron* 13, 4, 989–1002.
- [231] Mayers, R. M., Leighton, B., and Kilgour, E. 2005. PDH kinase inhibitors: a novel therapy for Type II diabetes? *Biochemical Society transactions* 33, Pt 2, 367–370.
- [232] McMahon, A. P. and Moon, R. T. 1989. Ectopic expression of the proto-oncogene int-1 in *Xenopus* embryos leads to duplication of the embryonic axis. *Cell* 58, 6, 1075–1084.
- [233] Meanwell, N. A. 2011. Improving drug candidates by design: a focus on physicochemical properties as a means of improving compound disposition and safety. *Chemical research in toxicology* 24, 9, 1420–1456.
- [234] Meggio, F., Perich, J. W., Marin, O., and Pinna, L. A. 1992. The comparative efficiencies of the Ser(P)-, Thr(P)- and Tyr(P)-residues as specificity determinants for casein kinase-1. *Biochemical and biophysical research communications* 182, 3, 1460–1465.
- [235] Meggio, F., Perich, J. W., Reynolds, E. C., and Pinna, L. A. 1991. A synthetic beta-casein phosphopeptide and analogues as model substrates for casein kinase-1, a ubiquitous, phosphate directed protein kinase. *FEBS letters* 283, 2, 303–306.
- [236] Mendoza, J., Sekiya, M., Taniguchi, T., Iijima, K. M., Wang, R., and Ando, K. 2013. Global analysis of phosphorylation of tau by the checkpoint kinases Chk1 and Chk2 in vitro. *Journal of proteome research* 12, 6, 2654–2665.
- [237] Meng, Q.-J., Maywood, E. S., Bechtold, D. A., Lu, W.-Q., Li, J., Gibbs, J. E., Dupré, S. M., Chesham, J. E., Rajamohan, F., Knafels, J., Sneed, B., Zawadzke, L. E., Ohren, J. F., Walton, K. M., Wager, T. T., Hastings, M. H., and Loudon, A. S. I. 2010. Entrainment of disrupted circadian behavior through inhibition of casein kinase 1 (CK1) enzymes. *Proceedings of the National Academy of Sciences of the United States of America* 107, 34, 15240–15245.

- [238] Meng, Z., Bischof, J., Ianes, C., Henne-Bruns, D., Xu, P., and Knippschild, U. 2016. CK1 δ kinase activity is modulated by protein kinase C α (PKC α)-mediated site-specific phosphorylation. *Amino acids* 48, 5, 1185–1197.
- [239] Meng, Z., Böhm, T., Xu, P., Henne-Bruns, D., Peifer, C., Witt, L., Knippschild, U., and Bischof, J. 2019. Kinase activity of casein kinase 1 delta (CK1 δ) is modulated by protein kinase C α (PKC α) by site-specific phosphorylation within the kinase domain of CK1 δ . *Biochimica et biophysica acta. Proteins and proteomics* 1867, 7-8, 710–721.
- [240] Milne, D. M., Palmer, R. H., Campbell, D. G., and Meek, D. W. 1992. Phosphorylation of the p53 tumour-suppressor protein at three N-terminal sites by a novel casein kinase I-like enzyme. *Oncogene* 7, 7, 1361–1369.
- [241] Minzel, W., Venkatachalam, A., Fink, A., Hung, E., Brachya, G., Burstain, I., Shaham, M., Rivlin, A., Omer, I., Zinger, A., Elias, S., Winter, E., Erdman, P. E., Sullivan, R. W., Fung, L., Mercurio, F., Li, D., Vacca, J., Kaushansky, N., Shlush, L., Oren, M., Levine, R., Pikarsky, E., Snir-Alkalay, I., and Ben-Neriah, Y. 2018. Small Molecules Co-targeting CK1 α and the Transcriptional Kinases CDK7/9 Control AML in Preclinical Models. *Cell* 175, 1, 171-185.e25.
- [242] Moon, R. T., Brown, J. D., and Torres, M. 1997. WNTs modulate cell fate and behavior during vertebrate development. *Trends in genetics : TIG* 13, 4, 157–162.
- [243] Morishima-Kawashima, M., Hasegawa, M., Takio, K., Suzuki, M., Yoshida, H., Titani, K., and Ihara, Y. 1995. Proline-directed and non-proline-directed phosphorylation of PHF-tau. *The Journal of biological chemistry* 270, 2, 823–829.
- [244] Morishima-Kawashima, M., Hasegawa, M., Takio, K., Suzuki, M., Yoshida, H., Watanabe, A., Titani, K., and Ihara, Y. 1995. Hyperphosphorylation of Tau in PHF. *Neurobiology of Aging* 16, 3, 365–371.
- [245] Mullan, M., Crawford, F., Axelman, K., Houlden, H., Lilius, L., Winblad, B., and Lannfelt, L. 1992. A pathogenic mutation for probable Alzheimer's disease in the APP gene at the N-terminus of beta-amyloid. *Nature genetics* 1, 5, 345–347.
- [246] 2023. *NanoBIT® Protein:Protein Interaction System Protocol*. Accessed 13 January 2023.
- [247] Němec, V., Khirsariya, P., Janovská, P., Moyano, P. M., Maier, L., Lesáková, P., Kebková, P., Gybel, T., Berger, B.-T., Chaikuad, A., Reinecke, M., Küster, B., Knapp, S., Bryja, V., and Paruch, K. 2023. Discovery of Potent and Exquisitely Selective Inhibitors of Kinase CK1 with Tunable Isoform Selectivity. *Angewandte Chemie (International ed. in English)*.
- [248] Nero, T. L., Morton, C. J., Holien, J. K., Wielens, J., and Parker, M. W. 2014. Oncogenic protein interfaces: small molecules, big challenges. *Nature reviews. Cancer* 14, 4, 248–262.
- [249] Niblock, M. and Gallo, J.-M. 2012. Tau alternative splicing in familial and sporadic tauopathies. *Biochemical Society transactions* 40, 4, 677–680.
- [250] Noble, W., Hanger, D. P., Miller, C. C. J., and Lovestone, S. 2013. The importance of tau phosphorylation for neurodegenerative diseases. *Frontiers in neurology* 4, 83.
- [251] 2022. *Nucleotide BLAST: Search nucleotide databases using a nucleotide query*. https://blast.ncbi.nlm.nih.gov/Blast.cgi?PROGRAM=blastn&PAGE_TYPE=BlastSearch&LINK_LOC=blasthome. Accessed 28 December 2022.
- [252] Obenaus, J. C., Cantley, L. C., and Yaffe, M. B. 2003. Scansite 2.0: Proteome-wide prediction of cell signaling interactions using short sequence motifs. *Nucleic acids research* 31, 13, 3635–3641.
- [253] Oddo, S., Caccamo, A., Kitazawa, M., Tseng, B. P., and LaFerla, F. M. 2003. Amyloid deposition precedes tangle formation in a triple transgenic model of Alzheimer's disease. *Neurobiology of Aging* 24, 8, 1063–1070.
- [254] Oka, M., Fujisaki, N., Maruko-Otake, A., Ohtake, Y., Shimizu, S., Saito, T., Hisanaga, S.-I., Iijima, K. M., and Ando, K. 2017. Ca²⁺/calmodulin-dependent protein kinase II promotes neurodegeneration caused by tau phosphorylated at Ser262/356 in a transgenic Drosophila model of tauopathy. *Journal of biochemistry* 162, 5, 335–342.
- [255] Okano, M., Yokoyama, T., Miyanaga, T., and Ohtsuki, K. 2004. Activation of C-kinase eta through its cholesterol-3-sulfate-dependent phosphorylation by casein kinase I in vitro. *Biological & pharmaceutical bulletin* 27, 1, 109–112.

- [256] Okochi, M., Walter, J., Koyama, A., Nakajo, S., Baba, M., Iwatsubo, T., Meijer, L., Kahle, P. J., and Haass, C. 2000. Constitutive phosphorylation of the Parkinson's disease associated alpha-synuclein. *The Journal of biological chemistry* 275, 1, 390–397.
- [257] Oliveira, J., Costa, M., Almeida, M. S. C. de, Da Cruz e Silva, O. A. B., and Henriques, A. G. 2017. Protein Phosphorylation is a Key Mechanism in Alzheimer's Disease. *Journal of Alzheimer's disease : JAD* 58, 4, 953–978.
- [258] Oumata, N., Bettayeb, K., Ferandin, Y., Demange, L., Lopez-Giral, A., Goddard, M.-L., Myrianthopoulos, V., Mikros, E., Flajolet, M., Greengard, P., Meijer, L., and Galons, H. 2008. Roscovitine-derived, dual-specificity inhibitors of cyclin-dependent kinases and casein kinases 1. *Journal of medicinal chemistry* 51, 17, 5229–5242.
- [259] Pan, D. 2007. Hippo signaling in organ size control. *Genes & development* 21, 8, 886–897.
- [260] Pan, D. 2010. The hippo signaling pathway in development and cancer. *Developmental cell* 19, 4, 491–505.
- [261] Papoff, G., Trivieri, N., Crielesi, R., Ruberti, F., Marsilio, S., and Ruberti, G. 2010. FADD-calmodulin interaction: a novel player in cell cycle regulation. *Biochimica et biophysica acta* 1803, 8, 898–911.
- [262] Peifer, C., Abadleh, M., Bischof, J., Hauser, D., Schattel, V., Hirner, H., Knippschild, U., and Laufer, S. 2009. 3,4-Diaryl-isoxazoles and -imidazoles as potent dual inhibitors of p38alpha mitogen activated protein kinase and casein kinase 1delta. *Journal of medicinal chemistry* 52, 23, 7618–7630.
- [263] Penas, C., Govek, E.-E., Fang, Y., Ramachandran, V., Daniel, M., Wang, W., Maloof, M. E., Rahaim, R. J., Bibian, M., Kawachi, D., Finkelstein, D., Han, J.-L., Long, J., Li, B., Robbins, D. J., Malumbres, M., Roussel, M. F., Roush, W. R., Hatten, M. E., and Ayad, N. G. 2015. Casein kinase 1δ is an APC/C(Cdh1) substrate that regulates cerebellar granule cell neurogenesis. *Cell reports* 11, 2, 249–260.
- [264] Penas, C., Ramachandran, V., Simanski, S., Lee, C., Madoux, F., Rahaim, R. J., Chauhan, R., Barnaby, O., Schurer, S., Hodder, P., Steen, J., Roush, W. R., and Ayad, N. G. 2014. Casein kinase 1δ-dependent Wee1 protein degradation. *The Journal of biological chemistry* 289, 27, 18893–18903.
- [265] Perez, D. I., Gil, C., and Martinez, A. 2011. Protein kinases CK1 and CK2 as new targets for neurodegenerative diseases. *Medicinal research reviews* 31, 6, 924–954.
- [266] Pernot, M., Vanderesse, R., Frochot, C., Guillemin, F., and Barberi-Heyob, M. 2011. Stability of peptides and therapeutic success in cancer. *Expert opinion on drug metabolism & toxicology* 7, 7, 793–802.
- [267] Perreau-Lenz, S., Vengeliene, V., Noori, H. R., Merlo-Pich, E. V., Corsi, M. A., Corti, C., and Spanagel, R. 2012. Inhibition of the casein-kinase-1-ε/δ/ prevents relapse-like alcohol drinking. *Neuropsychopharmacology : official publication of the American College of Neuropsychopharmacology* 37, 9, 2121–2131.
- [268] Petta, I., Lievens, S., Libert, C., Tavernier, J., and Bosscher, K. de. 2016. Modulation of Protein-Protein Interactions for the Development of Novel Therapeutics. *Molecular therapy : the journal of the American Society of Gene Therapy* 24, 4, 707–718.
- [269] Phadnis, N., Cipak, L., Polakova, S., Hyppa, R. W., Cipakova, I., Anrather, D., Karvaiova, L., Mechtler, K., Smith, G. R., and Gregan, J. 2015. Casein Kinase 1 and Phosphorylation of Cohesin Subunit Rec11 (SA3) Promote Meiotic Recombination through Linear Element Formation. *PLoS genetics* 11, 5, e1005225.
- [270] Price, M. A. 2006. CKI, there's more than one: casein kinase I family members in Wnt and Hedgehog signaling. *Genes & development* 20, 4, 399–410.
- [271] Randrup Hansen, C., Grimm, D., Bauer, J., Wehland, M., and Magnusson, N. E. 2017. Effects and Side Effects of Using Sorafenib and Sunitinib in the Treatment of Metastatic Renal Cell Carcinoma. *International journal of molecular sciences* 18, 2.
- [272] Rappsilber, J., Mann, M., and Ishihama, Y. 2007. Protocol for micro-purification, enrichment, pre-fractionation and storage of peptides for proteomics using StageTips. *Nature protocols* 2, 8, 1896–1906.
- [273] Rapuano, M. and Rosen, O. M. 1991. Phosphorylation of the insulin receptor by a casein kinase I-like enzyme. *The Journal of biological chemistry* 266, 20, 12902–12907.

- [274] Rebelo, S., Vieira, S. I., Esselmann, H., Wiltfang, J., Da Cruz e Silva, E. F., and Da Cruz e Silva, O. A. B. 2007. Tyr687 dependent APP endocytosis and Abeta production. *Journal of molecular neuroscience : MN* 32, 1, 1–8.
- [275] Rebelo, S., Vieira, S. I., Esselmann, H., Wiltfang, J., Da Cruz e Silva, E. F., and Da Cruz e Silva, O. A. B. 2007. Tyrosine 687 phosphorylated Alzheimer's amyloid precursor protein is retained intracellularly and exhibits a decreased turnover rate. *Neuro-degenerative diseases* 4, 2-3, 78–87.
- [276] Refaat, H. M. 2010. Synthesis and anticancer activity of some novel 2-substituted benzimidazole derivatives. *European journal of medicinal chemistry* 45, 7, 2949–2956.
- [277] Regad, T., Roth, M., Bredenkamp, N., Illing, N., and Papalopulu, N. 2007. The neural progenitor-specifying activity of FoxG1 is antagonistically regulated by CKI and FGF. *Nature cell biology* 9, 5, 531–540.
- [278] Rena, G., Bain, J., Elliott, M., and Cohen, P. 2004. D4476, a cell-permeant inhibitor of CK1, suppresses the site-specific phosphorylation and nuclear exclusion of FOXO1a. *EMBO reports* 5, 1, 60–65.
- [279] Reuter, S., Jensen, B., Buttenschoen, K., Kratzer, W., and Kern, P. 2000. Benzimidazoles in the treatment of alveolar echinococcosis: a comparative study and review of the literature. *The Journal of antimicrobial chemotherapy* 46, 3, 451–456.
- [280] Richter, J., Bischof, J., Zaja, M., Kohlhof, H., Othersen, O., Vitt, D., Alscher, V., Pospiech, I., García-Reyes, B., Berg, S., Leban, J., and Knippschild, U. 2014. Difluoro-dioxolo-benzimidazol-benzamides as potent inhibitors of CK1 δ and ϵ with nanomolar inhibitory activity on cancer cell proliferation. *Journal of medicinal chemistry* 57, 19, 7933–7946.
- [281] Ring, D. B., Johnson, K. W., Henriksen, E. J., Nuss, J. M., Goff, D., Kinnick, T. R., Ma, S. T., Reeder, J. W., Samuels, I., Slabiak, T., Wagman, A. S., Hammond, M.-E. W., and Harrison, S. D. 2003. Selective glycogen synthase kinase 3 inhibitors potentiate insulin activation of glucose transport and utilization in vitro and in vivo. *Diabetes* 52, 3, 588–595.
- [282] Rivers, A., Gietzen, K. F., Vielhaber, E., and Virshup, D. M. 1998. Regulation of casein kinase I epsilon and casein kinase I delta by an in vivo futile phosphorylation cycle. *The Journal of biological chemistry* 273, 26, 15980–15984.
- [283] Rocheleau, C. E., Downs, W. D., Lin, R., Wittmann, C., Bei, Y., Cha, Y. H., Ali, M., Priess, J. R., and Mello, C. C. 1997. Wnt signaling and an APC-related gene specify endoderm in early *C. elegans* embryos. *Cell* 90, 4, 707–716.
- [284] Roof, D. M., Meluh, P. B., and Rose, M. D. 1992. Kinesin-related proteins required for assembly of the mitotic spindle. *The Journal of cell biology* 118, 1, 95–108.
- [285] Roskoski, R. 2019. Small molecule inhibitors targeting the EGFR/ErbB family of protein-tyrosine kinases in human cancers. *Pharmacological research* 139, 395–411.
- [286] Roth, A., Gärtner, F., Mayer, K., Beyrle, J., König, I., Knippschild, U., and Bischof, J. 2021. CK1 δ -Derived Peptides as Novel Tools Inhibiting the Interactions between CK1 δ and APP695 to Modulate the Pathogenic Metabolism of APP. *International journal of molecular sciences* 22, 12.
- [287] Roth, A., Gihring, A., Bischof, J., Pan, L., Oswald, F., and Knippschild, U. 2022. CK1 Is a Druggable Regulator of Microtubule Dynamics and Microtubule-Associated Processes. *Cancers* 14, 5.
- [288] Roth, A., Gihring, A., Göser, F., Peifer, C., Knippschild, U., and Bischof, J. 2021. Assessing the Inhibitory Potential of Kinase Inhibitors In Vitro: Major Pitfalls and Suggestions for Improving Comparability of Data Using CK1 Inhibitors as an Example. *Molecules (Basel, Switzerland)* 26, 16.
- [289] Roth, A., Sander, A., Oswald, M. S., Gärtner, F., Knippschild, U., and Bischof, J. 2022. Comprehensive Characterization of CK1 δ -Mediated Tau Phosphorylation in Alzheimer's Disease. *Frontiers in molecular biosciences* 9, 872171.
- [290] Rousselle, C., Clair, P., Smirnova, M., Kolesnikov, Y., Pasternak, G. W., Gac-Breton, S., Rees, A. R., Scherrmann, J.-M., and Temsamani, J. 2003. Improved brain uptake and pharmacological activity of dalargin using a peptide-vector-mediated strategy. *The Journal of pharmacology and experimental therapeutics* 306, 1, 371–376.
- [291] Rousselle, C., Smirnova, M., Clair, P., Lefauconnier, J. M., Chavanieu, A., Calas, B., Scherrmann, J. M., and Temsamani, J. 2001. Enhanced delivery of doxorubicin into the brain

- via a peptide-vector-mediated strategy: saturation kinetics and specificity. *The Journal of pharmacology and experimental therapeutics* 296, 1, 124–131.
- [292] Rubin, L. L. and Sauvage, F. J. de. 2006. Targeting the Hedgehog pathway in cancer. *Nature reviews. Drug discovery* 5, 12, 1026–1033.
- [293] Rudrabhatla, P., Jaffe, H., and Pant, H. C. 2011. Direct evidence of phosphorylated neuronal intermediate filament proteins in neurofibrillary tangles (NFTs): phosphoproteomics of Alzheimer's NFTs. *FASEB journal : official publication of the Federation of American Societies for Experimental Biology* 25, 11, 3896–3905.
- [294] Sakuno, T. and Watanabe, Y. 2015. Phosphorylation of cohesin Rec11/SA3 by casein kinase 1 promotes homologous recombination by assembling the meiotic chromosome axis. *Developmental cell* 32, 2, 220–230.
- [295] Salado, I. G., Redondo, M., Bello, M. L., Perez, C., Liachko, N. F., Kraemer, B. C., Miguel, L., Lecourtois, M., Gil, C., Martinez, A., and Perez, D. I. 2014. Protein kinase CK-1 inhibitors as new potential drugs for amyotrophic lateral sclerosis. *Journal of medicinal chemistry* 57, 6, 2755–2772.
- [296] Salatin, S. and Yari Khosroushahi, A. 2017. Overviews on the cellular uptake mechanism of polysaccharide colloidal nanoparticles. *Journal of cellular and molecular medicine* 21, 9, 1668–1686.
- [297] Santos, J. A., Logarinho, E., Tapia, C., Allende, C. C., Allende, J. E., and Sunkel, C. E. 1996. The casein kinase 1 alpha gene of *Drosophila melanogaster* is developmentally regulated and the kinase activity of the protein induced by DNA damage. *Journal of cell science* 109 (Pt 7), 1847–1856.
- [298] Sato, S., Cerny, R. L., Buescher, J. L., and Ikezu, T. 2006. Tau-tubulin kinase 1 (TTBK1), a neuron-specific tau kinase candidate, is involved in tau phosphorylation and aggregation. *Journal of neurochemistry* 98, 5, 1573–1584.
- [299] Schitteck, B. and Sinnberg, T. 2014. Biological functions of casein kinase 1 isoforms and putative roles in tumorigenesis. *Molecular cancer* 13, 231.
- [300] Schmitt, M., Sinnberg, T., Nalpas, N. C., Maass, A., Schitteck, B., and Macek, B. 2019. Quantitative Proteomics Links the Intermediate Filament Nestin to Resistance to Targeted BRAF Inhibition in Melanoma Cells. *Molecular & cellular proteomics : MCP* 18, 6, 1096–1109.
- [301] Schneider, C. C., Kartarius, S., Montenarh, M., Orzeszko, A., and Kazimierzczuk, Z. 2012. Modified tetrahalogenated benzimidazoles with CK2 inhibitory activity are active against human prostate cancer cells LNCaP in vitro. *Bioorganic & medicinal chemistry* 20, 14, 4390–4396.
- [302] Schwab, C., DeMaggio, A. J., Ghoshal, N., Binder, L. I., Kuret, J., and McGeer, P. L. 2000. Casein kinase 1 delta is associated with pathological accumulation of tau in several neurodegenerative diseases. *Neurobiology of Aging* 21, 4, 503–510.
- [303] 2022. Search of: BTX-A51 - List Results - ClinicalTrials.gov. <https://clinicaltrials.gov/ct2/results?cond=&term=BTX-A51&cntry=&state=&city=&dist=>. Accessed 23 December 2022.
- [304] Selkoe, D. J. 1986. Altered structural proteins in plaques and tangles: what do they tell us about the biology of Alzheimer's disease? *Neurobiology of Aging* 7, 6, 425–432.
- [305] Servier Medical Art. 2022. SMART - Servier Medical ART. <https://smart.servier.com/>. Accessed 23 December 2022.
- [306] Sharma, P., Sharma, M., Amin, N. D., Albers, R. W., and Pant, H. C. 1999. Regulation of cyclin-dependent kinase 5 catalytic activity by phosphorylation. *Proceedings of the National Academy of Sciences of the United States of America* 96, 20, 11156–11160.
- [307] Shelton, S. B. and Johnson, G. V. W. 2004. Cyclin-dependent kinase-5 in neurodegeneration. *Journal of neurochemistry* 88, 6, 1313–1326.
- [308] Shin, S., Wolgamott, L., Roux, P. P., and Yoon, S.-O. 2014. Casein kinase 1 ϵ promotes cell proliferation by regulating mRNA translation. *Cancer research* 74, 1, 201–211.
- [309] Sillibourne, J. E., Milne, D. M., Takahashi, M., Ono, Y., and Meek, D. W. 2002. Centrosomal anchoring of the protein kinase CK1delta mediated by attachment to the large, coiled-coil scaffolding protein CG-NAP/AKAP450. *Journal of molecular biology* 322, 4, 785–797.

- [310] Silva, M. V. F., Loures, C. d. M. G., Alves, L. C. V., Souza, L. C. de, Borges, K. B. G., and Carvalho, M. d. G. 2019. Alzheimer's disease: risk factors and potentially protective measures. *Journal of biomedical science* 26, 1, 33.
- [311] Šimić, G., Babić Leko, M., Wray, S., Harrington, C., Delalle, I., Jovanov-Milošević, N., Bažadona, D., Buée, L., Silva, R. de, Di Giovanni, G., Wischik, C., and Hof, P. R. 2016. Tau Protein Hyperphosphorylation and Aggregation in Alzheimer's Disease and Other Tauopathies, and Possible Neuroprotective Strategies. *Biomolecules* 6, 1, 6.
- [312] Singh, T. J., Grundke-Iqbal, I., and Iqbal, K. 1995. Phosphorylation of tau protein by casein kinase-1 converts it to an abnormal Alzheimer-like state. *Journal of neurochemistry* 64, 3, 1420–1423.
- [313] Small, S. A. and Duff, K. 2008. Linking Abeta and tau in late-onset Alzheimer's disease: a dual pathway hypothesis. *Neuron* 60, 4, 534–542.
- [314] Smirlis, D., Dingli, F., Sabatet, V., Roth, A., Knippschild, U., Loew, D., Späth, G. F., and Rachidi, N. 2021. Identification of the Host Substratome of Leishmania-Secreted Casein Kinase 1 Using a SILAC-Based Quantitative Mass Spectrometry Assay. *Frontiers in cell and developmental biology* 9, 800098.
- [315] Smith, S. M. 2017. Strategies for the Purification of Membrane Proteins. *Methods in molecular biology (Clifton, N.J.)* 1485, 389–400.
- [316] Solari, F. A., Dell'Aica, M., Sickmann, A., and Zahedi, R. P. 2015. Why phosphoproteomics is still a challenge. *Mol. BioSyst.* 11, 6, 1487–1493.
- [317] Spittaels, K., van den Haute, C., van Dorpe, J., Geerts, H., Mercken, M., Bruynseels, K., Lasrado, R., Vandezande, K., Laenen, I., Boon, T., van Lint, J., Vandenheede, J., Moechars, D., Loos, R., and van Leuven, F. 2000. Glycogen synthase kinase-3beta phosphorylates protein tau and rescues the axonopathy in the central nervous system of human four-repeat tau transgenic mice. *The Journal of biological chemistry* 275, 52, 41340–41349.
- [318] Stachel, S. J., Coburn, C. A., Steele, T. G., Jones, K. G., Loutzenhiser, E. F., Gregro, A. R., Rajapakse, H. A., Lai, M.-T., Crouthamel, M.-C., Xu, M., Tugusheva, K., Lineberger, J. E., Pietrak, B. L., Espeseth, A. S., Shi, X.-P., Chen-Dodson, E., Holloway, M. K., Munshi, S., Simon, A. J., Kuo, L., and Vacca, J. P. 2004. Structure-based design of potent and selective cell-permeable inhibitors of human beta-secretase (BACE-1). *Journal of medicinal chemistry* 47, 26, 6447–6450.
- [319] Stamos, J. L. and Weis, W. I. 2013. The β -catenin destruction complex. *Cold Spring Harbor perspectives in biology* 5, 1, a007898.
- [320] Stelzl, U., Worm, U., Lalowski, M., Haenig, C., Brembeck, F. H., Goehler, H., Stroedicke, M., Zenkner, M., Schoenherr, A., Koeppen, S., Timm, J., Mintzlaff, S., Abraham, C., Bock, N., Kietzmann, S., Goedde, A., Toksöz, E., Droege, A., Krobitsch, S., Korn, B., Birchmeier, W., Lehrach, H., and Wanker, E. E. 2005. A human protein-protein interaction network: a resource for annotating the proteome. *Cell* 122, 6, 957–968.
- [321] Stöhr, J., Wu, H., Nick, M., Wu, Y., Bhate, M., Condello, C., Johnson, N., Rodgers, J., Lemmin, T., Acharya, S., Becker, J., Robinson, K., Kelly, M. J. S., Gai, F., Stubbs, G., Prusiner, S. B., and DeGrado, W. F. 2017. A 31-residue peptide induces aggregation of tau's microtubule-binding region in cells. *Nature chemistry* 9, 9, 874–881.
- [322] Stöter, M., Bamberger, A.-M., Aslan, B., Kurth, M., Speidel, D., Löning, T., Frank, H.-G., Kaufmann, P., Löhler, J., Henne-Bruns, D., Deppert, W., and Knippschild, U. 2005. Inhibition of casein kinase I delta alters mitotic spindle formation and induces apoptosis in trophoblast cells. *Oncogene* 24, 54, 7964–7975.
- [323] 2022. *Subcloning Efficiency™ DH5a kompetente Zellen*. <https://www.thermofisher.com/order/catalog/product/18265017>. Accessed 1 September 2022.
- [324] Sugiyama, Y., Hatano, N., Sueyoshi, N., Suetake, I., Tajima, S., Kinoshita, E., Kinoshita-Kikuta, E., Koike, T., and Kameshita, I. 2010. The DNA-binding activity of mouse DNA methyltransferase 1 is regulated by phosphorylation with casein kinase 1delta/epsilon. *The Biochemical journal* 427, 3, 489–497.
- [325] Sundaram, S., Nagaraj, S., Mahoney, H., Portugues, A., Li, W., Millsaps, K., Faulkner, J., Yunus, A., Burns, C., Bloom, C., Said, M., Pinto, L., Azam, S., Flores, M., Henriksen, A., Gamsby, J., and Gulick, D. 2019. Inhibition of casein kinase 1 δ /epsilon improves cognitive-affective

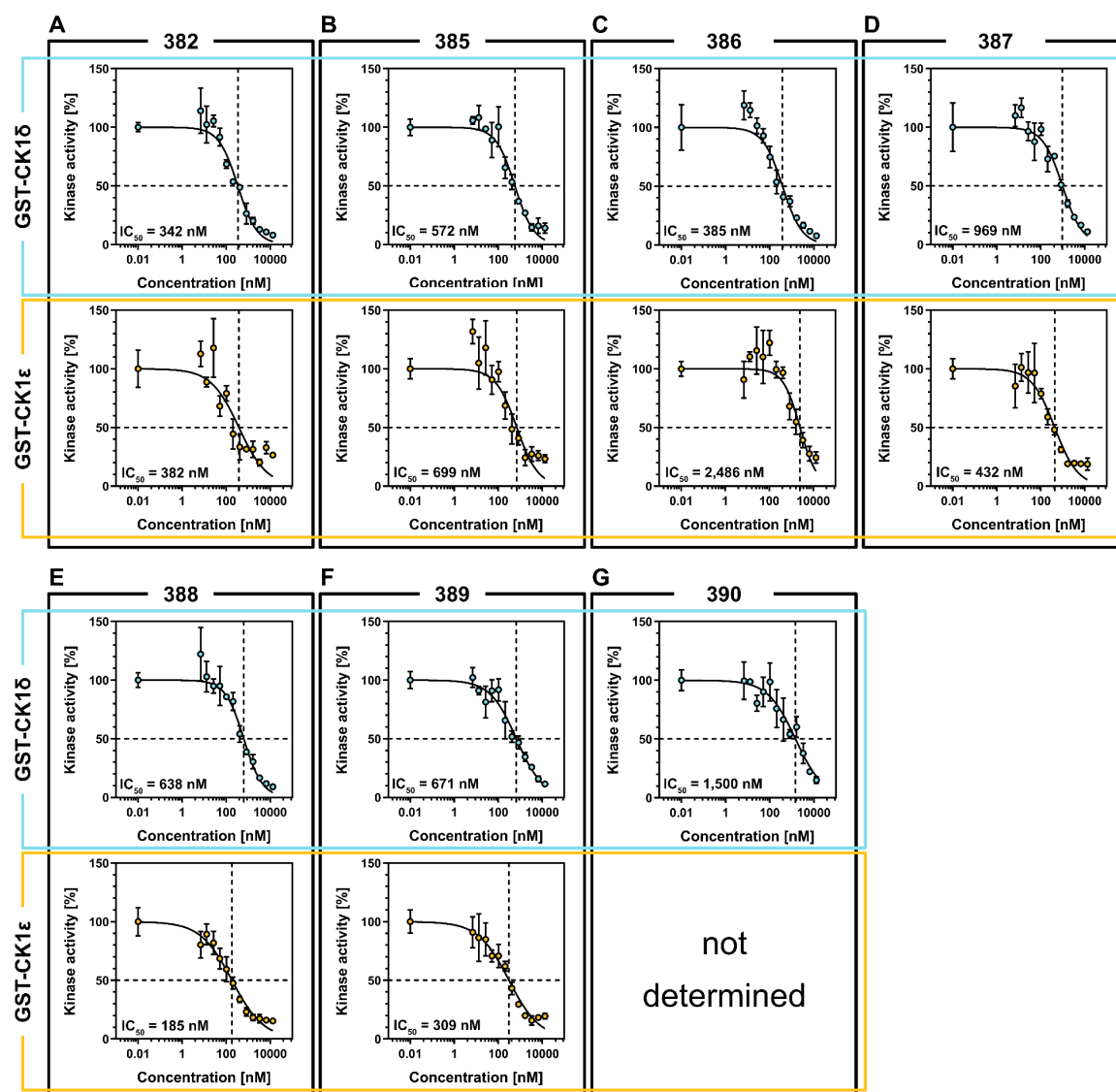
- behavior and reduces amyloid load in the APP-PS1 mouse model of Alzheimer's disease. *Scientific reports* 9, 1, 13743.
- [326] Suutari, T., Silen, T., S En Karaman, D., Saari, H., Desai, D., Kerkelä, E., Laitinen, S., Hanzlikova, M., Rosenholm, J. M., Yliperttula, M., and Viitala, T. 2016. Real-Time Label-Free Monitoring of Nanoparticle Cell Uptake. *Small (Weinheim an der Bergstrasse, Germany)* 12, 45, 6289–6300.
- [327] Suzuki, T., Oishi, M., Marshak, D. R., Czernik, A. J., Nairn, A. C., and Greengard, P. 1994. Cell cycle-dependent regulation of the phosphorylation and metabolism of the Alzheimer amyloid precursor protein. *The EMBO journal* 13, 5, 1114–1122.
- [328] Takashima, A., Honda, T., Yasutake, K., Michel, G., Murayama, O., Murayama, M., Ishiguro, K., and Yamaguchi, H. 1998. Activation of tau protein kinase I/glycogen synthase kinase-3beta by amyloid beta peptide (25-35) enhances phosphorylation of tau in hippocampal neurons. *Neuroscience research* 31, 4, 317–323.
- [329] Tamm, I., Bablanian, R., Nemes, M. M., Shunk, C. H., Robinson, F. M., and Folkers, K. 1961. Relationship between structure of benzimidazole derivatives and selective virus inhibitory activity. Inhibition of poliovirus multiplication and cytopathic effects by 2-(alpha-hydroxybenzyl)-benzimidazole, and its 5-chloroderivative. *The Journal of experimental medicine* 113, 4, 625–656.
- [330] Tamm, I., Folkers, K., Shunk, C. H., and Horsfall, F. L. 1954. Inhibition of influenza virus multiplication by N-glycosides of benzimidazoles-N. *The Journal of experimental medicine* 99, 3, 227–250.
- [331] Taylor, L. M., McMillan, P. J., Liachko, N. F., Strovas, T. J., Ghetti, B., Bird, T. D., Keene, C. D., and Kraemer, B. C. 2018. Pathological phosphorylation of tau and TDP-43 by TTBK1 and TTBK2 drives neurodegeneration. *Molecular neurodegeneration* 13, 1, 7.
- [332] Teo, J.-L. and Kahn, M. 2010. The Wnt signaling pathway in cellular proliferation and differentiation: A tale of two coactivators. *Advanced drug delivery reviews* 62, 12, 1149–1155.
- [333] Thornton, C., Bright, N. J., Sastre, M., Muckett, P. J., and Carling, D. 2011. AMP-activated protein kinase (AMPK) is a tau kinase, activated in response to amyloid β -peptide exposure. *The Biochemical journal* 434, 3, 503–512.
- [334] Toh, K. L., Jones, C. R., He, Y., Eide, E. J., Hinz, W. A., Virshup, D. M., Ptáček, L. J., and Fu, Y. H. 2001. An hPer2 phosphorylation site mutation in familial advanced sleep phase syndrome. *Science (New York, N.Y.)* 291, 5506, 1040–1043.
- [335] Traub, B., Roth, A., Kornmann, M., Knippschild, U., and Bischof, J. 2021. Stress-activated kinases as therapeutic targets in pancreatic cancer. *World journal of gastroenterology* 27, 30, 4963–4984.
- [336] Tuazon, P. T. and Traugh, J. A. 1991. Casein kinase I and II--multipotential serine protein kinases: structure, function, and regulation. *Advances in second messenger and phosphoprotein research* 23, 123–164.
- [337] 2021. UniProt: the universal protein knowledgebase in 2021. *Nucleic acids research* 49, D1, D480-D489.
- [338] Utz, A. C., Hirner, H., Blatz, A., Hillenbrand, A., Schmidt, B., Deppert, W., Henne-Bruns, D., Fischer, D., Thal, D. R., Leithäuser, F., and Knippschild, U. 2010. Analysis of cell type-specific expression of CK1 epsilon in various tissues of young adult BALB/c Mice and in mammary tumors of SV40 T-Ag-transgenic mice. *The journal of histochemistry and cytochemistry : official journal of the Histochemistry Society* 58, 1, 1–15.
- [339] Vandermarliere, E., Mueller, M., and Martens, L. 2013. Getting intimate with trypsin, the leading protease in proteomics. *Mass spectrometry reviews* 32, 6, 453–465.
- [340] Varela, L. and Garcia-Rendueles, M. E. R. 2022. Oncogenic Pathways in Neurodegenerative Diseases. *International journal of molecular sciences* 23, 6.
- [341] Vassar, R., Bennett, B. D., Babu-Khan, S., Kahn, S., Mendiaz, E. A., Denis, P., Teplow, D. B., Ross, S., Amarante, P., Loeloff, R., Luo, Y., Fisher, S., Fuller, J., Edenson, S., Lile, J., Jarosinski, M. A., Biere, A. L., Curran, E., Burgess, T., Louis, J. C., Collins, F., Treanor, J., Rogers, G., and Citron, M. 1999. Beta-secretase cleavage of Alzheimer's amyloid precursor protein by the transmembrane aspartic protease BACE. *Science (New York, N.Y.)* 286, 5440, 735–741.

- [342] Venkatesan, K., Rual, J.-F., Vazquez, A., Stelzl, U., Lemmens, I., Hirozane-Kishikawa, T., Hao, T., Zenkner, M., Xin, X., Goh, K.-I., Yildirim, M. A., Simonis, N., Heinzmann, K., Gebreab, F., Sahalie, J. M., Cevik, S., Simon, C., Smet, A.-S. de, Dann, E., Smolyar, A., Vinayagam, A., Yu, H., Szeto, D., Borick, H., Dricot, A., Klitgord, N., Murray, R. R., Lin, C., Lalowski, M., Timm, J., Rau, K., Boone, C., Braun, P., Cusick, M. E., Roth, F. P., Hill, D. E., Tavernier, J., Wanker, E. E., Barabási, A.-L., and Vidal, M. 2009. An empirical framework for binary interactome mapping. *Nature methods* 6, 1, 83–90.
- [343] Veronese, F. M. and Mero, A. 2008. The impact of PEGylation on biological therapies. *BioDrugs : clinical immunotherapeutics, biopharmaceuticals and gene therapy* 22, 5, 315–329.
- [344] Vieira, S. I., Rebelo, S., Esselmann, H., Wiltfang, J., Lah, J., Lane, R., Small, S. A., Gandy, S., Da Cruz e Silva, E. F., and Da Cruz E Silva, O. A. 2010. Retrieval of the Alzheimer's amyloid precursor protein from the endosome to the TGN is S655 phosphorylation state-dependent and retromer-mediated. *Molecular neurodegeneration* 5, 40.
- [345] Vuong, H. G., Ho, A. T. N., Tran, T. T. K., Capdevila, J., Benekli, M., Nakazawa, T., Katoh, R., and Kondo, T. 2019. Efficacy and toxicity of sorafenib in the treatment of advanced medullary thyroid carcinoma: A systematic review and meta-analysis. *Head & neck* 41, 8, 2823–2829.
- [346] Waddell, D. S., Liberati, N. T., Guo, X., Frederick, J. P., and Wang, X.-F. 2004. Casein kinase Iepsilon plays a functional role in the transforming growth factor-beta signaling pathway. *The Journal of biological chemistry* 279, 28, 29236–29246.
- [347] Wager, T. T., Chandrasekaran, R. Y., Bradley, J., Rubitski, D., Berke, H., Mente, S., Butler, T., Doran, A., Chang, C., Fisher, K., Knafels, J., Liu, S., Ohren, J., Marconi, M., DeMarco, G., Sneed, B., Walton, K., Horton, D., Rosado, A., and Mead, A. 2014. Casein kinase 1δ/ε inhibitor PF-5006739 attenuates opioid drug-seeking behavior. *ACS chemical neuroscience* 5, 12, 1253–1265.
- [348] Walker, J. R., Hall, M. P., Zimprich, C. A., Robers, M. B., Duellman, S. J., Machleidt, T., Rodriguez, J., and Zhou, W. 2017. Highly Potent Cell-Permeable and Impermeable NanoLuc Luciferase Inhibitors. *ACS chemical biology* 12, 4, 1028–1037.
- [349] Walter, J., Capell, A., Hung, A. Y., Langen, H., Schnölzer, M., Thinakaran, G., Sisodia, S. S., Selkoe, D. J., and Haass, C. 1997. Ectodomain phosphorylation of beta-amyloid precursor protein at two distinct cellular locations. *The Journal of biological chemistry* 272, 3, 1896–1903.
- [350] Walter, J., Fluhrer, R., Hartung, B., Willem, M., Kaether, C., Capell, A., Lammich, S., Multhaup, G., and Haass, C. 2001. Phosphorylation regulates intracellular trafficking of beta-secretase. *The Journal of biological chemistry* 276, 18, 14634–14641.
- [351] Walter, J., Grünberg, J., Schindzielorz, A., and Haass, C. 1998. Proteolytic fragments of the Alzheimer's disease associated presenilins-1 and -2 are phosphorylated in vivo by distinct cellular mechanisms. *Biochemistry* 37, 17, 5961–5967.
- [352] Walter, J., Schindzielorz, A., Hartung, B., and Haass, C. 2000. Phosphorylation of the beta-amyloid precursor protein at the cell surface by ectocasein kinases 1 and 2. *The Journal of biological chemistry* 275, 31, 23523–23529.
- [353] Walton, K. M., Fisher, K., Rubitski, D., Marconi, M., Meng, Q.-J., Sládek, M., Adams, J., Bass, M., Chandrasekaran, R., Butler, T., Griffor, M., Rajamohan, F., Serpa, M., Chen, Y., Claffey, M., Hastings, M., Loudon, A., Maywood, E., Ohren, J., Doran, A., and Wager, T. T. 2009. Selective inhibition of casein kinase 1 epsilon minimally alters circadian clock period. *The Journal of pharmacology and experimental therapeutics* 330, 2, 430–439.
- [354] Wang, L., Lu, A., Zhou, H.-X., Sun, R., Zhao, J., Zhou, C.-J., Shen, J.-P., Wu, S.-N., and Liang, C.-G. 2013. Casein kinase 1 alpha regulates chromosome congression and separation during mouse oocyte meiotic maturation and early embryo development. *PLoS one* 8, 5, e63173.
- [355] Wang, L., Wang, N., Zhang, W., Cheng, X., Yan, Z., Shao, G., Wang, X., Wang, R., and Fu, C. 2022. Therapeutic peptides: current applications and future directions. *Signal transduction and targeted therapy* 7, 1, 48.
- [356] Wang, S., Yin, J., Chen, D., Nie, F., Song, X., Fei, C., Miao, H., Jing, C., Ma, W., Wang, L., Xie, S., Li, C., Zeng, R., Pan, W., Hao, X., and Li, L. 2013. Small-molecule modulation of Wnt signaling via modulating the Axin-LRP5/6 interaction. *Nature chemical biology* 9, 9, 579–585.
- [357] Wang, X., Friesen, E., Müller, I., Lemieux, M., Dukart, R., Maia, I. B., Kalia, S., and Schmitt-Ulms, G. 2020. Rapid Generation of Human Neuronal Cell Models Enabling Inducible Expression of Proteins-of-interest for Functional Studies. *Bio-protocol* 10, 9, e3615.

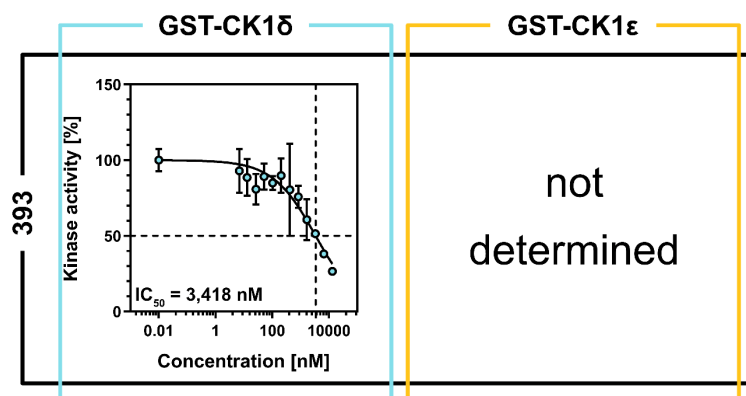
- [358] Wang, Z., Zhou, L., Wang, Y., Peng, Q., Li, H., Zhang, X., Su, Z., Song, J., Sun, Q., Sayed, S., Liu, S., and Lu, D. 2021. The CK1 δ/ϵ -AES axis regulates tumorigenesis and metastasis in colorectal cancer. *Theranostics* 11, 9, 4421–4435.
- [359] Weggen, S. and Beher, D. 2012. Molecular consequences of amyloid precursor protein and presenilin mutations causing autosomal-dominant Alzheimer's disease. *Alzheimer's research & therapy* 4, 2, 9.
- [360] Wei, X., Zhan, C., Chen, X., Hou, J., Xie, C., and Lu, W. 2014. Retro-inverso isomer of Angiopep-2: a stable d-peptide ligand inspires brain-targeted drug delivery. *Molecular pharmaceutics* 11, 10, 3261–3268.
- [361] Werner, H. M., Cabaltea, C. C., and Horne, W. S. 2016. Peptide Backbone Composition and Protease Susceptibility: Impact of Modification Type, Position, and Tandem Substitution. *Chembiochem : a European journal of chemical biology* 17, 8, 712–718.
- [362] Wesseler, F., Lohmann, S., Riege, D., Halver, J., Roth, A., Pichlo, C., Weber, S., Takamiya, M., Müller, E., Ketzler, J., Flegel, J., Gihring, A., Rastegar, S., Bertrand, J., Baumann, U., Knippschild, U., Peifer, C., Sievers, S., Waldmann, H., and Schade, D. 2022. Phenotypic Discovery of Triazolo1,5-cquinazolines as a First-In-Class Bone Morphogenetic Protein Amplifier Chemotype. *Journal of medicinal chemistry*.
- [363] West, H. L., Rebeck, G. W., and Hyman, B. T. 1994. Frequency of the apolipoprotein E epsilon 2 allele is diminished in sporadic Alzheimer disease. *Neuroscience letters* 175, 1-2, 46–48.
- [364] Wisniewski, H. M., Iqbal, K., Grundke-Iqbal, I., and Rubenstein, R. 1987. The solubility controversy of paired helical filaments: a commentary. *Neurochemical research* 12, 1, 93–95.
- [365] Wójcik, P. and Berlicki, Ł. 2016. Peptide-based inhibitors of protein-protein interactions. *Bioorganic & medicinal chemistry letters* 26, 3, 707–713.
- [366] Wolff, S., Xiao, Z., Wittau, M., Süßner, N., Stöter, M., and Knippschild, U. 2005. Interaction of casein kinase 1 delta (CK1 delta) with the light chain LC2 of microtubule associated protein 1A (MAP1A). *Biochimica et biophysica acta* 1745, 2, 196–206.
- [367] Wolozin, B. L., Pruchnicki, A., Dickson, D. W., and Davies, P. 1986. A neuronal antigen in the brains of Alzheimer patients. *Science (New York, N. Y.)* 232, 4750, 648–650.
- [368] Xu, J., Sato, S., Okuyama, S., Swan, R. J., Jacobsen, M. T., Strunk, E., and Ikezu, T. 2010. Tau-tubulin kinase 1 enhances prefibrillar tau aggregation and motor neuron degeneration in P301L FTDP-17 tau-mutant mice. *FASEB journal : official publication of the Federation of American Societies for Experimental Biology* 24, 8, 2904–2915.
- [369] Xu, P., Ianes, C., Gärtner, F., Liu, C., Burster, T., Bakulev, V., Rachidi, N., Knippschild, U., and Bischof, J. 2019. Structure, regulation, and (patho-)physiological functions of the stress-induced protein kinase CK1 delta (CSNK1D). *Gene* 715, 144005.
- [370] Xu, R. M., Carmel, G., Kuret, J., and Cheng, X. 1996. Structural basis for selectivity of the isoquinoline sulfonamide family of protein kinase inhibitors. *Proceedings of the National Academy of Sciences of the United States of America* 93, 13, 6308–6313.
- [371] Xu, R. M., Carmel, G., Sweet, R. M., Kuret, J., and Cheng, X. 1995. Crystal structure of casein kinase-1, a phosphate-directed protein kinase. *The EMBO journal* 14, 5, 1015–1023.
- [372] Xu, Y., Lee, S.-H., Kim, H. S., Kim, N. H., Piao, S., Park, S.-H., Jung, Y. S., Yook, J. I., Park, B.-J., and Ha, N.-C. 2010. Role of CK1 in GSK3beta-mediated phosphorylation and degradation of snail. *Oncogene* 29, 21, 3124–3133.
- [373] Yadav, S., Sinha, D., Singh, S. K., and Singh, V. K. 2012. Novel benzimidazole analogs as inhibitors of EGFR tyrosine kinase. *Chemical biology & drug design* 80, 4, 625–630.
- [374] Yanagawa, S., Matsuda, Y., Lee, J.-S., Matsubayashi, H., Sese, S., Kadowaki, T., and Ishimoto, A. 2002. Casein kinase I phosphorylates the Armadillo protein and induces its degradation in *Drosophila*. *The EMBO journal* 21, 7, 1733–1742.
- [375] Yang, P. and Sale, W. S. 2000. Casein kinase I is anchored on axonemal doublet microtubules and regulates flagellar dynein phosphorylation and activity. *The Journal of biological chemistry* 275, 25, 18905–18912.
- [376] Yasojima, K., Kuret, J., DeMaggio, A. J., McGeer, E., and McGeer, P. L. 2000. Casein kinase 1 delta mRNA is upregulated in Alzheimer disease brain. *Brain research* 865, 1, 116–120.

- [377] Yin, H., Laguna, K. A., Li, G., and Kuret, J. 2006. Dysbindin structural homologue CK1BP is an isoform-selective binding partner of human casein kinase-1. *Biochemistry* 45, 16, 5297–5308.
- [378] Yost, C., Torres, M., Miller, J. R., Huang, E., Kimelman, D., and Moon, R. T. 1996. The axis-inducing activity, stability, and subcellular distribution of beta-catenin is regulated in *Xenopus* embryos by glycogen synthase kinase 3. *Genes & development* 10, 12, 1443–1454.
- [379] Yung-Chi, C. and Prusoff, W. H. 1973. Relationship between the inhibition constant (KI) and the concentration of inhibitor which causes 50 per cent inhibition (I50) of an enzymatic reaction. *Biochemical Pharmacology* 22, 23, 3099–3108.
- [380] Zemp, I., Wandrey, F., Rao, S., Ashiono, C., Wyler, E., Montellese, C., and Kutay, U. 2014. CK1 δ and CK1 ϵ are components of human 40S subunit precursors required for cytoplasmic 40S maturation. *Journal of cell science* 127, Pt 6, 1242–1253.
- [381] Zhang, R., Qin, X., Kong, F., Chen, P., and Pan, G. 2019. Improving cellular uptake of therapeutic entities through interaction with components of cell membrane. *Drug delivery* 26, 1, 328–342.
- [382] Zhang, X. and Song, W. 2013. The role of APP and BACE1 trafficking in APP processing and amyloid- β generation. *Alzheimer's research & therapy* 5, 5, 46.
- [383] Zhao, B., Li, L., Tumaneng, K., Wang, C.-Y., and Guan, K.-L. 2010. A coordinated phosphorylation by Lats and CK1 regulates YAP stability through SCF(beta-TRCP). *Genes & development* 24, 1, 72–85.
- [384] Zhao, B., Tumaneng, K., and Guan, K.-L. 2011. The Hippo pathway in organ size control, tissue regeneration and stem cell self-renewal. *Nature cell biology* 13, 8, 877–883.
- [385] Zheng-Fischhöfer, Q., Biernat, J., Mandelkow, E. M., Illenberger, S., Godemann, R., and Mandelkow, E. 1998. Sequential phosphorylation of Tau by glycogen synthase kinase-3beta and protein kinase A at Thr212 and Ser214 generates the Alzheimer-specific epitope of antibody AT100 and requires a paired-helical-filament-like conformation. *European journal of biochemistry* 252, 3, 542–552.
- [386] Zhu, J., Shibasaki, F., Price, R., Guillemot, J. C., Yano, T., Dötsch, V., Wagner, G., Ferrara, P., and McKeon, F. 1998. Intramolecular masking of nuclear import signal on NF-AT4 by casein kinase I and MEKK1. *Cell* 93, 5, 851–861.
- [387] Zurdo, J., Guizarro, J. I., and Dobson, C. M. 2001. Preparation and characterization of purified amyloid fibrils. *Journal of the American Chemical Society* 123, 33, 8141–8142.
- [388] Zyss, D., Ebrahimi, H., and Gergely, F. 2011. Casein kinase I delta controls centrosome positioning during T cell activation. *The Journal of cell biology* 195, 5, 781–797.

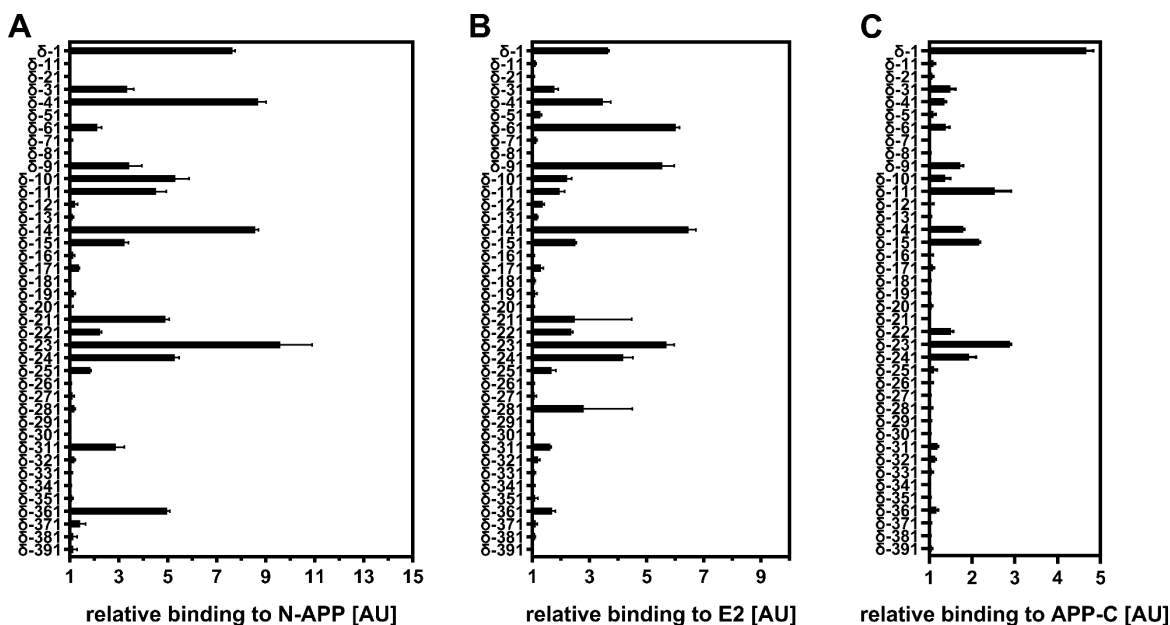
Supplement



Supplementary Figure 1: IC₅₀ determination of IWP-derived compounds. IC₅₀ determination was performed with GST-CK1 δ and GST-CK1 ϵ and IWP-derived compounds (A) 382, (B) 385, (C) 386, (D) 387, (E) 388, (F) 389 and (G) 390. Phosphate incorporation was quantified and normalized to DMSO as solvent control. Experiments were performed in triplicates. Results are shown as mean values and error bars represent the standard deviation. Data were fit to sigmoidal dose-response curve using GraphPad Prism 8.



Supplementary Figure 2: IC_{50} determination of isoxazole derivative 393. IC_{50} determination was performed with GST-CK1 δ and isoxazole derivative 393. Due to low inhibitory activity of 393 towards CK1 ϵ , IC_{50} value was not determined. Phosphate incorporation was quantified and normalized to DMSO as solvent control. Experiments were performed in triplicates. Results are shown as mean values and error bars represent the standard deviation. Data were fit to sigmoidal dose-response curve using GraphPad Prism 8.



Supplementary Figure 3: Initial streptavidin-linked interaction assay screening with APP695 fragments. Initial streptavidin-linked interaction assay indicates potential binding of CK1 δ -derived peptides to (A) N-APP, (B) E2 or (C) APP-C compared to control. Experiments were performed in triplicates. Results are shown as mean values and error bars represent the standard deviation. The figure was modified from [286], which is licensed under a Creative Commons Attribution 4.0 international license (CC BY 4.0), <https://creativecommons.org/licenses/by/4.0/>.

Acknowledgement

I would like to express my deepest appreciation to all the people that have encouraged, supported, and advised me during this unique journey as PhD candidate. I have been very fortunate to have many people who have helped and supported me directly or indirectly in performing experiments, preparing my PhD thesis and finally completing my work.

First, I am deeply indebted to Prof. Dr. Doris Henne-Bruns and Prof. Dr. Christoph Michalski for giving me the opportunity to prepare my PhD thesis in the Department of General and Visceral Surgery at the Ulm University Hospital.

Moreover, I am sincerely grateful for the wise and patient support of my first supervisor PD Dr. Joachim Bischof and the head of the working group Prof. Dr. Uwe Knippschild, both of whom made this project and work possible. I would like to thank you for your scientific guidance and advisory, which laid the foundation for my scientific understanding. In addition, I would like to acknowledge PD Dr. Joachim Bischof for his continuous support, even though his time was often very short.

This endeavor would not have been possible without Prof. Dr. Holger Barth and Prof. Dr. Gopal Sapkota, who kindly agreed to be my second and third supervisor. I appreciate that you always managed to take the time to read my progress reports, evaluate my intermediate examinations with your scientific expertise and suggest new experiments to improve my data. Your scientific advice has always been of great value to my project.

The identification of new CK1 δ -specific inhibitors would not have been possible without the support and the supply of new compounds by our cooperation partners from the working group of Prof. Dr. Christian Peifer and Dr. Andreas Luxenburger. Additionally, I would like to thank Dr. Ana Velic from the Proteome Center Tübingen for performing the LC-MS/MS analyses. My special thanks belong to Prof. Dr. Doo Kim at the Massachusetts General Hospital and Prof. Dr. Cagatay Günes for providing the lentiviral constructs, which enabled the establishment of the extremely useful “Alzheimer’s-in-a-dish” model. Furthermore, I thank Simona Ursu and Daniela Fröhlich of the Core Facility Ulm University for their helpful technical assistance with cell sorting.

I would like to extend my sincere thanks to the International Graduate School in Molecular Medicine at Ulm University, which is represented by the chairman Prof. Dr. Bernd Knöll, for accepting me as PhD candidate, providing an organizational framework and offering numerous industry-related trainings. Within the International Graduate School I especially want to thank Lina Zaveleva, Katrin Tenhumberg and Christiane Böhm, who always kept everything running smoothly.

Additionally, the work in this thesis would not have come so far without the help of numerous colleagues and students. At least I would like to name a few of the students, whom I thank very much for their work and efforts: Katja Mayer, Julian Beyrle, Irina König, Maxine Rustler, Annabelle Sander, Marleen Oswald, Laura Meier, Linda Grabe and Laura Mayer. Furthermore, I had the pleasure of working with aspiring and motivated scientists, such as Dr. Balbina Garcia-Reyes, Dr. Chiara lanes, Dr. Anna-Laura Kretz, Dr. Hend Abdelrasoul and Dr. Tamer Abdelaal. In this context I also would like to thank Dr. Fabian Gärtner for the helpful discussions, his excellent support in various (statistical) methods, entertaining coffee breaks and the friendship that has developed.

Finally, I could not have undertaken this journey without the help, love, emotional support, patience and motivation of my family, friends and my partner in life Adrian Gihring, who always believed in me and encouraged me. I apologize for the numerous stories about daily lab life and struggles you had to listen to. The fact that you always listened to me was of great value to me. I especially want to thank Adrian Gihring, who has always been a special and extremely valuable support to me, not only in science, but also in everyday life.

Statutory declaration

I hereby declare that I wrote the present dissertation with the topic

“Characterization of CK1δ-mediated phosphorylation of tau and development of novel pharmacological approaches targeting CK1δ in Alzheimer’s disease”

independently and used no other aids than those cited. In each individual case, I have clearly identified the source of the passages that are taken word for word according to the principles of good scientific practice in accordance with the current “Satzung der Universität Ulm zur Sicherung guter wissenschaftlicher Praxis”.

Ulm, 01.02.2023

Publications

A complete list of all publications published during the preparation of this thesis are shown in the following:

Gihring, A., Gärtner, F., Mayer, L., **Roth, A.**, Abdelrasoul, H., Kornmann, M., Elad, L., Knippschild, U. Influence of bariatric surgery on the peripheral blood immune system of female morbid obese patients revealed by high-dimensional mass cytometry. In preparation.

Meier, L., Gahr, B., **Roth, A.**, Gihring, A., Kirschner, S., Woitaske-Proske, C., Baier, J., Peifer, C., Just, S., and Knippschild, U. Zebrafish as model system for the characterization of CK1 inhibitors. In preparation.

Wesseler, F., Lohmann, S., Riege, D., Halver, J., **Roth, A.**, Pichlo, C., Weber, S., Takamiya, M., Müller, E., Ketzel, J., Flegel, J., Gihring, A., Rastegar, S., Bertrand, J., Baumann, U., Knippschild, U., Peifer, C., Sievers, S., Waldmann, H., and Schade, D. 2022. Phenotypic Discovery of Triazolo1,5-cquinazolines as a First-In-Class Bone Morphogenetic Protein Amplifier Chemotype. *Journal of medicinal chemistry*.

Roth, A., Sander, A., Oswald, M. S., Gärtner, F., Knippschild, U., and Bischof, J. 2022. Comprehensive Characterization of CK1 δ -Mediated Tau Phosphorylation in Alzheimer's Disease. *Frontiers in molecular biosciences* 9, 872171.

Roth, A., Gihring, A., Bischof, J., Pan, L., Oswald, F., and Knippschild, U. 2022. CK1 Is a Druggable Regulator of Microtubule Dynamics and Microtubule-Associated Processes. *Cancers* 14, 5.

Drathen, T. von, Ure, E. M., Kirschner, S., **Roth, A.**, Meier, L., Woolhouse, A. D., Cameron, S. A., Knippschild, U., Peifer, C., and Luxenburger, A. 2022. C5-Iminosugar modification of casein kinase 1 δ lead 3-(4-fluorophenyl)-5-isopropyl-4-(pyridin-4-yl)isoxazole promotes enhanced inhibitor affinity and selectivity. *Archiv der Pharmazie* 355, 5, e2100497.

Smirlis, D., Dingli, F., Sabatet, V., **Roth, A.**, Knippschild, U., Loew, D., Späth, G. F., and Rachidi, N. 2021. Identification of the Host Substratome of Leishmania-Secreted Casein Kinase 1 Using a SILAC-Based Quantitative Mass Spectrometry Assay. *Frontiers in cell and developmental biology* 9, 800098.

Gärtner, F., Gihring, A., **Roth, A.**, Bischof, J., Xu, P., Elad, L., Wabitsch, M., Burster, T., and Knippschild, U. 2021. Obesity Prolongs the Inflammatory Response in Mice After Severe Trauma and Attenuates the Splenic Response to the Inflammatory Reflex. *Frontiers in immunology* 12, 745132.

Traub, B., **Roth, A.**, Kornmann, M., Knippschild, U., and Bischof, J. 2021. Stress-activated kinases as therapeutic targets in pancreatic cancer. *World journal of gastroenterology* 27, 30, 4963–4984.

Roth, A., Gihring, A., Göser, F., Peifer, C., Knippschild, U., and Bischof, J. 2021. Assessing the Inhibitory Potential of Kinase Inhibitors In Vitro: Major Pitfalls and Suggestions for Improving Comparability of Data Using CK1 Inhibitors as an Example. *Molecules* (Basel, Switzerland) 26, 16.

Roth, A., Gärtner, F., Mayer, K., Beyrle, J., König, I., Knippschild, U., and Bischof, J. 2021. CK1 δ -Derived Peptides as Novel Tools Inhibiting the Interactions between CK1 δ and APP695 to Modulate the Pathogenic Metabolism of APP. *International journal of molecular sciences* 22, 12.